

RESEARCH LABORATORIES FOR THE ENGINEERING SCIENCES

SCHOOL OF ENGINEERING AND
APPLIED SCIENCE

University of Virginia
Charlottesville, Virginia 22901

A Report

OPTIMIZATION OF MLS RECEIVERS FOR
MULTIPATH ENVIRONMENTS

Submitted to:

NASA Scientific & Technical Information Facility
P.O. Box 8757
Baltimore/Washington International Airport
Maryland 21240

Submitted by:

G. A. McAlpine
J. H. Highfill, III
S. H. Irwin, Jr.
R. E. Nelson
Ghassem Koleyani

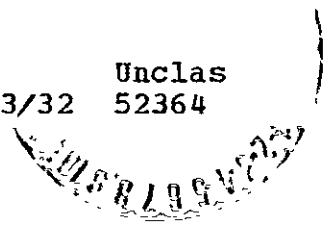
Report No. UVA/528062/EE77/104

November 1977

(NASA-CR-155230) OPTIMIZATION OF MLS
RECEIVERS FOR MULTIPATH ENVIRONMENTALS Annual
Report (Virginia Univ.) 250 p HC A11/MF A01
CSCL 17B



Unclas
G3/32 52364



RESEARCH LABORATORIES FOR THE ENGINEERING SCIENCES

Members of the faculty who teach at the undergraduate and graduate levels and a number of professional engineers and scientists whose primary activity is research generate and conduct the investigations that make up the school's research program. The School of Engineering and Applied Science of the University of Virginia believes that research goes hand in hand with teaching. Early in the development of its graduate training program, the School recognized that men and women engaged in research should be as free as possible of the administrative duties involved in sponsored research. In 1959, therefore, the Research Laboratories for the Engineering Sciences (RLES) was established and assigned the administrative responsibility for such research within the School.

The director of RLES—himself a faculty member and researcher—maintains familiarity with the support requirements of the research under way. He is aided by an Academic Advisory Committee made up of a faculty representative from each academic department of the School. This Committee serves to inform RLES of the needs and perspectives of the research program.

- In addition to administrative support, RLES is charged with providing certain technical assistance. Because it is not practical for each department to become self-sufficient in all phases of the supporting technology essential to present-day research, RLES makes services available through the following support groups: Machine Shop, Instrumentation, Facilities Services, Publications (including photographic facilities), and Computer Terminal Maintenance.

Annual Report

OPTIMIZATION OF MLS RECEIVERS FOR
MULTIPATH ENVIRONMENTS

NASA Grant NSG 1128

Submitted to:

NASA Scientific & Technical Information Facility
P. O. Box 8757
Baltimore/Washington International Airport
Maryland 21240

Submitted by:

G. A. McAlpine
J. H. Highfill, III
S. H. Irwin, Jr.
R. E. Nelson
Ghassem Koleyani

Department of Electrical Engineering
RESEARCH LABORATORIES FOR THE ENGINEERING SCIENCES
SCHOOL OF ENGINEERING AND APPLIED SCIENCE
UNIVERSITY OF VIRGINIA
CHARLOTTESVILLE, VIRGINIA

Report No. UVA/528062/EE77/104
November 1977

Copy No. 1

TABLE OF CONTENTS

	<u>Page No.</u>
I. Introduction	1
PART ONE: ANGLE-RECEIVER STUDY	
II. Signal Model and Approach	5
III. Scan Data Processor Design	11
IV. Tracking Loop Design	17
V. Simulation Studies	21
VI. Experimental System	49
PART TWO: DME-RECEIVER STUDY	
VII. DME Signal Model	53
VIII. DME Simulation	55
IX. Simulation Results - Transponder: Fixed Threshold Receiver	65
X. Simulation Results - Transponder: Delay and Compare Receiver	75
XI. Simulation Results - Interrogator: Adaptive Threshold Receiver	87
XII. Simulation Results - Interrogator: Delay and Compare Receiver	95
XIII. Overall Study Conclusions	101
References	103
Appendix A. Angle-Receiver Innovation's Study	
Appendix B. Adaptive Kalman Filtering Applied to Aircraft Position Estimation	

LIST OF FIGURES

Figures	Page No.
1. Receiver Error Time Histories, Crossing Multipath Simulation, No Multipath (reference) case . . .	28
2. Receiver Error Time Histories, Crossing Multipath Simulation, S/N = 14 db, $\rho = .8$, $F_{sc} = 51.3$ Hz., $\beta = -168.0^\circ$	29
3. Summary of Crossing Multipath Simulation Results for $F_{sc} = 5$ Hz., $\beta = 0^\circ$	31
4. Summary of Crossing Multipath Simulation Results for $F_{sc} = 51.3$ Hz., $\beta = -168^\circ$	32
5. Summary of Crossing Multipath Simulation Results for $F_{sc} = 500$ Hz., $\beta = 180^\circ$	33
6. Receiver Error time Histories, Crossing Multipath Simulation, S/N = 20 db, $\rho = .8$, $F_{sc} = 5.0$ Hz., $\beta = 0.0^\circ$	34
7. Receiver Error Time Histories, Crossing Multipath Simulation, S/N = 20 db, $\rho = .8$, $F_{sc} = 51.3$ Hz., $\beta = -168.0^\circ$	35
8. Receiver Error Time Histories, Crossing Multipath Simulation, S/N = 20 db, $\rho = .8$, $F_{sc} = 500.0$ Hz., $\beta = 180.0^\circ$	36
9. Receiver Error Time Histories, Crossing Multipath Simulation, S/N = 20 db, $\rho = .5$, $F_{sc} = 500.0$ Hz., $\beta = 180.0^\circ$	37
10. Optimal Receiver Error Time Histories, Crossing Multipath Simulation, S/N = 20 db, $\rho = 0.8$	38
11. Time-varying In-Beam Multipath Scenario, Receiver Error Time Histories, S/N = 20 db, $F_{sc} = 5$ Hz., $\beta = 0^\circ$, $\theta_{sep} = 0.5^\circ$	44
12. Representative Landing Scenario	46
13. Receiver Error Time Histories, Representative Landing Scenario, S/N = 20 db, $\beta = 0.0^\circ$	47

LIST OF FIGURES
CONTINUED

<u>Figures</u>	<u>Page No.</u>
14. Normalized Density Function for IF Envelope, Evaluated at Threshold Crossing Time	59
15. Landing Pattern, 14000 Ft Runway	60
16. Mean Error Vs. T/N, Fixed Threshold Receiver	66
17. Error Distribution, Fixed Threshold Receiver, T/N = 18 DB	68
18. Error Distribution, Fixed Threshold Receiver T/N = 6 DB	69
19. Mean Error Vs. S/N, Fixed Threshold Receiver.	71
20. Mean Error Vs. Multipath Delay, Fixed Threshold Receiver	72
21. Delay and Compare Receiver Signals	76
22. Mean Error Vs. Threshold Crossing Point, Delay and Compare Receiver, S/N = 46 DB.	77
23. Error Distribution, Delay and Compare Receiver, T/N = 25 DB.	79
24. Error Distribution, Delay and Compare Receiver, T/N = 29 DB.	80
25. Mean Error Vs. S/N, Delay and Compare Receiver, Nominal S/N = 46 DB.	82
26. Mean Error Vs. Multipath Delay, Delay and Compare Receiver, S/N = 46 DB.	83
27. Mean Error Vs. Threshold Crossing Point, Adaptive Threshold Receiver, S/N = 40 DB.	88
28. Mean Error Vs. S/N, Adaptive Threshold Receiver.	90
29. Mean Error Vs. Multipath Delay, Adaptive Threshold Receiver	91
30. Shift in Threshold Crossing Time with Multipath delay Adaptive Threshold Receiver	93

LIST OF FIGURES
CONTINUED

<u>Figures</u>	<u>Page No.</u>
31. Mean Error Vs. Threshold Crossing Point Delay and Compare Receiver, S/N = 40 DB	96
32. Mean Error Vs. S/N, Delay and Compare Receiver, Nominal S/N = 40 DB	97
33. Mean Error Vs. Multipath Delay, Delay and Compare Receiver, S/N = 40 DB	99

LIST OF TABLES

<u>Tables</u>	<u>Page No.</u>
1. Performance Comparisons of the Optimal, Threshold and Non-adaptive Receivers; Crossing Multipath Scenarios	39
2. Optimal Receiver Error Performance; Crossing Multipath Scenarios	40
3. Threshold Receiver Error Performance; Crossing Multipath Scenarios	41
4. Non-adaptive Receiver Error Performance; Crossing Multipath Scenarios	42
5. Experimental System Development Status, 10/77	50
6. Summary of Errors - Transponder, Fixed Threshold Receiver	74
7. Summary of Errors - Transponder, Delay and Compare Receiver	85
8. Summary of Errors - Interrogator, Adaptive Threshold Receiver	94
9. Summary of Errors - Interrogator, Delay and Compare Receiver	100

SECTION I

INTRODUCTION

This is an interim report concluding the third period of research under Grant NSG 1128, dealing with optimal design of subsystems of the proposed Microwave Landing System. The research reported includes both optimal design studies of MLS angle-receivers and a theoretical design-study of MLS DME-receivers.

The angle-receiver results include an integration of the scan data processor and tracking filter components of the optimal receiver into a unified structure and then an extensive simulation study comparing the performance of the optimal and threshold (Phase III) receivers in a wide variety of representative dynamical and interference environments. The optimal receiver was generally superior, offering improvements ranging up to 20:1 or better in certain situations.

The DME portion of this report includes a simulation study of the performance of the threshold and delay-and-compare receivers in various signal environments. This study provides an analysis of combined errors due to lateral reflections from vertical structures with small differential path delays, specular ground reflections with negligible differential path delays, and thermal noise in the receivers.

The angle-receiver research and DME-receiver research are two, completely independent studies and are documented accordingly in the following eleven sections, the first part, Section's II thru VI, dealing with the angle-receiver and the second part, Sections VII thru XII, dealing with the DME-receiver. No cross referencing occurs between

these major parts of this report, and also the symbol and notation systems used in the two parts are independent. For easy access, however, results and conclusions from both parts of the year's work are summarized in Section XII.

PART ONE
ANGLE-RECEIVER STUDY

SECTION II

SIGNAL MODEL AND APPROACH

The reader is referred to our prior reports [1], [2], [3] for details. This is a summary included to communicate minor revisions in prior results and establish notation.

GEOMETRY AND SIGNAL MODELING

The angular coordinate to be estimated and other relevant quantities that evolve are assembled into an N-dimensional state vector x , modeled as the solution of a suitable linear difference equation evolving in discrete-time, from scan-to-scan, and excited by a white zero-mean random process, $\{z(k), k = 0, 1, \dots\}$. The receiver log-envelope signal, a continuous-time signal within a scan, is sampled throughout a window on each semi-scan at a sampling rate approximately equal to the i-f bandwidth and then suitably exponentiated and squared; the resulting J samples of the amplitude-squared envelope taken within a given scan are then normalized to a suitable measure of receiver noise power and assembled into an observations, or measurement, vector u , which clearly is nonlinear in the state and also corrupted non-additively by receiver noise. For the k th scan, $k = 0, 1, 2, \dots$, therefore we have the model form

$$x(k+1) = F(k)x(k) + G(k)z(k) \tag{2.1}$$

$$u(k) = h(x(k), n(k))$$

relating state x , excitation z and observations u , generally.

More specifically, in terms of a discrete-time variable τ_j local to the scan, and assuming the presence of a direct-path component,

a single multipath component and receiver noise, the j th component of u , say u_j , $j = 1, \dots, J$, is approximated as follows with little error (see [

$$u_j = \{ \alpha_p [\theta - \theta_A(\tau_j)] + \alpha_R p[\theta_R - \theta_A(\tau_j)] \cos(\beta + \omega_{sc} \tau_j) + n_{c_j} \}^2 + \{ \alpha_R p[\theta_R - \theta_A(\tau_j)] \sin(\beta + \omega_{sc} \tau_j) + n_{s_j} \}^2 \quad (2.2)$$

where

$$\alpha = \alpha(k) = \text{direct path signal-to-noise ratio} \quad (2.3)$$

$$\theta = \theta(k) = \text{angular coordinate of own A/C} \quad (2.4)$$

$$\alpha_R = \alpha_R(k) = \text{multipath signal-to-noise ratio} \quad (2.5)$$

$$\theta_R = \theta_R(k) = \text{angular coordinate of reflector specular point} \quad (2.6)$$

$\beta = \beta(k) = \text{direct path-to-multipath phase difference at the beginning of the scan (propagating scan-to-scan as follows:}$

$$\beta(k+1) = \beta(k) + \omega_{sc} T_k$$

$$\text{where } T_k = \text{time interval, } k\text{th-to-}(k+1)\text{th scans.} \quad (2.7)$$

$$\omega_{sc} = \text{the scalloping rate} \quad (2.8)$$

$$\theta_A(\cdot) = \text{the transmitting antenna scanning function} \quad (2.9)$$

$$p[\cdot] = \text{the transmitting antenna selectivity function} \quad (2.10)$$

and

$$n_{c_j}, n_{s_j} \text{ are independent Gaussian random variables with mean zero, variance } 0.5. \quad (2.11)$$

On the basis of the above the state vector x is defined as follows:

$$x \triangleq (\alpha, \theta, \dot{\theta}, \alpha_R, \theta_R, \dot{\theta}_R, \beta, \omega_{sc})^T \quad (2.12)$$

where $(\quad)^T$ denotes transpose and $(\dot{\quad})$ denotes $\frac{d}{dt}$

Matrix F in (1) is then defined by

$$F \triangleq \begin{pmatrix} 1 & 0 & 0 & 0 & 0 & 0 & 0 & 0 \\ 0 & 1 & T_k & 0 & 0 & 0 & 0 & 0 \\ 0 & 0 & 1 & 0 & 0 & 0 & 0 & 0 \\ 0 & 0 & 0 & 1 & 0 & 0 & 0 & 0 \\ 0 & 0 & 0 & 0 & 1 & T_k & 0 & 0 \\ 0 & 0 & 0 & 0 & 0 & 1 & 0 & 0 \\ 0 & 0 & 0 & 0 & 0 & 0 & 1 & T_k \\ 0 & 0 & 0 & 0 & 0 & 0 & 0 & 1 \end{pmatrix} = F(k) \quad (2.13)$$

In (2.1) the vector process $\{z(k), k = 0, 1, \dots\}$ is a zero-mean white Gaussian sequence which excites the $\alpha, \theta, \alpha_R, \theta_R$ and ω_{sc} state components.

Consequently

$$G \triangleq \begin{pmatrix} 1 & 0 & 0 & 0 & 0 \\ 0 & 0 & 0 & 0 & 0 \\ 0 & 1 & 0 & 0 & 0 \\ 0 & 0 & 1 & 0 & 0 \\ 0 & 0 & 0 & 0 & 0 \\ 0 & 0 & 0 & 1 & 0 \\ 0 & 0 & 0 & 0 & 0 \\ 0 & 0 & 0 & 0 & 1 \end{pmatrix}, \text{ a constant matrix.} \quad (2.14)$$

Also

$$\langle z(k) z^T(k) \rangle \triangleq Q(k) = \text{Diag} (Q_{11}, Q_{22}, Q_{33}, Q_{44}, Q_{55}) \quad (2.15)$$

where $\langle \quad \rangle$ denotes mathematical expectation. This completes the modeling summary.

APPROACH

The objective of the desired MLS angle receiver is to produce an estimate of the A/C angular coordinate, θ , which is minimally affected by multipath interference. State estimation in conjunction with

the model (2.1) assumed is the approach used to develop the desired signal processor. Specifically, defining

$$U(k) \triangleq \{u(k_1), k_1 = 0, 1, \dots, k\}, \text{ the sequence of observations from some initial time through the present;} \quad (2.16)$$

$$\hat{x}(k|k) \triangleq \text{estimate of } x(k), \text{ given } U(k) \quad (2.17)$$

Then the estimate evolution is described as follows:

$$\hat{x}(k|k) = \hat{x}(k|k-1) + \xi(k|k) \quad (2.18)$$

where

$$\hat{x}(k|k-1) \triangleq F(k-1) \hat{x}(k-1|k-1) \quad (2.19)$$

$$\xi(k|k) \triangleq \text{estimate of the error in } \hat{x}(k|k-1), \text{ given } U(k) \quad (2.20)$$

The calculation of $\xi(k|k)$ in general, as defined, is complicated because of the form of $h(\cdot, \cdot)$ in (1), as implied by (2). A simpler form for ξ based in part on the "tracking assumption" that ξ is "small" in some sense (and the vector $G\hat{w}$ also) has been used thus far with good results (though without benefit of formal derivation from (2.20) as yet). This relation is

$$\xi(k|k) = K(k) \varepsilon(k|k) \quad (2.21)$$

where

$$\varepsilon(k|k) \triangleq \text{estimate of the error in } \hat{x}(k|k-1) \text{ in the neighborhood of zero error, given } u(k). \quad (2.22)$$

$$K(k) \triangleq \text{a gain matrix, depending on } \hat{x}(k|k-1), Q(k), \text{ and statistics of } \varepsilon(k|k) \quad (2.23)$$

The calculation of $\varepsilon(k|k)$ is based on the locally optimum estimation (LOE) criterion of Murphy [4] and does not make any use of the assumed dynamical model of state evolution, (2.1). This stage

of the computation processes the raw scan data $\{u(k), k = 0, 1, \dots\}$ and is described in summary form in the next section. The calculation of $K(k)$ represents the determination of a suitable weighting matrix such that use of the resulting $\xi(k|k)$, (2.21), in the estimate update equation, (2.18) gives a smoothly evolving state estimate which is appropriate to and consistent with the assumed dynamical model (2.1); in short, the constraints represented by the assumed state dynamics, heretofore ignored, are applied at this point. The quantity $K(k)$ is the Kalman gain of a recursive tracking loop (or filter), closed around the LOE. This aspect of the design is summarized in Section IV.

SECTION III

SCAN DATA PROCESSOR DESIGN

The observations taken on a scan have been modeled as a J-vector, u , with components u_j , $j = 1, 2, \dots, J$, as given in (2.2). The application of locally optimum estimation to this problem requires the conceptualization of a noise-free observation vector, say $q(k)$, whose j th- component q_j has the form

$$q_j \stackrel{\Delta}{=} \tilde{u}_j \left| \begin{array}{l} = [\alpha p_j(\theta) + \alpha_R p_j(\theta_R) \cos \beta_j]^2 + [\alpha_R p_j(\theta_R) \sin \beta_j]^2 \\ n_{c_j} = 0 \\ n_{s_j} = 0 \end{array} \right. \quad (3.1)$$

$$= \alpha^2 p_j^2(\theta) + 2 \alpha \alpha_R p_j(\theta) p_j(\theta_R) \cos \beta_j + \alpha_R^2 p_j^2(\theta_R) \quad (3.2)$$

where

$$\beta_j \stackrel{\Delta}{=} \beta + \omega_{sc} \tau_j \quad (3.3)$$

$$p_j(\theta) \stackrel{\Delta}{=} p[\theta - \theta_A(\tau_j)] \quad (3.4)$$

and similarly for $p_j(\theta_R)$. Using the q_j - formulization, it is possible to write u_j as follows:

$$u_j = q_j + 2 \sqrt{q_j [n_{c_j} \cos \beta_j + n_{s_j} \sin \beta_j]} + n_{c_j}^2 + n_{s_j}^2 \quad (3.5)$$

$$= q_j + 2 \sqrt{q_j} (\cos \beta_j \sin \beta_j) \begin{pmatrix} n_{c_j} \\ n_{s_j} \end{pmatrix} + \begin{pmatrix} n_{c_j} & n_{s_j} \end{pmatrix} \begin{pmatrix} n_{c_j} \\ n_{s_j} \end{pmatrix} \quad (3.6)$$

Letting the noise vector, $(n_{c_j} \ n_{s_j})^T$, be modeled as follows

$$\begin{pmatrix} n_{c_j} \\ n_{s_j} \end{pmatrix} \triangleq \begin{pmatrix} \cos \beta_j & -\sin \beta_j \\ \sin \beta_j & \cos \beta_j \end{pmatrix} \begin{pmatrix} \eta_{c_j} \\ \eta_{s_j} \end{pmatrix} \quad (3.7)$$

where

$$\langle \eta_{c_j} \rangle = \langle \eta_{s_j} \rangle = 0 \quad (3.8)$$

$$\langle \eta_{c_j} \ \eta_{s_l} \rangle = 0, \forall j, l \quad (3.9)$$

$$\langle \eta_{c_j} \ \eta_{c_l} \rangle = \langle \eta_{s_j} \ \eta_{s_l} \rangle = \frac{1}{2} \delta_{jl} \quad (3.10)$$

clearly assures these same assumed properties in $(n_{c_j} \ n_{s_j})^T$, and

in addition simplifies u_j in (3.6)

$$u_j = q_j + 2 \eta_{c_j} \sqrt{q_j} + \eta_{c_j}^2 + \eta_{s_j}^2 \quad (3.11)$$

Henceforth, references to receiver noise will refer to the new vector

$(\eta_{c_j} \ \eta_{s_j})^T$ unless otherwise noted.

Paralleling the prior development somewhat [3], the likelihood ratio $\lambda(u|q)$, in terms of the revised formulations of u and q , is .

given now by

$$\lambda(u|q) = \prod_{j=1}^J \left[M_0(4q_j u_j) \exp(-q_j) \right] \quad (3.12)$$

where, as before, $M_0(\cdot)$ [for positive argument--as is the case here]

is defined in relation to $I_0(\cdot)$, the modified Bessel function of the first kind, zeroth order, as follows

$$M_0(z) \triangleq I_0(\sqrt{z}), \quad z > 0, \text{ real} \quad (3.13)$$

The theory of locally optimum estimation is applied to the scan data processing problem by first assembling a selected subset of the state variables into a parameter vector γ and then processing the observations u to obtain an estimate, \hat{e} , of the error in the current γ -estimate, as follows:

$$\hat{e} \triangleq \Phi^{-1} \Lambda(u|\hat{q}) \quad (3.14)$$

where

$$\Phi \triangleq \left\langle \Lambda(u|\hat{q}) \Lambda^T(u|\hat{q}) \mid \hat{q} \right\rangle \quad (3.15)$$

$$\hat{q} \triangleq q(\gamma) \Big|_{\gamma=\hat{\gamma}}(q(\gamma)), \text{ given in (3.2)} \quad (3.16)$$

and

$$\Lambda(u|\hat{q}) \triangleq \left[\frac{\partial}{\partial \gamma} \ln \lambda(u|q(\gamma)) \right]_{\gamma=\hat{\gamma}} \quad (3.17)$$

The estimate \hat{e} is both locally unbiased at zero error (i.e. when $\gamma = \hat{\gamma}$) and has minimum mean square error of all estimates locally unbiased at zero error. The matrix Φ^{-1} is the covariance matrix for the error in the estimate \hat{e} when $\gamma = \hat{\gamma}$. The averaging done in the calculation of Φ , (3.15), is taken under the assumption that $\gamma = \hat{\gamma}$, i.e. that the parameter value entering the \hat{q} calculation equals the true value giving the u observation; the result is independent of the observation and is a function only of \hat{q} . The observations u , enter

calculation of \hat{e} only through $\Lambda(u|\hat{q})$, which is a function of both u and \hat{q} . Substituting (3.12) into (3.17) we may write, specifically

$$\Lambda(u|q) = \frac{\partial}{\partial \gamma} \sum_{j=1}^J \left[\ln M_0(4q_j u_j) - q_j \right] \quad (3.18)$$

$$= \sum_{j=1}^J \left\{ \frac{\partial q_j}{\partial \gamma} \left[4u_j \frac{M_1}{M_0} (4q_j u_j) - 1 \right] \right\} \quad (3.19)$$

$$= D(q) w(u|q) \quad (3.20)$$

where

$$D(q) \triangleq \left(\frac{\partial q_1}{\partial \gamma}, \frac{\partial q_2}{\partial \gamma}, \dots, \frac{\partial q_J}{\partial \gamma} \right), \text{ a matrix} \quad (3.21)$$

$$w(u|q) = \begin{pmatrix} \vdots \\ 4u_j \frac{M_1}{M_0} (4q_j u_j) - 1 \\ \vdots \end{pmatrix}, \text{ a J-vector} \quad (3.22)$$

and, as before

$$M_1(z) \triangleq \frac{d}{dz} M_0(z) \quad (3.23)$$

Using the previously developed asymptotic approximation for M_1/M_0 ,
i.e. [3, eqn (III-42p)]

$$\frac{M_1}{M_0}(z) \approx \frac{1}{2 \sqrt{4+z}} \quad (3.24)$$

The vector $w(u|q)$, through which the observations, u , enter the computations, has representative element

$$w_j(u|q) = \frac{u_j}{\sqrt{1+q_j u_j}} - 1 \quad (3.25)$$

Substituting (3.20) into (3.15) results in an expression for matrix $\Phi(\hat{q})$, as follows:

$$\Phi(\hat{q}) = D(\hat{q}) \left\langle w(u|\hat{q}) w^T(u|\hat{q}) \mid \hat{q} \right\rangle D^T(\hat{q}) \quad (3.26)$$

$$= D(\hat{q}) H_w(\hat{q}) D^T(\hat{q}) \quad (3.27)$$

where

$$H_w(\hat{q}) \triangleq \left\langle w(u|\hat{q}) w^T(u|\hat{q}) \mid \hat{q} \right\rangle \quad (3.28)$$

A simulation study was performed of the statistics of $w_j(u|q)$, (3.25), involving up to 10,000 samples. Refer to Appendix A for details.

Conclusions reached are as follows:

$$\left\langle w_j(u|\hat{q}) \mid \hat{q} \right\rangle = 0, \text{ independent of } \hat{q} \quad (3.29)$$

$$\left\langle w_j(u|\hat{q}) w_k(u|\hat{q}) \mid \hat{q} \right\rangle = \delta_{jk} h_j(\hat{q}) \quad (3.30)$$

where δ_{jk} is the Kronecker delta, and

$$h_j(\hat{q}) \triangleq \left\langle w_j^2(u|\hat{q}) \mid \hat{q} \right\rangle \quad (3.31)$$

The process $\{w_j(u|q), j=1, \dots, J\}$ is white; consequently,

$$H_w(\hat{q}) = \text{Diag} [h_1(\hat{q}), h_2(\hat{q}), \dots, h_J(\hat{q})] \quad (3.32)$$

The sample statistics study also produced an asymptotic approximation for $h_j(\hat{q})$:

$$h_j(\hat{q}) \approx \frac{1}{1 + 2 \hat{q}_j} \quad (3.33)$$

whose error peaked briefly at 20% (for $\hat{q}_j = 2$), but which produced good results in the receiver simulation studies.

All receiver simulation studies to date dealt with a receiver design based on the following choice of the parameter vector γ :

$$\gamma \triangleq \begin{pmatrix} \alpha \\ \theta \\ \alpha_R \\ \theta_R \\ \beta \end{pmatrix} \quad (3.34)$$

The corresponding D-matrix is the following:

$$D(q) = \begin{pmatrix} \dots 2\alpha p_j^2(\theta) + 2\alpha_R p_j(\theta) p_j(\theta_R) \cos \beta_j \dots \\ \dots 2\alpha^2 \dot{p}_j(\theta) p_j(\theta) + 2\alpha \alpha_R \dot{p}_j(\theta) p_j(\theta_R) \cos \beta_j \dots \\ \dots 2\alpha p_j(\theta) p_j(\theta_R) \cos \beta_j + 2\alpha_R p_j^2(\theta_R) \dots \\ \dots 2\alpha \alpha_R p_j(\theta_R) \dot{p}_j(\theta_R) \cos \beta_j + 2\alpha_R^2 \dot{p}_j(\theta_R) p_j(\theta_R) \dots \\ \dots -2\alpha \alpha_R p_j(\theta) p_j(\theta_R) \sin \beta_j \dots \end{pmatrix} \quad (3.35)$$

where $\dot{(\)}$ denotes $\frac{d}{dt} (\)$.

SECTION IV

TRACKING LOOP DESIGN

The scan data processor produces an estimate \hat{e} of the error e in the last estimate $\hat{\gamma}$ of parameter vector γ , a masked version of the state x . The algorithm employed provides that \hat{e} is locally optimum at $e = 0$ in a least mean square error sense and supplies also the associated covariance matrix

$$R \triangleq \left. \left\langle (\hat{e} - e) (\hat{e} - e)^T \mid \hat{q} \right\rangle \right|_{e=0} = \Phi^{-1}(\hat{q}) \quad (4.1)$$

The tracking loop design was obtained as follows:

1. Generation of a pre-estimate of γ by simply adding the estimate \hat{e} to the value of $\hat{\gamma}$ used in the calculation of \hat{e} .
2. Interpretation of the pre-estimate as a synthetic measurement of γ , additively corrupted by white, discrete-time noise with covariance R .
3. Use of a linear Kalman filter designed to accept the synthetic measurements produced (and the matrix R), for generating an update estimated, \hat{x} of the full state.

The method embodies certain assumptions, including specifically

1. The whiteness of the synthetic measurement noise.
2. A knowledge of matrix Q , defined in (2.15)
3. The form of state-estimate error in (2.21).

The algorithm therefore is deemed suboptimal; nevertheless the tracking performance results were good and probably represent the limiting performance obtainable from the standpoint of algorithmic complexity.

We will now formalize the approach mathematically and present in summary form the algorithm, which benefits from some simplifications that are possible.

Pre-estimate: $\hat{\gamma}(k|k) \triangleq \hat{\gamma}(k|k-1) + \hat{e}(k) = H\hat{x}(k|k-1) + \hat{e}(k)$ (4.2)

$$= [\gamma(k) - e(k)] + \hat{e}(k) \quad (4.3)$$

$$= Hx(k) + v(k) \quad (4.4)$$

where $H \triangleq$ masking matrix associated with choice of $\hat{\gamma}$ (4.5)

$$v(k) \triangleq \hat{e}(k) - e(k) \quad (4.6)$$

and

$$\langle v(k) \rangle \Big|_{e=0} = 0 \text{ (locally unbiasedness)} \quad (4.7)$$

$$\langle v(k)v^T(k) \rangle \Big|_{e=0} = R(k) = \Phi^{-1}(\hat{q}(k)) \text{ (by 4-1)} \quad (4.8)$$

Kalman filter: $\hat{x}(k|k-1) = F(k-1) \hat{x}(k-1|k-1)$ (4.9)

$$P(k|k-1) = F(k-1)P(k-1|k-1)F^T(k-1) + G(k-1)Q(k-1)G^T(k-1) \quad (4.10)$$

$$K(k) = P(k|k-1)H^T [HP(k|k-1)H^T + R(k)]^{-1} \quad (4.11)$$

$$\hat{x}(k|k) = \hat{x}(k|k-1) + K(k) [\hat{\gamma}(k|k) - H\hat{x}(k|k-1)] \quad (4.12)$$

$$P(k|k) = P(k|k-1) - K(k)HP(k|k-1) \quad (4.13)$$

$$= [I-K(k)H]P(k|k-1)[I-K(k)H]^T + K(k)R(k)K^T(k) \quad (4.14)$$

(4.14) is preferred to (4.13) for preservation of symmetry and positive-definiteness properties.

Substantial simplification follows from substitution of (4.2) into (4.12), giving

$$\hat{x}(k|k) = \hat{x}(k|k-1) + K(k) \hat{e}(k) \quad (4.15)$$

where

$$K(k)\hat{e}(k) = P(k|k-1)H^T [HP(k|k-1)H^T + \Phi^{-1}]^{-1} \Phi^{-1} \Lambda = K\Phi^{-1}\Lambda \quad (4.16)$$

$$= PH^T \{ \Phi [HPH^T + \Phi^{-1}] \}^{-1} \Lambda \quad (4.17)$$

$$= M(k)\Lambda (u|\hat{q}) \quad (4.18)$$

in which

$$M(k) \triangleq P(k|k-1)H^T [I + \Phi HPH^T]^{-1} \quad (4.19)$$

Thus the state estimate update operation, i.e.

$$\hat{x}(k|k) = \hat{x}(k|k-1) + M(k)\Lambda(u|\hat{q}), \quad (4.20)$$

does not require the inversion of matrix Φ .

The error covariance update equation (4.14) can be written in terms of Φ also by first noting from (4.16) and (4.18) above that $M = K\Phi^{-1}$, or more specifically

$$K(k) = M(k) \Phi \quad (4.21)$$

Substituting this into (4.14) and recalling that $R \triangleq \Phi^{-1}$, gives

$$P(k|k) = [I - M\Phi H] P(k|k-1) [I - M\Phi H]^T + M\Phi M^T \quad (4.22)$$

SECTION V

SIMULATION STUDIES

The principal simulation models with which we were concerned during the past year are the following:

- i. The environment and baseband receiver signal;
- ii. The LOE/Kalman filter recursive receiver structure, and specifically both multipath-adaptive and non-adaptive variants, thereof;
- iii. A representation of the phase III MLS receiver, denoted the threshold receiver

Simulation studies conducted, included principally the following:

- i. Crossing multipath interference, initiating as out-of-beam interference.
- ii. Time-varying in-beam multipath interference
- iii. Simulated landing scenarios

Results are presented below and discussed; programs developed and used will be transmitted to the sponsor under separate cover.

Simulation Models

A. Environment and Baseband Receiver Signal

Generally, the environmental dynamics are simulated with a state model of the form (2.1) (without the random excitation), using the state vector (2.12). To provide some commonality between the optimal and threshold receiver simulations, however, the observations are generated in absolute-amplitude form. The full model is as follows:

$$x(k+1) = Fx(k) \quad , \quad x(0) = x_0 \quad (5.1)$$

$$v(k) = h_v(x(k), \sigma, n(k)) \quad (5.2)$$

where x_0 = the initial state at the start of the simulation.

$F =$ the matrix (2.13) except T_k is a selected constant in the simulation (1/13.5 sec. for AZ, 1/40.5 sec. for EL).

$\sigma =$ rms value of receiver noise at a point in the I-F channel having the same signal amplitude as the demodulator output. The parameter σ is assumed known, being a receiver characteristic.

$h_v(\) =$ a matrix-valued function of its arguments which compiles the J-vector $v(k)$ as one with representative element $v_j(k)$, $j=1, \dots, J$,

where

$$v_j(k) = \sigma \sqrt{2u_j}$$

and u_j is as given in (2.2).

All other quantities are as previously defined. The components of x_0 are specified either in program DATA statements or read in at run time.

The quantity β_j , (3.3) is reduced to its principal value on $(-\Pi, \Pi)$ after each change.

Signal data samples are generated only during sampling windows of $J/2$ samples each, located in the T0 and FRO scans respectively, and centered where the centroid of the received signal pulses are expected. For all runs to date

$$J = 130 \tag{5.3}$$

corresponding (at the sampling rate of 160 kHz) to window widths of 8° in each semi-scan.

B. The Optimal Receiver Simulation

The optimal receiver simulation consists basically of the following:

- i. Extrapolation of \hat{x} to the present, via (4.9).
- ii. Scan data processor calculations of Λ , via (3.20), and Φ , via (3.27).
- iii. Kalman filter calculations as follows:
 - (a) $P(k|k-1)$, via (4.10)
 - (b) Gain matrix, $M(k)$, via (4.19)
 - (c) $\hat{x}(k|k)$, via (4.20)
 - (d) $P(k|k)$, via (4.22)

The scan data processor calculations begin with a computation of the squared amplitude observations vector u component-wise as follows:

$$u_j = \frac{v_j^2}{2\sigma^2}$$

In the subsequent calculations the following models for the antenna selectivity function, $p(\theta)$, and its derivative $\dot{p}(\theta)$ were used:

$$p(\theta) = \begin{cases} \frac{\pi}{4}, & \theta = B/2.4 \\ \frac{\cos(1.2)\pi\theta/B}{1-(2.4\theta/B)^2}, & \text{elsewhere} \end{cases} \quad (5.5)$$

and

$$\dot{p}(\theta) = \begin{cases} -\frac{0.3\pi}{B} \text{Signum}(\theta), & \theta = B/2.4 \\ \frac{0.3\pi^2}{B} \left[\frac{\cos \frac{\pi}{2}(Z+1) - \frac{\sin \frac{\pi}{2}(Z+1)}{\frac{\pi}{2}(Z+1)}}{\frac{\pi}{2}(Z+1)} \right. \\ \left. + \frac{\cos \frac{\pi}{2}(Z-1) - \frac{\sin \frac{\pi}{2}(Z-1)}{\frac{\pi}{2}(Z-1)}}{\frac{\pi}{2}(Z-1)} \right], & \text{elsewhere} \end{cases} \quad (5.6)$$

$Z = \frac{2.4\theta}{B}$

in which B, the -3db beam width in degrees, was given the value of 1 degree.

In the Kalman filter calculations the diagonal elements of the diagonal matrix Q were given values as follows:

$$Q_{11} = Q_{33} = \max [0.25, 0.01\hat{\alpha}^2(k)] \quad (5.7)$$

where $\hat{\alpha}$ is the estimated direct path signal-to-noise ratio, thus giving some adaptation on the basis of 10% uncertainty in $\alpha(k+1)$, given $\alpha(k)$ (for $\alpha(k) > 5$).

$$Q_{22} = Q_{44} = |\ddot{\theta}_{\max}|^2 T, \quad (5.8)$$

where T is the interscan interval. All runs to date were made with the AZ receiver simulation, and, based on a prior study of representative landing patterns [3,p.40], a value of $|\ddot{\theta}_{\max}| = 0.1^\circ \text{sec}^2$ was used.

$$Q_{55} = 0.04/T^2 \quad (5.9)$$

corresponding to a mean-square uncertainty in $\omega_{sc}(k+1)$, given $\omega_{sc}(k)$, no greater than that which would cause an interscan extrapolation error in $\hat{\beta}$ of about 10° while tracking.

The optimal receiver simulation is programmed with maximum dimensions of 8 and 5 for the vectors x and γ respectively (and all associated matrices). The actual dimensions used in the calculations however are parameterized with the integer variables NS and NG respectively. When NS=8 and NG=5, the optimal multipath-adaptive receiver, which has been described, obtains; when NS=3, NG=2, a lesser dimensional model of the same basic structure results for which

$$x = (\alpha, \theta, \dot{\theta})^T \quad (5.10)$$

$$\gamma = (\alpha, \theta)^T \quad (5.11)$$

corresponding to an optimal receiver design predicated on the assumption of a multipath-free environment. Clearly, in the current work this latter design is a suboptimal one, nevertheless it served as a comparison standard in this work and is referred to as the suboptimal design or the nonadaptive design.

C. The Threshold Receiver

The threshold receiver simulation first computes the log-amplitude envelope observations signal, v_{\log} , component-wise as follows:

$$v_{\log_j} = 20 \log_{10} (1 + Av_j) \quad (5.12)$$

where $A = 100$, corresponding to 40 db of logging action. The result is then filtered by a 25 kHz bandwidth low pass digital filter with transfer function

$$H_{25}(z) = \frac{0.34831(1 + z^{-1})}{1 - 0.30336z^{-1}} \quad (5.13)$$

The signal that results is then passed to the thresholding and interference-rejection logic that characterizes the standard phase III MLS angle receiver design. This is described as follows:

1. On each the TO- and FRO-semi-scans the signal peak within the tracking gate (located as described below) is determined and a threshold level 3db below the peak established.
2. Dwell gates are defined for those intervals during which the log video signal exceeds the thresholds. The tracking gate for the next TO-scan will be symmetrically located about the expected dwell gate centroid position with a duration of 1.5 times the present TO-scan dwell gate duration; similarly for the FRO-scan.
3. Dwell gates less than 15 μ s or greater than 350 μ s cause the scan

to be aborted and the prior estimate of θ to be used again.

4. When the dwell gates are acceptable, the interval from the center of the TO dwell gate to that of the FRO dwell gate is determined, quantized to $0.5\mu\text{sec}$, and used to calculate the new estimate $\hat{\theta}$, which is output.

The threshold receiver simulation was programmed to be interchangeable with the optimal receiver simulation as far as the main simulation program (and sampling window positioning) is concerned. Performance evaluation, however, was based on the angle estimate error filtered as follows:

$$\underline{\text{AZ:}} \quad H(z) = \frac{0.5}{1 - 0.5z^{-1}} \quad (5.14)$$

$$\underline{\text{EL:}} \quad H(z) = \frac{0.25}{1 - 0.75z^{-1}} \quad (5.15)$$

corresponding to available evaluation data. In this respect, however, the simulated threshold receiver is more like the phase II model than the phase III model (which apparently uses an α - β filtered error for performance evaluation).

Simulation Runs and Results

Four key parameters important to the performance of an MLS receiver are the following:

$$S/N \triangleq \text{Direct-path signal-to-noise ratio (denoted DSNRDB in the simulation), (db).} \quad (5.16)$$

$$\rho \triangleq \text{Multipath-to-direct path signal amplitude ratio} \quad (5.17)$$

$$F_{sc} = \text{scalloping frequency (Hertz)} \quad (5.18)$$

$$\theta_{sep} = \theta - \theta_R, \text{ the separation angle of the multipath interference} \quad (5.19)$$

The MLS receivers are expected to operate with S/N ratios of 8 db or higher; values in the range 8 to 20 db were used in the simulation study.

A recent MIT study of multipath interference at air terminal areas [5] shows relative multipath amplitudes, ρ , to 1.0 or more and scalloping frequencies, F_{sc} , to 1300 Hz. Representative values are as follows:

$$\begin{aligned} \rho &= 0.9, F_{sc} = 2,22,51 \text{ Hz} \\ \rho &= 0.8, F_{sc} = 63,81,130 \text{ Hz} \\ \rho &= 0.5, F_{sc} = 381 \text{ Hz} \end{aligned} \tag{5.20}$$

Values spanning these ranges of ρ , F_{sc} were used in the study. Separation angles, θ_{sep} , corresponding to both in-beam and out-of-beam multipath were considered.

A fifth parameter, β , the r-f phase difference initial values (at the start of the simulation run) also affected results somewhat. Its effect is studied some and its value is always noted.

A. Crossing Multipath Studies

This scenario begins with

$$\begin{aligned} \theta_{sep} &= - 2.75^\circ \text{ (AZ)} \\ \frac{d\theta_{sep}}{dt} &= + 0.7^\circ/\text{sec constant} \end{aligned} \tag{5.21}$$

and runs for 100 scans (approx. 7.4 sec). Forty runs each for the threshold, optimal and suboptimal receivers were made in this series, corresponding to various values of key parameters S/N, ρ , and F_{sc} . In all runs the receivers were initialized in the track mode, i.e. all estimated variables produced by each receiver were initialized to true values. Figures 1 thru 10 show comparative results of selected runs for the optimal and threshold receivers; Fig. 1 presents time histories of error for S/N = 14 db, no multipath; note the two plots are made to the same scale for easy comparison. Fig. 2 is the same, but with heavy multipath interference, $\rho=0.8$, $F_{sc} = 51.3$ Hz. (This scalloping rate and the associated value of β , $- 168^\circ$, produces maximum enhancement

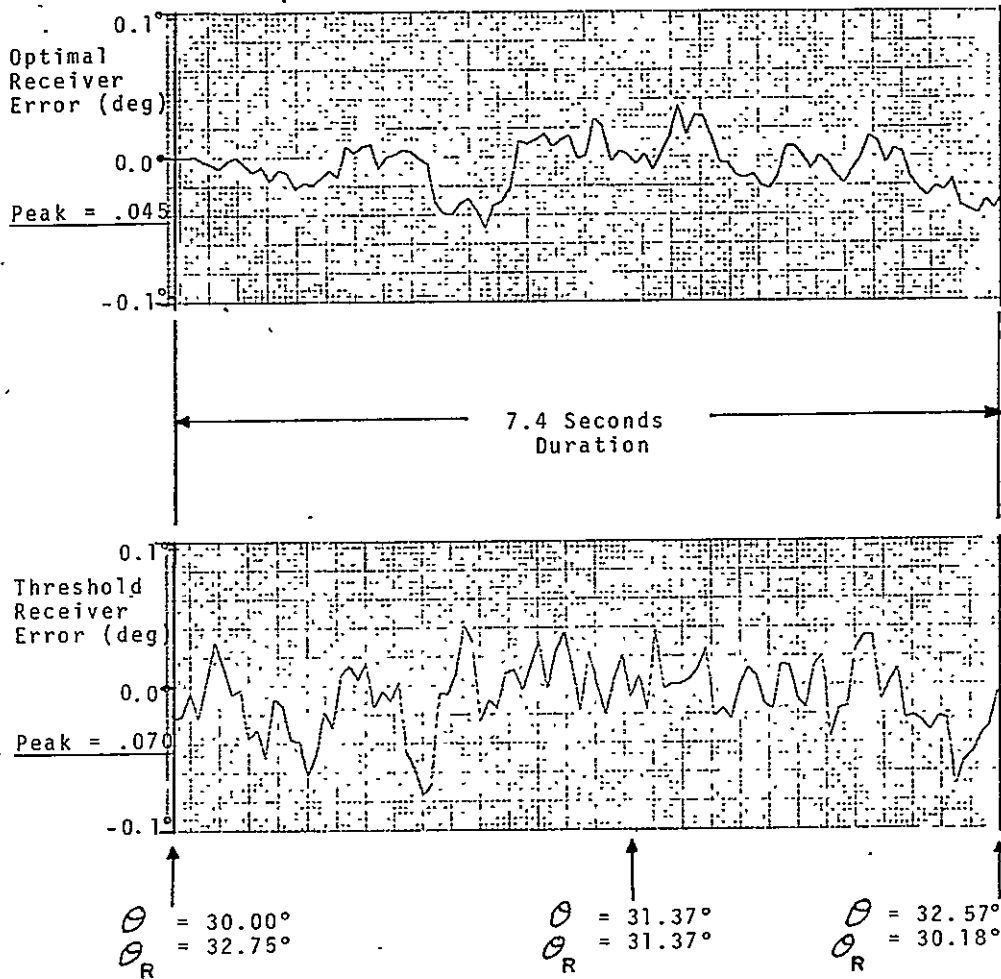


Figure 1. Receiver Error Time Histories, Crossing Multipath Simulation, No Multipath (reference) case.

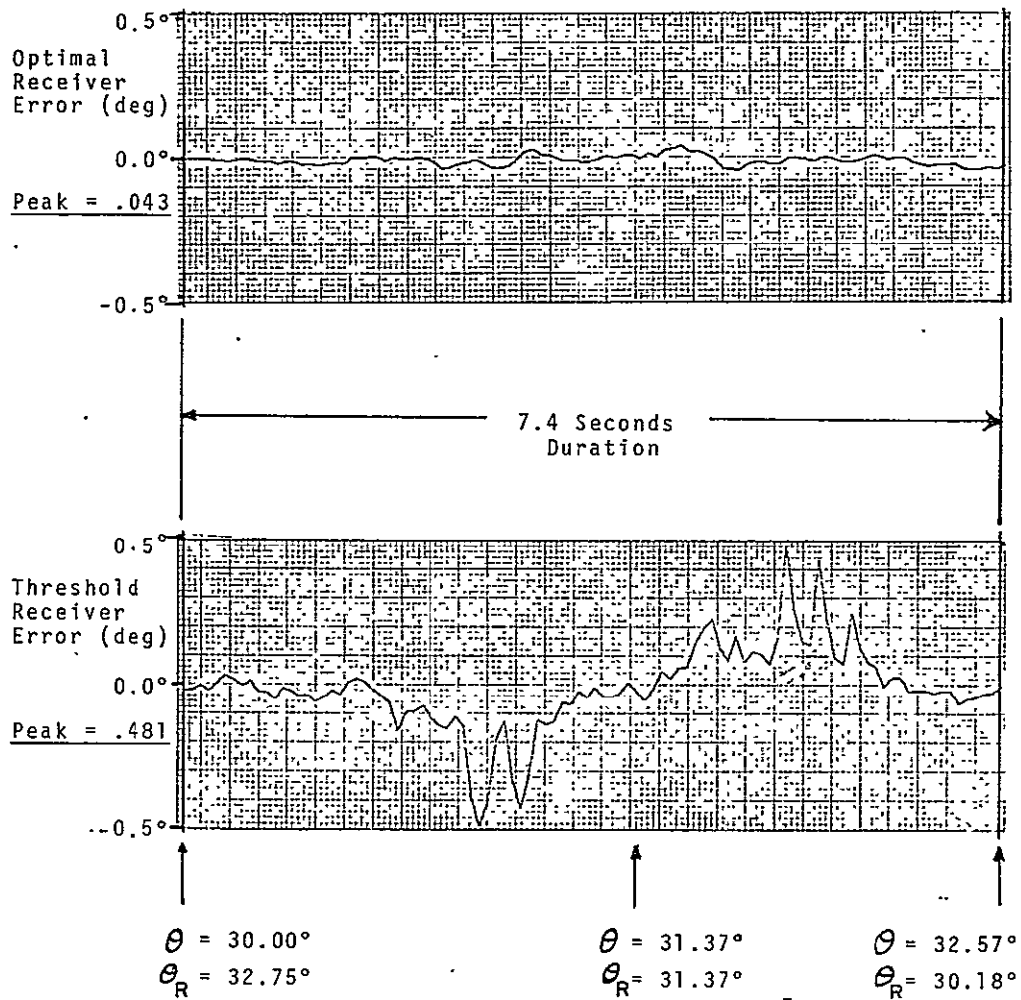


Figure 2. Receiver Error Time Histories, Crossing Multipath Simulation, $S/N = 14$ db, $\rho = .8$, $F_{sc} = 51.3$ Hz., $\beta = -168.0^\circ$.

by the multipath on the TO scan and maximum cancellation on the FRO scan as the separation angle traverses zero). Figures 3, 4 and 5 summarize for $F_{sc} = 5, 51.3$ and 500 Hz, respectively, comparative studies of peak absolute error versus S/N and ρ . Figures 6, 7, 8 and 9 present time histories of error for runs corresponding to selected points in Figure 3, 4 and 5 representing both moderate and heavy multipath interference. The high ratios of improvement provided by the optimal receivers are especially noteworthy -- typically about 20:1 for the $\rho=0.8$ cases. Figure 10 shows, for the $S/N = 20$ db, $\rho=0.8$ cases, only optimal receiver results, plotted with enlarged scales to show more clearly the sample functions of the error process, which appears to be more random than that of the threshold receiver (See Figures 6, 7 and 8).

Tables 1, 2, 3, and 4 summarize all the crossing multipath studies. Table 1 presents a comparison of the 3 receivers, optimal, threshold and sub-optimal (or non-adaptive), in terms of peak-absolute-error. Tables 2, 3 and 4 each summarize the performance of respectively one receiver in terms of several error measures computed over the set of 100 scans per run for each case.

The crossing multipath scenario represents a strenuous test of the tracking capabilities of a receiver algorithm. Conclusions drawn are as follows:

1. The optimal receiver generally outperformed the threshold receiver, sometimes by a wide margin.
2. The optimal receiver is algorithmically much more complex than the threshold receiver.

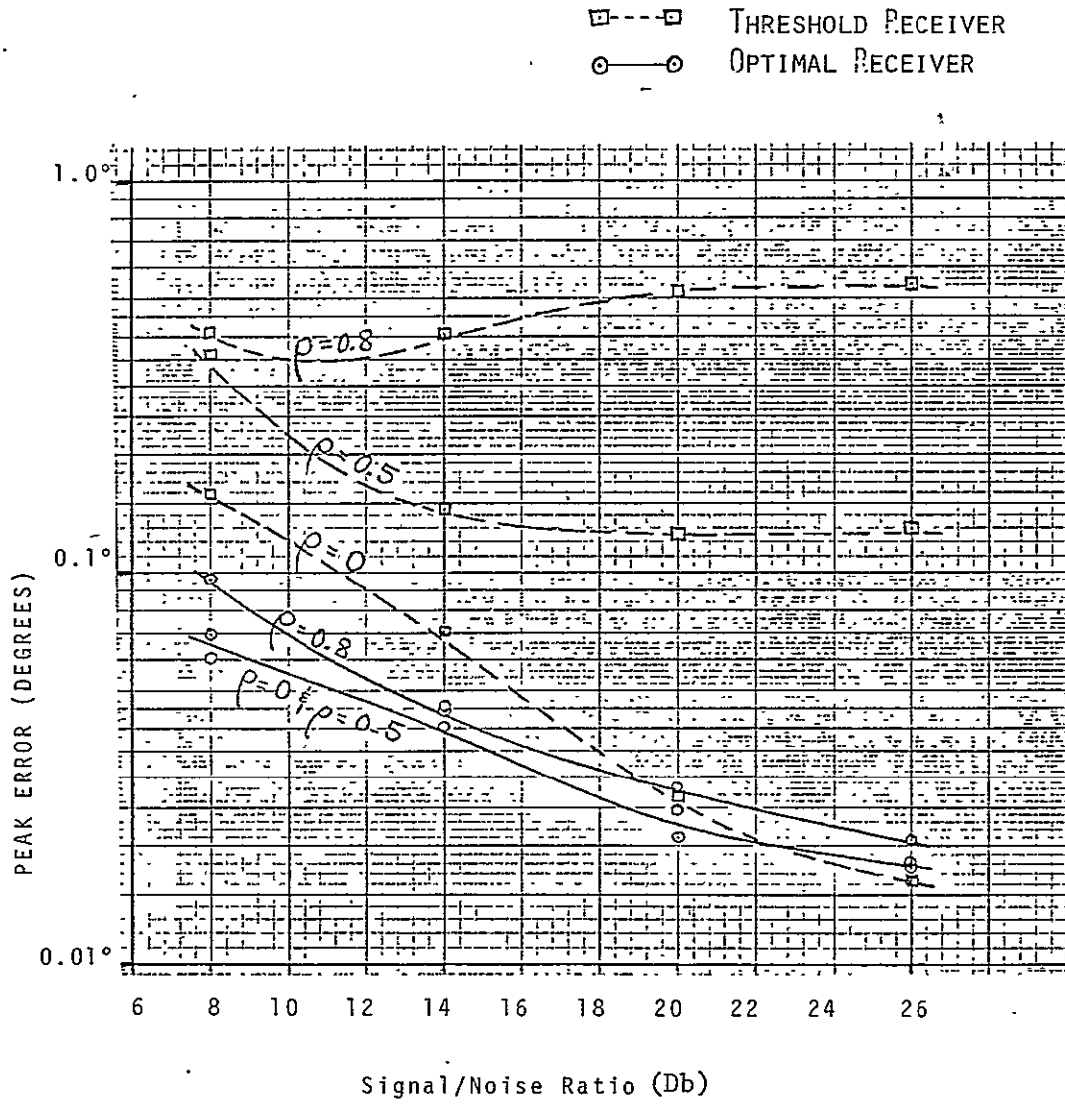


Figure 3. Summary of Crossing Multipath Simulation Results for $F_{sc} = 5$ Hz., $\beta = 0^\circ$.

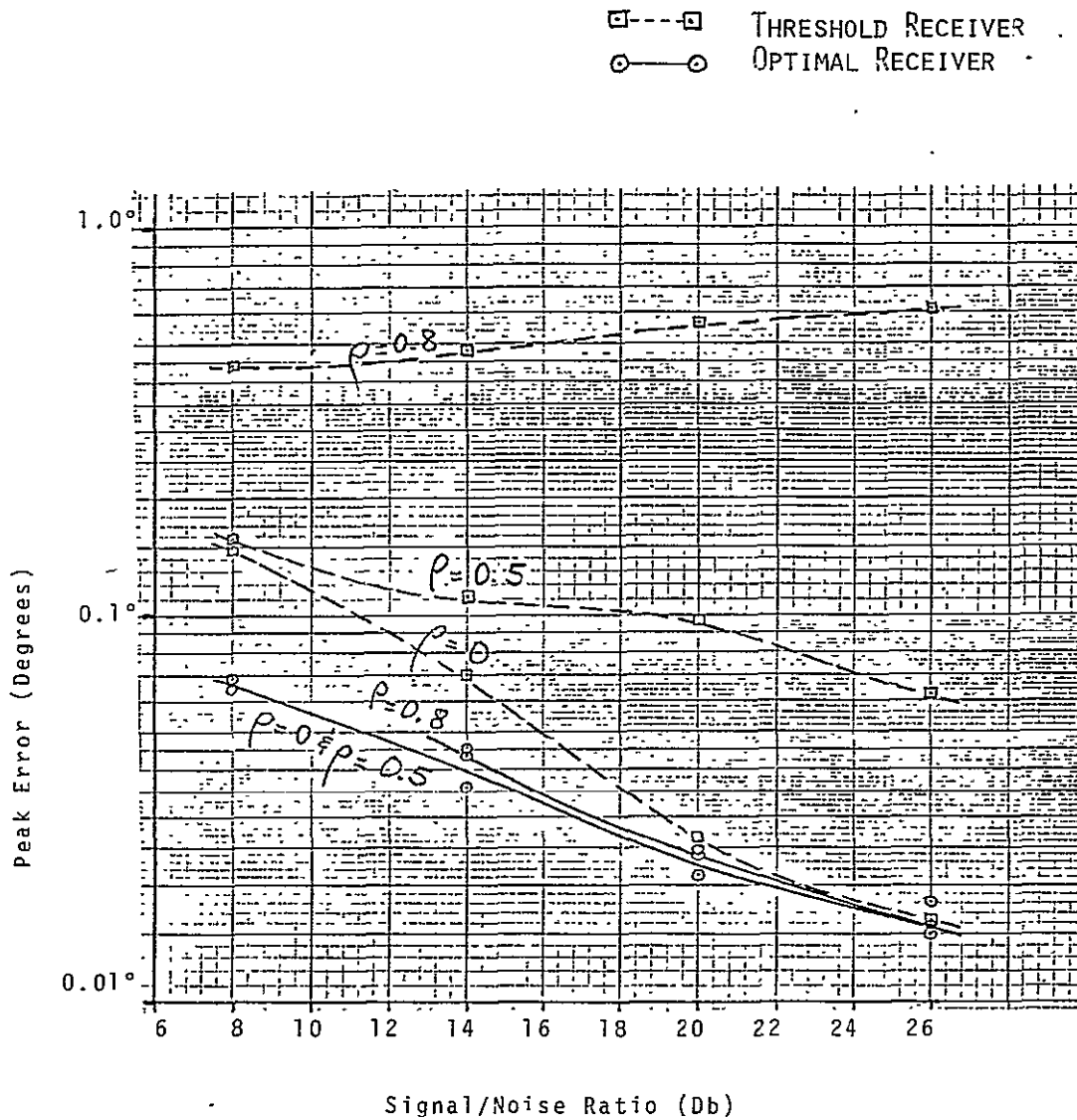


Figure 4. Summary of Crossing Multipath Simulation Results for $F_{sc} = 51.3 \text{ Hz.}$, $\beta = -168^\circ$.

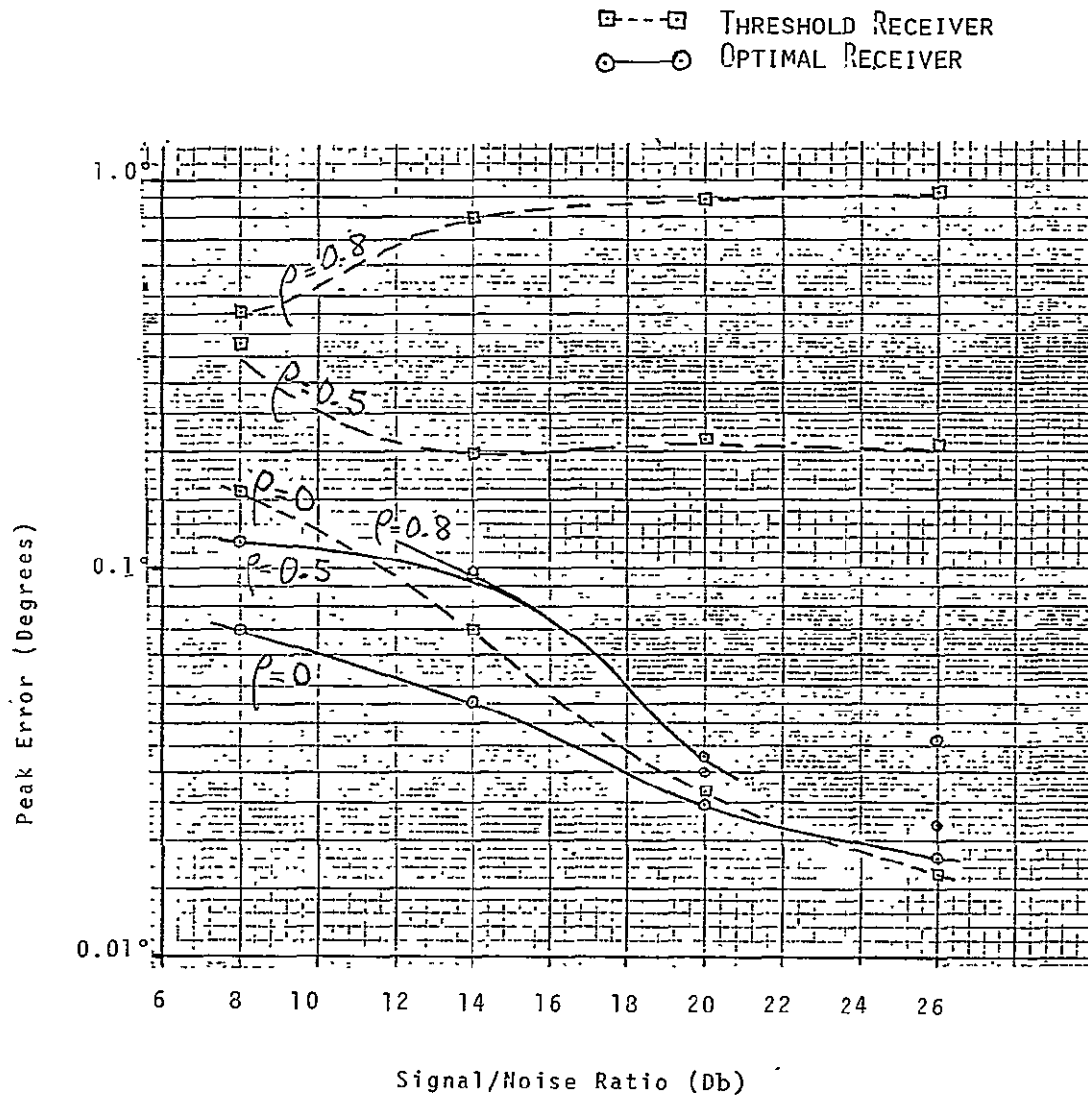


Figure 5. Summary of Crossing Multipath Simulation Results for $F_{sc} = 500$ Hz., $\beta = 180^\circ$.

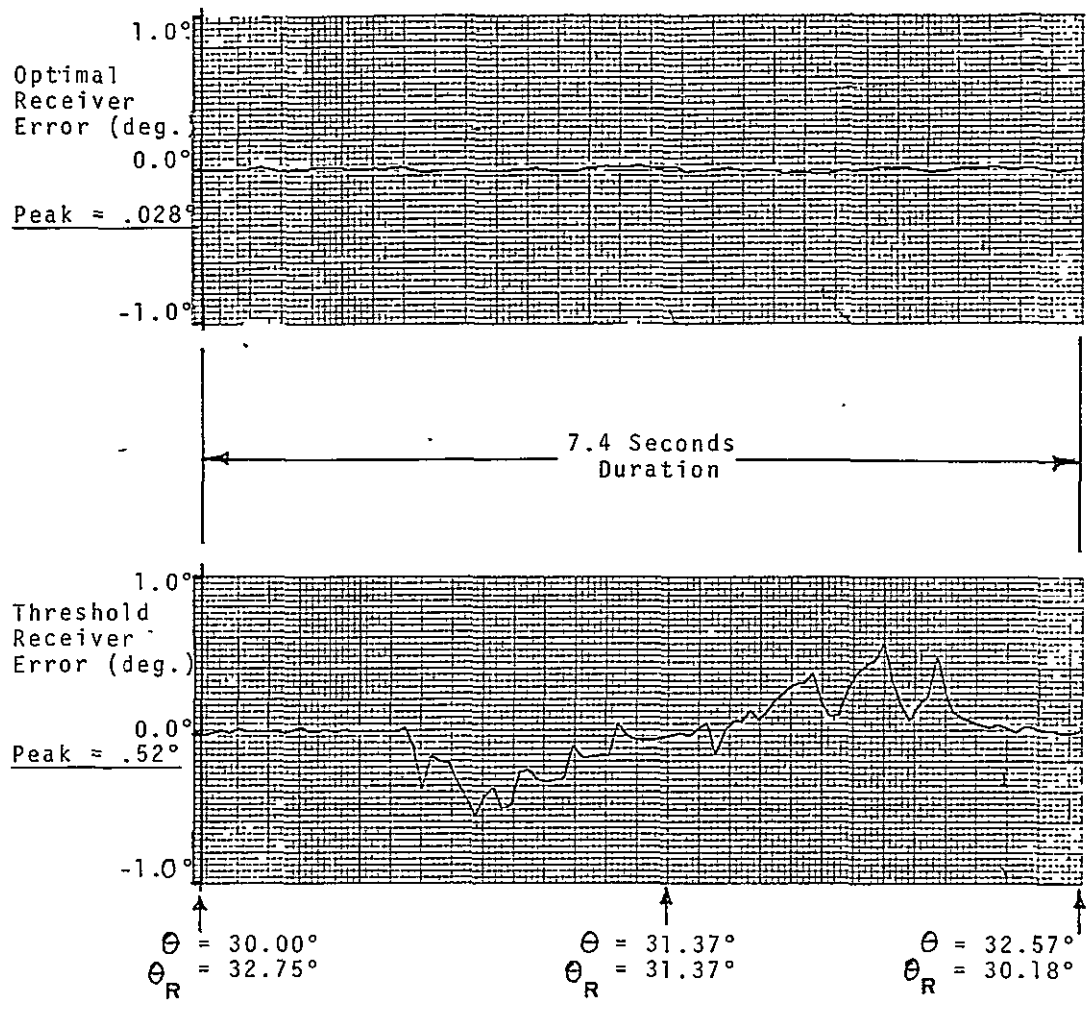


Figure 6. Receiver Error time Histories, Crossing Multipath Simulation, $S/N = 20$ db, $\rho = .8$, $F_{sc} = 5.0$ Hz., $\beta = 0.0^\circ$

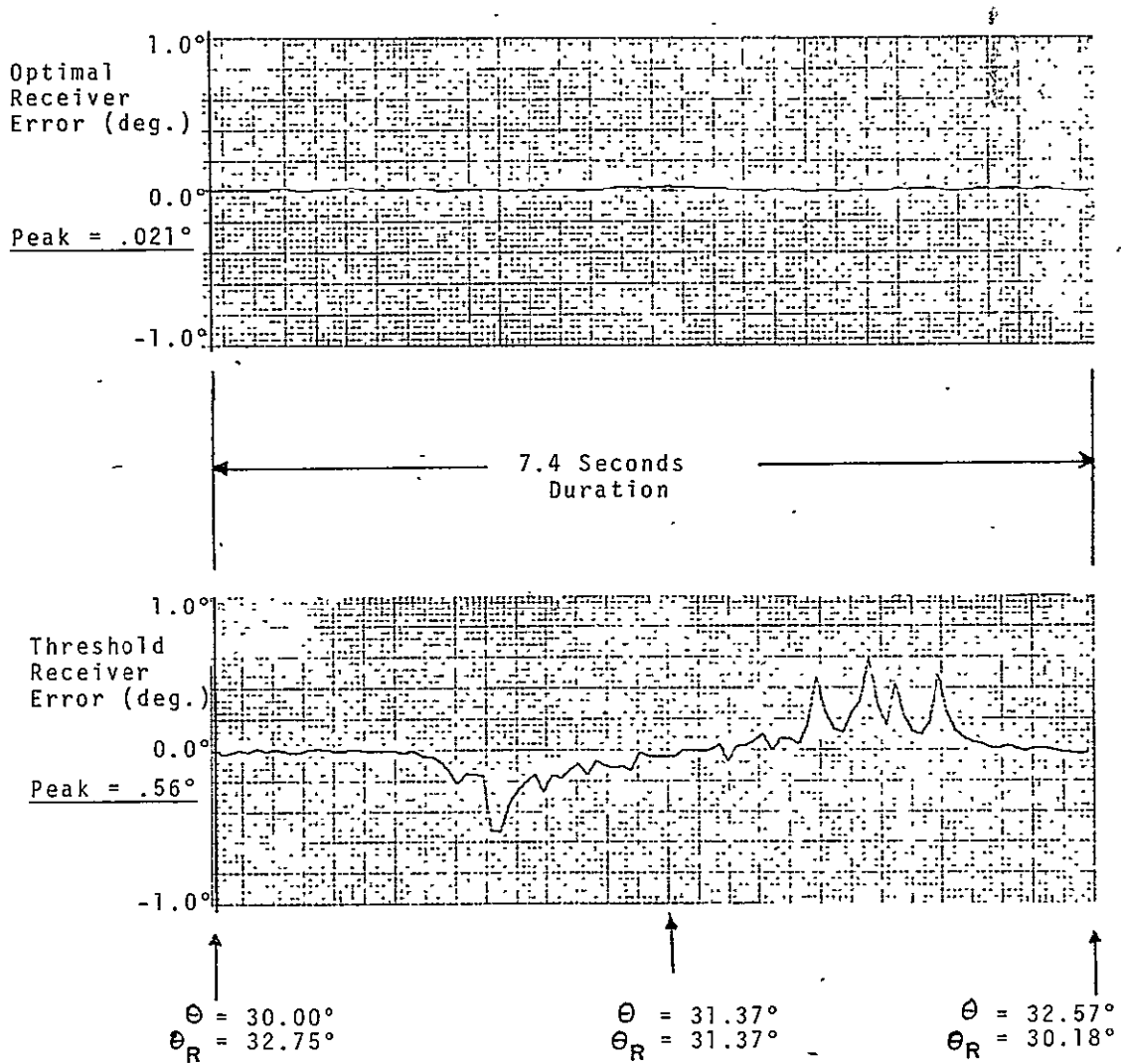


Figure 7. Receiver Error Time Histories, Crossing Multipath
 Simulation, S/N = 20 db, $\rho = .8$, $F_{sc} = 51.3$ Hz., $\beta = -168.0^\circ$

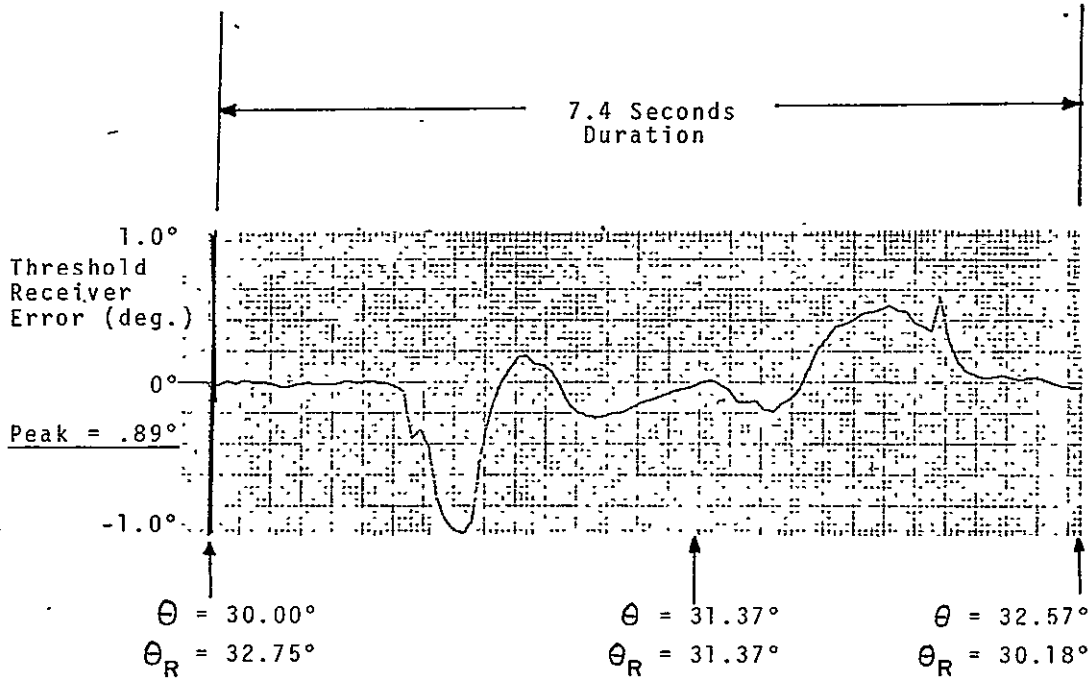
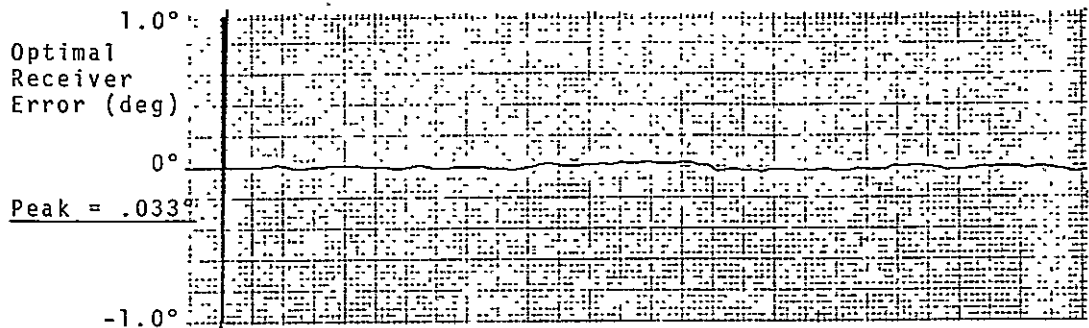


Figure 8. Receiver Error Time Histories, Crossing Multipath
 Simulation, S/N = 20 db, $\rho = .8$, $F_{sc} = 500.0$ Hz., $\beta = 180.0^\circ$.

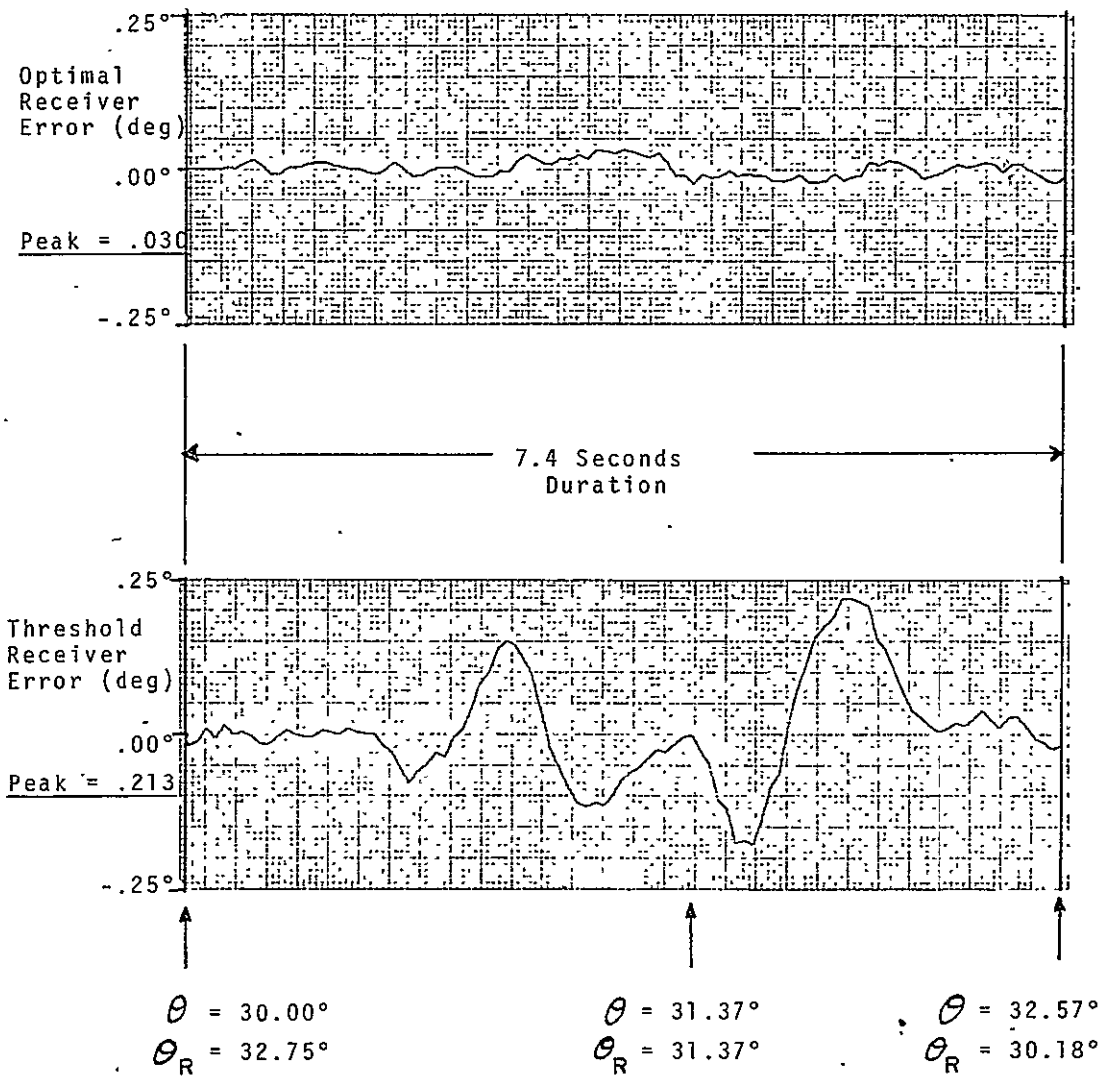


Figure 9. Receiver Error Time Histories, Crossing Multipath
 Simulation, $S/N = 20$ db, $\rho = .5$, $F_{sc} = 500.0$ Hz., $\beta = 180.0^\circ$

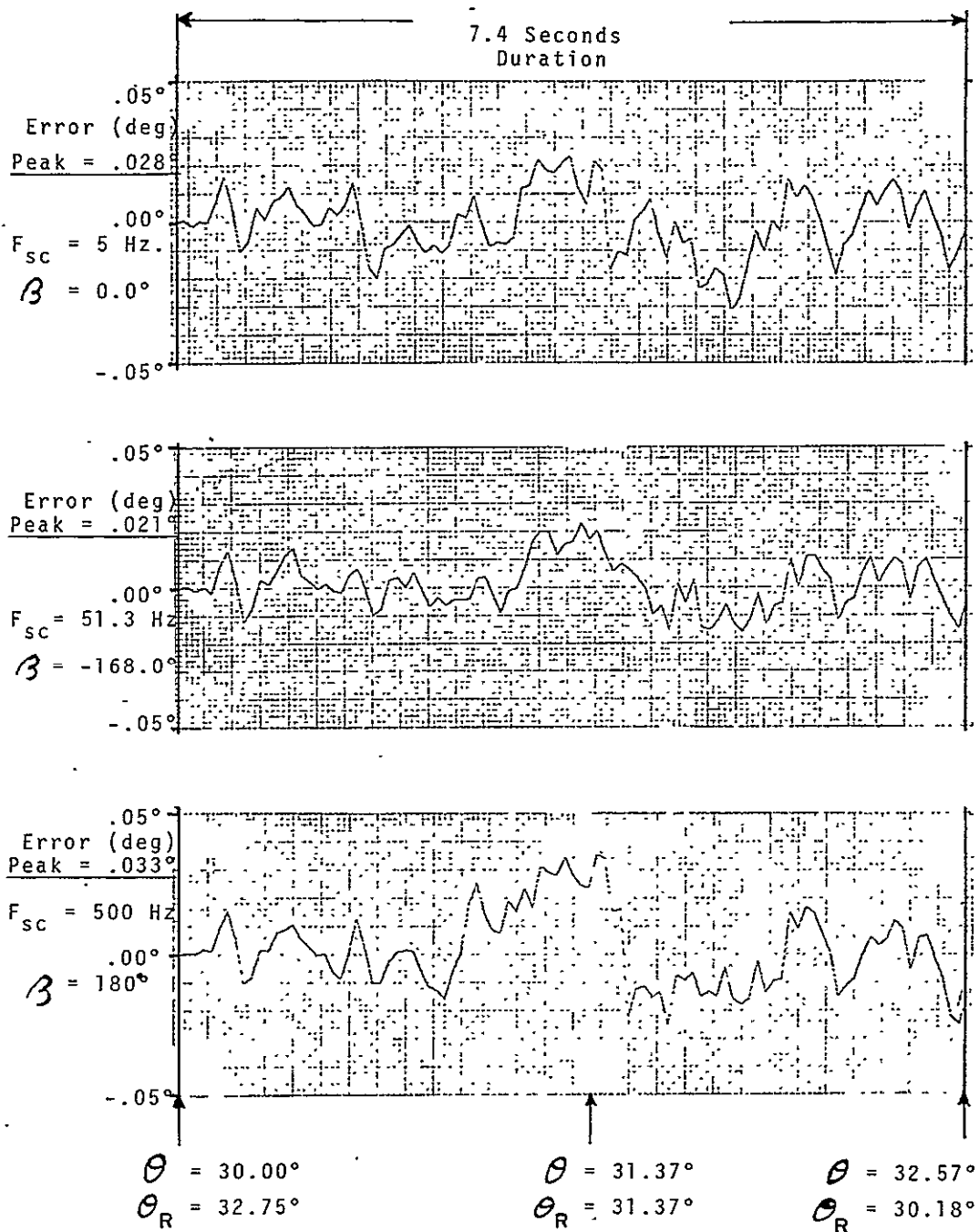


Figure 10. Optimal Receiver Error Time Histories, Crossing Multipath Simulation, $S/N = 20 \text{ db}$, $\rho = 0.8$.

COMPARISON OF PEAK-ABSOLUTE-ERROR PERFORMANCE
FOR OPTIMAL, THRESHOLD & NON-ADAPTIVE MFS RECEIVERS

NRUN	DSNRDB	RHO	FSC	BETA	OPT RCVR	THRESHOLD	NON-ADAPT.	NRUN
1	20.0	0.80	500.0	-180.0	0.03272	0.89128	0.52575	1
2	20.0	0.80	500.0	-150.0	0.03074	0.75318	0.47096	2
3	20.0	0.80	500.0	-120.0	0.02720	0.47984	0.44490	3
4	20.0	0.80	500.0	-90.0	0.02715	0.40911	0.41781	4
5	20.0	0.80	500.0	-60.0	0.04362	0.37478	0.41174	5
6	20.0	0.80	500.0	-30.0	0.03516	0.37707	0.44284	6
7	20.0	0.80	500.0	0.0	0.05699	0.44524	0.46339	7
8	20.0	0.80	500.0	30.0	0.03367	0.44057	0.50667	8
9	20.0	0.80	500.0	60.0	0.04565	0.54822	0.51262	9
10	20.0	0.80	500.0	90.0	0.04443	0.60415	0.52711	10
11	20.0	0.80	500.0	120.0	0.03097	0.74053	0.54248	11
12	20.0	0.80	500.0	150.0	0.03708	0.80374	0.51792	12
13	8.0	0.00	0.0	0.0	0.06981	0.15672	0.05538	13
14	14.0	0.00	0.0	0.0	0.04557	0.07016	0.03748	14
15	20.0	0.00	0.0	0.0	0.02473	0.02655	0.01892	15
16	26.0	0.00	0.0	0.0	0.01813	0.01619	0.01021	16
17	8.0	0.50	5.0	0.0	0.06054	0.35890	0.17831	17
18	14.0	0.50	5.0	0.0	0.04065	0.14388	0.16824	18
19	20.0	0.50	5.0	0.0	0.02188	0.12499	0.16479	19
20	26.0	0.50	5.0	0.0	0.01756	0.12927	0.16535	20
21	8.0	0.80	5.0	0.0	0.09599	0.41537	0.37735	21
22	14.0	0.80	5.0	0.0	0.04413	0.40627	0.38814	22
23	20.0	0.80	5.0	0.0	0.02802	0.57193	0.35944	23
24	26.0	0.80	5.0	0.0	0.02069	0.54139	0.37256	24
25	8.0	0.50	51.3	-168.0	0.06429	0.14716	0.16951	25
26	14.0	0.50	51.3	-168.0	0.03600	0.11148	0.15234	26
27	20.0	0.50	51.3	-168.0	0.02379	0.09691	0.13425	27
28	26.0	0.50	51.3	-168.0	0.01496	0.06221	0.11955	28
29	8.0	0.80	51.3	-168.0	2.35204	0.43984	0.38284	29
30	14.0	0.80	51.3	-168.0	0.04350	0.48091	0.38693	30
31	20.0	0.80	51.3	-168.0	0.02112	0.56204	0.34870	31
32	26.0	0.80	51.3	-168.0	0.01603	0.61010	0.34102	32
33	8.0	0.50	500.0	180.0	0.11694	0.37920	0.27490	33
34	14.0	0.50	500.0	180.0	0.09875	0.19877	0.26974	34
35	20.0	0.50	500.0	180.0	0.02992	0.21320	0.28787	35
36	26.0	0.50	500.0	180.0	0.03611	0.20749	0.27048	36
37	8.0	0.80	500.0	180.0	2.38019	0.45202	0.53748	37
38	14.0	0.80	500.0	180.0	0.09727	0.79227	0.49249	38
39	20.0	0.80	500.0	180.0	0.03272	0.89128	0.52575	39
40	26.0	0.80	500.0	180.0	0.02180	0.92404	0.49073	40
STOP								

Table 1. Performance Comparisons of the Optimal, Threshold and Non-adaptive Receivers; Crossing Multipath Scenarios.

ORIGINAL PAGE IS
OF POOR QUALITY

OPTIMAL RECEIVER ERROR PERFORMANCE										
RUN	DSNRDB	RHO	FSC	BETA	PK AD ER	MEAN ERR	RMS ERR	ER ST DV	NRUN	
1	20.0	0.80	500.0	-180.0	0.03272	0.00188	0.01293	0.01279	1	
2	20.0	0.80	500.0	-150.0	0.03074	-0.00374	0.01141	0.01078	2	
3	20.0	0.80	500.0	-120.0	0.25720	-0.00616	0.04131	0.04085	3	
4	20.0	0.80	500.0	-90.0	0.02715	-0.00439	0.01189	0.01105	4	
5	20.0	0.80	500.0	-60.0	0.04362	-0.00106	0.01335	0.01231	5	
6	20.0	0.80	500.0	-30.0	0.03516	-0.00184	0.01164	0.01149	6	
7	20.0	0.80	500.0	0.0	0.05699	-0.00330	0.01445	0.01407	7	
8	20.0	0.80	500.0	30.0	0.03367	-0.00035	0.01222	0.01222	8	
9	20.0	0.80	500.0	60.0	0.04565	-0.00024	0.01217	0.01216	9	
10	20.0	0.80	500.0	90.0	0.04443	0.00218	0.01278	0.01259	10	
11	20.0	0.80	500.0	120.0	0.03097	-0.00112	0.01185	0.01180	11	
12	20.0	0.80	500.0	150.0	0.03708	0.00087	0.01377	0.01375	12	
13	8.0	0.00	0.0	0.0	0.06981	-0.00684	0.02845	0.02762	13	
14	14.0	0.00	0.0	0.0	0.04557	-0.00557	0.01689	0.01595	14	
15	20.0	0.00	0.0	0.0	0.02473	-0.00113	0.00933	0.00926	15	
16	26.0	0.00	0.0	0.0	0.01813	-0.00128	0.00635	0.00622	16	
17	8.0	0.50	5.0	0.0	0.06054	0.00020	0.02582	0.02582	17	
18	14.0	0.50	5.0	0.0	0.04065	-0.00419	0.01791	0.01742	18	
19	20.0	0.50	5.0	0.0	0.02188	0.00028	0.00901	0.00900	19	
20	26.0	0.50	5.0	0.0	0.01756	-0.00106	0.00614	0.00605	20	
21	8.0	0.80	5.0	0.0	0.09599	-0.00344	0.03248	0.03230	21	
22	14.0	0.80	5.0	0.0	0.04413	-0.00509	0.01648	0.01567	22	
23	20.0	0.80	5.0	0.0	0.02802	-0.00023	0.01030	0.01030	23	
24	26.0	0.80	5.0	0.0	0.02069	-0.00121	0.00633	0.00621	24	
25	8.0	0.50	51.3	-168.0	0.06429	0.00001	0.02391	0.02391	25	
26	14.0	0.50	51.3	-168.0	0.03600	-0.00543	0.01532	0.01433	26	
27	20.0	0.50	51.3	-168.0	0.02379	0.00066	0.00863	0.00861	27	
28	26.0	0.50	51.3	-168.0	0.01496	-0.00139	0.00499	0.00480	28	
29	8.0	0.80	51.3	-168.0	2.35204*****	LOST TRACK*****				
30	14.0	0.80	51.3	-168.0	0.04350	-0.00474	0.01667	0.01598	30	
31	20.0	0.80	51.3	-168.0	0.02112	0.00099	0.00821	0.00815	31	
32	26.0	0.80	51.3	-168.0	0.01603	-0.00096	0.00587	0.00549	32	
33	8.0	0.50	500.0	180.0	0.11694	-0.00312	0.04637	0.04627	33	
34	14.0	0.50	500.0	180.0	0.09875	-0.01269	0.02422	0.02063	34	
35	20.0	0.50	500.0	180.0	0.02992	0.00066	0.01237	0.01236	35	
36	26.0	0.50	500.0	180.0	0.03611	-0.00255	0.00807	0.00766	36	
37	8.0	0.80	500.0	180.0	2.38019*****	LOST TRACK*****				
38	14.0	0.80	500.0	180.0	0.09727	-0.00998	0.02571	0.02370	38	
39	20.0	0.80	500.0	180.0	0.03272	0.00188	0.01293	0.01279	39	
40	26.0	0.80	500.0	180.0	0.02180	-0.00179	0.00658	0.00634	40	
STOP										

Table 2. Optimal Receiver Error Performance;
Crossing Multipath Scenarios.

THRESHOLD RECEIVER ERROR PERFORMANCE										
RUN	DSNRDB	RHO	FSC	BETA	PK AN ER	MEAN ERR	RMS CRR	ER SI DV	NRUN	
1	20.0	0.80	500.0	-180.0	0.89128	-0.00990	0.20795	0.25776	1	
2	20.0	0.80	500.0	-150.0	0.75318	-0.00188	0.20507	0.20506	2	
3	20.0	0.80	500.0	-120.0	0.47984	0.02712	0.16613	0.16390	3	
4	20.0	0.80	500.0	-90.0	0.40911	0.00716	0.15240	0.15224	4	
5	20.0	0.80	500.0	-60.0	0.37478	0.00729	0.15888	0.15871	5	
6	20.0	0.80	500.0	-30.0	0.37707	0.00112	0.15581	0.15580	6	
7	20.0	0.80	500.0	0.0	0.44524	-0.01031	0.16421	0.16388	7	
8	20.0	0.80	500.0	30.0	0.44057	-0.02538	0.16048	0.15846	8	
9	20.0	0.80	500.0	60.0	0.54822	-0.02498	0.19843	0.19686	9	
10	20.0	0.80	500.0	90.0	0.60415	-0.05196	0.23655	0.22983	10	
11	20.0	0.80	500.0	120.0	0.74053	-0.01257	0.27644	0.27140	11	
12	20.0	0.80	500.0	150.0	0.80374	-0.02568	0.26999	0.26876	12	
13	8.0	0.00	0.0	0.0	0.15672	-0.00416	0.05312	0.05295	13	
14	14.0	0.00	0.0	0.0	0.07016	-0.00680	0.02463	0.02368	14	
15	20.0	0.00	0.0	0.0	0.02655	0.00009	0.01056	0.01056	15	
16	26.0	0.00	0.0	0.0	0.01619	-0.00230	0.00635	0.00592	16	
17	8.0	0.50	5.0	0.0	0.35890	0.00019	0.08461	0.08461	17	
18	14.0	0.50	5.0	0.0	0.14388	-0.00385	0.04818	0.04802	18	
19	20.0	0.50	5.0	0.0	0.12499	-0.00125	0.04315	0.04313	19	
20	26.0	0.50	5.0	0.0	0.12927	-0.00142	0.04301	0.04299	20	
21	8.0	0.80	5.0	0.0	0.41537	0.02204	0.10813	0.10586	21	
22	14.0	0.80	5.0	0.0	0.40627	-0.02241	0.12229	0.12022	22	
23	20.0	0.80	5.0	0.0	0.52193	-0.00226	0.18854	0.18852	23	
24	26.0	0.80	5.0	0.0	0.54139	-0.01188	0.20017	0.19981	24	
25	8.0	0.50	51.3	-168.0	0.14716	0.01853	0.06355	0.06079	25	
26	14.0	0.50	51.3	-168.0	0.11148	-0.00493	0.03668	0.03634	26	
27	20.0	0.50	51.3	-168.0	0.09691	0.00016	0.03077	0.03077	27	
28	26.0	0.50	51.3	-168.0	0.06221	-0.00148	0.02930	0.02926	28	
29	8.0	0.80	51.3	-168.0	0.43984	0.03806	0.12373	0.11773	29	
30	14.0	0.80	51.3	-168.0	0.48091	-0.01119	0.13931	0.13886	30	
31	20.0	0.80	51.3	-168.0	0.56204	0.01236	0.15342	0.15292	31	
32	26.0	0.80	51.3	-168.0	0.61010	-0.01379	0.18963	0.18913	32	
33	8.0	0.50	500.0	180.0	0.37920	0.00227	0.11241	0.11239	33	
34	14.0	0.50	500.0	180.0	0.19877	-0.00317	0.07561	0.07555	34	
35	20.0	0.50	500.0	180.0	0.21320	0.00570	0.08075	0.08055	35	
36	26.0	0.50	500.0	180.0	0.20749	0.00334	0.07812	0.07804	36	
37	8.0	0.80	500.0	180.0	0.45202	0.01674	0.12708	0.12598	37	
38	14.0	0.80	500.0	180.0	0.79227	-0.00454	0.22294	0.22289	38	
39	20.0	0.80	500.0	180.0	0.89128	-0.01001	0.25795	0.25776	39	
40	26.0	0.80	500.0	180.0	0.92404	-0.03378	0.29673	0.29480	40	
STOP										

Table 3. Threshold Receiver Error Performance;
Crossing Multipath Scenarios.

NON-ADAPTIVE RECEIVER ERROR PERFORMANCE

RUN	ISNRDD	RHO	FSC	BETA	PK AB ER	MEAN ERR	RMS ERR	CR ST IV	NRUN
1	20.0	0.80	500.0	-180.0	0.52575	0.01921	0.20634	0.20544	1
2	20.0	0.80	500.0	-150.0	0.47096	0.01963	0.18588	0.18485	2
3	20.0	0.80	500.0	-120.0	0.44490	0.02396	0.18211	0.18053	3
4	20.0	0.80	500.0	-90.0	0.41781	0.01490	0.17675	0.17612	4
5	20.0	0.80	500.0	-60.0	0.41174	0.01405	0.17726	0.17671	5
6	20.0	0.80	500.0	-30.0	0.44284	0.00198	0.17740	0.17739	6
7	20.0	0.80	500.0	0.0	0.46339	-0.00037	0.18007	0.18007	7
8	20.0	0.80	500.0	30.0	0.50667	-0.00033	0.18610	0.18591	8
9	20.0	0.80	500.0	60.0	0.51262	-0.00723	0.19588	0.19574	9
10	20.0	0.80	500.0	90.0	0.52711	-0.00810	0.21378	0.21363	10
11	20.0	0.80	500.0	120.0	0.54248	0.00084	0.23252	0.23252	11
12	20.0	0.80	500.0	150.0	0.51792	0.00222	0.23210	0.22209	12
13	8.0	0.00	0.0	0.0	0.05538	-0.00200	0.02483	0.02475	13
14	14.0	0.00	0.0	0.0	0.03748	-0.00610	0.01481	0.01350	14
15	20.0	0.00	0.0	0.0	0.01892	-0.00067	0.00777	0.00774	15
16	26.0	0.00	0.0	0.0	0.01021	-0.00149	0.00456	0.00431	16
17	8.0	0.50	5.0	0.0	0.17831	-0.00026	0.06822	0.06822	17
18	14.0	0.50	5.0	0.0	0.16824	-0.00691	0.06792	0.06756	18
19	20.0	0.50	5.0	0.0	0.16479	-0.00095	0.06713	0.06712	19
20	26.0	0.50	5.0	0.0	0.16535	-0.00229	0.06852	0.06848	20
21	8.0	0.80	5.0	0.0	0.37735	0.01436	0.19664	0.19611	21
22	14.0	0.80	5.0	0.0	0.38814	-0.00217	0.18959	0.18958	22
23	20.0	0.80	5.0	0.0	0.35944	0.00285	0.18331	0.18329	23
24	26.0	0.80	5.0	0.0	0.37256	-0.00091	0.17940	0.17940	24
25	8.0	0.50	51.3	-168.0	0.16951	-0.00012	0.07246	0.07246	25
26	14.0	0.50	51.3	-168.0	0.15234	-0.00692	0.06936	0.06901	26
27	20.0	0.50	51.3	-168.0	0.13425	-0.00066	0.06456	0.06456	27
28	26.0	0.50	51.3	-168.0	0.11955	-0.00209	0.06073	0.06069	28
29	8.0	0.80	51.3	-168.0	0.38284	0.01402	0.19630	0.19580	29
30	14.0	0.80	51.3	-168.0	0.38693	-0.00202	0.18968	0.18967	30
31	20.0	0.80	51.3	-168.0	0.34870	0.00246	0.17866	0.17864	31
32	26.0	0.80	51.3	-168.0	0.34102	-0.00143	0.16963	0.16963	32
33	8.0	0.50	500.0	180.0	0.27490	0.00814	0.09365	0.09330	33
34	14.0	0.50	500.0	180.0	0.26974	0.00014	0.09715	0.09715	34
35	20.0	0.50	500.0	180.0	0.28787	0.00538	0.10647	0.10634	35
36	26.0	0.50	500.0	180.0	0.27048	0.00234	0.10093	0.10090	36
37	8.0	0.80	500.0	180.0	0.53748	0.03641	0.21513	0.21203	37
38	14.0	0.80	500.0	180.0	0.49249	0.00937	0.20930	0.20909	38
39	20.0	0.80	500.0	180.0	0.52575	0.01921	0.20634	0.20544	39
40	26.0	0.80	500.0	180.0	0.49073	0.01601	0.19639	0.19574	40

STOP

Table 4. Non-adaptive Receiver Error Performance; Crossing Multipath Scenarios.

4. Generally the suboptimal (non-adaptive) receiver performed as well or better than the threshold receiver.
5. Generally the suboptimal design performs less well than the optimal design, though it was never observed to lose track.

It is felt that the optimal and suboptimal receivers represent, within this family of receiver structures, two extremes in use of any information in the received signal concerning the multipath interference -- both being generally superior to the threshold receiver. Further, it is felt that a carefully drawn design intermediate to these extremes can effect a substantial reduction in complexity at little loss in tracking performance with respect to the optimal design described. This, in part, is our recommendation for future work; the reader is referred to Section III for more details.

B. Time-Varying In-Beam Multipath Scenario

This is primarily a test of the multipath-acquisition capabilities of the optimal receiver. Figure 11 presents the result of a simulation run, which began with no multipath, the receivers tracking and $S/N = 20$ db. After about a second, multipath interference begins to appear at a constant separation angle of 0.5° , growing in amplitude to about 0.8 of the direct path signal amplitude, then diminishing, again to zero. The optimal receiver offers a 10:1 improvement in peak error performance.

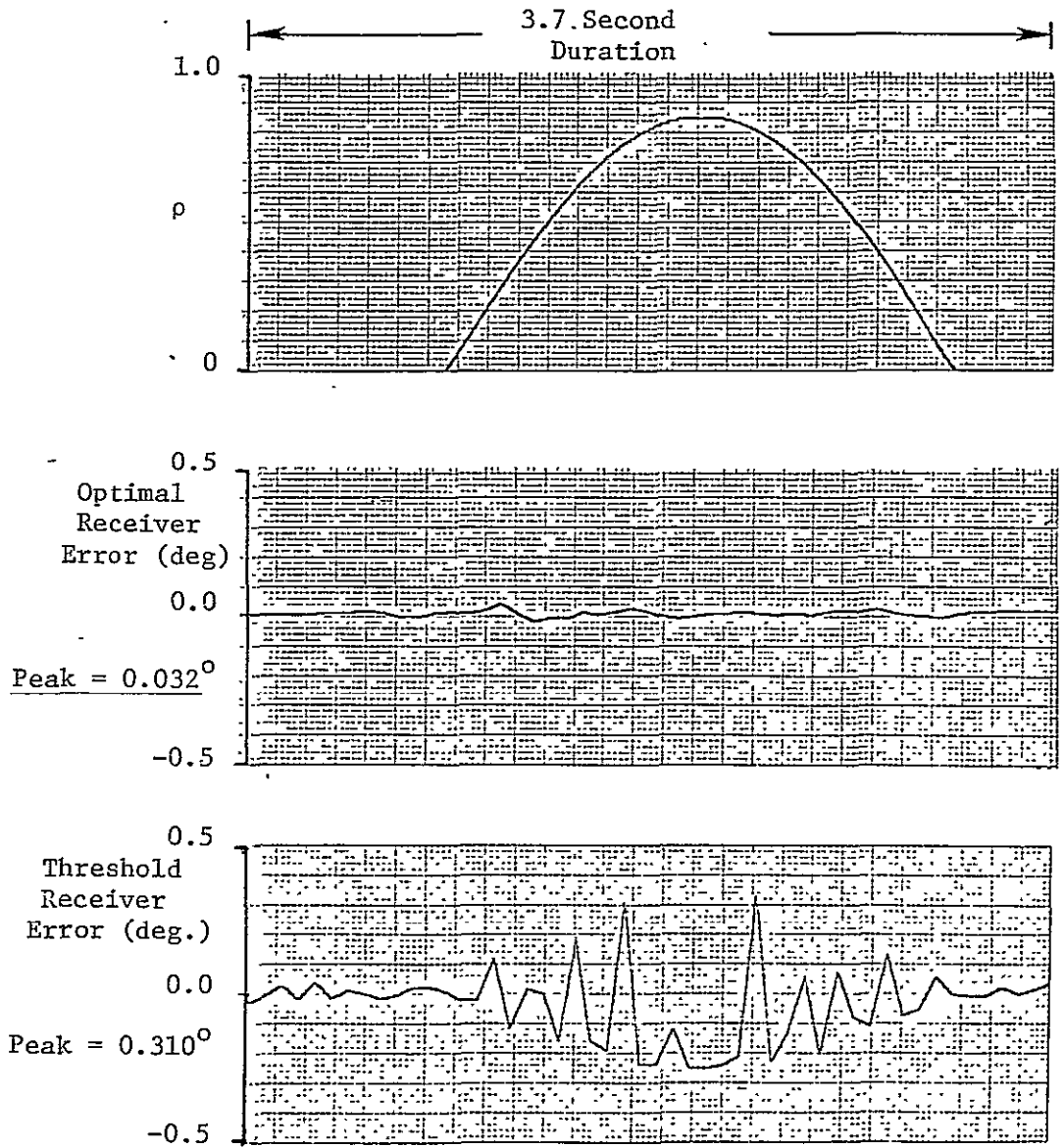


Figure 11. Time-varying In-Beam Multipath Scenario,
 Receiver Error Time Histories,
 $S/N = 20 \text{ db}$, $F_{sc} = 5 \text{ Hz.}$, $\beta = 0^\circ$, $\theta_{sep} = 0.5^\circ$

C. Simulated Landing Scenarios

A landing scenario in general is characterized, in terms of our simulation parameters, by simultaneously varying ρ , θ_{sep} and F_{sc} [5]. A case that was simulated is shown in Figure 12, suggestive of heavy in-beam multipath, a Fresnel reflection pattern and closing ranges. Error time-histories for the optimal and threshold receivers, operating, at 20 db S/N ratios, are shown in Figure 13. The receiver simulations were initialized in the track mode.

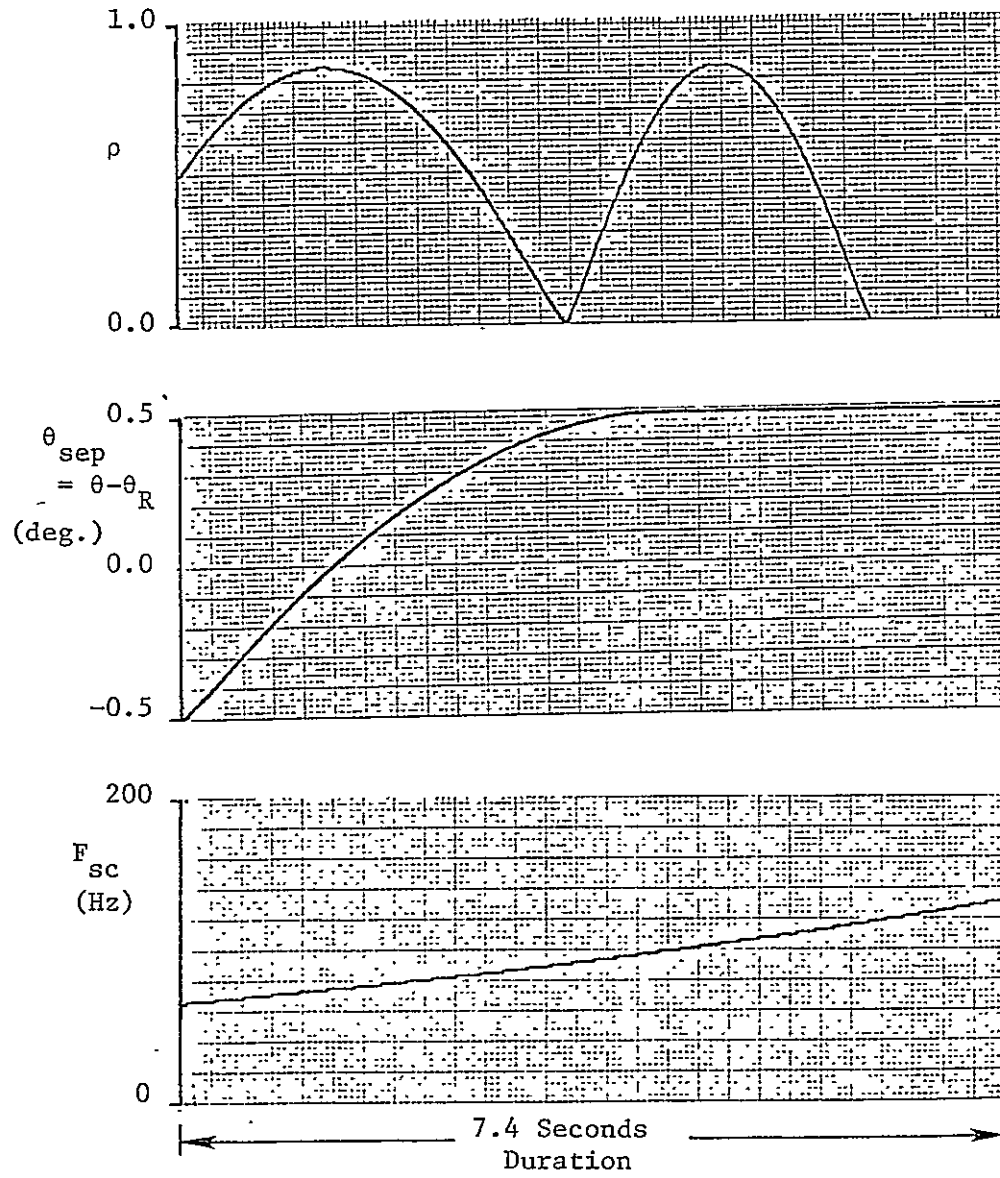


Figure 12. Representative Landing Scenario

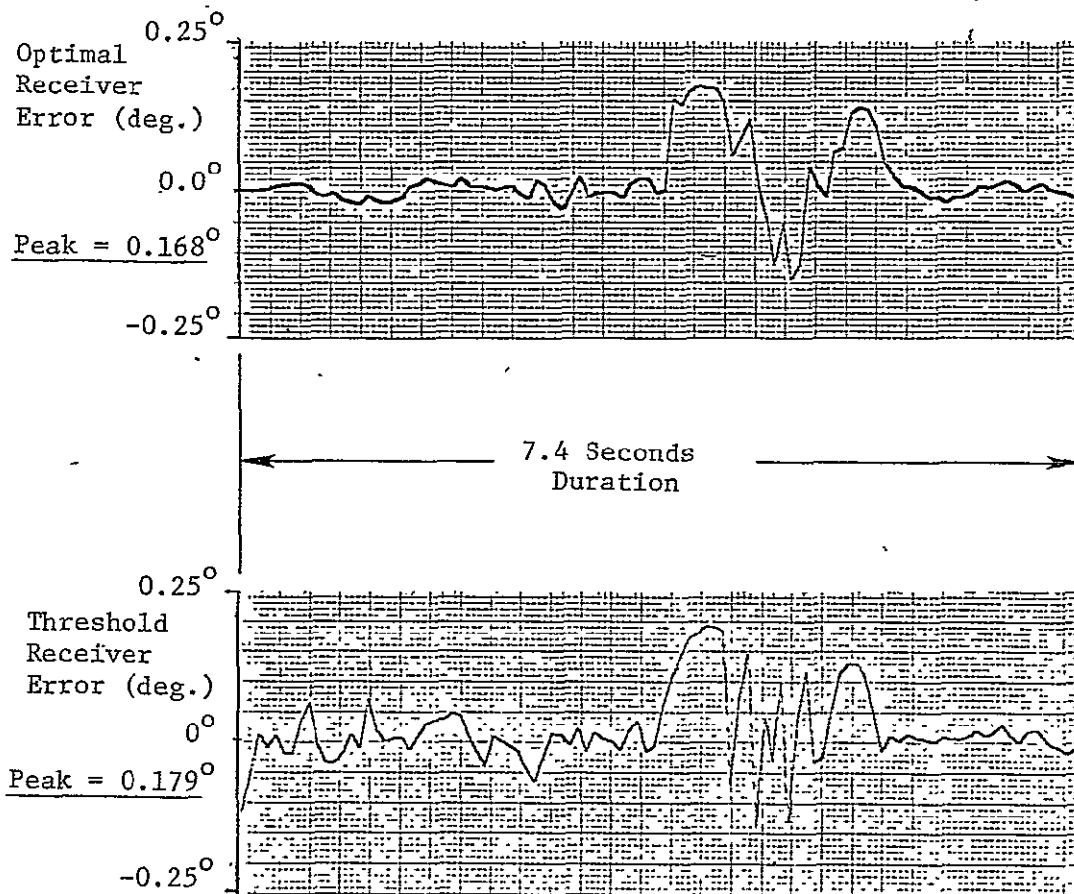


Figure 13. Receiver Error Time Histories,
 Representative Landing Scenario,
 $S/N = 20 \text{ db}$, $\beta = 0.0^\circ$

SECTION VI

THE EXPERIMENTAL SYSTEM

A philosophy and design plan for an experimental system was described in the last report [3]. Three small circuit boards under construction at that time have been completed, but aside from that, no effort during the current grant period was expended on the experimental system. This task was halted because it was becoming increasingly apparent the computational requirements of the optimal receiver algorithm, as it was evolving, would be beyond the capacities of the PDP-11/03 microcomputer to supply as a real-time processor synchronized to the MLS time-frame. Also, all project personnel were needed on the simulation studies (angle-and DME-receivers). The status of the experimental system development, as it stands, is summarized in Table 5.

The immediate objective with respect to an experimental system is the specification of the functional characteristics of a mini-or micro-computer suitable to the computational load of the receiver algorithm as it becomes firm. The work done to date is nearly machine independent, and the experience obtained will facilitate the drawing of a computer specification when appropriate.

PRECEDING PAGE BLANK NOT FILMED

50

MODULE	Breadboarded or Simulated?	Built or Programmed?	Documentation	Tested ?	FINISHED VERSIONS			Remarks
					Estimated % of Next Higher Sub-Assy	Est. % Completion @ various levels of Sub-Assy		
Hardware:					50	40.2	20.1	40% of Hardware Compl
Input:					80	47.75	38.2	43% of Input
5v. to ±15v. Power Supply *	No	Yes	BreadBoard Schematic only	N	5	75	3.75	Hardware Completed
3.54MHz Oscillator	N	Y	N	↓	5	75	3.75	
A/D & S/H	Y	N	BB schematic only	↓	10	20	2.0	
St. Controller & Ferr. ID *	Y	N	Final schematic	↓	25	25	6.25	
Scan Timer *	Y	N	BB schematic only	↓	25	20	5.0	
Sample Timer & Buffer *	Y	Y	Final schematic, layout	↓	30	70	27.0	
Output:					10	0	0	0% of Output
Display *	N	N	N	N	50	0	0	Hardware Compl.
Recorder Interface *	N	N	N	N	50	0	0	
Chassis & Backplane *	N	N	Wiring Table	N	100	20	20.0	20% of Chassis- Backplane Compl.
Software:					50	16.0	8.0	16% of Software Compl.
Assembly Language Routines *					60	0.0	0.0	0% of Assembly lang. Software Completed
DATA Ready Interrupt Service	N	N	N	N		0	0	
Real Time Clock Int. Service	↓	↓	↓	↓		0	0	
ts-Request Interrupt Service	↓	↓	↓	↓		0	0	
Background EXEC.	↓	↓	↓	↓		0	0	
FORTRAN Routines					40	40.0	16.0	40% of FORTRAN Software Compl.
Extimpark (default/scan-init?)	Y	almost	N	N	20	50	10	
If scan, Convert data, process & update	Y	almost		↓	60	50	30	
Calculate values need by foreground	N	N	↓	↓	10	0	0	
Output variables as needed	N	N	↓	↓	10	0	0	
							28.1	28% of total job completed.

*These modules affected to varying degrees by choice of Computer used.

Table 5. Experimental System Development Status, 10/77.

ORIGINAL PAGE IS
OF POOR QUALITY

PART TWO

DME-RECEIVER STUDY

PRECEDING PAGE BLANK NOT FILMED

SECTION VII

DME SIGNAL MODEL

The DME signal model is initiated at the RF stage of the receiver. At this point, the signal consists of a direct path signal, a reflected path signal, and added noise. It can be modeled as:

$$X(t) = R(t) \cos(\omega_c t) + \rho R(t-\tau) \cos(\omega_c(t-\tau) + \beta_1) + n(t) \quad (7.1)$$

where $R(t)$ = direct path envelope

ρ = amplitude of reflected signal relative to the direct signal

τ = time delay of reflected signal

β_1 = phase shift of carrier wave upon reflection

$n(t)$ = receiver noise assumed to be covariant stationary, Gaussian, and bandpass with spectrum centered at the RF carrier, ω_c

$$X(t) = R(t) \cos(\omega_c t) + \rho R(t-\tau) \cos(\omega_c t + \beta_2) + n(t) \quad (7.2)$$

$$= R(t) \cos(\omega_c t) + \rho R(t-\tau) [\cos(\beta_2) \cos(\omega_c t) - \sin(\beta_2) \sin(\omega_c t)] + n(t)$$

where $\beta_2 = \beta_1 - \omega_c \tau$

Because of the assumed properties of the receiver noise process, it can be expanded into quadrature components with respect to the carrier frequency, ω_c .

$$n(t) = n_c(t) \cos(\omega_c t) - n_s(t) \sin(\omega_c t) \quad (7.3)$$

consequently $X(t)$ can be written

$$X(t) = [R(t) + \rho R(t-\tau) \cos(\beta_2) + n_c(t)] \cos(\omega_c t) - [\rho R(t-\tau) \sin(\beta_2) + n_s(t)] \sin(\omega_c t) \quad (7.4)$$

$$X(t) = X_c(t) \cos(\omega_c t) + X_s(t) \sin(\omega_c t) \quad (7.5)$$

After heterodyning, the IF signal is

$$Y_1(t) = X_c(t) \cos(\omega_0 t) + X_s(t) \sin(\omega_0 t) + \text{higher harmonics} \quad (7.6)$$

With good tracking of the IF frequency, the output of the IF filter can be approximated as

$$Y_2(t) = Y_c(t) \cos(\omega_0 t) + Y_s(t) \sin(\omega_0 t) \quad (7.7)$$

where $Y_c(t) = X_c(t) * h(t)$

$Y_s(t) = X_s(t) * h(t)$

$h(t)$ is the impulse response of the lowpass analog of the IF filter

* denotes convolution

It follows that the IF envelope is

$$V(t) = [Y_c^2(t) + Y_s^2(t)]^{1/2} \quad (7.8)$$

SECTION VIII

DME SIMULATION

The DME signal is simulated by generating the functions $R(t)$, $n_c(t)$, and $n_s(t)$ and combining them as in (7.4) to produce the quadrature components, $X_c(t)$ and $X_s(t)$. Each component is filtered by separate but identical lowpass filters to produce the IF components, $Y_c(t)$ and $Y_s(t)$. The IF envelope is obtained by (7.8) and examined to determine when a threshold crossing has occurred. A large number of simulation runs are made (about 250) for each set of multipath and noise conditions so that an approximate statistical average and distribution function for the error will result. The error itself is then passed through a ten radian per second bandwidth filter to reduce random pulse-to-pulse errors. Another average and distribution function are obtained for the filtered error.

8.1 IF Filters

The quadrature components of the DME signal are filtered through a five-pole Butterworth lowpass filter. The effect of this filter is equivalent to that of the Butterworth bandpass filter used in the Hazeltine DME system. It is implemented in the simulation as a digital lowpass filter with a sampling frequency of 100 MHz. Although a sampling frequency of this magnitude might be impractical in a real time situation, its use on the computer is justified since the response of the digital filter should be as close to that of the analog filter as possible. The bandwidth of the filter is 1.75 MHz so that the simulation results will be directly comparable to the Hazeltine study [6].

8.2 False Alarms

In any type of receiver, there is a danger of mistaking an early threshold crossing due to noise as the final crossing due to the DME pulse. The rate of these "false alarms" varies with the proximity of the threshold level to the noise level and has the potential for causing a high negative bias in the error. Therefore, there is a need for some logic in the receivers to recognize and eliminate some of these false alarms.

The primary factor that distinguishes a false alarm from the actual threshold crossing is the amount of time the signal stays above threshold. Samples of the signal which are separated by a time constant (reciprocal of the bandwidth of the bandpass IF filter) are nearly uncorrelated so that the probability of the signal remaining above the threshold due to noise alone for a period of time greater than a time constant is very small. The half-amplitude pulse width is over ten times the length of a time constant so it should be possible to distinguish between false alarms and the actual threshold crossing due to the DME pulse. It is on this basis that false alarms are reduced in the simulation.

8.3 Error

Errors due to multipath and noise are combined here instead of being treated separately as in the Hazeltine and M.I.T. studies, [6], [7]. These two sources of error are not independent of each other since the signal to noise ratio (S/N) is affected whenever multipath is present. Of course, if the threshold is placed at a very high point

on the pulse, multipath will be the primary source of error with noise errors being negligible. The opposite is true if the threshold is placed at a very low point on the signal, but since one tries to place the threshold at a point where there is an effective trade-off between the two it is not realistic to analyze each separately.

Previous studies [6], [8] have assumed that the noise effects on the IF signal envelope, $V(t)$ are Gaussian. The density function under these conditions is

$$P_{V(t)} = \frac{1}{(2\pi\sigma^2)^{1/2}} \exp [V(t) - V_0(t)]^2 / 2\sigma^2 \quad (8.1)$$

where $V_0(t)$ is the IF signal envelope uncorrupted by noise.

This kind of assumption ignores the non-linear effects of the envelope detection process and as Rice [9] has shown, the density function for the envelope is actually.

$$P_{V(t)} = \frac{V(t)}{\sigma} \exp [-(V^2(t) + V_0^2(t))/2\sigma^2] I_0 [V(t)V_0(t)/\sigma^2] \quad (8.2)$$

where $I_0 [V(t)V_0(t)/\sigma^2]$ is the Bessel function.

Rearranging terms, this density function is

$$P_{V(t)} = \frac{V(t)}{\sigma} \exp \frac{1}{2} [(V(t)/\sigma)^2 + (V_0(t)/\sigma)^2] I_0 [(V(t)/\sigma)(V_0(t)/\sigma)] \quad (8.3)$$

If $\alpha(t) = V(t)/\sigma$ and $\gamma(t) = V_0(t)/\sigma$, then a new density function for the random process, $\alpha(t)$, will result.

$$P\alpha(t) = \alpha(t) \exp \frac{1}{2} [\alpha^2(t) + \gamma^2(t)] I_0 [\alpha(t)\gamma(t)] \quad (8.4)$$

This is a normalized density function for the envelope with the parameter $\gamma(t)$ representing the signal to noise ratio.

When (8.4) is evaluated at the threshold crossing time, a density function for the amplitude variations in the I.F. envelope at this point in time results. Figure 14 shows this Rician density function for various values of γ . The distribution is Rayleigh when γ is zero and approaches a Gaussian distribution as γ is increased. γ in this case is the threshold to noise ratio (T/N).

A variation in the amplitude of the envelope can either shorten or lengthen the time it takes to reach threshold. If the error in the measurement of the arrival time of the pulse is considered to be the shift in the threshold crossing time from the ideal (the crossing time on an incoming pulse uncorrupted by interference from any form of multipath or noise), then this density function also applies to the error. Positive and negative variations in the envelope amplitude cause early and late threshold crossings, respectively, so one would expect from the graph in Figure 14 that there would be a negative bias in the error at low T/N. Therefore, the assumption of a Gaussian distribution of error is only valid for relatively high T/N.

8.5 Power Budgets

The power budgets for the ground-based and airborne receivers are based on the landing pattern shown in Figure 15. The flight path is at a three degree angle with respect to a 14000 foot runway with the groundbased receiver at one end. Signal attenuation is incurred along the flight path due to the antenna pattern [6]. This effect must be compensated for if accuracy is to be maintained as the plane approaches the runway.

$$\gamma = T/N$$
$$\rho = V/N$$

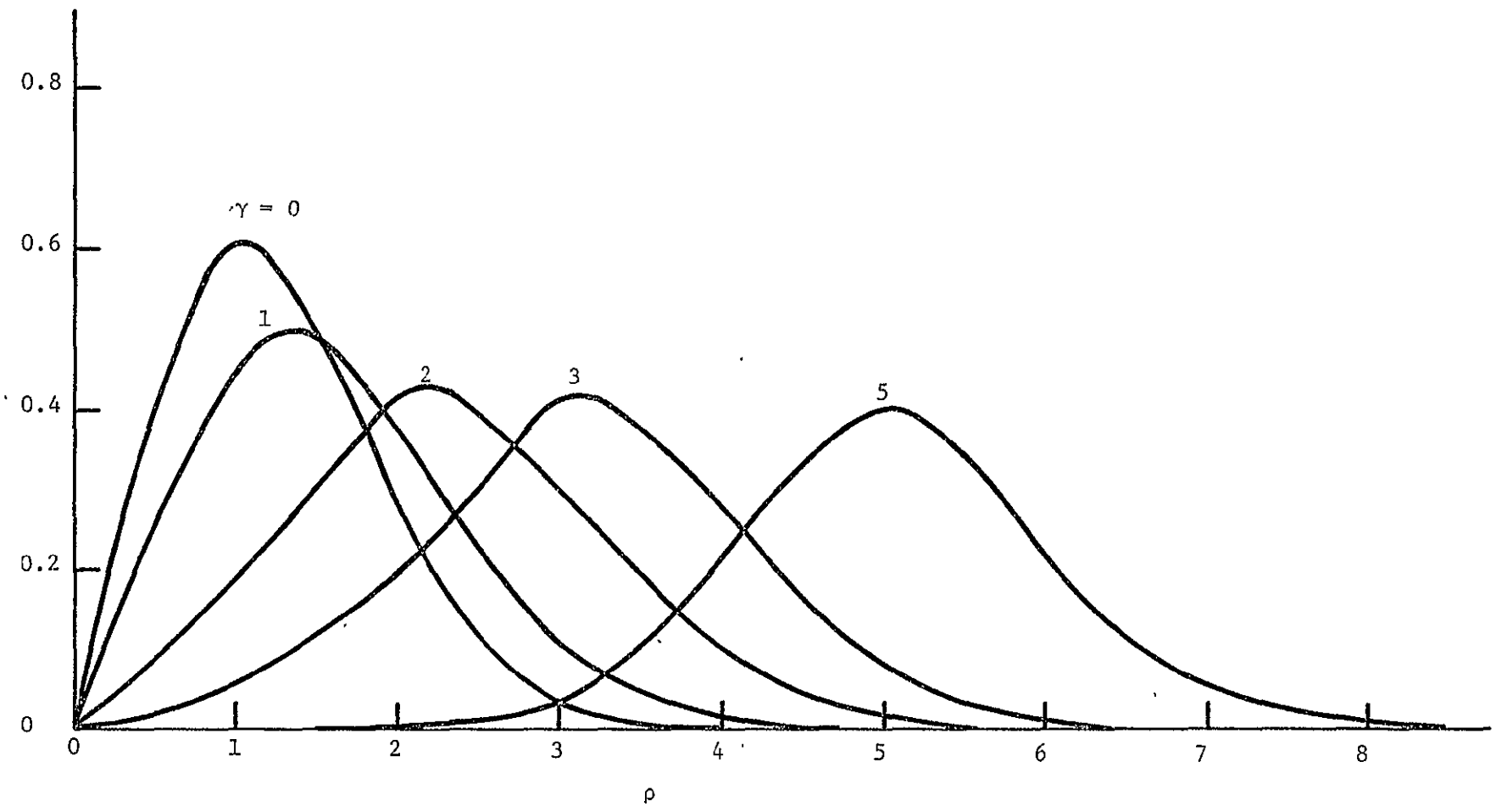


Figure 14 Normalized Density Function for IF Envelope, Evaluated at Threshold Crossing Time

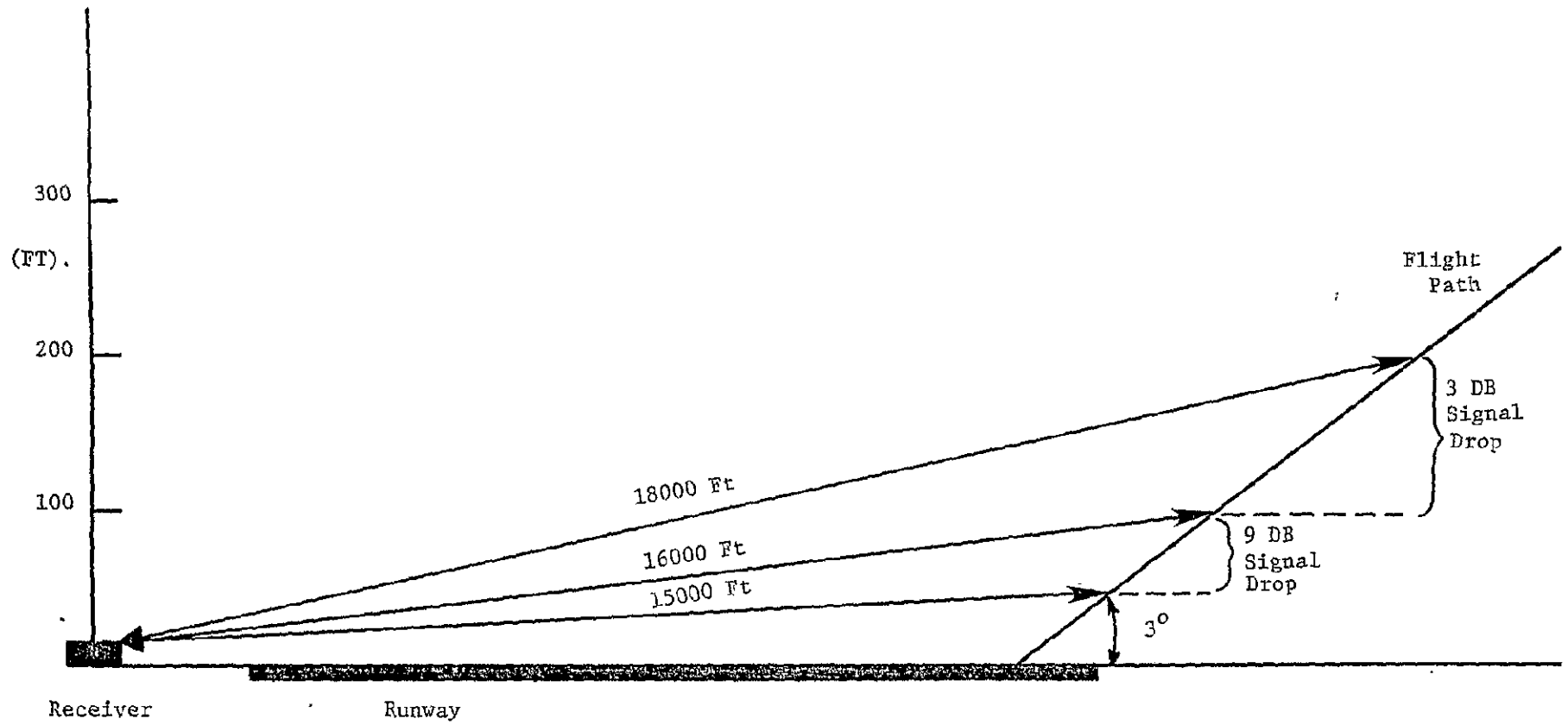


Figure 15 Landing Pattern, 14000 Ft Runway

For a $\cos\text{-}\cos^2$ pulse shape with a 3.5 μ sec half-amplitude pulse width, the ratio of pulse peak to RMS amplitude is 3.7 decibels (DB). The average power allowable for this pulse shape under the ICAO Annex 10 specification on effective radiated power in adjacent channels is 55 DB. This is obtained by integrating the pulse spectrum over all frequencies and comparing it with the power allowed in a 0.5 MHz band, 2 MHz from the carrier. The peak is then 58.7 DBM.

The assumed power budgets follow. The signal to noise ratios in the assumed budgets are defined as the ratio of peak signal level to RMS noise level and are defined at the input of the receiver before any power loss occurs (antenna losses are neglected). Under these circumstances the noise power used is $4 \text{ kTB} + \text{NF}$ instead of $\text{kTB} + \text{NF}$ which is used to describe the available noise power in many cases.

AIR TO GROUND POWER BUDGET [6]

ERP (peak)	58.7 DBM
Transponder Antenna Gain	8.0 DB
Path Loss (18000 Ft)	107.0 DB
Peak Signal (18000 Ft)	-43.3 DBM
Noise ($4\text{kTB} + \text{NF}$) NF = 15 DB	-87.5 DBM
S/N (18000 Ft)	47.2 DB
S/N (16000 Ft)	44.2 DB
S/N (15000 Ft)	38.2 DB

GROUND TO AIR POWER BUDGET [6]

ERP (peak)	61.7 DBM
Path Loss	107.0 DB
Peak Signal	-45.3 DBM
Noise (4 ktB + NF) NF = 15 DB	-87.5 DBM
S/N (18000 Ft)	42.2 DBM
S/N (16000 Ft)	39.2 DBM
S/N (15000 Ft)	33.2 DBM

SECTIONS IX - XII

The following sections give simulation results for both the threshold and delay and compare receivers in the ground-based transponder and the airborne interrogator. Each section is broken up into subsections which describe how the receiver performs as each parameter is varied in turn with the others remaining constant. This allows one to extrapolate as to the performance of the receiver under a wide range of conditions.

An error summary is provided at the end of each section to provide a more detailed accounting of the performance of each receiver. This includes the performance under varying multipath conditions at the signal to noise ratio outlined in the power budget and also with a 6 DB drop in the signal to noise ratio as might occur with a specular reflection. The threshold level for this summary is chosen to be within a range of values where the receiver provides the best performance with respect to noise and multipath errors. The error in the summary has been filtered through a 10 rad/sec lowpass filter. This process has very little effect on the mean but reduces σ by a factor of approximately 2.2.

SECTION IX

SIMULATION RESULTS - TRANSPONDER FIXED THRESHOLD RECEIVER

The threshold level is assumed to be set at a constant voltage level in the fixed threshold receiver. This means that the position of the threshold with respect to the pulse shape changes with the strength of the signal. A subtractive multipath with a relatively small delay would lower the signal to noise ratio (S/N) of the pulse. The resulting shift of the threshold to a higher point on the signal would cause a late threshold crossing and bias the error in the positive direction. An additive multipath signal would cause the opposite effect and negatively bias the error.

This type of receiver is assumed to be limited to the ground-based transponder so that the air to ground power budget applies here.

9.1 Threshold Levels

The performance of the fixed threshold receiver is greatly dependent on the threshold setting. For a threshold to noise ratio (T/N) of 6 DB, the mean error is negatively biased for both additive and subtractive multipath signals (Figure 16). Early threshold crossings are due to the proximity of the threshold to the noise level and multipath has little effect under these conditions. A subtractive multipath signal, however, can provide a slight improvement since it causes a positive shift in the mean error bringing it closer to zero.

The noise errors are diminished and a positive shift in the error results when the threshold is raised to higher levels. For

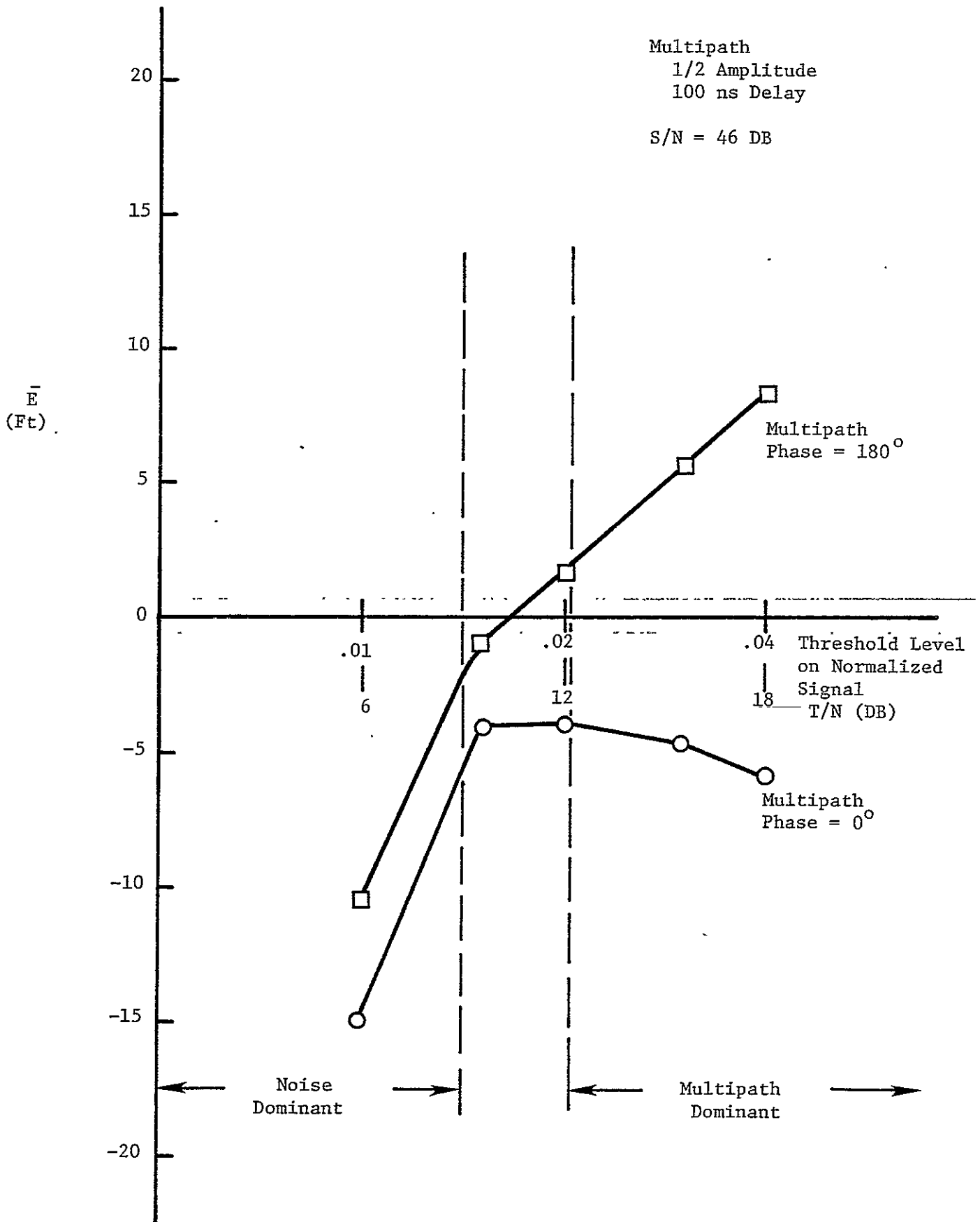


Figure 16 Mean Error Vs. T/N, Fixed Threshold Receiver

subtractive multipath, it increases almost linearly and becomes positive as the threshold level is increased. For additive multipath, the error reaches a minimum and shifts toward the negative again. The graph in Figure 16 can be separated into regions where noise is the primary cause of error (up to $T/N = 9\text{DB}$) and where multipath is the primary cause of error ($T/N = 12\text{DB}$ and above). The region between these two is where an effective tradeoff between the two sources of error occurs.

9.2 Error Distribution

The density function for the error has been described in section 8.4. Figure 17 shows the error distribution for a threshold to noise ratio of 18 DB and a subtractive half-amplitude multipath. This is a nearly Gaussian distribution with a narrow spread about the mean. A very different distribution of error results when the threshold level is lowered to 6 DB (Figure 18). The mean is shifted into the negative region and the spread of error is no longer nearly symmetrical about this point. The error has now approached a Rayleigh form with the error spread over a large range below the mean and concentrated in small range above the mean.

When the error is filtered through a 10 rad/sec lowpass filter, the spread is reduced by a factor of two to three but the original shape remains. This makes it difficult to obtain one expression which accurately expresses the spread of error about the mean. Using the standard deviation, σ , as a measure disguises the fact that the error is not symmetrical about the mean in all cases,

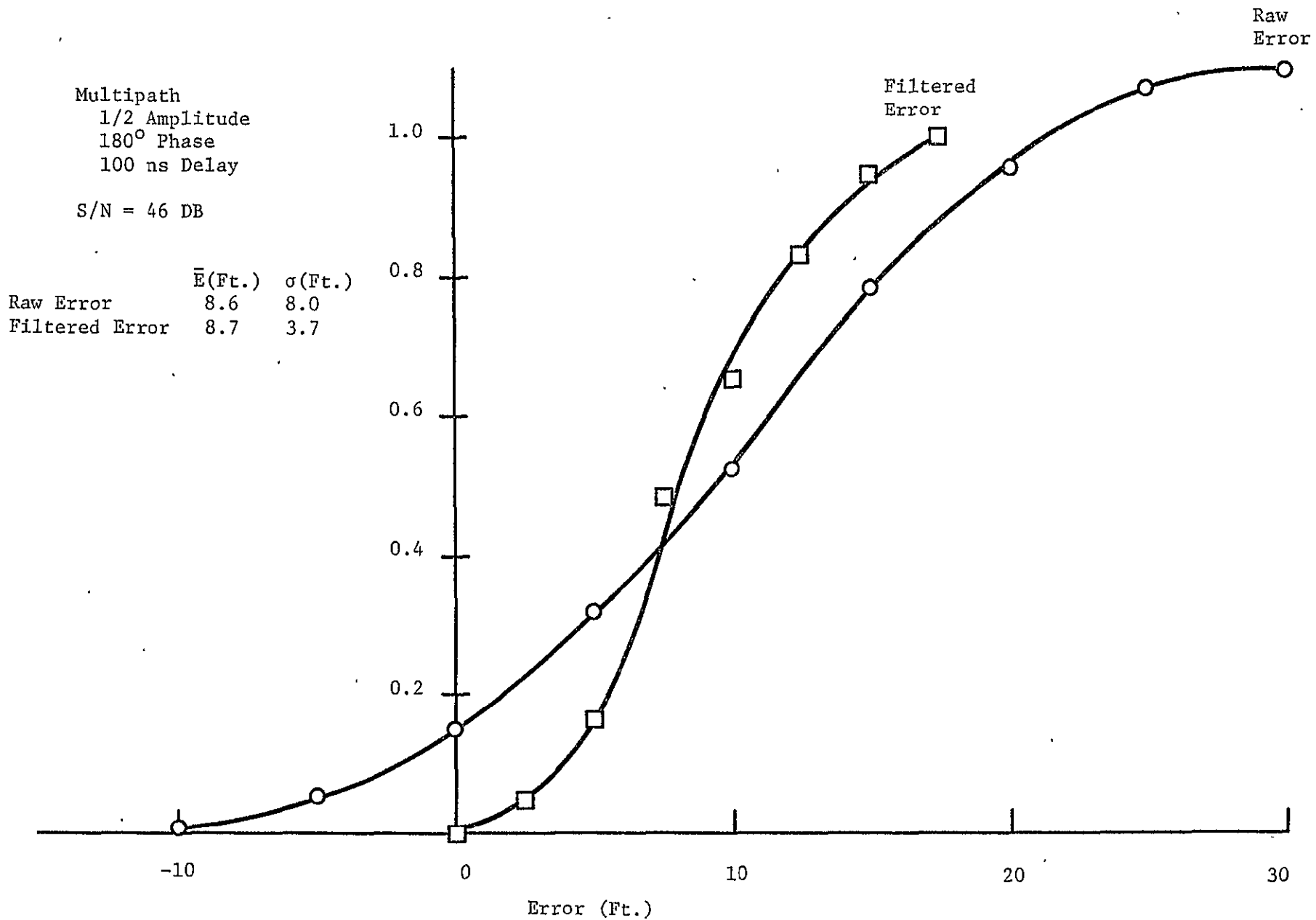


Figure 17 Error Distribution, Fixed Threshold Receiver, T/N = 18 DB

Multipath
 1/2 Amplitude
 180° Phase
 100 ns Delay

S/N = 46 DB

	\bar{E} (Ft.)	σ (Ft.)
Raw Error:	-11.5	34.1
Filtered Error:	-11.3	14.5

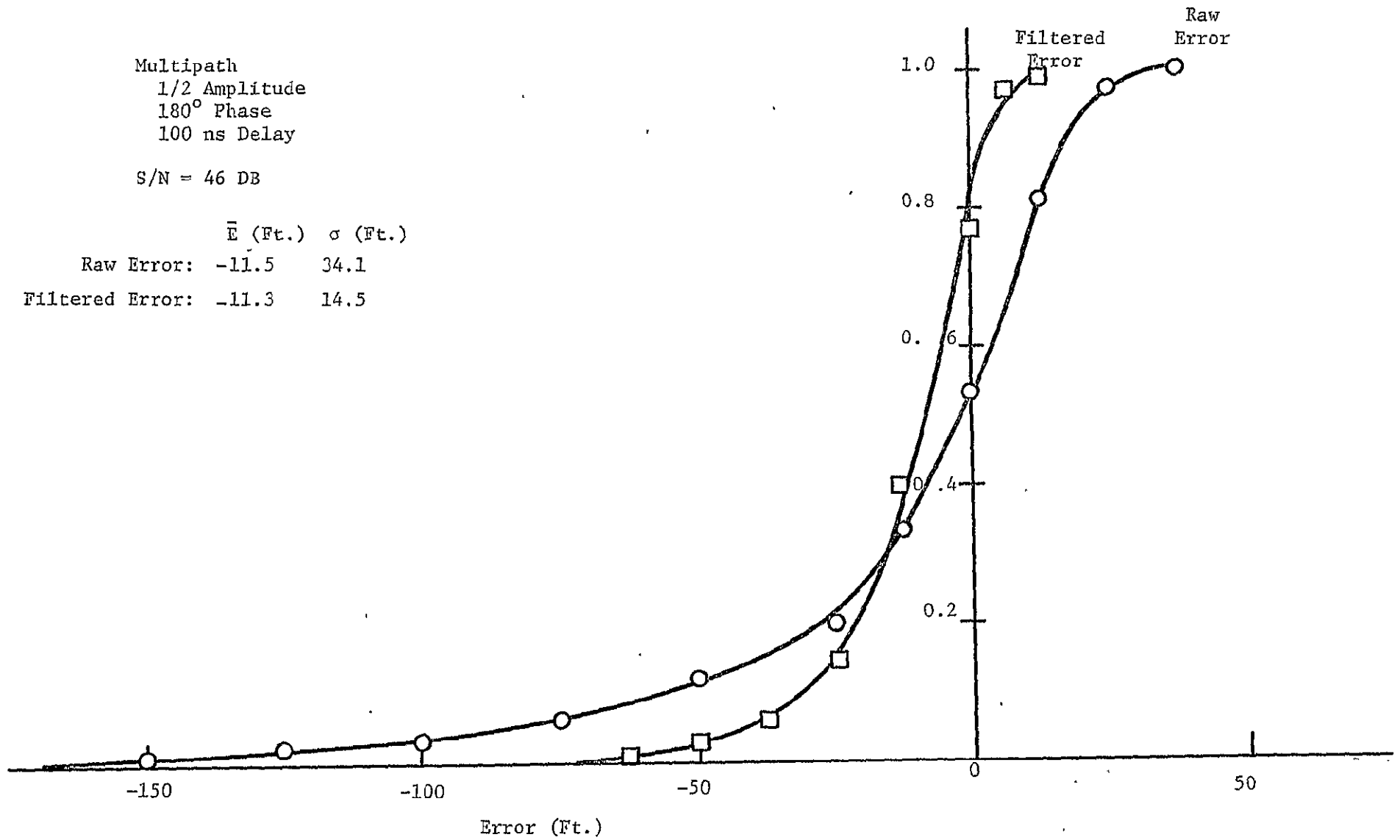


Figure 18 Error Distribution, Fixed Threshold Receiver, T/N = 6DB

but should provide a good approximation for thresholds in the range of interest.

9.3 Changes in the Signal to Noise Ratio

A change in S/N shifts the position of the threshold on the pulse and therefore changes the threshold crossing time. S/N is affected by changes in the signal strength due to specular ground reflections and receiver to receiver gain variations due to temperature, aging and other factors.

Ground reflections have very short differential path delays with respect to the direct path signal and this makes them recognizable only as changes in S/N at the receiver. Lateral reflections (multipath) have longer delays and are treated as a separate problem.

Figure 19 shows the changes in the error bias for ± 6 DB changes in S/N while under the influence of a subtractive half-amplitude multipath signal. The 6 DB change can cause a shift in the error bias of up to 33 feet. This shift generally increases as the threshold is raised.

9.4 Multipath Effects

Multipath in the fixed threshold receiver causes a shift in S/N which in turn causes error as explained above. The magnitude of the error is dependent upon the multipath parameters with error increasing as amplitude increases or as the differential path delay decreases.

The error is most severe at short delay times as shown in Figure 20. It levels out to a relatively small error at about 150 nanoseconds (ns). In the noise-free case, one would expect the error to level out at zero.

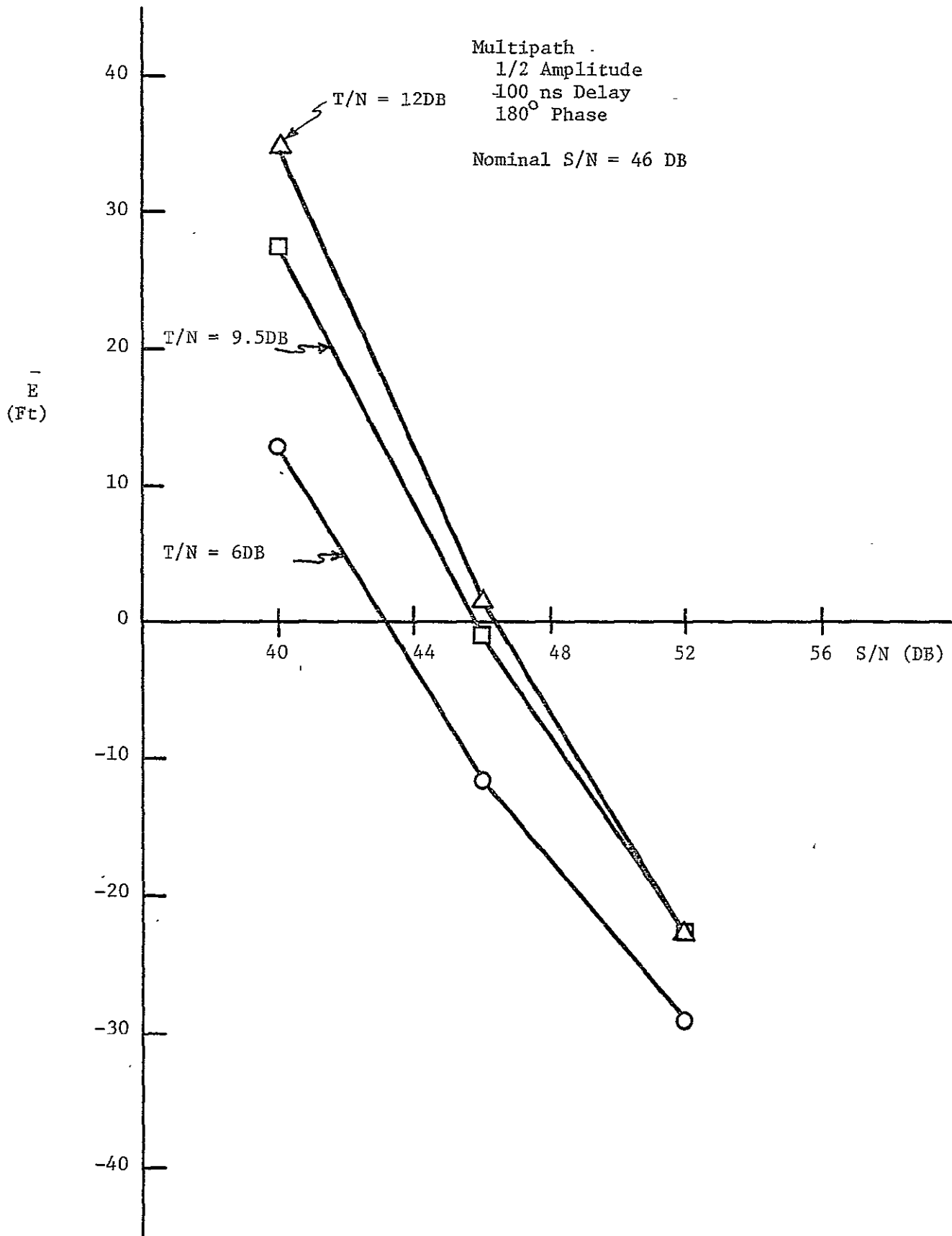


Figure 19 Mean Error Vs. S/N, Fixed Threshold Receiver

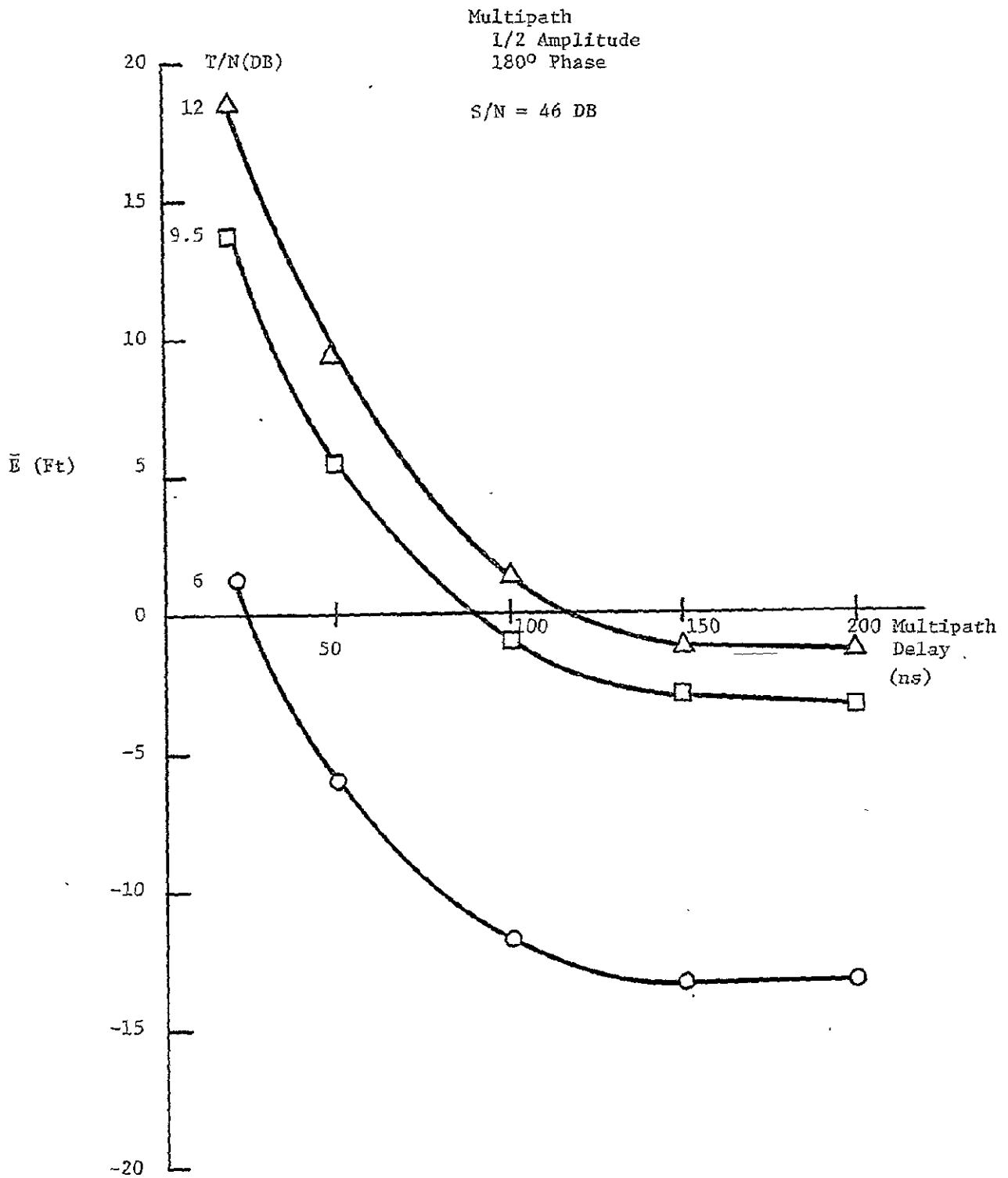


Figure 20 Mean Error Vs. Multipath Delay, Fixed Threshold Receiver

When noise is added in, there is a negative bias in the error, the magnitude of which depends upon T/N. At T/N = 6DB, the noise bias is large so that short multipath delay times can actually cause an improvement in the error. When T/N is raised to 12 DB, the noise bias decreases and the error is near zero for multipath delays above 150 ns.

T/N = 9.5 DB
 Nominal S/N = 46 DB

Multipath Phase:		0°		0°		180°		180°	
Multipath Delay:		100ns		200ns		100ns		200ns	
Multipath Amplitude	S/N (DB)	\bar{E} (Ft)	σ (Ft)	\bar{E} (Ft)	σ (Ft)	\bar{E} (Ft)	σ (Ft)	\bar{E} (Ft)	σ (Ft)
0.2	46	-4.4	6.2	-3.5	6.4	-2.6	6.5	-3.5	6.4
0.2	40	20.7	8.1	22.3	8.4	24.5	8.8	22.6	8.5
0.5	46	-5.5	6.0	-3.7	6.3	-1.0	6.8	-3.5	6.4
0.5	40	18.3	7.7	22.1	8.3	28.1	9.5	22.9	8.5
0.8	46	-6.8	6.2	-3.6	6.3	0.5	7.6	-3.4	6.4
0.8	40	16.3	7.4	21.4	7.9	32.8	10.5	23.2	8.9

Table 6 Summary of Errors - Transponder, Fixed Threshold Receiver

SECTION X

SIMULATION RESULTS - TRANSPONDER DELAY AND COMPARE RECEIVER

A delay and compare receiver compares the IF envelope with a delayed and slightly amplified version of itself to determine the arrival time of the DME pulse. A diagram of this type of receiver is shown in Figure 21. The threshold crossing time is given by the negative going zero crossing of the difference signal, $d(t)$, and the threshold level is set by the delay and gain parameters, τ and k . A form of automatic gain control is inherent in this type of receiver since the input signal is being compared with itself.

Before the pulse arrives, the receiver will essentially be comparing noise signals which are highly correlated with each other due to the short time delay. The delayed signal will also be amplified so that there is a high probability that the difference signal will be below zero during this period. Therefore, the false alarm rate for this receiver is more significant than that of the fixed threshold receiver under similar conditions and must be reduced as outlined in section 8.2.

10.1 Threshold Crossing Point

Figure 22 shows the mean error as a function of the threshold crossing point. The negative bias in the error due to noise occurs at higher levels on the pulse than it does in the fixed threshold receiver under the same circumstances. Assuming that the receiver delay, τ , is fixed, it is necessary to increase the gain, k , to lower the threshold. This results in an increase in the noise level

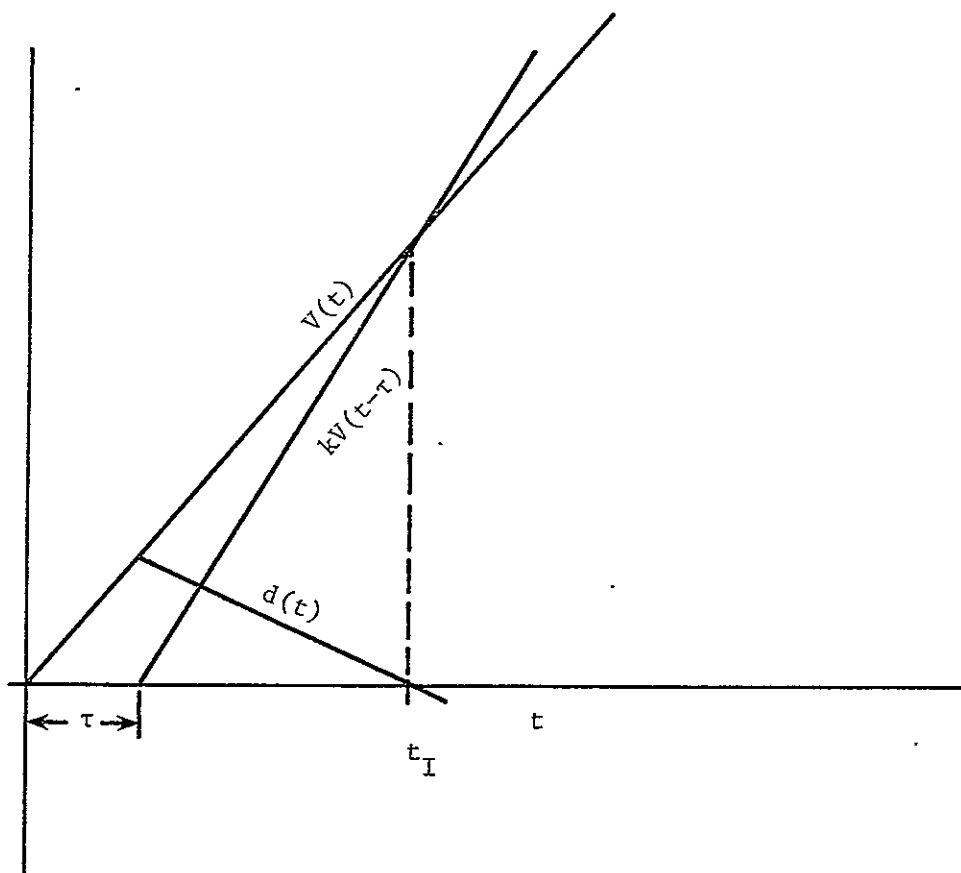
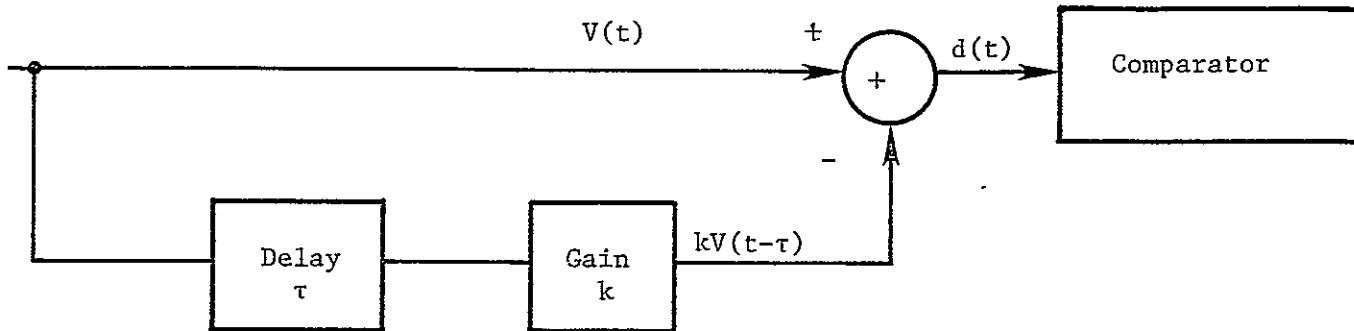


Figure 21 Delay and Compare Receiver Signals

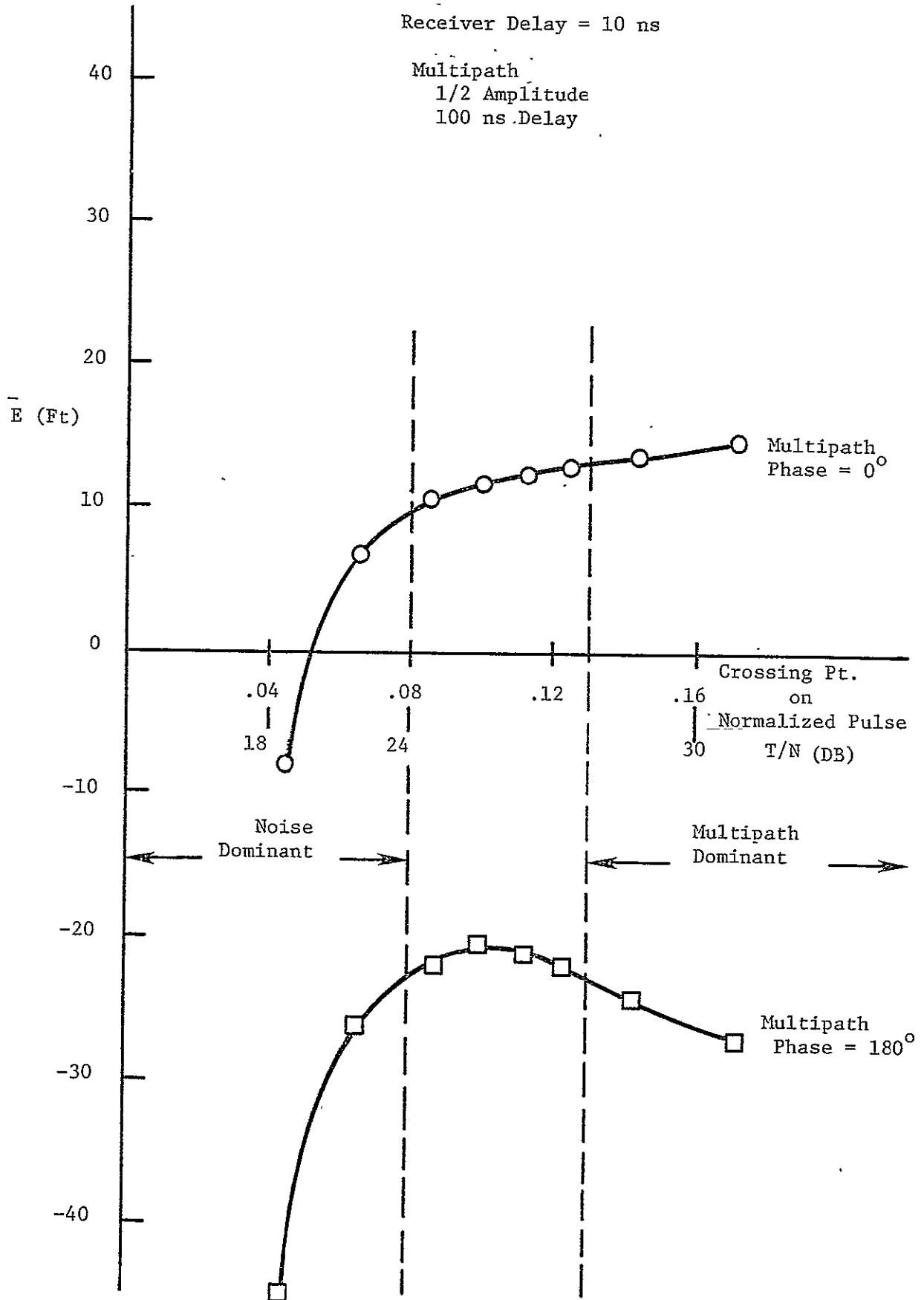


Figure 22 Mean Error Vs. Threshold Crossing Point, Delay and Compare Receiver S/N = 46 DB

in the delayed signal which in turn causes an increase in early threshold crossings and contributes to this effect.

It is possible to separate the graph in Figure 22 into a region where noise is the primary source of error (up to $T/N = 24$ DB) and a region where multipath is the primary source of error ($T/N = 29$ DB and above). The region between these two is where the minimum over-all bias in the error due to multipath and noise occurs. Subtractive multipaths signals cause the most significant errors and also reach an overall minimum in this region, so these are studied in more detail.

10.2 Error Distribution

The density function for the error developed in section 8.4 does not apply directly to the error in the delay and compare receiver. The error density function applies only to the direct IF envelope signal, $V(t)$, and not to the difference signal, $d(t)$. However, the overall effect is much the same. Figure 23 shows the error distribution for a subtractive half-amplitude multipath signal at a T/N of 25 DB. This distribution is in the Rician form and is similar to that found at a 6 DB threshold level in the fixed threshold receiver. A threshold level of 29 DB gives an error distribution which is more nearly Gaussian (Figure 24).

The most significant difference between the error distributions in the two receivers is the difference in the threshold levels where the near Gaussian distribution is achieved. This point is of interest because it indicates the signal level at which the receiver becomes relatively

Receiver Delay = 10ns

Multipath
1/2 Amplitude
180° Phase
100ns Delay

S/N = 46 DB

	\bar{E} (Ft.)	σ (Ft.)
Raw Error:	-22.2	28.4
Filtered Error:	-22.2	12.0

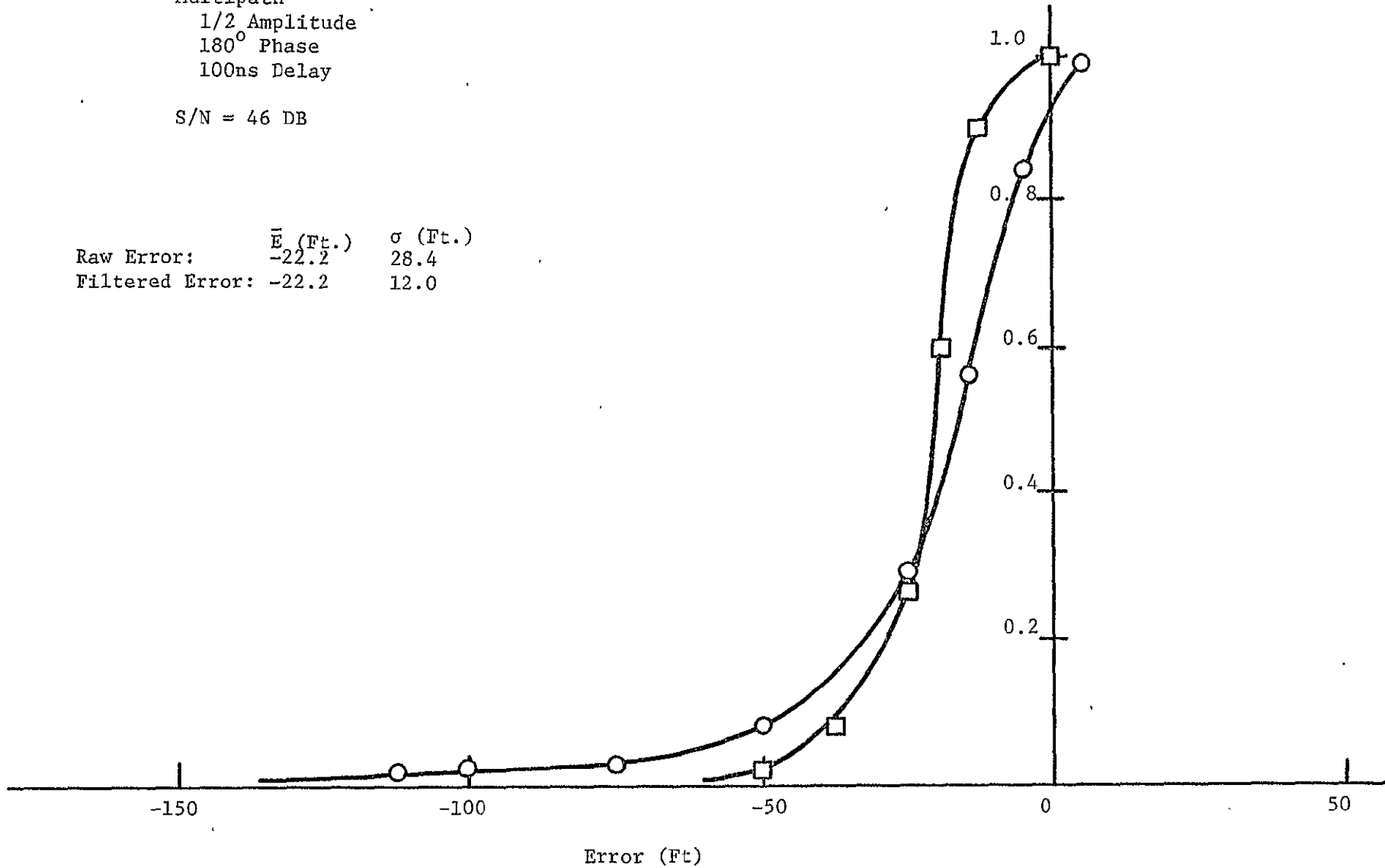


Figure 23 Error Distribution, Delay and Compare Receiver, T/N = 25 DB.

Receiver Delay = 10ns

Multipath
1/2 Amplitude
180° Phase
100ns Delay

S/N = 46 DB

	$\bar{E}(\text{Ft.})$	$\sigma(\text{Ft.})$
Raw Error:	-22.8	9.4
Filtered Error:	-22.8	4.4

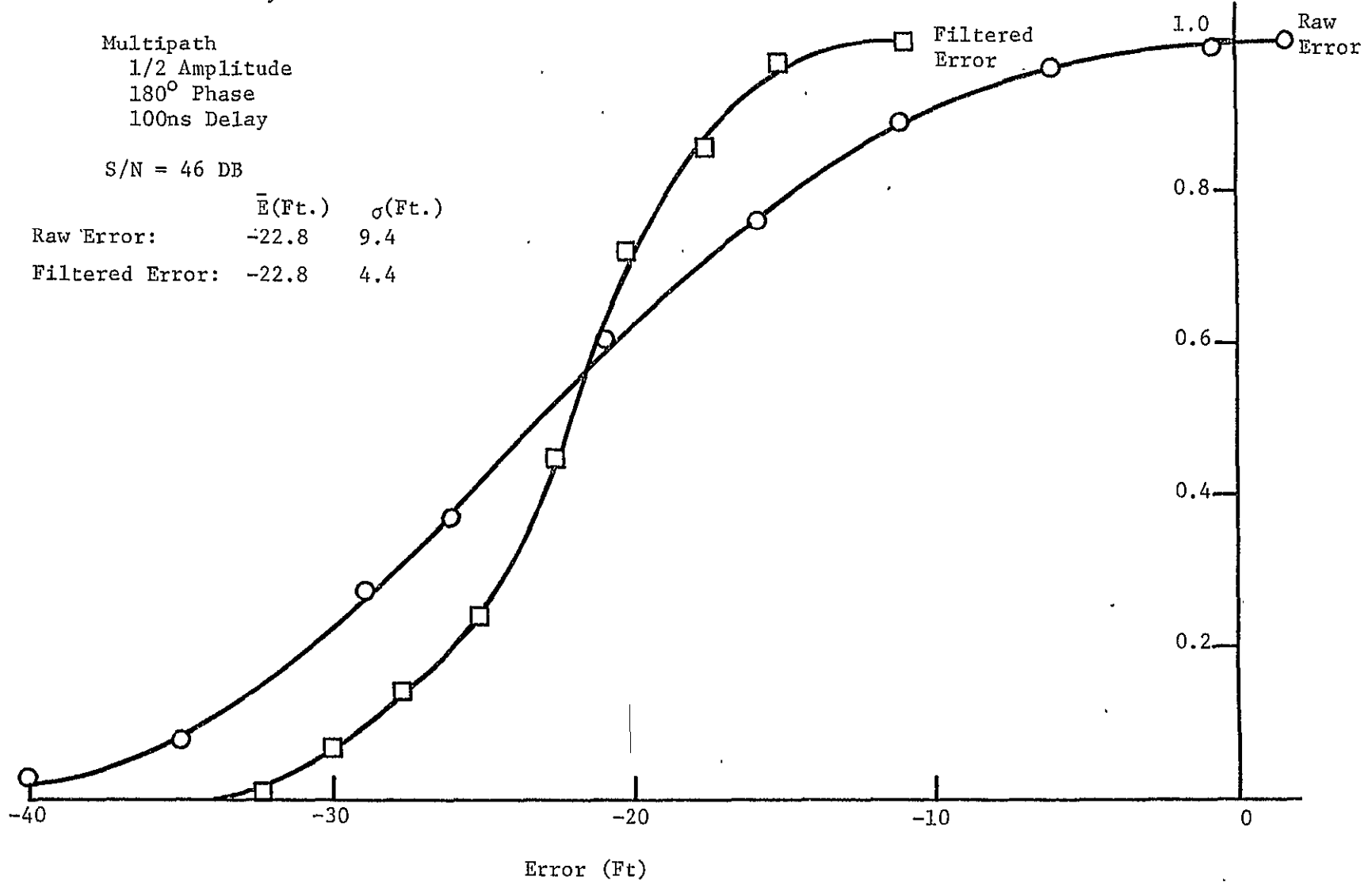


Figure 24 Error Distribution, Delay and Compare Receiver, T/N = 29 DB

insensitive to noise effects. It takes an increase in the threshold level of approximately .12 DB for the delay and compare receiver to approach the same level of insensitivity as the fixed threshold receiver. This is significant because the higher threshold levels mean more susceptibility to multipath errors.

10.3 Changes in the Signal to Noise Ratio

Positive or negative shifts in the signal to noise ratio may be caused by specular ground reflections or receiver to receiver gain variations. The effect of these shifts on the error bias is most pronounced in the case of a drop in gain (Figure 25). The inherent automatic gain control of the delay and compare receiver does not allow the threshold level to shift with respect to the pulse shape as S/N changes. The result is that the greatest penalty is incurred when S/N drops since this increases noise errors. A 6 DB S/N increase causes the error bias to improve slightly.

The variations in the error bias decrease as the threshold level is raised due to a lessening of noise errors.

10.4 Multipath Effects

The M.I.T. study [7] has shown that the error caused by multipath alone in this receiver is small when the multipath delay is small, increases to a peak, and then diminishes steadily as the delay time is increased with all other factors remaining constant. This is also true when multipath and noise errors are considered together (Figure .26). However, in this case when subtractive multipath is involved, the point where the peak error bias occurs

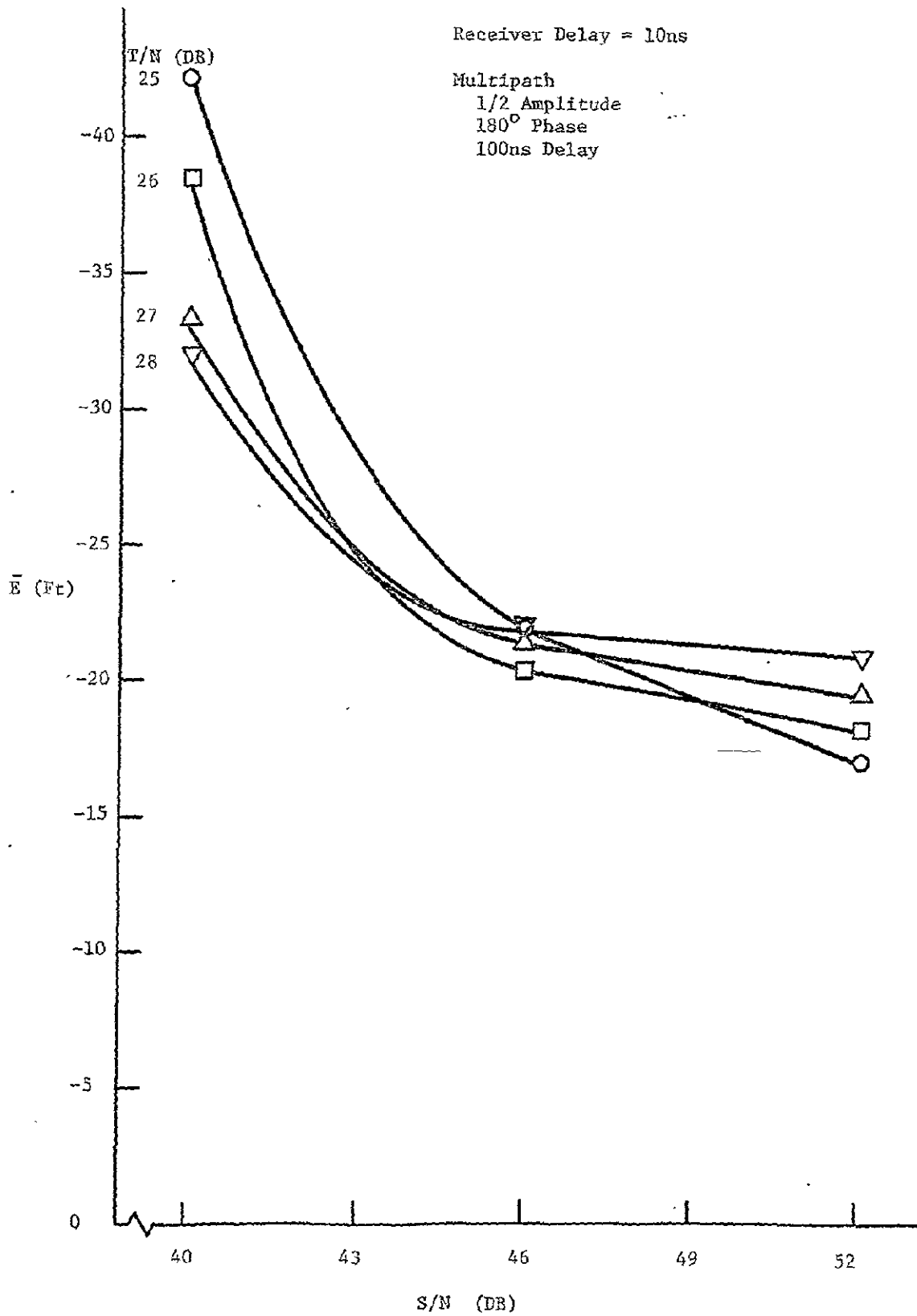


Figure 25 Mean Error Vs. S/N, Delay and Compare Receiver, Nominal S/N = 46 DB

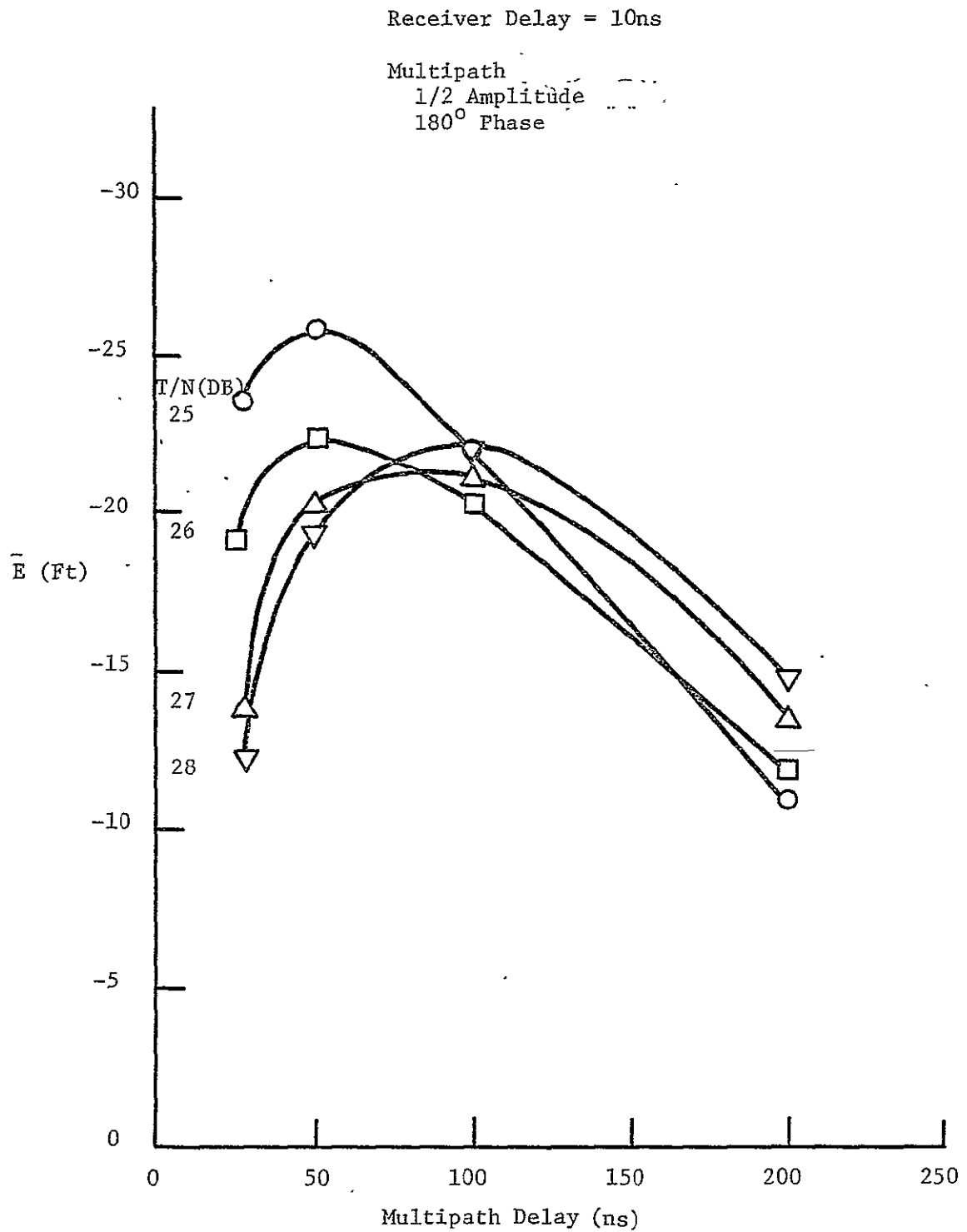


Figure 26 Mean Error Vs. Multipath Delay, Delay and Compare Receiver, S/N = 46 DB

is dependent on the threshold level. The error bias at the 25 DB threshold level peaks at a multipath delay of approximately 50 ns. As the threshold is increased to 28 DB the peak error point shifts forward to about 100 ns.

The key to understanding this is the fact that subtractive multipath causes a change in the signal to noise ratio and at the point where the threshold is crossed there is a relatively larger change when the multipath delay is small. Low signal to noise ratios cause more noise errors (Figure 25) as do low threshold levels (Figure 26) so that the combined effect of both of these causes a shift in the peak error.

Receiver Delay = 10ns

T/N = 28DB
Nominal S/N = 46 DB

		0°		0°		180°		180°	
		100ns		200ns		100ns		200ns	
Multipath	Phase:								
Multipath	Delay:								
Multipath	S/N	\bar{E} (Ft)	σ (Ft)	\bar{E} (Ft)	σ (Ft)	\bar{E} (Ft)	σ (Ft)	\bar{E} (Ft)	σ (Ft)
Amplitude	(DB)								
0.2	46	5.3	3.0	5.4	3.4	-8.4	4.0	-6.9	3.5
0.2	40	3.1	6.8	1.9	9.4	-14.4	13.1	-11.7	11.0
0.5	46	12.9	2.4	15.1	3.2	-22.0	5.0	-15.1	3.5
0.5	40	11.2	5.1	12.8	7.4	-30.8	16.6	-20.5	12.1
0.8	46	18.0	2.0	24.4	2.8	-38.6	6.3	-22.4	3.5
0.8	40	17.2	4.2	22.7	7.1	-50.6	19.9	-28.7	13.7

Table 7 Summary of Errors - Transponder, Delay and Compare Receiver

SECTION XI

SIMULATION RESULTS - INTERROGATOR
ADAPTIVE THRESHOLD RECEIVER

The adaptive threshold receiver takes the DME pulse at the IF stage and uses automatic gain control to normalize it. The threshold is set at a constant voltage level below the pulse peak and so does not shift its position on the pulse due to varying signal strengths as in the fixed threshold receiver.

The effect of the AGC is such that the noise level is increased whenever a loss of signal strength occurs as in subtractive multipath conditions. This is in contrast to the delay and compare receiver which is self-AGC'd and thus does not change the noise levels. In cases of severe signal loss, the noise level could potentially be multiplied to the point that it approaches the threshold level. There should be a limit on the range of the AGC to prevent this.

11.1 Threshold Crossings

Under the influence of additive multipath, the error bias is positive and relatively constant through a large range of threshold levels (Figure 27). Under these conditions, noise errors are insignificant due to the decrease in the noise level caused by the AGC and as a result there is no negative shift in the bias at the lower threshold levels.

The noise levels are increased by subtractive multipath causing a subsequent negative shift in the error bias at low threshold crossing points (up to $T/N = 15.5$ DB). The error reaches a minimum point in the 15.5-20 DB region and again shifts toward the negative at higher threshold points due to the larger error penalties caused by the multipath.

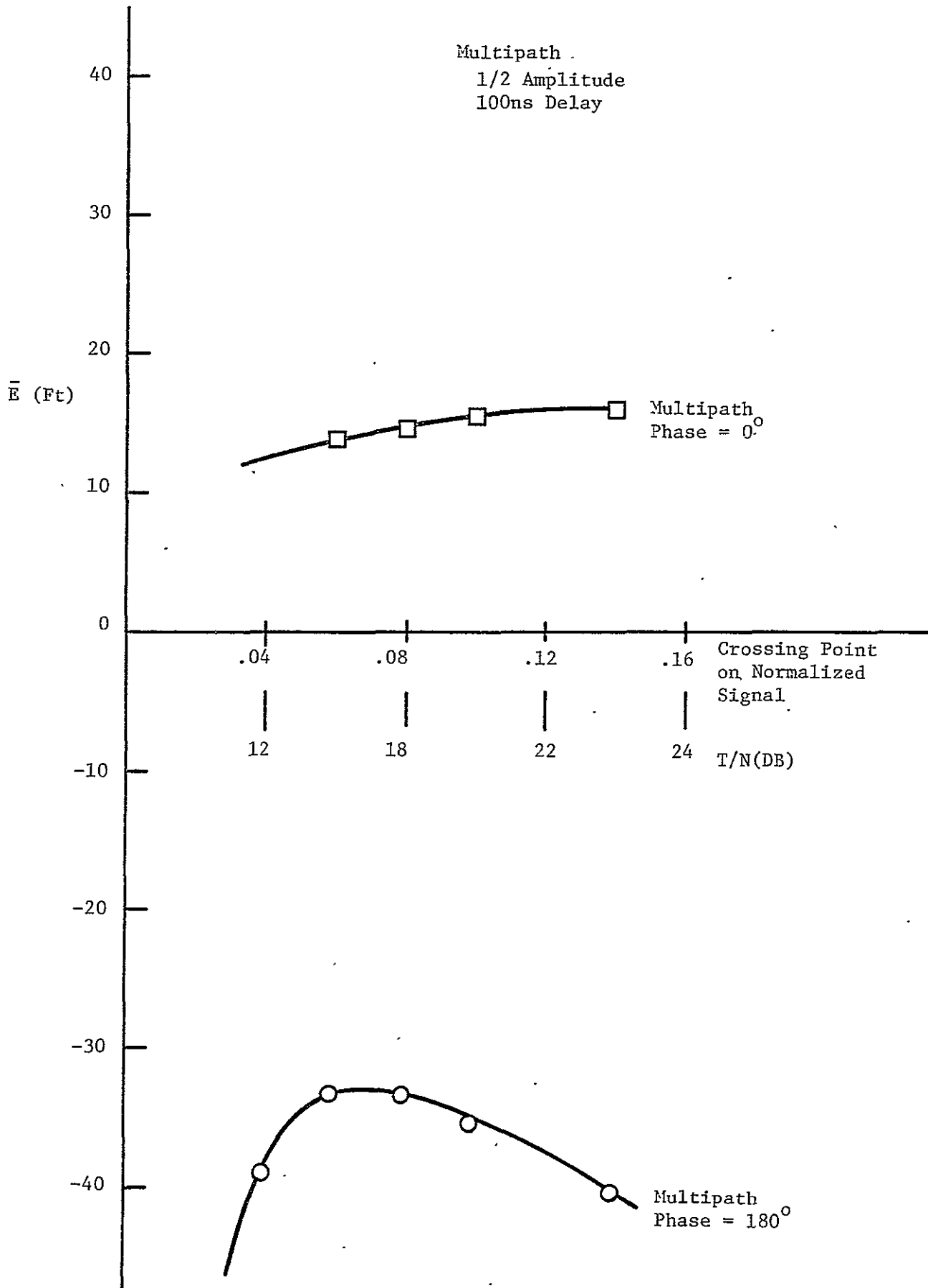


Figure 27 Mean Error Vs. Threshold Crossing Point, Adaptive Threshold Receiver, S/N = 40 DB

Multipath and noise are not necessarily the primary causes of error for this receiver as they were for the delay and compare and fixed threshold receivers. Any loss of signal strength can potentially cause large errors due to the multiplication of the noise level by the AGC. This dictates the investigation of a somewhat larger range of threshold levels than in previous receivers.

11.2 Changes in the Signal to Noise Ratio

The shift in the error bias due to a 6 DB drop in the signal to noise ratio is about 24 feet at a threshold level of 15.5 DB (Figure 28). This is a larger shift than any encountered in the two transponder receivers. As the threshold level is raised the shift decreases and finally reaches a value of about 2 feet at the 23 DB level. This suggests that the increased penalties in error bias incurred at the higher threshold levels may be offset by less sensitivity to signal degradation.

11.3 Multipath Effects

When the multipath delay is increased with all other factors remaining constant, the error increases to a peak at about 300 ns (Figure 29). The adaptive threshold receiver is therefore sensitive to a larger range of multipath delays than either the fixed threshold or the delay and compare receiver.

For multipath delays between 0 and 300 ns, the peak value of the pulse is approximately constant and as a result the AGC compensation is the same throughout this range. The effect on the leading edge of the pulse, however, is greatly dependent on the multipath delay

Multipath
1/2 Amplitude
180° Phase
100ns Delay

Nominal S/N = 46 DB

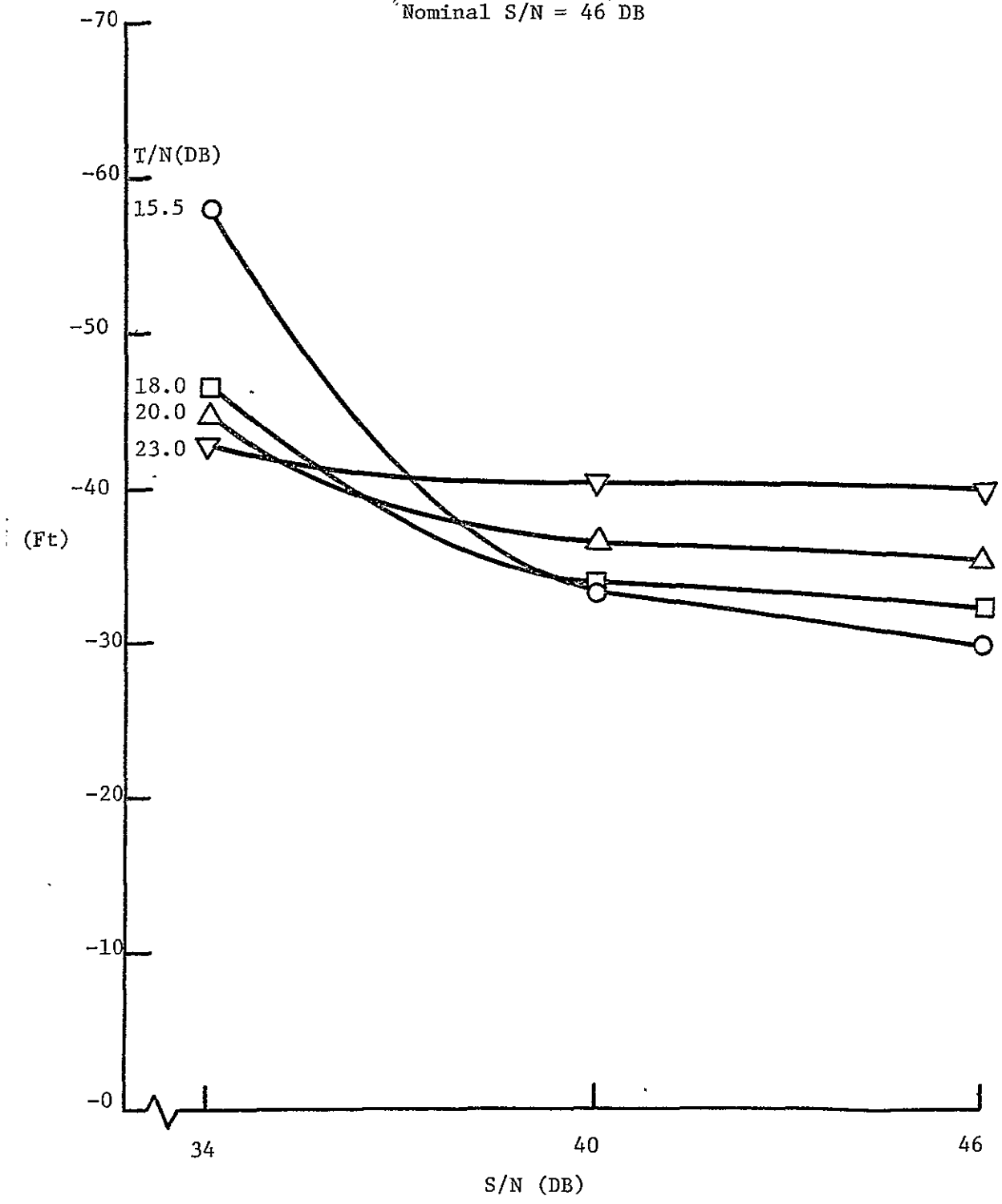


Figure 28 Mean Error Vs. S/N, Adaptive Threshold Receiver

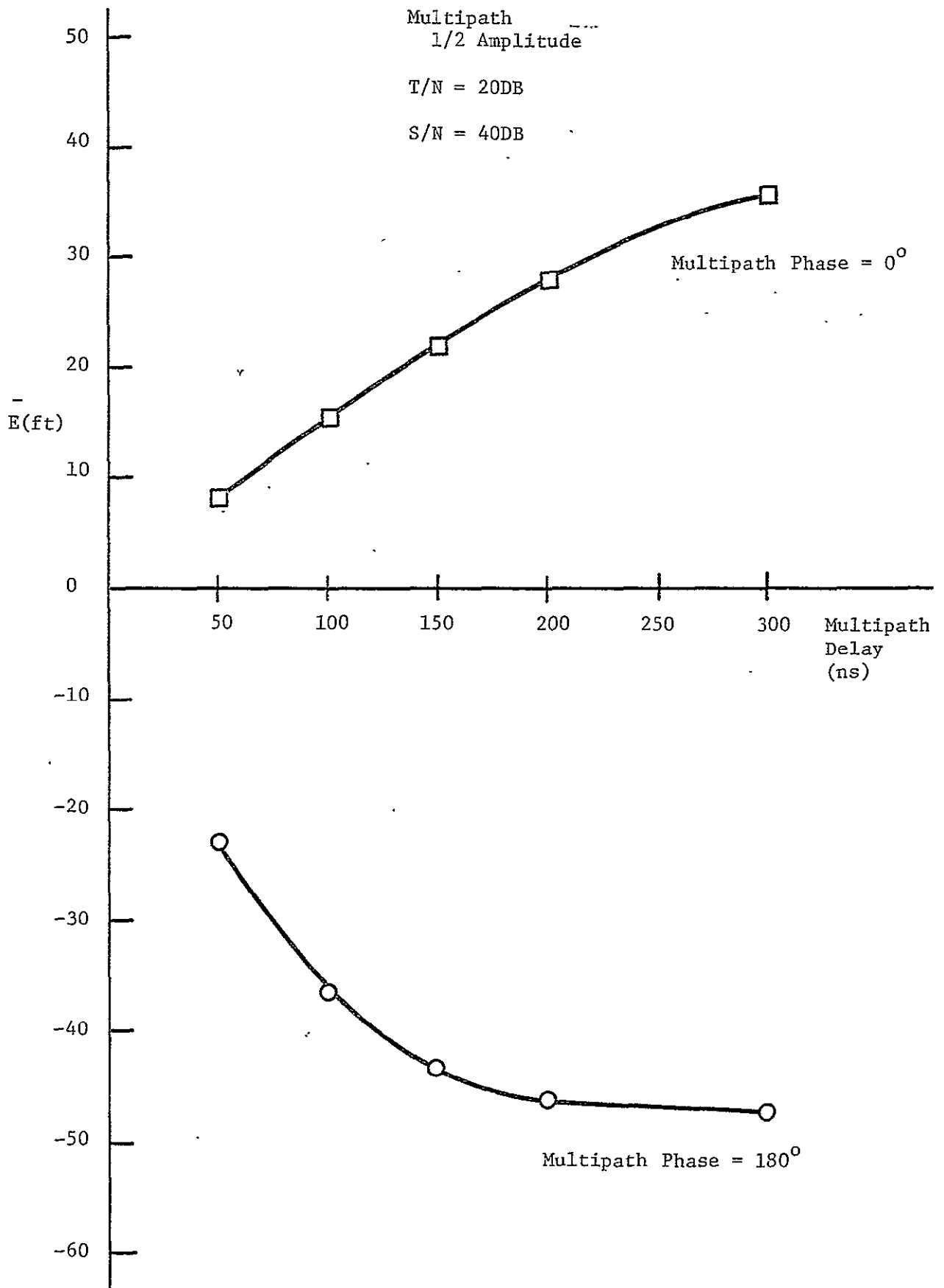
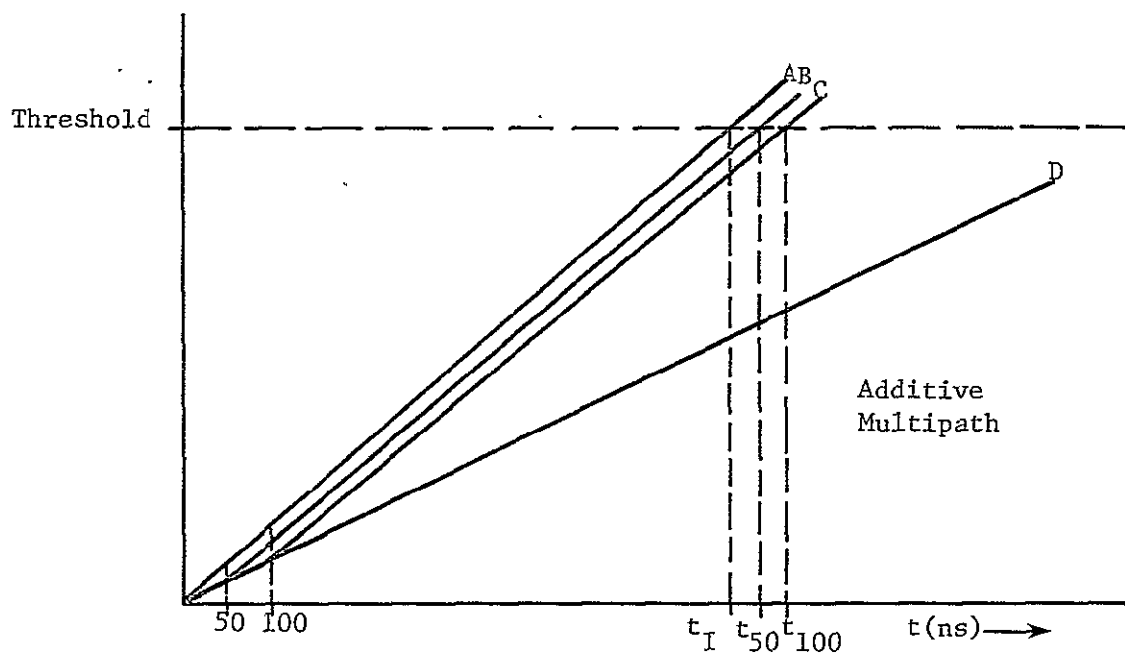
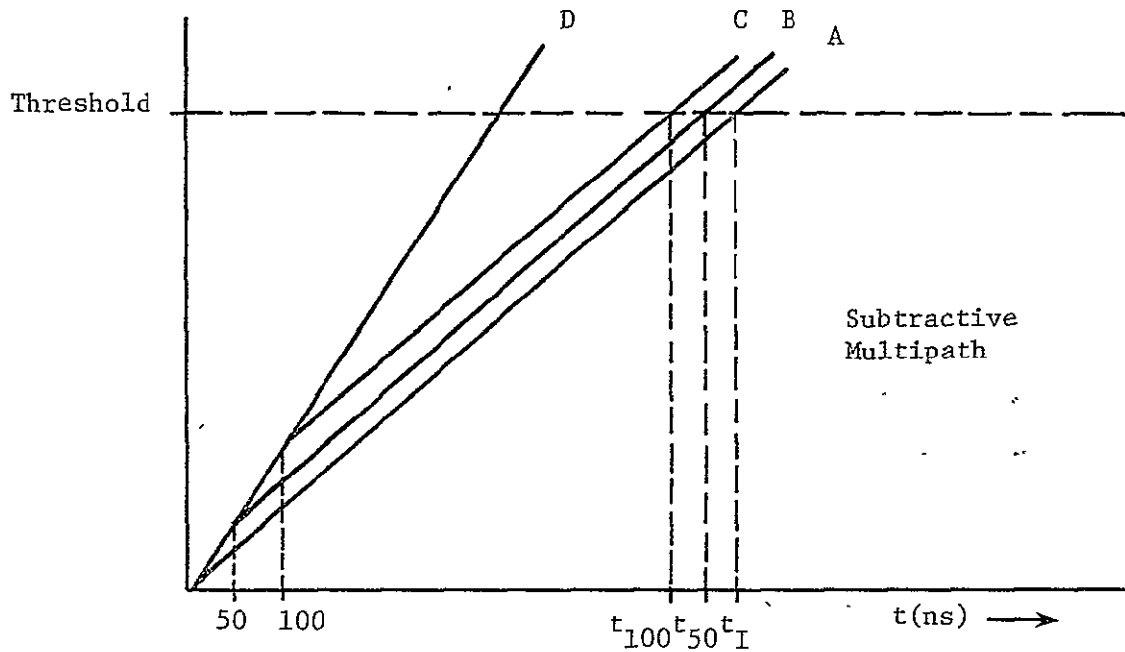


Figure 29 Mean Error Vs. Multipath Delay, Adaptive Threshold Receiver

and the AGC compensation. The first portion of the leading edge is unaffected by the multipath so that when the AGC normalizes the pulse, it either sharpens or flattens this part of it. This causes the threshold crossing time to be pushed either backward or forward, respectively, from the ideal crossing time (Figure 30). This effect increases as multipath delay increases and the direction of the error shift is dependent only on the phase of the multipath.



t_I - Ideal Threshold Crossing Time
 t_{50} - Crossing Time for 50 ns Multipath and AGC
 t_{100} - Crossing Time for 100 ns Multipath and AGC

- A - Direct Signal with No AGC
- B - Signal with 50 ns Multipath and AGC
- C - Signal with 100 ns Multipath and AGC
- D - Direct Signal with AGC

Figure 30 Shift in Threshold Crossing Time with Multipath Delay, Adaptive Threshold Receiver

T/N = 20DB
 Nominal S/N = 40 DB

<u>Multipath Phase:</u>		0°		0°		180°		180°	
<u>Multipath Delay:</u>		100 ns		200 ns		100 ns		200 ns	
<u>Multipath</u>	<u>S/N</u>	<u>\bar{E} (Ft)</u>	<u>σ (ft)</u>	<u>\bar{E} (Ft)</u>	<u>σ (Ft)</u>	<u>\bar{E} (Ft)</u>	<u>σ (Ft)</u>	<u>\bar{E} (Ft)</u>	<u>σ (Ft)</u>
<u>Amplitude</u>	<u>(DB)</u>								
0.2	40	7.8	3.2	12.3	3.2	-10.8	4.5	-15.9	3.9
0.2	34	6.9	6.5	11.2	6.2	-12.7	9.2	-17.8	8.4
0.5	40	15.8	2.6	27.9	2.8	-36.6	6.1	-46.2	5.2
0.5	34	15.4	5.3	26.5	5.2	-44.3	15.1	-53.7	12.7
0.8	40	21.2	2.2	38.6	2.2	-92.5	13.3	-97.9	12.4
0.8	34	21.0	4.4	37.9	4.4	-130.4	29.3	-135.5	27.3

Table 8 Summary of Errors - Interrogator, Adaptive Threshold Receiver

SECTION XII

SIMULATION RESULTS - INTERROGATOR DELAY AND COMPARE RECEIVER

The delay and compare receiver used in the interrogator is identical to that used in the transponder. The conditions under which it operates are different, however, and are outlined in the ground-to-air power budget.

12.1 Threshold Crossings

The increased noise level in the interrogator results in a larger region where noise is the dominant source of error (Figure 31). The minimum error bias with respect to both noise and multipath occurs in the 0.13 to 0.17 level range on a normalized pulse which translates into a range of threshold to noise ratios between 22 and 25 DB.

12.2 Changes in the Signal to Noise Ratio

A 6 DB drop in the signal to noise ratio causes an increase in the error bias of 9 to 12 ft. depending on the threshold level (Figure 32). This degradation in performance is caused by an increase in noise errors. A 6 DB gain in the signal to noise ratio results in a slight improvement in each case.

12.3 Multipath Effects

The error caused by multipath in the delay and compare receivers under these conditions is larger than it is in the transponder. The higher threshold levels that are necessary here are the reason for this, making multipath and noise errors the major constituent in the combined error.

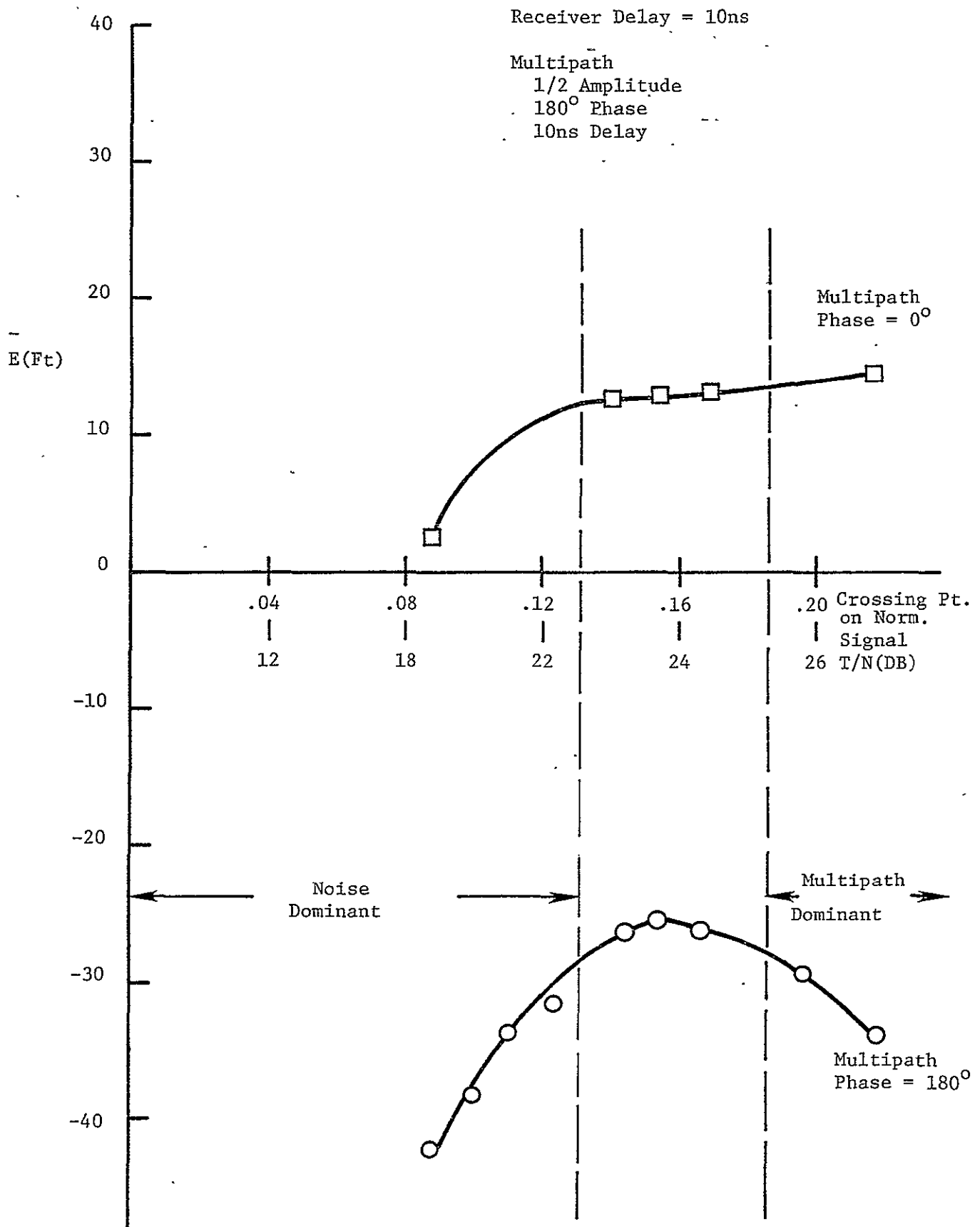


Figure 31 Mean Error Vs. Threshold Crossing Point, Delay and Compare Receiver, S/N = 40DB

Receiver Delay = 10ns

Multipath
1/2 Amplitude
180° Phase
100ns Delay

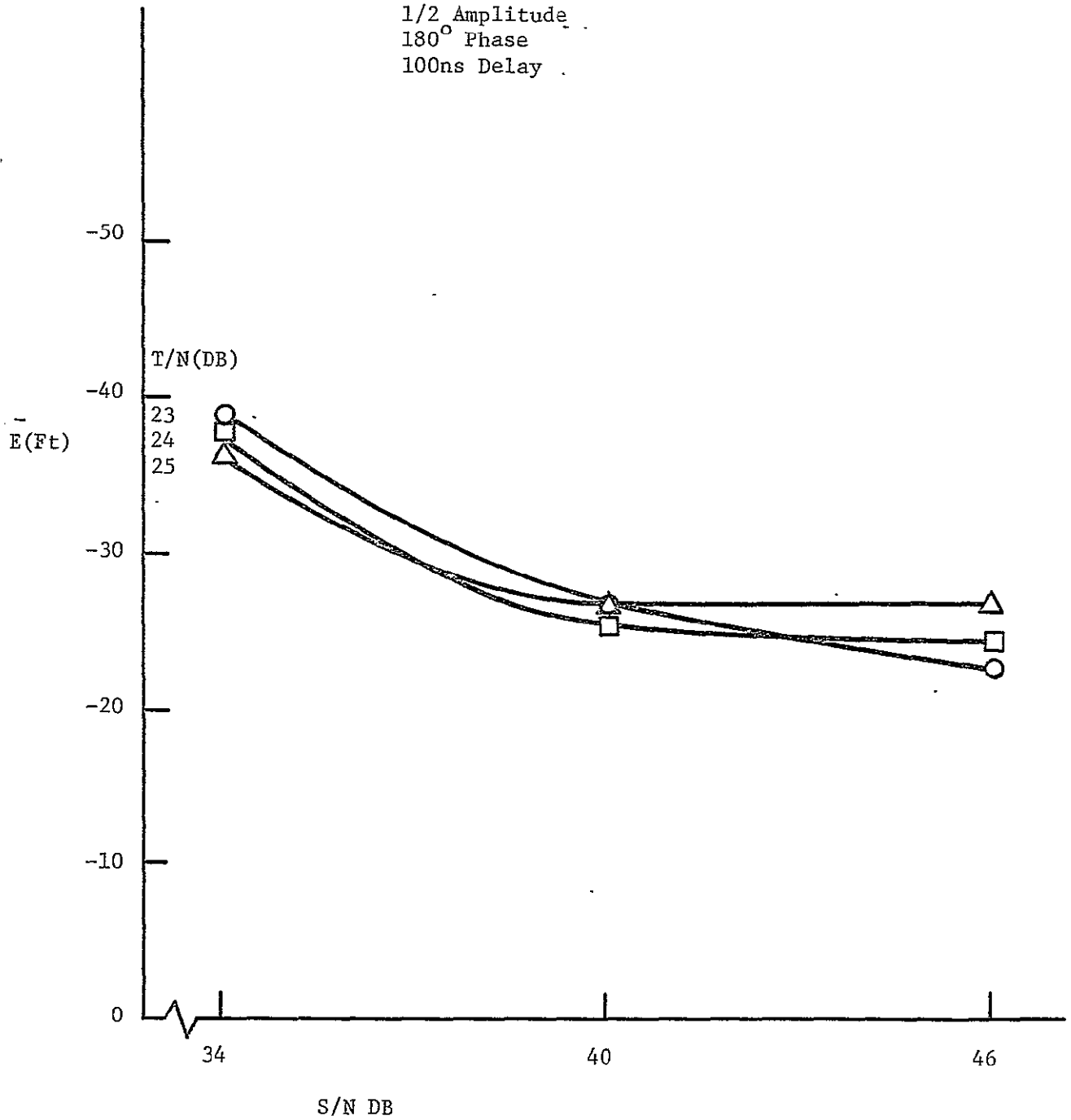


Figure 32 Mean Error Vs. S/N, Delay and Compare Receiver, Nominal S/N = 40DB

Multipath errors peak at delay times of approximately 100 ns for threshold levels between 23 and 25 DB (Figure 33). One would expect a shift of the peak point to shorter delay times and an increase in error at lower thresholds as in the delay and compare transponder.

0-2

Receiver Delay = 10ns

Multipath
1/2 Amplitude
180° Phase

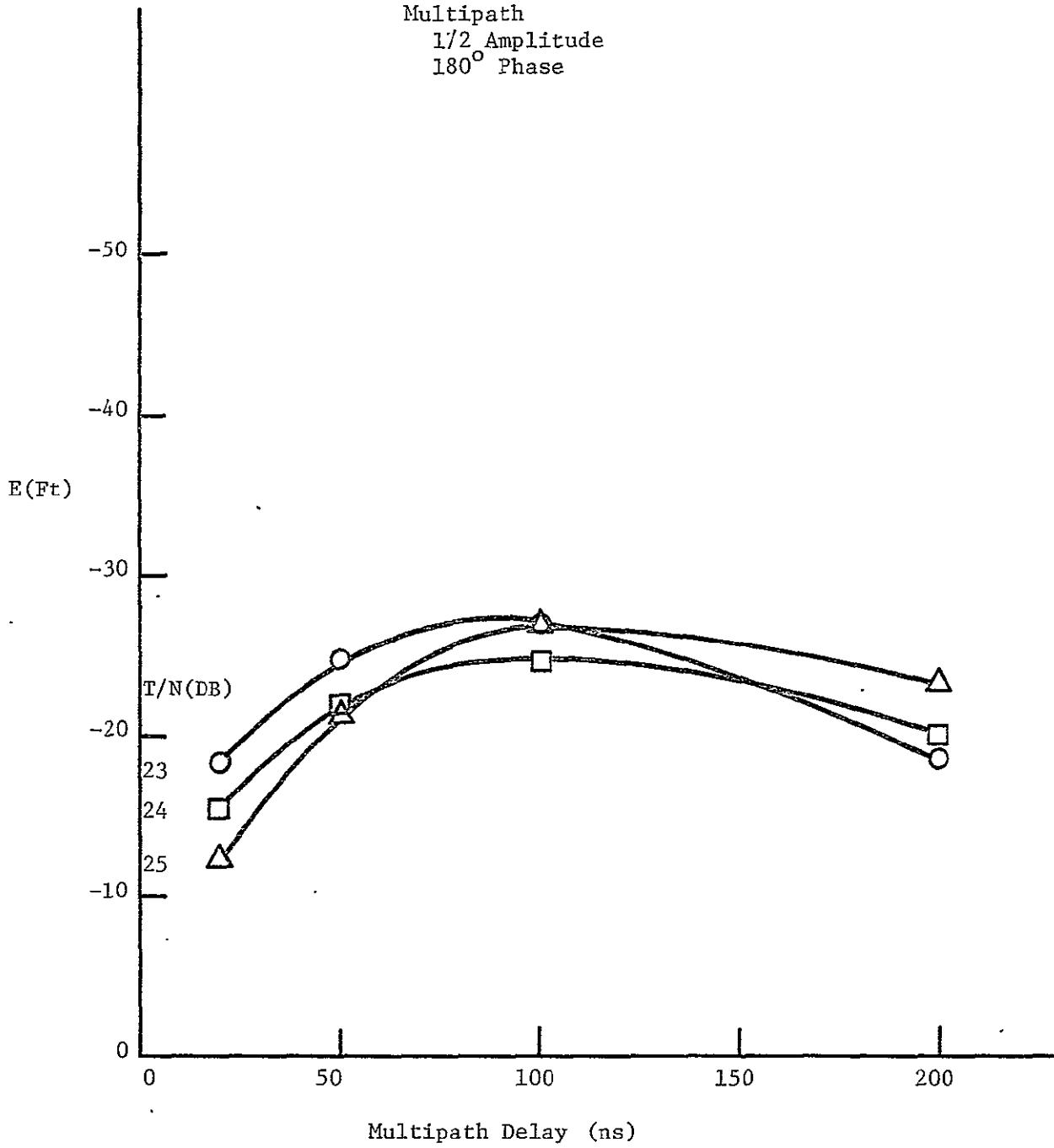


Figure 33 Mean Error Vs. Multipath Delay, Delay and Compare Receiver, S/N = 40 DB

Receiver Delay $\gamma = 10\text{ns}$

T/N = 25 DB

Nominal S/N = 40 DB

<u>Multipath Phase:</u>		0°		0°		180°		180°		
<u>Multipath Delay:</u>		100ns		200ns		100ns		200ns		
<u>Multipath</u>	<u>S/N</u>	<u>\bar{E} (Ft)</u>	<u>σ (Ft)</u>	<u>\bar{E} (Ft)</u>	<u>σ (Ft)</u>	<u>\bar{E} (Ft)</u>	<u>σ (Ft)</u>	<u>\bar{E} (Ft)</u>	<u>σ (Ft)</u>	
<u>Amplitude</u>	<u>(DB)</u>									
100	0.2	40	5.8	5.4	8.0	6.0	-9.9	7.1	-10.3	6.2
	0.2	34	3.0	11.3	4.4	12.7	-14.2	17.9	-14.2	16.2
	0.5	40	13.6	4.5	21.0	5.5	-27.3	8.8	-23.2	6.1
	0.5	34	11.4	9.1	17.5	11.4	-36.4	23.2	-29.1	17.6
	0.8	40	19.2	3.8	32.3	4.7	-54.4	16.0	-34.6	5.9
	0.8	34	17.5	7.5	29.2	9.8	-58.0	29.6	-43.7	20.5

Table 9 Summary of Errors - Interrogator, Delay and Compare Receiver

SECTION XIII

OVERALL STUDY CONCLUSIONS

Angle-Receiver Study

The integrated LOE/Kalman filter receiver algorithm tested in simulation as generally superior to the threshold receiver. Specifically, in the crossing-multipath scenario, primarily a test of tracking performance, improvement ratios (in peak absolute error) ranged to 20:1 and better in certain situations involving high multipath interference. In the in-beam multipath and representative landing scenarios the optimal receiver superiority was confirmed, though less dramatically, partly because of the element of multi-path acquisition present in these runs.

A distinct disadvantage of the optimal receiver is its complexity. The non-adaptive receiver (of the same structure), evaluated as a suboptimal alternative, retained some of the superiority of the optimal receiver in multipath environments at a fraction of the computational demand. This suggests a carefully drawn compromise of performance and complexity might result in a computationally more efficient algorithm offering most of the principal benefits of the optimal receiver demonstrated. This problem area along with multipath acquisition (identification) have been included in our plans for next year's effort.

DME Study

Under the assumed operating conditions of the transponder, the fixed threshold receiver seems to provide marginally better performance

than the delay and compare receiver. The fixed threshold receiver can have considerable immunity to both multipath and noise effects if the noise level is relatively low and the threshold is set at the proper point above this level. A disadvantage of this receiver is its sensitivity to changes in S/N which may be caused by specular reflections, receiver to receiver gain variations, and other causes. The delay and compare receiver has an inherent automatic gain control and is insensitive to these effects.

The adaptive threshold receiver used in the interrogator performs poorly under any condition which reduces the input signal amplitude. The AGC under these conditions multiplies the noise level and increases noise errors. The AGC also causes this receiver to be susceptible to multipaths with a large range of differential path delays. The delay and compare receiver with its inherent AGC can provide performance superior to the adaptive threshold receiver under all of these conditions.

REFERENCES

1. G. A. McAlpine, J. H. Highfill, III, S. H. Irwin, Jr., J. E. Padgett, "Optimization of MLS Receivers for Multipath Environments," Report No. EE-4033-101-75, Research Laboratories for the Engineering Sciences, School of Engineering and Applied Science, University of Virginia, Charlottesville, Virginia, December 1975.
2. G. A. McAlpine, J. H. Highfill, III, "Optimization of MLS Receivers for Multipath Environments," Report No. EE-4033-102-76, Research Laboratories for the Engineering Sciences, School of Engineering and Applied Science, University of Virginia, Charlottesville, Virginia, March 1976.
3. G. A. McAlpine, J. H. Highfill, III, S. H. Irwin, Jr., "Optimization of MLS Receivers for Multipath Environments," Report No. UVA/528062/EE76/102, Research Laboratories for the Engineering Sciences, School of Engineering and Applied Science, University of Virginia, Charlottesville, Virginia, December 1976.
4. James T. Murphy, Jr., "Locally Optimum Estimation with Applications to Communications Theory," Ph.D. dissertation, University of Florida, 1968.
5. D. A. Shnidman, J.E. Evans, "Multipath Characteristics of AWOP WG-A Multipath Scenarios," Massachusetts Institute of Technology, March 31, 1976.
6. C. A. Palmieri, "Evaluation of L-Band DME for MLS", Report No. 11083, Hazeltine Corporation, Greenlawn, N.Y., February 20, 1976.
7. Richard S. Orr, "Multipath Performance of MLS DME Candidates" ATC Working Paper No. 44WP-5029 Lincoln Laboratory, Massachusetts Institute of Technology, March 31, 1976.
8. C. J. Hirsch, "L-Band DME for the Microwave-Landing System", Systems Research and Development Service, Federal Aviation Administration, Contract No. W1-71-3086-1, February 1972.
9. S. O. Rice, "Mathematical Analysis of Random Noise," From Bell System Technical Journal, Vols. 23 and 24; included in "Selected Papers on Noise and Stochastic Processes", Edited by N. Wax, Dover Publications, Inc., New York, 1954.
10. C. J. Hirsh, "Experimentation for Use of L-Band DME With the Microwave Landing System", Systems Research and Development Service, Federal Aviation Administration. Contract No. W1-74-1245-1, April 1974.

APPENDIX A

(164)

PRECEDING PAGE BLANK NOT FILMED

ANGLE-RECEIVER INNOVATIONS STUDY

In the scan data processor, new observations data are entered via a random process represented by the J-vector $w(u|q)$ with representative element w_j , defined in (3.25), and repeated here with index j suppressed:

$$w \triangleq \frac{u}{\sqrt{1 + qu}} \quad -1 \quad (A.1)$$

where

$$u \triangleq q + 2n_c \sqrt{q + n_c^2 + n_s^2} \quad (A.2)$$

$$q \text{ is a real number } \geq 0 \quad (A.3)$$

$$n_c, n_s \text{ are independent Gaussian random variables with mean } 0, \text{ variance } 0.5 \quad (A.4)$$

The results of a simulation study of the first and second-order statistics of w (A.1) are given in Table A.1. The sample size was 1000 points; the quantity RI in the table is an independent variable equivalent to twice the q parameter in (A.1) above. The autocorrelations shown are really values of the sample correlation coefficient, having been normalized to the appropriate sample mean square value.

Conclusions drawn are as follows:

1. The sample mean (MEAN) is much less than the sample rms value (WRMS) for all 5 RI values used and also it seems, as a random variable, to be well dispersed about zero; hence, it seemed plausible that

$$\langle w|q \rangle = 0, \text{ independent of } q \quad (A.5)$$

and this conclusion was drawn.

2. The sample correlation coefficients for non-zero shifts are much less than unity for all 5 RI values used, suggesting that a sequence of w -values with q fixed is a white process; the whiteness property was assumed to extend to the more general non-fixed q case.

1000 POINT SAMPLE					
RJ-	0.0000000	0.1000000	1.0000000	10.0000000	100.0000000
MFAN-	0.0113773	-0.0362046	0.0034937	0.0198567	-0.0053797
WMS-	1.0740432	0.7874628	0.5339779	0.0904930	-0.0093178
WRMS-	1.0363606	0.8873910	0.7307379	0.3008206	0.0967359

SHIFT AND AUTOCORRELATION

0	1.0000000	1.0000000	1.0000000	1.0000000	1.0000000
1	-0.0270604	-0.0272451	0.0415108	0.0627663	0.0012036
2	0.0478279	-0.0679387	-0.0244034	0.0239389	0.0348052
3	0.0028992	0.0148117	-0.0160504	-0.0339244	-0.0044730
4	0.0213317	-0.0272186	-0.0107524	0.0331980	-0.0058701
5	-0.0316544	0.0182481	-0.0043104	0.0054010	-0.0081583
6	0.0138999	0.0227231	-0.0268710	0.0447955	0.0108709
7	-0.0438014	0.0190700	0.0149515	0.0481430	-0.0353028
8	-0.0027386	0.0175632	-0.0074245	-0.0274951	0.0262319
9	-0.0559775	0.0175616	-0.0318451	0.0718726	-0.0420408
10	-0.0162943	0.0149989	-0.0301198	0.0332770	-0.0002008
11	-0.0476010	-0.0262103	0.0151127	0.0001841	0.0271018
12	0.0443660	0.0348354	0.0063709	-0.0150879	-0.0143412
13	-0.0267694	-0.0109377	0.0022143	0.0062216	0.0341044
14	0.0180384	0.0174614	0.0707840	0.0253326	-0.0030641
15	-0.0100571	0.0275735	-0.0063971	0.0031010	-0.0289168
16	0.0665258	0.0020313	0.0091793	0.0078576	-0.0077510
17	-0.0235868	0.0398531	0.0298906	-0.0053596	0.0280460
18	-0.0107038	0.0168095	-0.0266094	0.0101925	-0.0133703
19	0.0065942	0.0194152	0.0006231	-0.0324720	0.0200613
20	0.0236151	-0.0338185	0.0031682	-0.0120829	0.0173313

Table A.1 First-and Second-Order Sample Statistics of w.

ORIGINAL PAGE IS
OF POOR QUALITY

4-3

The further observations, concerning the sample mean square value (WMS), that

1. $WMS \approx 1$, for $RI = 0$
2. $WMS \approx \frac{1}{RI}$, for RI large

suggested a tentative approximation formula, in terms of q , as follows:

$$\langle w^2 | q \rangle \triangleq h(q) \approx \frac{1}{1 + 2q} \quad (A.6)$$

The results of a more extensive simulation, involving 10,000 samples and values of q ($= \frac{RH0}{2}$) from 0 to 50 (corresponding to $S/N = 34\text{db}$), are shown in Table A.2 and in Figures A.1 and A.2, comparing plots of the sample mean square value and the approximation (A.6). The error in the approximation peaks at about 20% for $q = 2$ ($RH0 = 4$) and seems in an average sense to be asymptotic to zero for smaller and larger values of q . The approximation (A.6) was employed in the scan data processor with good results.

N=10000	RHO	WMEAN	WMS	HAPPROX	ERROR	FRAC. ERR.
	0.000000	0.009305	1.001360	1.000000	0.001360	0.001360
	0.100000	-0.012796	0.908855	0.909091	-0.000236	-0.000260
	0.126000	0.004004	0.870778	0.888099	0.017321	0.019504
	0.158000	0.009553	0.874085	0.863558	0.010527	0.012190
	0.200000	0.006881	0.863670	0.836633	0.030337	0.036405
	0.251000	0.004705	0.840683	0.799460	0.041322	0.051694
	0.316000	0.006111	0.760954	0.759078	0.001076	0.001416
	0.400000	-0.002090	0.722546	0.714286	0.008260	0.011564
	0.500000	0.023802	0.715980	0.666667	0.049321	0.073982
	0.631000	0.008241	0.654265	0.613121	0.041144	0.062706
	0.797000	0.021374	0.624964	0.555483	0.069481	0.123060
	1.000000	0.013065	0.513909	0.500000	0.053909	0.107818
	1.260000	0.021621	0.501466	0.442478	0.058988	0.133314
	1.580000	0.022029	0.444415	0.387597	0.056818	0.146591
	2.000000	0.032890	0.385830	0.336633	0.052496	0.157489
	2.510000	0.033994	0.331448	0.284900	0.046548	0.163382
	3.160000	0.026900	0.284580	0.240385	0.043995	0.183021
	4.000000	0.032815	0.238072	0.200000	0.038079	0.190397
	5.000000	0.046330	0.190665	0.166667	0.023998	0.143990
	6.310000	0.046346	0.158290	0.136799	0.021491	0.157097
	7.970000	0.029785	0.124781	0.111483	0.013298	0.119284
	10.000000	0.030040	0.095069	0.090909	0.007160	0.078760
	12.600000	0.023735	0.081435	0.073539	0.007905	0.107515
	15.800000	0.026278	0.063646	0.059524	0.004122	0.069255
	20.000000	0.020595	0.050599	0.047519	0.002980	0.062571
	25.100000	0.017782	0.038760	0.038614	0.000446	0.011634
	31.600000	0.014009	0.031787	0.030675	0.001112	0.036250
	40.000000	0.013242	0.025283	0.024390	0.000893	0.036601
	50.000000	0.007723	0.019840	0.019608	0.000232	0.011848
	63.099998	0.008502	0.015699	0.015601	0.000099	0.006315
	79.699997	0.003263	0.012350	0.012392	0.000042	0.003384
	100.000000	0.005247	0.010000	0.009901	0.000099	0.010004

Table A.2 Tabulation of WMS and H_{approx} versus RHO (= 2q).ORIGINAL PAGE IS
OF POOR QUALITY

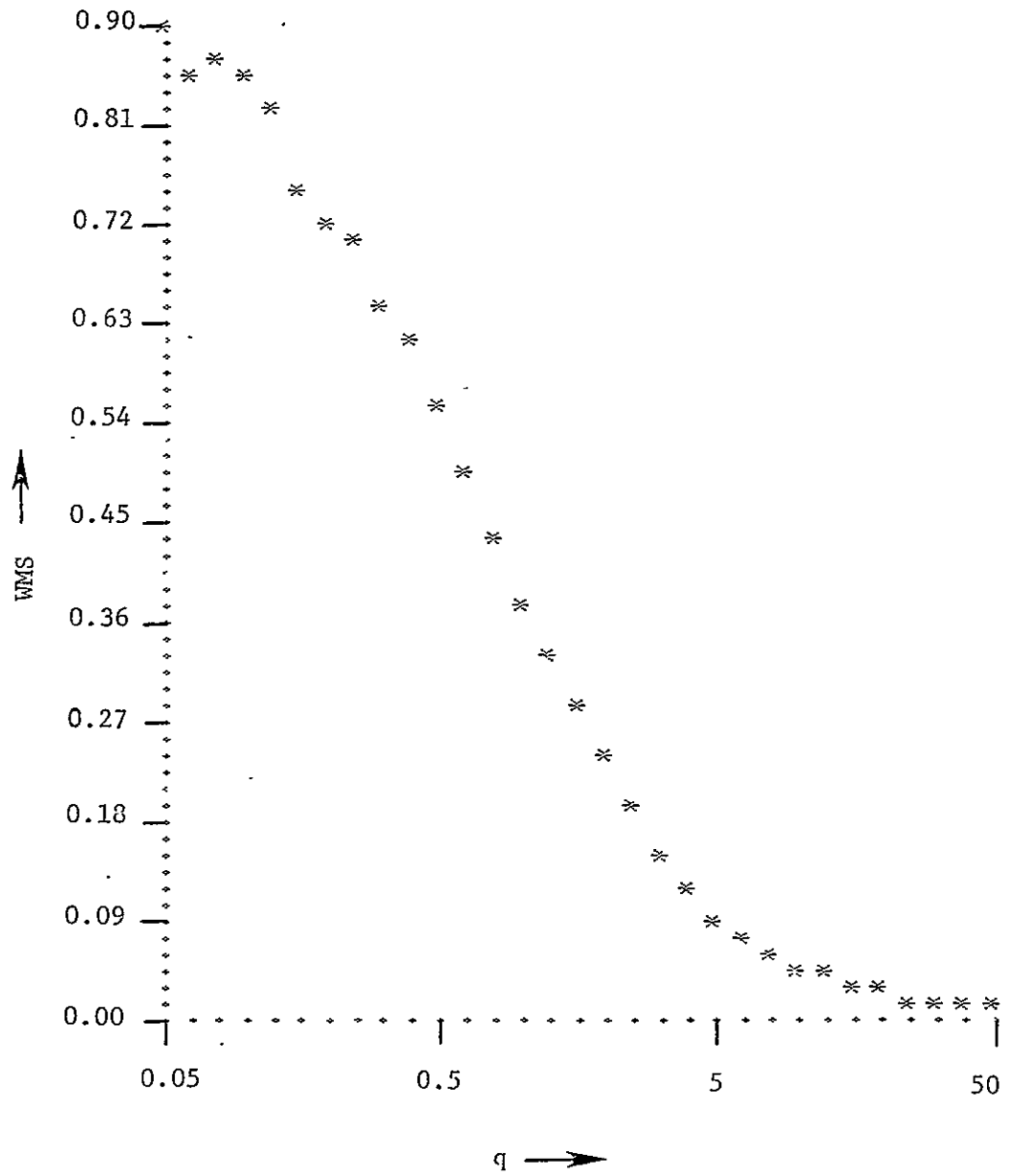


Figure A.1 Sample Mean Square of w versus q.

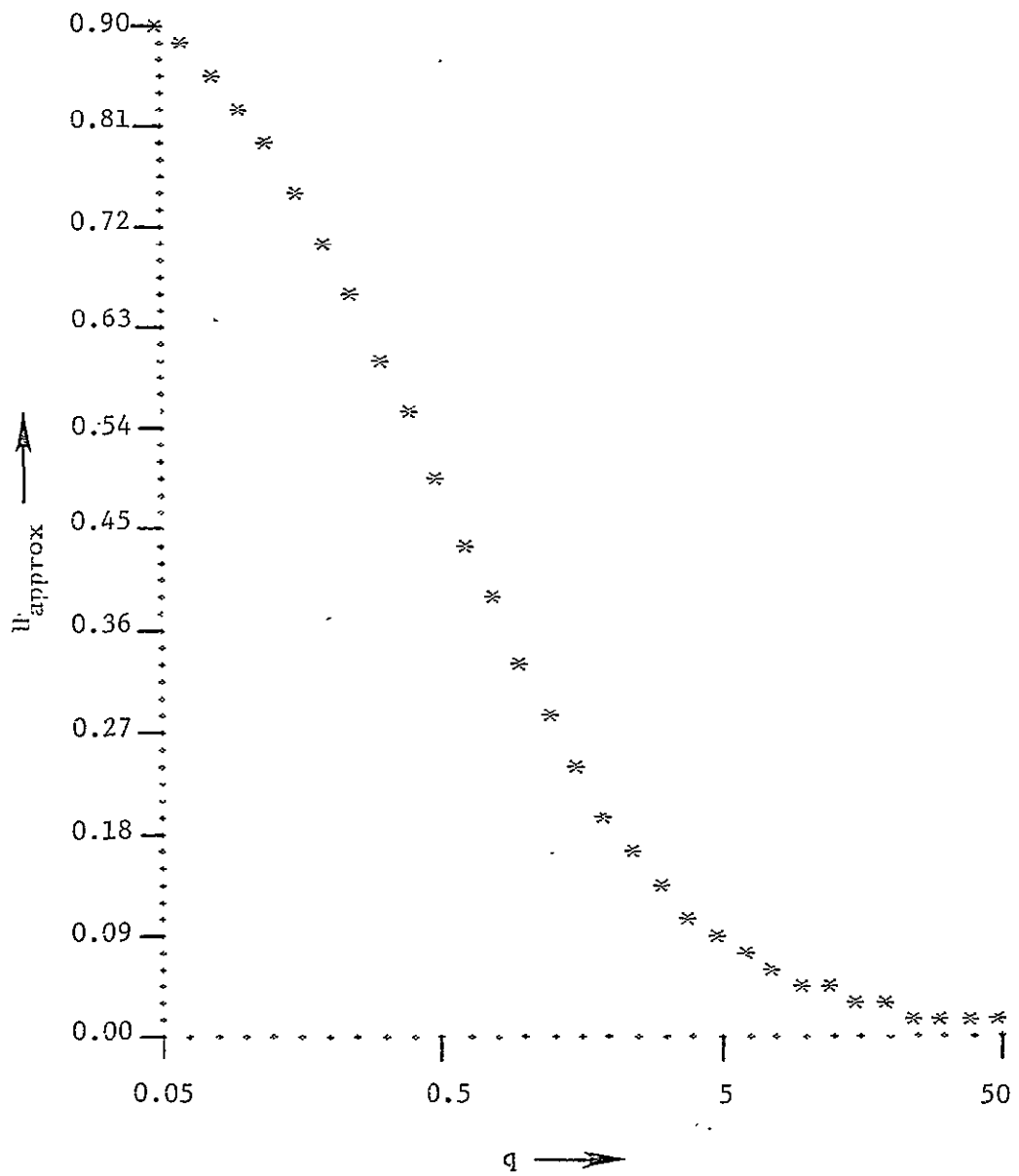


Figure A.2 Plot of $H_{\text{approx}}(q)$.

APPENDIX B

(A8)

PRECEDING PAGE BLANK NOT FILMED

ADAPTIVE KALMAN FILTERING APPLIED TO AIRCRAFT POSITION ESTIMATION

A Thesis

Presented to

the Faculty of the School of Engineering and Applied Science

University of Virginia

In Partial Fulfillment

of the Requirements for the Degree

Master of Science (Electrical Engineering)

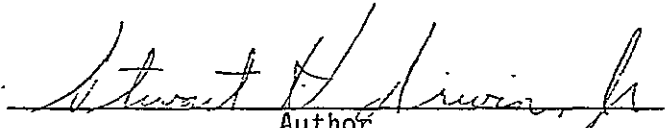
by

Stewart H. Irwin, Jr.

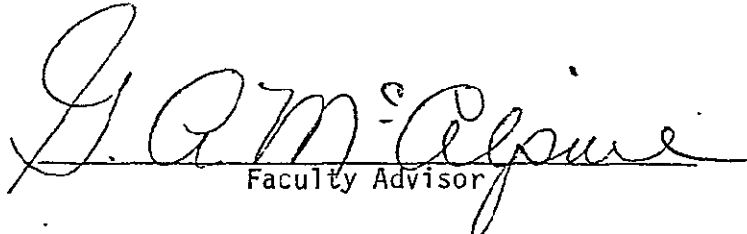
August 1977

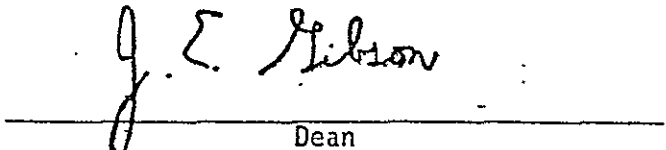
APPROVAL SHEET

This thesis is submitted in partial fulfillment of
the requirements for the degree of
Master of Science in Electrical Engineering


Author

Approved:


Faculty Advisor


Dean
School of Engineering and Applied Science

August 1977

ABSTRACT

This paper addresses an estimation problem in which a landing aircraft uses ground-transmitted microwave information to determine its azimuth angular position $\theta(t)$ relative to a fixed reference. State estimation is used to lower the mean-square error in estimates of $\theta(t)$ produced by an envelope processor in the airborne receiver. $\theta(t)$ is modeled as part of the state of a linear dynamic system driven by white Gaussian noise of unknown covariance. The envelope processor estimates become linear observations of the state corrupted by additive Gaussian noise of known covariance. Adaptive Kalman filtering is examined as a means of computing estimates of $\theta(t)$ having minimum mean-square error. Adaptive filtering methods are found in the technical literature which work for systems where the noise is stationary. They are then modified for use in the aircraft position estimation problem, where the noise statistics are time varying. The adaptive filters are tested in a digital computer simulation, where $\theta(t)$ is updated according to aircraft motion along an unknown flightpath. Several of the adaptive filters work very well, though not significantly better than suboptimal estimators of less complexity.

TABLE OF CONTENTS

	<u>PAGE</u>
ABSTRACT	i
LIST OF SYMBOLS	iv
LIST OF FIGURES	vi
 <u>CHAPTER</u>	
I. INTRODUCTION	1
Background on Microwave Landing System	1
Thesis Overview	6
II. PROBLEM DEFINITION AND MODEL DEVELOPMENT	8
Problem Definition	8
Stochastic Model	11
III. THE DISCRETE KALMAN FILTER	16
IV. ADAPTIVE KALMAN FILTERING: THE STATIONARY NOISE CASE	29
The Innovations Sequence	30
The Method of Sage and Husa	37
The Method of Magill	51
The Method of Alspach	56
The Minimum Innovations Covariance Method	64

<u>CHAPTER</u>	<u>PAGE</u>
V. ADAPTIVE KALMAN FILTERING WITH TIME VARYING NOISE STATISTICS	67
The Method of Alspach	67
The Minimum Innovations Covariance Method	71
The Method of Sage and Husa	74
The Method of Magill	76
VI. COMPUTER SIMULATION TESTING	83
The Landing Approach	85
Computer Simulation Structure	93
Simulation Testing: The Stochastic Model Case	96
Simulation Testing: The Deterministic Case	105
VII. CONCLUSION	115
REFERENCES	118

LIST OF SYMBOLS

$E\{\cdot\}$	Expectation operator
$f(k)$	Function describing evolution of $\theta(k)$ for aircraft motion along a given flightpath
H	Observation or measurement matrix
Hz	Hertz
$J(k j)$	Loss function relating the error performance of the state estimate $\hat{x}(k j)$
k	Number of the present azimuth scan period
$K(k)$	Kalman gain
$\hat{K}(k)$	Adaptive Kalman gain
m	Dimension of measurement $y(k)$ in general system model (VI-1)-(VI-4)
n	Dimension of state $x(k)$ in general system model
N	Fading memory constant for computing sample innovations covariance
$N[m, P]$	Denotes Gaussian density function with mean m and covariance P
$p[\cdot]$	Probability density function
$P(k j)$	Error covariance of state estimate $\hat{x}(k j)$
$Q(k)$	State (plant) noise covariance
r	Slant range from azimuth antenna to aircraft
$R(k)$	Measurement noise covariance
t	Time
T	Superscript denoting the transpose of a matrix
$v(k)$	Measurement noise term on k th scan

$W(k)$	Innovations covariance
$\hat{W}(k)$	Sample innovations covariance
$WN[m, P]$	Denotes white Gaussian distribution with mean m and covariance P
$x(k)$	State of general system on k th scan
$\hat{x}(k j)$	Estimate of $x(k)$ based on measurements through $y(k)$
X_k	Set of all past states from $x(1)$ to $x(k)$
$y(k)$	Additively corrupted measurement or observation of the state
Y_k	Set of all past measurements from $y(1)$ to $y(k)$
α	Vector containing unknown elements of Q and R for the stationary noise case
Δt	Time between consecutive measurements (period of azimuth scan update rate)
Γ	Input matrix multiplying state noise term in the general state model (IV-1)
$\theta(k)$	Aircraft's azimuth angle during k th scan period
$\hat{\theta}(k j)$	Estimate of $\hat{\theta}(k)$ based on measurements up to and including $y(j)$
$v(k)$	Innovations residual during k th scan period
ϕ	Aircraft's elevation angle
Φ	State transition matrix in general state model (IV-1)
$\omega(k)$	State noise term on k th scan

LIST OF FIGURES

		<u>PAGE</u>
I-1	Coordinate System; Scanning Beam Boresight; Signal Envelope	3
III-1	Mean-Square Error in $\hat{\theta}(k k)$ vs. Suboptimal Gain	28
IV-1	Innovations Covariance vs. Suboptimal Gain	36
IV-2	$WT(k K)$ vs. $\hat{W}(k K)/W_{MAX}(K)$	62
<u>FLOWCHARTS OF ADAPTIVE KALMAN FILTERING ALGORITHMS</u>		
V-1	The Adaptive Algorithm of Alspach	72
V-2	Modifications to the Block Diagram of Alspach for Implementation of Minimum Innovations Covariance Algorithm	75
V-3	The Adaptive Algorithm of Sage-Husa	77
V-4	The Adaptive Algorithm of Magill	81
VI-1	S-Curve Flightpath Used in the Simulation	87
VI-2	General S-Curve Flightpath	88
VI-3	Flightpath Subroutine	90
VI-4	Azimuth Angle $\theta(t)$ and Derivatives for S-Curve Flightpath	94
VI-5	Main Simulation Flowchart	95
<u>SIMULATION RESULTS: STATE DRIVEN BY WHITE NOISE</u>		
VI-6	Gain \hat{K}_1 vs. Time for Adaptive Filters	99
VI-7	Error in $\hat{\theta}(k k)$ for Different Estimators	101
VI-8	Error in $\hat{\theta}(k k)$ for Adaptive Kalman Filters	102

	<u>PAGE</u>
VI-9	Sample RMS Error in $\hat{\theta}(k k)$ 104
<u>SIMULATION RESULTS: $\theta(k)$ UPDATED DETERMINISTICALLY</u>	
VI-10	Gain \hat{K}_1 for Adaptive Filters 107
VI-11	Error in $\hat{\theta}(k k)$ 108
VI-12	Error in $\hat{\theta}(k k)$ for Adaptive Filters 109
VI-13	Sample RMS Error in $\hat{\theta}(k k)$ 111

CHAPTER I

INTRODUCTION

This paper describes the application of state estimation theory to an aircraft landing problem where the system model is incompletely defined. In general the problem requires estimation of the state of a linear dynamic system driven by white Gaussian noise with unknown covariance. The state is observed by a linear function of the state corrupted by additive white Gaussian noise. When all model parameters are known, the optimal minimum variance estimator becomes the Kalman filter [1, pp. 228-229], [2, pp. 195-201]. However, when the model noise covariances are unknown, the optimal estimator cannot be achieved, and some suboptimal approach must be employed. Several adaptive Kalman filtering methods from the literature are examined in this paper as possible solutions to the aircraft landing problem.

Before giving a formal description of the state estimation problem, let us first provide a background description of the aircraft landing problem. A more rigorous problem definition can then be presented, along with a proposed course of solution.

Background on Microwave Landing System

The problem examined in this paper is part of an airborne receiver study for the Microwave Landing System (MLS). The MLS, developed by the

Federal Aviation Administration (FAA) and the National Aeronautical and Space Administration (NASA), provides electronic guidance in an air terminal area for landing aircraft [3], [4]. The system enables an approaching aircraft to compute its position in space relative to a fixed ground reference. The required coordinate information is derived by the aircraft's receiver from ground-transmitted microwave signals.

Let us establish a cartesian coordinate system, with its origin at the stop end of the runway. Referring to Fig. I-1.A, the runway centerline forms the X axis, while the Z axis is normal to the ground plane. We also establish a spherical reference system centered at the same origin. At time t , the aircraft's position shall be defined by the following spherical coordinates:

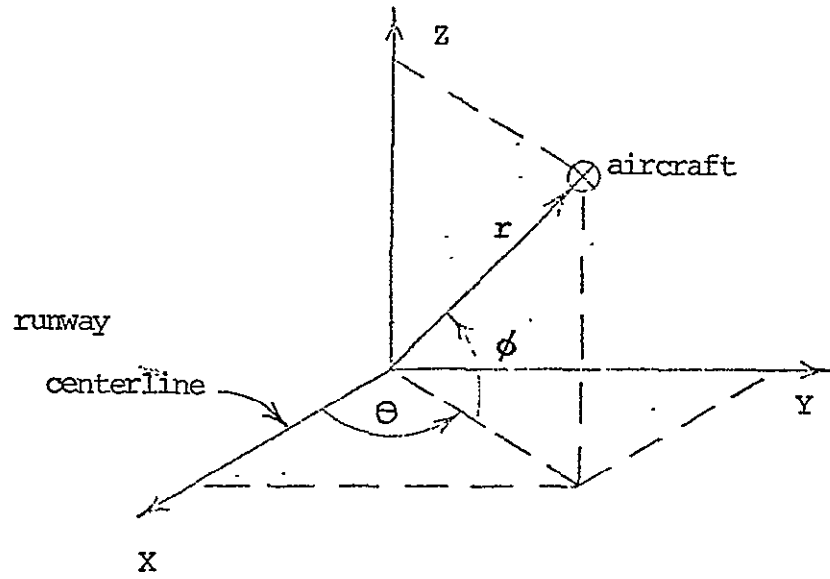
$r(t)$ = direct path distance from the origin to the aircraft.

$\theta(t)$ = azimuth angle from the X axis to the projection onto the ground plane of a ray from the origin to the aircraft.

$\phi(t)$ = elevation angle from the ground plane up to this ray.

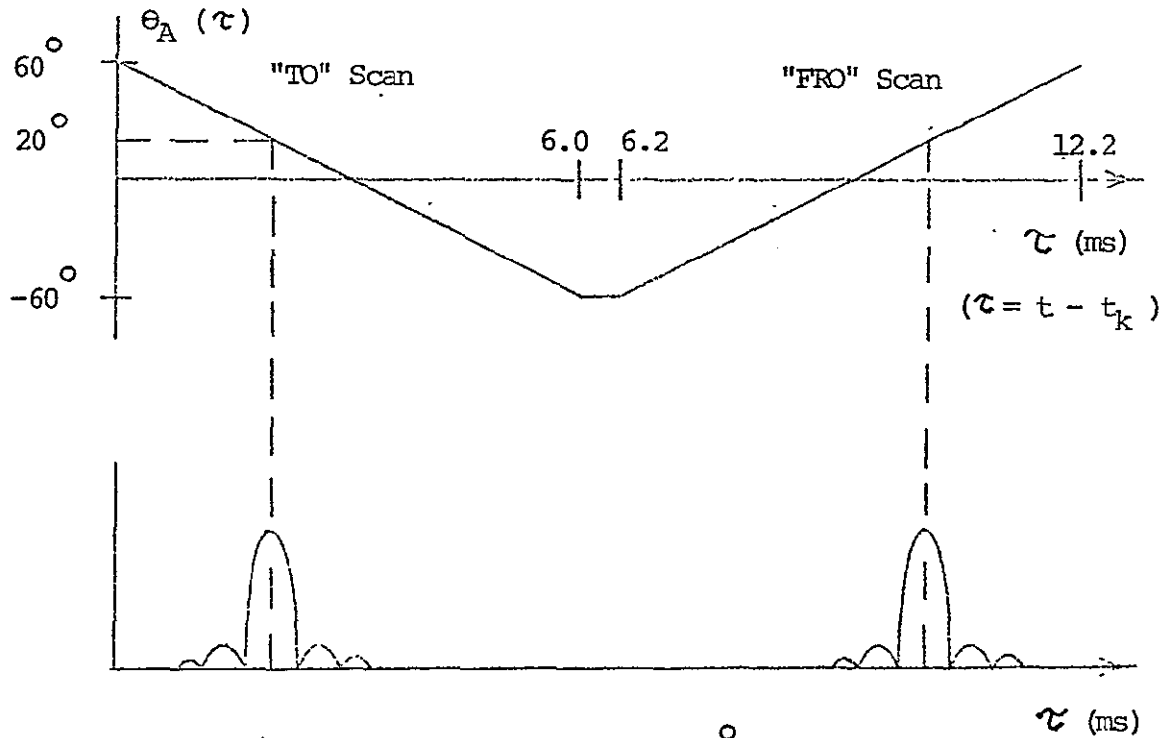
The MLS enables the aircraft to compute these three coordinates. We restrict ourselves in this paper to considering only the azimuth angle $\theta(t)$. First we present a brief description of the azimuth channel in the MLS.

An antenna, located at the coordinate origin, electronically scans a $\pm 60^\circ$ azimuth coverage sector with a narrow fan-shaped microwave beam. The beam is narrow only in the azimuth sense (1° between -3 db points),



A. Coordinate System

B. Scanning Beam Boresight vs. Time



C. Noiseless Signal Envelope for $\theta(t_k) = 20^\circ$

Figure I - 1

while being wide in elevation coverage. The beam is scanned in a "TO-FRO" fashion, as shown in Fig. I-1.B: the beam boresight $\theta_A(t)$ starts at $+60^\circ$ azimuth, moves at constant rate to -60° , holds there for a brief "dead time," and then moves back. This scanning procedure takes 12.2 milliseconds and repeats at a $13 \frac{1}{3}$ Hz update rate [3, pp. I-10, 11, 27].

We define t_k as the time at the start of the k th scanning procedure. We also assume that $\theta(t)$ is constant at $\theta(t_k)$ during the 12.2 millisecond duration of the scan. During this time the scanning beam signal, viewed at the input to a receiver at the aircraft, is amplitude-modulated, having large amplitude when the boresight $\theta_A(t)$ is near $\theta(t_k)$. The envelope-detected signal, shown in Fig. I-1.C, has two pulses: one which peaks when $\theta_A(t) = \theta(t_k)$ during the "TO" scan; and the second which peaks when $\theta_A(t) = \theta(t_k)$ during the "FRO" scan. As seen in Figs. I-1.B, C, the time differential between the centroids of the two pulses is directly related to the value of $\theta(t_k)$. The aircraft can therefore determine its azimuth angle by receiving and envelope detecting the ground-transmitted signal and measuring this time differential.

This scheme for computing $\theta(t_k)$ runs into difficulty when we realize that the received signal is corrupted by front-end noise in the airborne receiver. This front-end noise produces random distortions in the envelope so that any attempt to estimate $\theta(t_k)$ from envelope information will have random errors as well.

An optimal envelope processor has been designed which, given the noise-corrupted signal envelope for the k th scanning interval, computes an estimate of $\theta(t_k)$ which minimizes mean square error. The

envelope-detected IF signal is sampled in the vicinity of the two large pulses during the 12.2 millisecond scanning process. Then, during the "down time," before the next scanning process begins, the envelope samples are sent to a minicomputer. Here a "locally optimum estimation" algorithm computes an estimate of $\theta(t_k)$ [5, pp. 8-29], [6, pp. 4-28, 52-61]. Using a stochastic model for the signal envelope, this algorithm provides an estimate of $\theta(t_k)$, given the envelope samples for the k th scanning process, which is optimal in terms of minimum mean square error.

The optimal envelope processor estimates $\theta(t_k)$ based only upon the envelope samples taken on the k th scanning interval. At a 13 1/3 Hz azimuth update rate, we would expect the effects of thermal noise upon the signal envelope to be independent between consecutive scans. The error in consecutive estimates should therefore be independent as well. On the other hand, the true angle $\theta(t_k)$ cannot change appreciably between scans for a large aircraft. In plotting a time sequence of estimates we therefore expect to see random fluctuations about a slowly changing mean.

Since the estimates change much more rapidly than the true azimuth angle, it seems reasonable that the estimate of $\theta(t_k)$ could be improved by averaging it with past estimate values. This would produce a new estimate based on all past envelope information and not just that obtained on scan k . This is the objective of the work presented in this paper. Adaptive Kalman filtering is examined as a means of producing an estimate of $\theta(t_k)$ having a smaller mean square error than that of the envelope processor estimate.

Thesis Overview

The above-stated problem is presented mathematically in Chapter II, where a stochastic system model is derived. The Kalman filter requires a state variable model, where an n th-order linear dynamic system is driven by white noise of known covariance. We therefore model $\theta(t_k)$ as part of the state of such a system. The discrete Kalman filter is presented in Chapter III as the optimal estimator of $\theta(t_k)$, given the state model of Chapter II. It is also shown that the Kalman filter requires knowledge of the plant noise covariance, which is unknown in our problem model. Adaptive Kalman filtering is therefore studied as a suboptimal estimation approach in which the unknown Kalman gain is estimated from measurement information.

Several candidate adaptive-filtering methods from the literature are presented in Chapter IV. Each filtering scheme is developed under the assumption of stationary noise. In Chapter V we modify each of the candidate filters to work for our specific problem, where the unknown noise covariances are time varying.

The adaptive Kalman filters are tested in digital computer simulation in Chapter VI. This testing proceeds in two stages. First the assumed stochastic model of Chapter II is simulated with additively corrupted measurements of the state sent to a candidate adaptive filter. The error in the filter's estimate $\hat{\theta}(t_k)$ is plotted as a function of time. If a candidate filter performs well here, it is then tested in a second simulation phase where the stochastic model assumption is removed. $\theta(t_k)$ is now updated deterministically as the aircraft moves along a prescribed flight path. Additively corrupted measurements of

$\theta(t_k)$ are again sent to the candidate filter which then computes the estimate $\hat{\theta}(t_k)$. That adaptive filter is sought which minimizes the mean square error in $\hat{\theta}(t_k)$. A conclusion is given in Chapter VII.

CHAPTER II

PROBLEM DEFINITION AND MODEL DEVELOPMENT

In this chapter we offer a more rigorous problem description and then develop a stochastic model describing the evolution of the azimuth angle $\theta(t_k)$. This model is then used in subsequent chapters to develop an estimate of $\theta(t_k)$, based on all past envelope information.

Problem Definition

Before formally describing the estimation problem, we place some mild restrictions on the aircraft's azimuth coordinate and its estimate produced by the envelope processor. We first change notation, using $\theta(k)$ instead of $\theta(t_k)$ to represent the azimuth coordinate at the start of the k th scanning interval.

Let us assume that the aircraft is making a landing approach along some prescribed flight path unknown to us. As the aircraft moves along this path, let its azimuth angle be given by

$$\theta(k) = f(k) \quad (II-1)$$

While we do not know the relation $f(\cdot)$, we shall assume that it is a member of a known "class" of functions representing evolutions in $\theta(k)$ for typical landing approaches. For example, we can limit the aircraft's maximum air speed or minimum radius of turn. More is said about this in Chapter VI.

We define $y(k)$ as the estimate of $\theta(k)$ produced by the envelope processor using the locally optimum estimation algorithm. This estimate is unbiased and can therefore be given by

$$y(k) = \theta(k) + v(k) \quad (\text{II-2})$$

where $v(k)$ is a zero-mean additive error term with covariance $R(k)$. $R(k)$ is computed by the locally optimum estimation algorithm so that we know its value [6, p. 5]. The probability distribution of $v(k)$ is unknown. Here, we assume that it is Gaussian. This does not appear to be an unreasonable assumption insofar as we would intuitively expect the error density to be symmetric about a single mode at zero. Also, the Gaussian assumption makes the state estimation problem to follow mathematically tractable. We therefore write the probability density of $v(k)$ as

$$p[v(k)] = N[0, R(k)] \quad (\text{II-3})$$

We hereafter denote the first-order density of an n -dimensional Gaussian process $x(k)$ with mean $m(k)$ and covariance $P(k)$ as

$$p[x(k)] = N[m(k), P(k)] \quad (\text{II-4})$$

where

$$N[m(k), P(k)] \triangleq (2\pi)^{-\frac{n}{2}} |P(k)|^{-\frac{1}{2}} \exp\left\{-\frac{1}{2}[x(k)-m(k)]^T P^{-1}(k)[x(k)-m(k)]\right\} \quad (\text{II-5})$$

If $x(k)$ is white or uncorrelated in time, we write:

$$p[x(k)] = WN[m(k), P(k)] \quad (\text{II-6})$$

The envelope processor error $v(k)$ is produced by the effects of front-end noise on the IF signal. These effects are independent from one scan interval to the next, so that $v(k)$ is uncorrelated. We therefore write

$$p[v(k)] = WN[0, R(k)] \quad (\text{II-7})$$

As mentioned in Chapter I, the envelope processor estimate $y(k)$ uses only the envelope information from the k th scan interval. Our objective is to develop an estimate of $\theta(k)$ based on Y_k , the set of all past values of $y(k)$:

$$Y_k \triangleq \{y(1), y(2), \dots, y(k)\} \quad (\text{II-8})$$

For a slowly changing azimuth angle there is a high correlation between $\theta(k)$ and $\theta(k+1)$, while the estimates $y(k)$ have uncorrelated errors from scan to scan. As mentioned in Chapter I, we intuitively expect to improve the estimate $y(k)$ by averaging it in some way with past values. This could be viewed as a low-pass filtering approach.

Let us consider a stochastic state model, driven by noise, as a representation for the evolution of $\theta(k)$. Given a valid state model, we could then, by treating the estimates $y(k)$ as observations of the state, produce a new state estimate which minimizes error in some mean-square sense. This is the approach taken here.

We now offer a formal problem description. Given in the problem is an unknown azimuth coordinate $\theta(k)$ described by (II-1), where $f(\cdot)$ is a member of a known class of functions. Also given is the set Y_k of past envelope processor estimates. The estimate $y(k)$ has zero-mean, white

Gaussian error with known covariance, described by (II-2) and (II-7). The objective can be stated as follows: using an assumed stochastic model for the evolution of $\theta(k)$, develop an adaptive Kalman filter which estimates $\theta(k)$ so as to minimize mean-square error in the estimate. Several adaptive Kalman filtering methods are obtained from the literature and modified for use in this problem. Each candidate filter is tested in computer simulation, with error in the estimate of $\theta(k)$ being the quantity of interest.

Stochastic Model

The Kalman filter requires a state variable model where an nth-order linear system is driven by white Gaussian noise. We therefore use such a stochastic model in representing the evolution of the azimuth angle $\theta(k)$. In order to keep the resulting Kalman filter computationally feasible we elect to use a two-dimensional model where the angular acceleration is set equal to white Gaussian noise:

$$\begin{bmatrix} \dot{\theta}(t) \\ \ddot{\theta}(t) \end{bmatrix} = \begin{bmatrix} 0 & 1 \\ 0 & 0 \end{bmatrix} \begin{bmatrix} \theta(t) \\ \dot{\theta}(t) \end{bmatrix} + \begin{bmatrix} 0 \\ 1 \end{bmatrix} u(t) \quad (\text{II-9})$$

$$p[u(t)] = \text{WN}[0, S(t)] \quad (\text{II-10})$$

Our decision to model acceleration as white noise provides us with the lowest order stochastic model for which both $\theta(t)$ and $\dot{\theta}(t)$ can be estimated. As shown in Chapter III, $\dot{\theta}(t)$ is used to linearly extrapolate the estimate of $\theta(t)$ between measurement times.

In using the noise process $u(t)$ to model $\ddot{\theta}(t)$, we must relate the

noise covariance $S(t)$ to the actual value which $\ddot{\theta}(t)$ takes on. Since $S(t)$ is the expected value of the square of $u(t)$, we set it equal to the square of the actual acceleration:

$$S(t) = \ddot{\theta}^2(t) \quad (\text{II-11})$$

Of course, in estimating $\theta(t)$ we do not know $\ddot{\theta}(t)$, since the only available information is the set Y_k of envelope processor estimates. $S(t)$ is therefore unknown in our model, at least from the aircraft's point of view.

As stated in the problem definition, we are interested in estimating $\theta(k)$, the value of $\theta(t)$ at the start of the k th scanning interval. We therefore obtain a discrete-time representation of the state model in (II-9). Let us first replace (II-9) with a more general state equation:

$$\dot{\tilde{x}}(t) = A\tilde{x}(t) + Gu(t) \quad (\text{II-12})$$

where $x(t)$ is a general state vector driven by a vector noise process $u(t)$. (II-10) can still be used to describe $u(t)$. A general discrete state model is given by:

$$x(k) = \phi(\Delta t)x(k-1) + \Gamma\omega(k-1) \quad (\text{II-13})$$

$$p[\omega(k-1)] = WN[0, Q(k-1)] \quad (\text{II-14})$$

where $\Delta t \triangleq t_k - t_{k-1}$. (II-14) becomes the discrete equivalent of (II-9) with $x(k)$ representing $x(t)|_{t=t_k}$ when we use the following transformations [7, pp. 60-61, 72-75]:

$$\phi(\Delta t) = \exp\{A\Delta t\} \quad (\text{II-15.A})$$

$$rQ(k-1)r^T = \int_{t_k-1}^{t_k} \phi(t_k-t)GS(t)G^T\phi^T(t_k-t)dt \quad (\text{II-15.B})$$

Substituting the A matrix of (II-9) into (II-15.A), we obtain for our model:

$$\phi(\Delta t) = \begin{bmatrix} 1 & \Delta t \\ 0 & 1 \end{bmatrix} \quad (\text{II-16})$$

We assume Δt to be constant, so that $\phi(\Delta t)$ also becomes a constant and is written hereafter as ϕ . For evaluation of (II-15.B) we assume that $S(t)$ is constant at $S(t_k)$ over the limits of integration. This seems reasonable, as $\ddot{\theta}(t)$ cannot change appreciably during one scan period at a 13 1/3 Hz update rate. Moving the scalar $S(t_k)$ outside the integral and changing variables we obtain:

$$rQ(k-1)r^T = S(t_k) \int_0^{\Delta t} \phi(\tau)GG^T\phi^T(\tau)d\tau \quad (\text{II-17})$$

We then substitute for G and $\phi(\tau)$ from (II-9) and (II-16) and evaluate the integral:

$$rQ(k-1)r^T = S(t_k) \begin{bmatrix} \frac{1}{3}\Delta t^3 & \frac{1}{2}\Delta t^2 \\ \frac{1}{2}\Delta t^2 & \Delta t \end{bmatrix} \quad (\text{II-18})$$

The linear Δt term in the matrix dominates for small Δt , as is the case

for our problem, where $\Delta t = .075$ (the period of a 13 1/3 Hz update rate). We approximate the other terms as zero:

$$\Gamma Q(k-1) \Gamma^T = \begin{bmatrix} 0 & 0 \\ 0 & \Delta t S(t_k) \end{bmatrix} \quad (\text{II-19})$$

With this approximation $Q(k-1)$ becomes a scalar, so that the state equation becomes

$$\begin{bmatrix} \theta(k) \\ \dot{\theta}(k) \end{bmatrix} = \begin{bmatrix} 1 & \Delta t \\ 0 & 1 \end{bmatrix} \begin{bmatrix} \theta(k-1) \\ \dot{\theta}(k-1) \end{bmatrix} + \begin{bmatrix} 0 \\ 1 \end{bmatrix} \omega(k-1) \quad (\text{II-20})$$

$$p[\omega(k-1)] = WN[0, Q(k-1)] \quad (\text{II-21})$$

$$Q(k-1) = \Delta t S(t_k) \quad (\text{II-22})$$

Since $S(t)$ is unknown in the continuous-time model, $Q(k-1)$ is unknown as well.

We can see from (II-20) that the effect of our assumption in (II-19) is to add noise only to the velocity $\dot{\theta}(k)$, so that $\theta(k)$ becomes piecewise linear between measurement updates. If we were to assume a constant acceleration between times t_{k-1} and t_k , $\theta(k)$ would be described by:

$$\theta(k) = \theta(k-1) + \Delta t \dot{\theta}(k-1) + \frac{1}{2} \Delta t^2 \ddot{\theta}(k-1) \quad (\text{II-23})$$

In (II-20) we have discarded the nonlinear term $\frac{1}{2} \Delta t^2 \ddot{\theta}(k-1)$, assuming it to be negligible. For reasonable landing approaches we do not expect $\ddot{\theta}$

to exceed $0.1^\circ/\text{sec}^2$ [6, p. 40]. For a $13\frac{1}{3}$ Hz update rate, Δt is 75 milliseconds, and the error in neglecting the nonlinear term is always less than $\frac{1}{2}(.075 \text{ sec})^2(.1^\circ/\text{sec}^2)$, or 2.8×10^{-4} degrees. Since 0.01° is given as a desired r.m.s. error specification, (II-20) is a valid approximation.

We now have a discrete time state model describing the evolution of $\theta(k)$. We recall from (II-2) and (II-7) that the envelope processor estimate $y(k)$ equals $\theta(k)$ plus a Gaussian error term. We can therefore view $y(k)$ as a linear observation, or "measurement" of the state corrupted by additive noise:

$$y(k) = [1 \quad 0] \begin{bmatrix} \theta(k) \\ \dot{\theta}(k) \end{bmatrix} + v(k) \quad (\text{II-24})$$

Finding the value of $\theta(k)$ now becomes a state estimation problem. We must estimate the state of a linear dynamic system excited by white Gaussian noise of unknown covariance, given linear measurements of the state corrupted by additive white Gaussian noise of known covariance.

CHAPTER III

THE DISCRETE KALMAN FILTER

In this chapter we examine the discrete Kalman filter, which is the optimal estimator for the assumed state and measurement models in our problem. As previously mentioned, the optimal estimator cannot be used here, as the state noise covariance is unknown. The optimal estimator is of use, however, in obtaining the suboptimal solutions to follow, and provides a lower bound on error performance.

Let us first provide the state and measurement equations in concise form. From (II-7), (II-20), (II-21), and (II-24) we have:

$$\begin{bmatrix} \theta(k) \\ \dot{\theta}(k) \end{bmatrix} = \begin{bmatrix} 1 & \Delta t \\ 0 & 1 \end{bmatrix} \begin{bmatrix} \theta(k-1) \\ \dot{\theta}(k-1) \end{bmatrix} + \begin{bmatrix} 0 \\ 1 \end{bmatrix} \omega(k-1) \quad (\text{III-1})$$

$$y(k) = [1 \quad 0] \begin{bmatrix} \theta(k) \\ \dot{\theta}(k) \end{bmatrix} + v(k) \quad (\text{III-2})$$

$$p[\omega(k-1)] = WN[0, Q(k-1)] \quad (\text{III-3})$$

$$p[v(k)] = WN[0, R(k)] \quad (\text{III-4})$$

where $Q(k-1)$ is unknown. Equations (III-1) and (III-2) describe a specific member within a general class of linear systems given by:

$$x(k) = \Phi x(k-1) + \Gamma \omega(k-1) \quad (\text{III-5})$$

$$y(k) = Hx(k) + v(k) \quad (\text{III-6})$$

where $x(k)$ is an n -dimensional state vector, $y(k)$ is an m -dimensional measurement of $x(k)$, and where $\omega(k-1)$ and $v(k)$ are Gaussian noise vectors of dimension r and m . The noise sequences for the general case are still described by (III-3) and (III-4), where $Q(k-1)$ and $R(k)$ are now symmetric, non-negative definite matrices of respective dimensions $r \times r$ and $m \times m$.

Let us consider the general system of (III-5) and (III-6). We assume in this chapter that the state noise covariance $Q(k-1)$ is known. Our objective is to estimate the state $x(k)$ given the set Y_k of all past measurements:

$$Y_k \triangleq \{y(1), y(2), \dots, y(k)\} \quad (\text{III-7})$$

Let us define $\hat{x}(k|j)$ as an estimate of $x(k)$, given Y_j . We are concerned with finding the optimum state estimate $\hat{x}(k|k)$.

In order to have a quantitative measure for optimality we define a performance index, or loss function $J(k|k)$:

$$J(k|k) = E\{[x(k) - \hat{x}(k|k)]^T W [x(k) - \hat{x}(k|k)]\} \quad (\text{III-8})$$

where W is an $n \times n$ symmetric, non-negative definite matrix. When W is diagonal $J(k|k)$ becomes a weighted sum of the mean-square errors in the elements of $\hat{x}(k|k)$. We define the optimal state estimate of $x(k)$ as that estimate $\hat{x}(k|k)$ which minimizes $J(k|k)$. It can be shown that $J(k|k)$ is a

member of a class of loss functions which are minimized by that estimate given by the conditional mean of the state given all past measurements; i.e., the optimal estimate $\hat{x}(k|k)$ becomes

$$\hat{x}(k|k) = E\{x(k)|Y_k\} \quad (\text{III-9})$$

[1, pp. 227, 231], [2, pp. 147-148]. This is true for any non-negative definite W .

We again reference the general linear system (II-3)-(II-6), and still assume that the noise covariances are known. It is well known that the optimal estimate of $x(k)$ for this system, the conditional mean which minimizes $J(k|k)$, is given by the discrete Kalman filter [1, pp. 228-229], [2, pp. 195-201]. The Kalman filter is described by the following equations [2, p. 201]:

$$\hat{x}(k|k-1) = \Phi \hat{x}(k-1|k-1) \quad (\text{III-10})$$

$$P(k|k-1) = \Phi P(k-1|k-1) \Phi^T + \Gamma Q(k-1) \Gamma^T \quad (\text{III-11})$$

$$K(k) = P(k|k-1) H^T [H P(k|k-1) H^T + R(k)]^{-1} \quad (\text{III-12})$$

$$\hat{x}(k|k) = \hat{x}(k|k-1) + K(k) [y(k) - H \hat{x}(k|k-1)] \quad (\text{III-13})$$

$$P(k|k) = P(k|k-1) - K(k) H P(k|k-1) \quad (\text{III-14})$$

where $\hat{x}(k|k-1)$ denotes the optimal predicted, or extrapolated estimate of $x(k)$ given Y_{k-1} , while $\hat{x}(k|k)$ is the optimal updated estimate using all measurements Y_k up to the present time. The term $P(k|j)$ is the error

covariance in the estimate $\hat{x}(k|j)$:

$$P(k|j) = E\{[x(k) - \hat{x}(k|j)][x(k) - \hat{x}(k|j)]^T\} \quad (\text{III-15})$$

$K(k)$ is the Kalman gain, which determines the weighting given the present measurement $y(k)$ in computing $\hat{x}(k|k)$. Note that $K(k)$ is not a function of measurement values, so that $\hat{x}(k|k)$ is a linear estimate of $x(k)$.

Returning to our original problem of (III-1) to (III-4), we define the state estimate $\hat{x}(k|k)$ by

$$\hat{x}(k|k) = [\hat{\theta}(k|k), \hat{\theta}(k|k)]^T \quad (\text{III-16})$$

We seek to minimize mean-square error in $\hat{\theta}(k|k)$, so that our performance index becomes

$$PI(k|k) = E\{[\theta(k) - \hat{\theta}(k|k)]^2\} \quad (\text{III-17})$$

From (III-8) we see that $PI(k|k)$ is a special case of the general loss function $J(k|k)$ where W is the diagonal matrix $\text{diag}\{1, 0\}$. Therefore the Kalman filter produces the optimal estimate for our problem when the noise covariances are known. We now give the Kalman filter equations for our specific model:

$$\hat{\theta}(k|k-1) = \hat{\theta}(k-1|k-1) + \Delta t \hat{\theta}(k-1|k-1) \quad (\text{III-18})$$

$$P_{11}(k|k-1) = P_{11}(k-1|k-1) + 2\Delta t P_{12}(k-1|k-1) + \Delta t^2 P_{22}(k-1|k-1) \quad (\text{III-19})$$

$$P_{12}(k|k-1) = P_{12}(k-1|k-1) + \Delta t P_{22}(k-1|k-1) \quad (\text{III-20})$$

$$P_{22}(k|k-1) = P_{22}(k-1|k-1) + Q(k-1) \quad (\text{III-21})$$

$$K_1(k) = P_{11}(k|k-1)/[P_{11}(k|k-1) + R(k)] \quad (\text{III-22})$$

$$K_2(k) = P_{12}(k|k-1)/[P_{11}(k|k-1) + R(k)] \quad (\text{III-23})$$

$$\hat{\theta}(k|k) = \hat{\theta}(k|k-1) + K_1(k)[y(k) - \hat{\theta}(k|k-1)] \quad (\text{III-24})$$

$$\hat{\theta}(k|k) = \hat{\theta}(k-1|k-1) + K_2(k)[y(k) - \hat{\theta}(k|k-1)] \quad (\text{III-25})$$

$$P_{11}(k|k) = P_{11}(k|k-1)[1 - K_1(k)] \quad (\text{III-26})$$

$$P_{12}(k|k) = P_{12}(k|k-1)[1 - K_1(k)] \quad (\text{III-27})$$

$$P_{22}(k|k) = P_{22}(k|k-1) - K_2(k)P_{12}(k|k-1) \quad (\text{III-28})$$

Let us consider the Kalman filter for the general case of an n-dimensional state vector with scalar noise and measurements. From (III-12) we can see that the optimal gain matrix $K(k)$ becomes an n-dimensional vector. Some of the properties of this gain vector are useful for the adaptive Kalman filter development of Chapter IV.

We first note that for stationary noise where $Q(k-1)$ and $R(k)$ are scalar constants, the gain $K(k)$ as well as the error covariances $P(k|k-1)$ and $P(k|k)$ reach constant steady-state values. If $Q(k-1)$ and $R(k)$ are constant or slowly varying, $K(k)$ is a function of the ratio $Q(k-1)/R(k)$. Furthermore, $K(k)$ can be specified if only one of its elements are known; all remaining entries are deterministic functions of

the one known element. The dependence of the gain on Q and R as well as the functional relationships between gain elements can be observed numerically, but we cannot usually find closed-form expressions for such properties, especially when n is large [8, p. 274]. Another useful property of the gain for the scalar measurement case is given by Alspach [8, p. 272]:

$$0 \leq HK(k) \leq 1 \quad (\text{III-29})$$

We offer a proof for (III-29), but first we rewrite the general Kalman gain equation (III-12):

$$W(k) = HP(k|k-1)H^T + R(k) \quad (\text{III-30})$$

$$K(k) = P(k|k-1)H^TW^{-1}(k) \quad (\text{III-31})$$

$P(k|k-1)$ and $R(k)$ are non-negative definite matrices, so that $W(k)$ is non-negative definite as well, having the same form as a covariance matrix. More is said about this property of $W(k)$ in Chapter IV. Alspach notes that $W(k)$ can be written:

$$W(k) = [I - HK(k)]^{-1}R(k) \quad (\text{III-32})$$

[8, p. 270]. We can prove this by starting with the right-hand side and substituting:

$$[I - HK(k)]^{-1}R(k) \quad (\text{III-32.A})$$

$$= [I - HP(k|k-1)H^TW^{-1}(k)]^{-1}R(k) \quad (\text{III-32.B})$$

$$= W(k)[W(k) - HP(k|k-1)H^T]^{-1}R(k) \quad (\text{III-32.C})$$

$$= W(k)[R(k)]^{-1}R(k) \quad (\text{III-32.D})$$

$$= W(k) \quad (\text{III-32.E})$$

(III-32.B) is obtained by substituting for $K(k)$ from (III-31), while (III-32.D) is obtained from (III-30). For the scalar noise and measurement case $R(k)$ and $W(k)$ become positive scalars, and (III-32) can be rewritten:

$$1 - HK(k) = R(k)/W(k) \quad (\text{III-33})$$

Since $R(k)$ and $W(k)$ are positive, their ratio cannot be negative. From (III-30) we know that $W(k)$ must be greater than or equal to $R(k)$, so that the ratio in (III-33) cannot exceed unity. We therefore have:

$$0 \leq 1 - HK(k) \leq 1 \quad (\text{III-34})$$

or

$$0 \leq HK(k) \leq 1 \quad (\text{III-35})$$

For the two-dimensional aircraft problem we can show that the gain of the filter given by (III-18)-(III-28) is a function of $Q(k-1)/R(k)$. We can also obtain a closed-form expression for the second gain element in terms of the first. We first need to express the error covariances $P(k|k-1)$ and $P(k|k)$ in terms of $K(k)$. From (III-22) we can write:

$$P_{11}(k|k-1) = K_1(k)R(k)/[1 - K_1(k)] \quad (\text{III-36})$$

Substituting this expression for $P_{11}(k|k-1)$ into (III-26) we obtain:

$$P_{11}(k|k) = K_1(k)R(k) \quad (\text{III-37})$$

Substituting (III-36) for $P_{11}(k|k-1)$ into (III-23), we have:

$$P_{12}(k|k-1) = K_2(k)R(k)/[1 - K_1(k)] \quad (\text{III-38})$$

And substituting this expression for $P_{12}(k|k-1)$ into (III-27) we have:

$$P_{12}(k|k) = K_2(k)R(k) \quad (\text{III-39})$$

We now make the assumption that the noise covariances are slowly varying in time. This seems reasonable, as $Q(k-1)$ is determined by the acceleration $\ddot{\alpha}(t_k)$ and $R(k)$ depends on the signal-to-noise ratio. Neither of these quantities can change appreciably between scan intervals at a 13 1/3 Hz update rate. We therefore approximate the error covariance $P(k|k-1)$ as having the same value for two consecutive time periods:

$$P(k+1|k) \approx P(k|k-1) \quad (\text{III-40})$$

Using this approximation, we substitute (III-38) and (III-39) into (III-20) and obtain:

$$P_{22}(k|k) = K_1(k)K_2(k)R(k)/[\Delta t(1 - K_1(k))] \quad (\text{III-41})$$

We can now represent the second entry of the optimal gain in terms of the first. Using the approximation of (III-40), we substitute (III-36), (III-37), (III-39), and (III-41) for the needed covariances into (III-19)

and simplify, obtaining:

$$K_2(k) = K_1^2(k)/[\Delta t(2 - K_1(k))] \quad (\text{III-42})$$

We observe that $K_2(k)$ is a monotone-increasing function of $K_1(k)$. Using (III-35) and (III-42) and noting that here $HK(k)$ equals $K_1(k)$, we establish bounds on the gain:

$$\begin{aligned} 0 \leq K_1(k) \leq 1 \\ 0 \leq K_2(k) \leq 1/\Delta t \end{aligned} \quad (\text{III-43})$$

Keeping the assumption of (III-40), we find from (III-21) and (III-28) that we have two expressions for the difference $P_{22}(k|k-1) - P_{22}(k|k)$. Equating these we have:

$$Q(k-1) = K_2(k)P_{12}(k|k-1) \quad (\text{III-44})$$

Substituting (III-38) for $P_{12}(k|k-1)$, we have:

$$Q(k-1)/R(k-1) = K_2^2(k)/[1 - K_1(k)] \quad (\text{III-45})$$

And by using (III-42) for $K_2(k)$ we finally have:

$$Q(k-1)/R(k) = K_1^4(k)/[\Delta t(2 - K_1(k))^2(1 - K_1(k))] \quad (\text{III-46})$$

$Q(k-1)/R(k)$ is clearly a monotone-increasing function of $K_1(k)$, ranging from zero when $K_1(k)$ is zero to infinity when $K_1(k)$ is unity. Since $Q(k-1)/R(k)$ and $K_1(k)$ are both positive, we can infer that $K_1(k)$ is a

monotone-increasing function of $Q(k-1)/R(k)$ as well.

We can make some intuitive observations from this about the optimal filter of (III-18)-(III-28). From (III-18) we see that $\hat{\theta}(k|k-1)$ is a linear extrapolation of $\hat{\theta}(k-1|k-1)$, based upon the velocity estimate $\hat{\theta}(k-1|k-1)$. We then accept a new measurement $y(k)$ of $\theta(k)$, and use the weighted difference between $y(k)$ and $\hat{\theta}(k|k-1)$ to update our estimate to $\hat{\theta}(k|k)$ in (III-24). The weighting applied to this difference is $K_1(k)$, varying from 0 to 1. We have just found $K_1(k)$ to be a monotone-increasing function of $Q(k-1)/R(k)$. We might view $Q(k-1)/R(k)$ as the ratio of uncertainty in our knowledge of the state $x(k)$ to uncertainty in the measurement $y(k)$. When this ratio is low, indicating high confidence in our estimate of the state, $K(k)$ is small, so that $y(k)$ has little effect on the new estimate $\hat{x}(k|k)$. When this ratio is high, we have greater confidence in our new measurement $y(k)$. $K(k)$ becomes large, and $y(k)$ has more weighting in determining $\hat{x}(k|k)$. Of course when $Q(k-1)/R(k)$ approaches infinity, we have no prior knowledge of the state: $\hat{x}(k-1|k-1)$ gives no information about $x(k)$. $K_1(k)$ becomes unity, causing $\hat{\theta}(k|k)$ to become $y(k)$.

Before leaving the subject of optimal filters, let us study the effects of using a Kalman filter with incorrect or suboptimal gain. This would be the case if incorrect values were used for the noise covariances $Q(k-1)$ and $R(k)$. Assume that the filter of (III-10) and (III-13) is implemented, with a suboptimal gain $\hat{K}(k)$. From (III-5), (III-10), and (III-13) we can write the error in the state estimate:

$$\begin{aligned}
 x(k) - \hat{x}(k|k) &= \Phi x(k-1) + \Gamma \omega(k-1) - \Phi \hat{x}(k-1|k-1) \\
 &\quad - \hat{K}(k)[y(k) - H\Phi \hat{x}(k-1|k-1)]
 \end{aligned} \tag{III-47}$$

Substituting for $y(k)$ from (III-6) we have:

$$\begin{aligned}
 x(k) - \hat{x}(k|k) &= \Phi[x(k-1) - \hat{x}(k-1|k-1)] + \Gamma \omega(k-1) \\
 &\quad - \hat{K}(k)[H\Phi x(k-1) + H\Gamma \omega(k-1) + v(k) - H\Phi \hat{x}(k-1|k-1)]
 \end{aligned} \tag{III-48}$$

$$\begin{aligned}
 x(k) - \hat{x}(k|k) &= [I - \hat{K}(k)H]\Phi[x(k-1) - \hat{x}(k-1|k-1)] \\
 &\quad + [I - \hat{K}(k)H]\Gamma \omega(k-1) - \hat{K}(k)v(k)
 \end{aligned} \tag{III-49}$$

We recall that $\omega(k-1)$ and $v(k)$ are samples of white sequences and are independent of each other. Since $\hat{x}(k|j)$ is a combination of measurements through $y(j)$, we can make the following assertions:

$$[x(k) - \hat{x}(k|j)] \text{ is independent of } \omega(i): \begin{array}{l} k \leq i \\ j \leq i \end{array} \tag{III-50}$$

$$[x(k) - \hat{x}(k|j)] \text{ is independent of } v(i): \begin{array}{l} \text{all } k \\ j < i \end{array} \tag{III-51}$$

Therefore all three terms in (III-49) are independent, and we write the suboptimal error covariance:

$$P(k|k) = E\{[x(k) - \hat{x}(k|k)][x(k) - \hat{x}(k|k)]^T\} \tag{III-52.A}$$

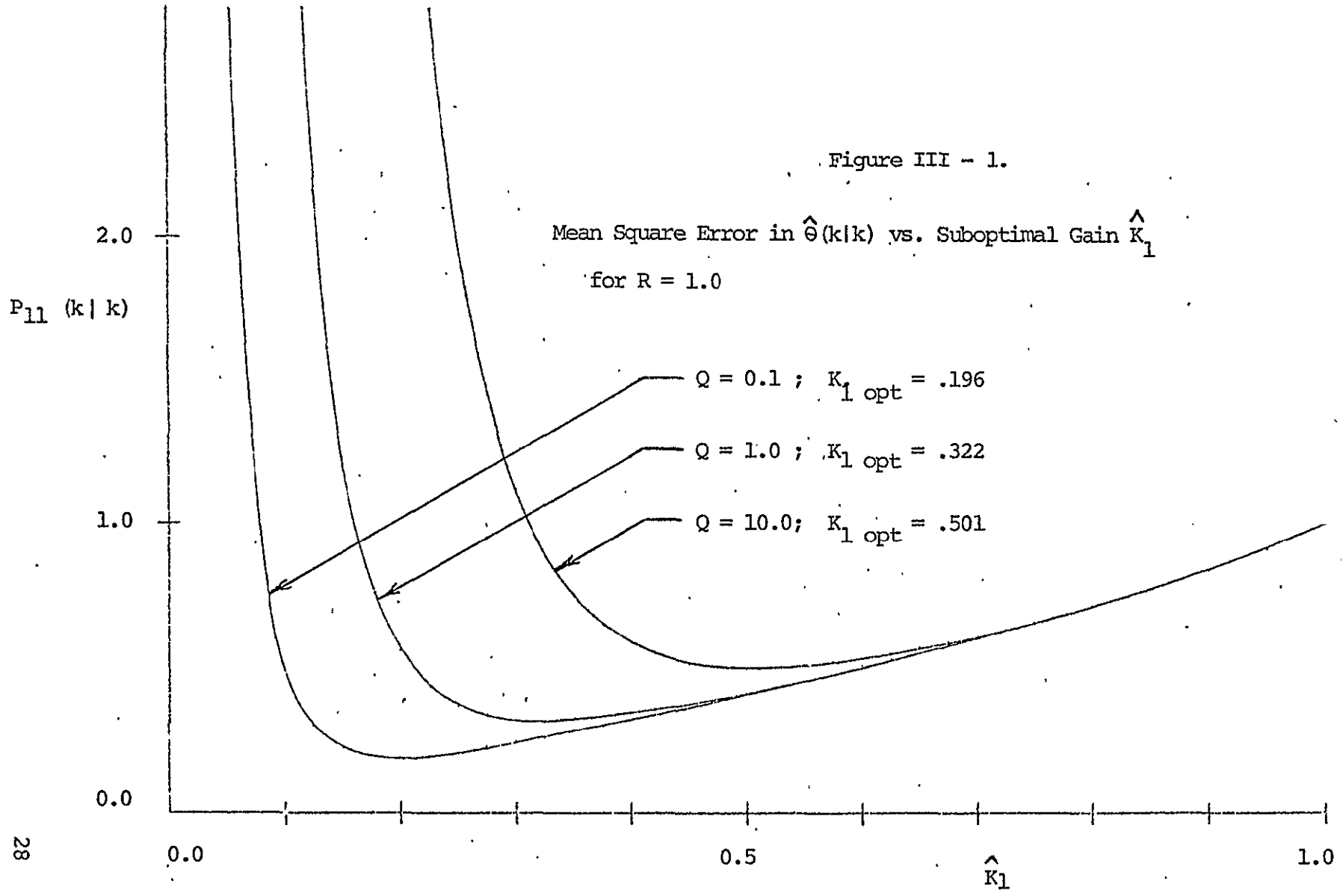
$$\begin{aligned}
&= [I - \hat{K}(k)H] \Phi E\{[x(k-1) - \hat{x}(k-1|k-1)][x(k-1) - \hat{x}(k-1|k-1)]^T\} \Phi^T [I - \hat{K}(k)H]^T \\
&+ [I - \hat{K}(k)H] \Gamma E\{\omega(k-1)\omega^T(k-1)\} \Gamma^T [I - \hat{K}(k)H]^T + \hat{K}(k) E\{v(k)v^T(k)\} \hat{K}^T(k)
\end{aligned}
\tag{III-52.B}$$

Simplifying this expression, we obtain:

$$\begin{aligned}
P(k|k) &= [I - \hat{K}(k)H] [\Phi P(k-1|k-1) \Phi^T + \Gamma Q(k-1) \Gamma^T] [I - \hat{K}(k)H]^T \\
&+ \hat{K}(k) R(k) \hat{K}^T(k)
\end{aligned}
\tag{III-53}$$

Equation (III-53) has been iterated until steady-state is reached for our problem of (III-1)-(III-4) with stationary noise. Figure III-1 shows $P_{11}(k|k)$, the steady-state mean-square error in $\hat{\theta}(k|k)$, as a function of suboptimal gain. $P_{11}(k|k)$ versus $\hat{K}_1(k|k)$ is plotted for three ratios of $Q(k-1)/R(k)$. Note that for each case $P_{11}(k|k)$ is minimum for the optimal gain and then rises to $R(k)$ as $\hat{K}_1(k)$ approaches unity. We can see that as long as the suboptimal gain is near or above the optimal value, the estimate $\hat{\theta}(k|k)$ will have a lower mean-square error than $y(k)$. When the suboptimal gain becomes less than the optimal value, however, $P_{11}(k|k)$ rises rapidly, approaching infinity as the gain goes to zero. Here the suboptimal filter diverges. The gain is so small that insufficient weighting is given to the most recent measurement $y(k)$ in updating the state estimate $\hat{x}(k|k)$. Too much emphasis is placed on old measurement information, so that the filter cannot follow the true dynamics of $\theta(k)$.

Figure III - 1.



CHAPTER IV

ADAPTIVE KALMAN FILTERING: THE STATIONARY NOISE CASE

In Chapter III we introduced the discrete Kalman filter as the optimal state estimator for the linear system described by:

$$x(k) = \Phi x(k-1) + \Gamma \omega(k-1) \quad (\text{IV-1})$$

$$y(k) = Hx(k) + v(k) \quad (\text{IV-2})$$

$$p[\omega(k-1)] = \text{WN}[0, Q(k-1)] \quad (\text{IV-3})$$

$$p[v(k)] = \text{WN}[0, R(k)] \quad (\text{IV-4})$$

We made the assumption, however, that the noise covariances were known. Reviewing the Kalman filter equations (III-10)-(III-14) we note that both $Q(k-1)$ and $R(k)$ are needed for computing the optimal gain $K(k)$ and the error covariances $P(k|k-1)$ and $P(k|k)$. If either $Q(k-1)$ or $R(k)$ is unknown, as is the case for our problem, the gain $K(k)$ cannot be found. We could implement the Kalman filter equations by substituting estimates for the unknown noise covariances, but the performance of the resulting estimator could be highly suboptimal if these estimates are poor.

In this chapter we introduce adaptive Kalman filter as a suboptimal estimation scheme when the noise covariances are unknown. The adaptive Kalman filter takes the form of the optimal filter:

$$\hat{x}(k|k-1) = \Phi \hat{x}(k-1|k-1) \quad (\text{IV-5})$$

$$\hat{x}(k|k) = \hat{x}(k|k-1) + \hat{K}(k)[y(k) - H\hat{x}(k|k-1)] \quad (\text{IV-6})$$

where $\hat{K}(k)$ is an estimate of the unknown optimal gain $K(k)$. The suboptimal $\hat{K}(k)$ is a function of the measurements Y_k : we use the measurements to either estimate $K(k)$ directly or to estimate the unknown noise covariances for use in the Kalman equations (III-10)-(III-14). The adaptive filter is therefore a nonlinear estimator, unlike the optimal Kalman filter, which is linear since the gain $K(k)$ is independent of the measurements.

Here we present three adaptive Kalman filtering methods for the stationary noise case from the literature, as well as a simpler intuitive scheme. Each method assumes the system model of (IV-1)-(IV-4), with both $Q(k-1)$ and $R(k)$ unknown and constant. Some methods assume a model of general dimension, while others assume scalar noise and measurements. In this chapter we present the development of each method for the general stationary case. In Chapter V we modify the adaptive filters to work when the noise covariances are time-varying and apply them to our specific problem of (III-1) to (III-4).

The Innovations Sequence

Before presenting a development of the adaptive Kalman filtering methods, let us first define the innovations sequence. This concept is useful in the filtering developments to follow.

We first recall the general Kalman filter equations (III-10)-(III-14). Specifically, the updated estimate is given by (III-13);

$$\hat{x}(k|k) = \hat{x}(k|k-1) + K(k)[y(k) - H\hat{x}(k|k-1)] \quad (\text{IV-7})$$

We shall define the innovations residual $v(k)$ by:

$$v(k) = y(k) - H\hat{x}(k|k-1) \quad (\text{IV-8})$$

The time sequence of these residuals is called the innovations sequence. We can show that the residual $v(k)$ is actually the error in the optimal predicted estimate of the measurement $y(k)$ given Y_{k-1} . From Chapter III we recall that the optimal, least-mean-square error estimate of $y(k)$ is the conditional mean of $y(k)$ given the available measurements. From (III-9) we write the optimal predicted estimate as:

$$\hat{y}(k|k-1) = E\{y(k)|Y_{k-1}\} \quad (\text{IV-9.A})$$

$$= E\{Hx(k) + v(k)|Y_{k-1}\} \quad (\text{IV-9.B})$$

$$= HE\{x(k)|Y_{k-1}\} + E\{v(k)\} \quad (\text{IV-9.C})$$

Equation (IV-9.B) results from substituting (IV-2) for $y(k)$, while the second term in (IV-9.C) results from noting that $v(k)$ is from a white sequence and thus independent of Y_{k-1} . Recalling that the optimal predicted state estimate is given by the Kalman filter, and that $v(k)$ is zero-mean, we have:

$$\hat{y}(k|k-1) = H\hat{x}(k|k-1) \quad (\text{IV-10})$$

where $\hat{x}(k|k-1)$ is from the Kalman equation (III-10). The innovations

residual $v(k)$ is therefore the difference between the measurement $y(k)$ and its optimal predicted estimate. This error is then multiplied by the Kalman gain $K(k)$ and used to correct $\hat{x}(k|k-1)$ in (IV-7) to produce the optimal state estimate $\hat{x}(k|k)$.

The residual $v(k)$ can easily be shown to be zero-mean:

$$E\{v(k)\} = E\{y(k) - H\hat{x}(k|k-1)\} \quad (\text{IV-11.A})$$

$$= HE\{x(k) - \hat{x}(k|k-1)\} + E\{v(k)\} = 0 \quad (\text{IV-11.B})$$

(IV-11.B) is obtained by substituting (IV-2) for $y(k)$. It equals zero because the Kalman estimate $\hat{x}(k|k-1)$ is by definition unbiased, while $v(k)$ is zero-mean. We can also find the innovations covariance $W(k)$:

$$W(k) = E\{v(k)v^T(k)\} \quad (\text{IV-12.A})$$

$$= E\{[H(x(k) - \hat{x}(k|k-1)) + v(k)][H(x(k) - \hat{x}(k|k-1)) + v(k)]^T\} \quad (\text{IV-12.B})$$

From (III-51), $[x(k) - \hat{x}(k|k-1)]$ and $v(k)$ are independent, so that (IV-12.B) becomes:

$$W(k) = HE\{[x(k) - \hat{x}(k|k-1)][x(k) - \hat{x}(k|k-1)]^T\}H^T + E\{v(k)v^T(k)\} \quad (\text{IV-13.A})$$

$$= HP(k|k-1)H^T + R(k) \quad (\text{IV-13})$$

From (III-12) we see that the optimal filter computes $W(k)$ in

finding the Kalman gain $K(k)$. The gain was written as a function of $W(k)$ in (III-30), (III-31), although no physical interpretation was given for $W(k)$ at the time. We sometimes find it convenient to express the Kalman gain and updated state estimate of (III-12), (III-13) in terms of the innovations sequence:

$$v(k) = y(k) - H\hat{x}(k|k-1) \quad (\text{IV-14})$$

$$W(k) = HP(k|k-1)H^T + R(k) \quad (\text{IV-15})$$

$$K(k) = P(k|k-1)H^TW^{-1}(k) \quad (\text{IV-16})$$

$$\hat{x}(k|k) = \hat{x}(k|k-1) + K(k)v(k) \quad (\text{IV-17})$$

The innovations residual $v(k)$ can be shown to be Gaussian. Assuming the initial state $x(0)$ to be Gaussian, we can see from (IV-1) that $x(k)$ is Gaussian, since it is a linear combination of Gaussian random variables. Similarly from (IV-2) we see that $y(k)$ is the linear combination of Gaussian random variables and must be Gaussian as well. Finally we recall that for the optimal filter $\hat{x}(k|k-1)$ is a linear combination of the measurement values in Y_{k-1} , and is therefore Gaussian. Since $v(k)$ is a linear combination of $y(k)$ and $\hat{x}(k|k-1)$, it must also be Gaussian:

$$p[v(k)] = N[0, W(k)] \quad (\text{IV-18})$$

We have already established in (IV-8)-(IV-10) that $v(k)$ is the zero-mean difference between $y(k)$ and its optimal estimate $\hat{y}(k|k-1)$.

Since $\hat{y}(k|k-1)$ is the conditional mean $E\{y(k)|Y_{k-1}\}$, we can represent the conditional density $p[y(k)|Y_{k-1}]$ as the density of $v(k)$ with its mean displaced to $\hat{y}(k|k-1)$:

$$p[y(k)|Y_{k-1}] = N[H\hat{x}(k|k-1), W(k)] \quad (\text{IV-19})$$

The innovations sequence becomes important when we realize that it is an obtainable measure of the estimator's performance. From (IV-13) we know that the innovations covariance $W(k)$ is directly related to the predicted estimate error covariance $P(k|k-1)$. The derivation of (IV-13) makes no assumptions of filter optimality, so that this relation holds whether the filter gain is optimal or not. (Of course $P(k|k-1)$ and $P(k|k)$ are computed for the optimal case, and $W(k)$ is not needed). For our specific aircraft model of (III-1)-(III-4), equation (IV-13) is given by (III-22):

$$W(k) = P_{11}(k|k-1) + R(k) \quad (\text{IV-20})$$

For a constant $R(k)$, we see that the innovations covariance rises and falls with the mean-square error in $\hat{\theta}(k|k-1)$. $W(k)$ should therefore be minimum when the state estimator is optimal.

We can solve for $W(k)$ as a function of suboptimal gain $\hat{K}(k)$ for our specific system model of (III-1)-(III-4) when the noise is stationary. We have already obtained the error covariance $P(k|k)$ as a function of suboptimal gain \hat{K} and constant covariances Q and R in Chapter III by iterating (III-53) until steady-state is reached. From (IV-20) we have $W(k)$ as a function of $P(k|k-1)$. We can therefore express $W(k)$ in terms

of \hat{K} by relating $P(k|k-1)$ to $P(k|k)$ for the suboptimal filter. Using (IV-1) and (IV-5) we write the error in the predicted estimate:

$$x(k) - \hat{x}(k|k-1) = \Phi[x(k-1) - \hat{x}(k-1|k-1)] + r\omega(k-1) \quad (IV-21)$$

Recalling from (III-50) that $[x(k-1) - \hat{x}(k-1|k-1)]$ and $\omega(k-1)$ are independent, we have:

$$P(k|k-1) = E\{[x(k) - \hat{x}(k|k-1)][x(k) - \hat{x}(k|k-1)]^T\} \quad (IV-22.A)$$

$$= \Phi P(k-1|k-1) \Phi^T + rQ(k-1)r^T \quad (IV-22)$$

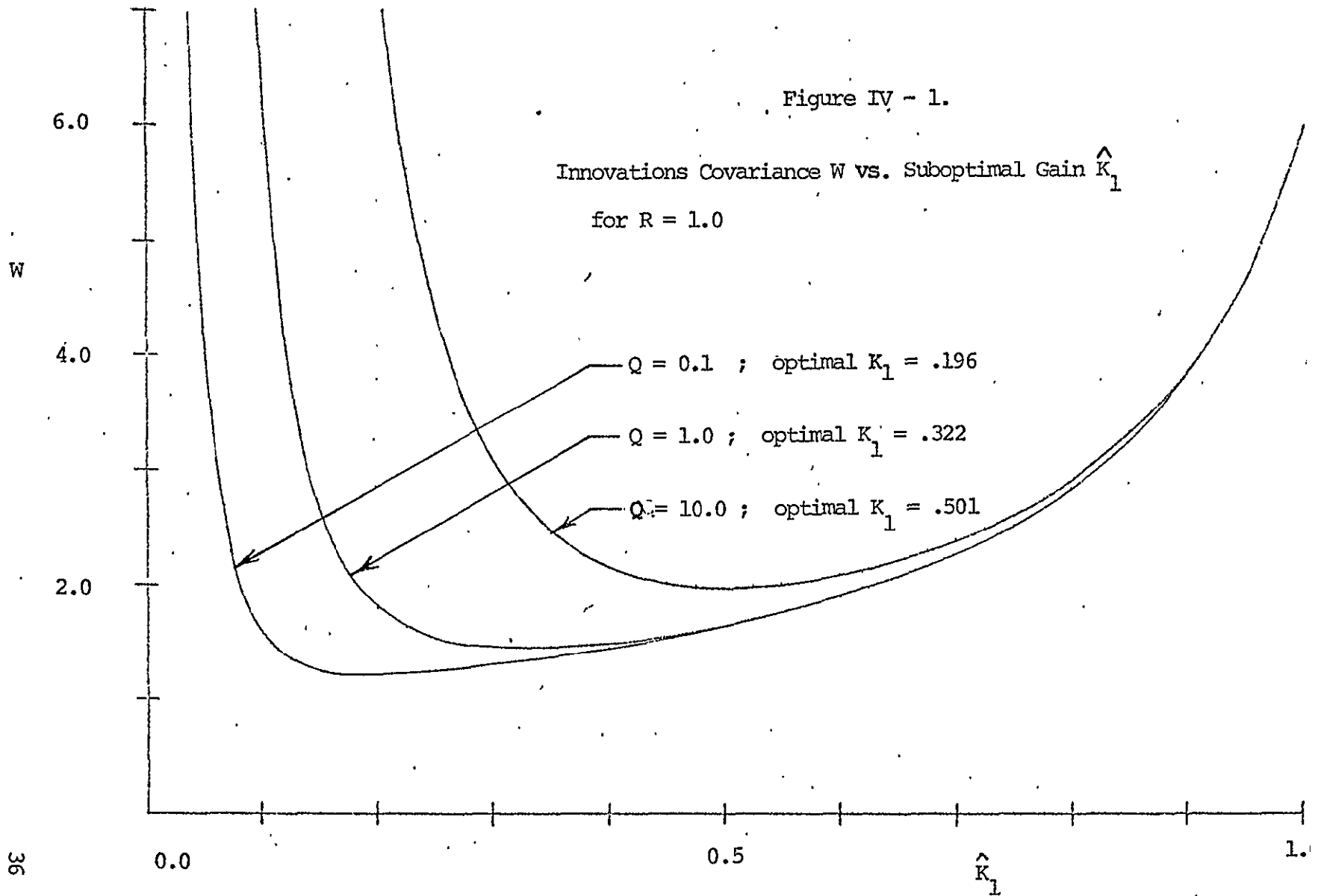
This is the same relation as (III-10) for the optimal filter, which is given by (III-19)-(III-21) for our specific aircraft problem. To obtain $W(k)$ we only need $P_{11}(k|k-1)$, given by (III-19):

$$P_{11}(k|k-1) = P_{11}(k-1|k-1) + 2\Delta t P_{12}(k-1|k-1) + \Delta t^2 P_{22}(k-1|k-1) \quad (IV-23)$$

We can therefore find $W(k)$ as a function of \hat{K} , Q , and R by first obtaining $P(k|k)$ from the steady-state solution of (III-53) and then applying (IV-21) and (IV-20).

Figure IV-1 shows plots of $W(k)$ versus suboptimal gain \hat{K}_1 with constant $Q(k-1)$ and $R(k)$ for aircraft system model (III-1)-(III-4). We note that $W(k)$ is minimum when \hat{K}_1 equals the optimal gain K_1 . This is expected, since $W(k)$ is the sum of $P_{11}(k|k-1)$ plus $R(k)$, and both $P_{11}(k|k-1)$ and $P_{11}(k|k)$ are minimized when the filter gain is optimal. We also note that $W(k)$ rises toward infinity as \hat{K}_1 approaches zero; here $P_{11}(k|k-1)$ and $P_{11}(k|k)$ are both approaching infinity as the suboptimal

Figure IV - 1.



filter diverges. We observe this same effect in Figure III-1.

The properties of the innovations sequence presented here are of immense value in the adaptive Kalman filtering developments which follow. It has been shown that the innovations sequence contains all new state information obtained by the measurements Y_k [9, p. 176]. In addition to the properties stated above, Mehra shows that the innovations sequence is white for the optimal filter and correlated when the filter gain becomes suboptimal [9, p. 177]. This property is not used by the adaptive filtering methods presented here.

We are now ready to present methods of adaptive Kalman filtering for general stationary noise problems.

The Method of Sage and Husa

Let us assume the general system model of (IV-1)-(IV-4), where the state vector $x(k)$ has dimension n and the measurement $y(k)$ has dimension m :

$$x(k) = \Phi x(k-1) + \Gamma \omega(k-1) \quad (IV-24)$$

$$y(k) = Hx(k) + v(k) \quad (IV-25)$$

$$p[\omega(k-1)] = WN[0, Q(k-1)] \quad (IV-26)$$

$$p[v(k)] = WN[0, R(k)] \quad (IV-27)$$

The noise covariance matrices $Q(k-1)$ and $R(k)$ are unknown constants, and shall be written hereafter as Q and R . We recall from (II-8) that Y_k is the set of all past measurements, and we define X_k as the set of all past state values:

$$Y_k = \{y(1), y(2), \dots, y(k)\} \quad (\text{IV-28})$$

$$X_k = \{x(1), x(2), \dots, x(k)\} \quad (\text{IV-29})$$

Sage and Husa develop maximum a posteriori (MAP) estimates $\hat{x}(k|k)$, $\hat{Q}(k|k)$, and $\hat{R}(k|k)$ which maximize the conditional probability density of the unknowns given the measurements. They actually address the more general problem where the noise terms of (IV-26) and (IV-27) have unknown means to be estimated as well. This more general procedure is not applicable for our problem, however, and is not covered here. The reader is referred to the works of Sage and Husa for a description of their general method [10], [11].

Let us form the a posteriori density of the unknown states and noise covariances given the measurements, i.e., the conditional probability density of X_k , Q , and R given Y_k :

$$p[X_k, Q, R|Y_k] = \frac{p[Y_k|X_k, Q, R]p[X_k, Q, R]}{p[Y_k]} \quad (\text{IV-30})$$

The right-hand side of (IV-30) is obtained from Bayes Law, where $p[X_k, Q, R]$ is the a priori density of the unknowns given no measurement information. For maximum a posteriori estimation we need to find those values of $x(k)$, Q , and R which maximize (IV-30). Noting that the denominator $p[Y_k]$ is unaffected by the choice of these values, we seek to maximize the function:

$$J(k) = p[Y_k|X_k, Q, R]p[X_k, Q, R] \quad (\text{IV-31})$$

Sage and Husa assume that the unknowns are independent in the absence of measurement information, yielding:

$$J(k) = p[Y_k | X_k, Q, R] p[X_k] p[Q] p[R] \quad (\text{IV-32})$$

They next assume that the a priori densities of Q and R are uniform between some known limits. For example:

$$p[Q_{ij}] = \begin{cases} \frac{1}{Q_{ijMAX} - Q_{ijMIN}}, & Q_{ijMIN} \leq Q_{ij} \leq Q_{ijMAX} \\ 0 & \text{otherwise} \end{cases} \quad (\text{IV-33})$$

All we know about the ij th element of Q is that it lies somewhere between Q_{ijMIN} and Q_{ijMAX} . All values between these limits are equally likely. Of course, if we have no information on how large Q and R become, we can allow the limits to approach infinity (Q_{ijMIN} must be positive for diagonal elements, as Q is non-negative definite). As long as we remain within the allowable limits on Q_{ij} and R_{ij} the densities $p[Q]$ and $p[R]$ are constant and do not affect the maximization of $J(k)$. We therefore write:

$$J(k) = C p[Y_k | X_k, Q, R] p[X_k] \quad (\text{IV-34})$$

where C is a constant.

We now solve for $J(k)$ in terms of its component densities. $p[X_k]$ can be expressed:

$$p[X_k] = p[x(k), X_{k-1}] \quad (\text{IV-35.A})$$

$$= p[x(k) | X_{k-1}] p[X_{k-1}] \quad (\text{IV-35})$$

where the last step results from the definition of conditional probability. We then substitute (IV-24) to write:

$$p[x(k)|X_{k-1}] = p[\phi x(k-1) + \Gamma\omega(k-1)|X_{k-1}] \quad (\text{IV-36})$$

Given X_{k-1} , $x(k-1)$ is known. No new information about $\Gamma\omega(k-1)$ is obtained, since from (III-50) $\omega(k-1)$ and $x(j)$ are independent for $j \leq k-1$. $p[x(k)|X_{k-1}]$ therefore assumes the density of $\Gamma\omega(k-1)$ shifted in mean by $\phi x(k-1)$:

$$p[x(k)|X_{k-1}] = N[\phi x(k-1), \Gamma Q \Gamma^T] \quad (\text{IV-37})$$

Reapplying (IV-35) and the substituting (IV-37) we have:

$$p[X_k] = p[x(0)] \prod_{j=1}^k p[x(j)|X_{j-1}] \quad (\text{IV-38.A})$$

$$= N[\hat{x}(0), P(0)] \prod_{j=1}^k N[\phi x(j-1), \Gamma Q \Gamma^T] \quad (\text{IV-38})$$

We now reapply the definition of conditional probability to obtain:

$$p[Y_k | X_k, Q, R] = p[Y(k), Y_{k-1} | X_k, Q, R] \quad (\text{IV-39.A})$$

$$= p[Y(k) | Y_{k-1}, X_k, Q, R] p[Y_{k-1} | X_k, Q, R] \quad (\text{IV-39})$$

Using (IV-25) for $y(k)$ we write:

$$p[Y(k) | Y_{k-1}, X_k, Q, R] = p[Hx(k) + v(k) | Y_{k-1}, X_k, Q, R] \quad (\text{IV-40})$$

Given X_k , we know the value of $x(k)$. Knowledge of the conditioning variables gives no new information about $v(k)$, which is independent of X_k and $y(j)$ for $j < k$. (IV-40) therefore becomes the density of $v(k)$ with mean displaced by $Hx(k)$:

$$p[y(k) | Y_{k-1}, X_k, Q, R] = N[Hx(k), R] \quad (IV-41)$$

In the same manner used to obtain (IV-38) we reapply (IV-39) and then substitute (IV-41):

$$p[Y_k | X_k, Q, R] = \prod_{j=1}^k p[y(j) | Y_{j-1}, X_k, Q, R] \quad (IV-42)$$

$$= \prod_{j=1}^k N[Hx(j), R] \quad (IV-43)$$

We can now solve for $J(k)$ by substituting (IV-38) and (IV-43) into (IV-34):

$$J(k) = CN[\hat{x}(0), P(0)] \prod_{j=1}^k N[\phi x(j-1), \Gamma Q \Gamma^T] \prod_{j=1}^k N[Hx(j), R] \quad (IV-44.A)$$

$$= CN[\hat{x}(0), P(0)]$$

$$\times \prod_{j=1}^k (2\pi)^{-\frac{n}{2}} |\Gamma Q \Gamma^T|^{-\frac{1}{2}} \exp\left\{-\frac{1}{2} [x(j) - \phi x(j-1)]^T (\Gamma Q \Gamma^T)^{-1} [x(j) - \phi x(j-1)]\right\} \quad (IV-44)$$

$$\times \prod_{j=1}^k (2\pi)^{-\frac{m}{2}} |R|^{-\frac{1}{2}} \exp\left\{-\frac{1}{2} [y(j) - Hx(j)]^T R^{-1} [y(j) - Hx(j)]\right\}$$

Incorporating into C all components of $J(k)$ which are unaffected by X_k , Q , and R and therefore constant for the maximization procedure, we have:

$$J(k) = C |RQ\Gamma^T|^{-\frac{k}{2}} |R|^{-\frac{k}{2}} \exp\left\{-\frac{1}{2} \sum_{j=1}^k [x(j) - \phi x(j-1)]^T (RQ\Gamma^T)^{-1} [x(j) - \phi x(j-1)]\right. \\ \left. - \frac{1}{2} \sum_{j=1}^k [y(j) - Hx(j)]^T R^{-1} [y(j) - Hx(j)]\right\} \quad (IV-45)$$

We now have $J(k)$ as a function of X_k , Q , and R . Needed at time k are the values $\hat{x}(k|k)$, $\hat{Q}(k|k)$, and $\hat{R}(k|k)$ which maximize $J(k)$. Sage and Husa solve this problem by using a "discrete maximum principle" [10, p. 770]. Here we offer an alternate approach yielding the same results. We first maximize $J(k)$ with respect to Q and R .

To obtain the MAP estimate $\hat{Q}(k|k)$ we rewrite (IV-45):

$$J_Q(k) = C |RQ\Gamma^T|^{-\frac{k}{2}} \exp\left\{-\frac{1}{2} \sum_{j=1}^k [x(j) - \phi x(j-1)]^T (RQ\Gamma^T)^{-1} [x(j) - \phi x(j-1)]\right\} \quad (IV-46)$$

where C contains all factors of $J(k)$ which are not functions of Q . We choose to redefine J in terms of $\ln(J)$ and maximize this function instead. This is allowable, since $\ln(\cdot)$ is a monotone increasing function:

$$J_Q(k) = -k \ln |RQ\Gamma^T| - \frac{k}{2} \sum_{j=1}^k [x(j) - \phi x(j-1)]^T (RQ\Gamma^T)^{-1} [x(j) - \phi x(j-1)] \quad (IV-47)$$

Note that $J_Q(k)$ is a function of $RQ\Gamma^T$, so that we cannot estimate Q directly. Substituting P for $RQ\Gamma^T$ and $z(j)$ for $[x(j) - \phi x(j-1)]$, we

have:

$$J(P) = -k \ln |P| - \sum_{j=1}^k z^T(j) P^{-1} z(j) \quad (\text{IV-48})$$

We seek that value P_0 of P which maximizes (IV-48).

Let us define ϵ as a scalar arbitrarily close to zero, such that $P_0 + \epsilon A$ represents a small deviation in P from P_0 . Since P represents $\Gamma Q \Gamma^T$, both P_0 and A are non-negative definite. We can write:

$$J(P_0 + \epsilon A) = J(P_0) - \delta J(P_0, \epsilon) \quad (\text{IV-49})$$

Obviously, $\delta J = 0$ when $\epsilon = 0$. Since $J(P)$ is maximum at P_0 , δJ cannot go negative and is minimum at $P = P_0$, or at $\epsilon = 0$:

$$\left. \frac{\partial}{\partial \epsilon} \{\delta J(P_0, \epsilon)\} \right|_{\epsilon=0} = 0 \quad (\text{IV-50})$$

We now must obtain a functional relation for $\delta J(P_0, \epsilon)$ in order to solve for P_0 . Using (IV-48), we write:

$$J(P_0 + \epsilon A) = -k \ln |P_0 + \epsilon A| - \sum_{j=1}^k z^T(j) (P_0 + \epsilon A)^{-1} z(j) \quad (\text{IV-51})$$

where

$$|P_0 + \epsilon A| = |P_0 (I + \epsilon P_0^{-1} A)| = |P_0| |I + \epsilon P_0^{-1} A| \quad (\text{IV-52})$$

We use the approximation, valid for small ϵ :

$$|I + \epsilon B| \approx 1 + \epsilon \text{trace}(B) \quad (\text{IV-53})$$

to write:

$$|P_0 + \epsilon A| = |P_0| [1 + \epsilon \text{trace}(P_0^{-1}A)] \quad (\text{IV-54})$$

We next use the matrix identity [12, p. 79]:

$$(B + C)^{-1} = B^{-1} - B^{-1}(B^{-1} + C^{-1})^{-1}B^{-1} \quad (\text{IV-55})$$

to write:

$$(P_0 + \epsilon A)^{-1} = P_0^{-1} - P_0^{-1}[P_0^{-1} + (\epsilon A)^{-1}]^{-1}P_0^{-1} \quad (\text{IV-56})$$

For small ϵ , $(\epsilon A)^{-1} \gg P_0^{-1}$, yielding the approximation:

$$(P_0 + \epsilon A)^{-1} \approx P_0^{-1} - \epsilon P_0^{-1} A P_0^{-1} \quad (\text{IV-57})$$

Now we substitute (IV-54) and (IV-57) into (IV-51):

$$\begin{aligned} J(P_0 + \epsilon A) = & -k \ln |P_0| - k \ln [1 + \epsilon \text{trace}(P_0^{-1}A)] \\ & - \sum_{j=1}^k z^T(j) P_0^{-1} z(j) + \epsilon \sum_{j=1}^k z^T(j) P_0^{-1} A P_0^{-1} z(j) \end{aligned} \quad (\text{IV-58})$$

We recognize the first and third terms of (IV-58) as $J(P_0)$ from (IV-48).

The second and fourth terms give us $\delta J(P_0, \epsilon)$, so that we have:

$$\frac{\partial}{\partial \epsilon} \{\delta J(P_0, \epsilon)\} = -k [1 + \epsilon \text{trace}(P_0^{-1}A)]^{-1} [\text{trace}(P_0^{-1}A)] + \sum_{j=1}^k z^T(j) P_0^{-1} A P_0^{-1} z(j) \quad (\text{IV-59})$$

From (IV-50), we let this become zero for $\epsilon = 0$, yielding:

$$k \text{ trace}(P_0^{-1}A) = \sum_{j=1}^k z^T(j)P_0^{-1}AP_0^{-1}z(j) \quad (\text{IV-60})$$

Using the matrix identity for symmetric, non-negative definite B [1, p. 231]:

$$x^T Bx = \text{trace}(Bxx^T) \quad (\text{IV-61})$$

we have:

$$k \text{ trace}(P_0^{-1}A) = \sum_{j=1}^k \text{trace}[P_0^{-1}AP_0^{-1}z(j)z^T(j)] \quad (\text{IV-62})$$

$$\text{trace}(kP_0^{-1}A) = \text{trace}[P_0^{-1}AP_0^{-1} \sum_{j=1}^k z(j)z^T(j)] \quad (\text{IV-63})$$

Equating trace arguments and simplifying:

$$P_0 = \frac{1}{k} \sum_{j=1}^k z(j)z^T(j) \quad (\text{IV-64})$$

Recalling from before (IV-48) that $z(j) = [x(j) - \phi x(j-1)]$ and that P_0 is that value of $\Gamma Q \Gamma^T$ that maximizes $J_0(k)$, we have:

$$\hat{\Gamma} \hat{Q}(k|k) \Gamma^T = \frac{1}{k} \sum_{j=1}^k [x(j) - \phi x(j-1)][x(j) - \phi x(j-1)]^T \quad (\text{IV-65})$$

The state $x(j)$ is unknown and will be replaced by the optimal smoothed estimate of $x(j)$ given the measurements Y_k :

$$\Gamma \hat{Q}(k|k) \Gamma^T = \frac{1}{k} \sum_{j=1}^k [\hat{x}(j|k) - \phi \hat{x}(j-1|k)][\hat{x}(j|k) - \phi \hat{x}(j-1|k)]^T \quad (\text{IV-66})$$

We obtain the MAP estimate $\hat{R}(k|k)$ in similar fashion, defining $J_R(k)$ those factors of $J(k)$ in (IV-45) which are functions of R :

$$J_R(k) = C|R|^{-\frac{k}{2}} \exp\{-\frac{1}{2} \sum_{j=1}^k [y(j) - Hx(j)]^T R^{-1} [y(j) - Hx(j)]\} \quad (\text{IV-67})$$

$J_R(k)$ has the same form as $J_Q(k)$ in (IV-46), with R replacing $\Gamma Q \Gamma^T$ and $[y(j) - Hx(j)]$ replacing $[x(j) - \phi x(j-1)]$. Maximization of $J_R(k)$ with respect to R should therefore yield an estimate $\hat{R}(k|k)$ of the same form as $\hat{Q}(k|k) \Gamma^T$ in (IV-65):

$$\hat{R}(k|k) = \frac{1}{k} \sum_{j=1}^k [y(j) - Hx(j)][y(j) - Hx(j)]^T \quad (\text{IV-68})$$

We again replace $x(j)$ with the optimal smoothed estimate $\hat{x}(j|k)$:

$$\hat{R}(k|k) = \frac{1}{k} \sum_{j=1}^k [y(j) - H\hat{x}(j|k)][y(j) - H\hat{x}(j|k)]^T \quad (\text{IV-69})$$

We make the assumption that the optimal MAP estimates of (IV-66) and (IV-69) are very nearly equal to the true noise covariances:

$$\hat{Q}(k|k) \Gamma^T \approx \Gamma Q \Gamma^T, \quad \hat{R}(k|k) \approx R \quad (\text{IV-70})$$

Under this assumption we can obtain the optimal MAP state estimate $\hat{x}(k|k)$ from the linear Kalman filter of (III-10)-(III-14), where $\Gamma Q \Gamma^T$ and R are replaced by their MAP estimates. This assumption also allows us to

obtain the estimates $\hat{x}(j|k)$, needed by $r\hat{Q}(k|k)\Gamma^T$ and $\hat{R}(k|k)$, from optimal linear smoothing.

In using the Kalman equations (III-10)-(III-14) to compute $\hat{x}(k|k)$, we must substitute $\hat{R}(k-1|k-1)$ for R . $\hat{x}(k|k)$ requires R in the gain equation (III-12), and since $\hat{R}(k|k)$ requires $\hat{x}(k|k)$ in (IV-69), it does not yet exist. $\hat{R}(k-1|k-1)$ is the best available estimate of R for computing $\hat{x}(k|k)$, and is therefore redefined:

$$\hat{R}(k|k-1) \triangleq \hat{R}(k-1|k-1) = \frac{1}{k-1} \sum_{j=1}^{k-1} [y(j) - H\hat{x}(j|k)][y(j) - H\hat{x}(j|k)]^T \quad (IV-71)$$

Sage and Husa develop an estimation algorithm which uses (IV-66) and (IV-71) to compute $r\hat{Q}(k|k)\Gamma^T$ and $\hat{R}(k|k-1)$ for use in the Kalman filter. However the result quickly becomes complicated and impractical, because of the need to process smoothed estimates $\hat{x}(j|k)$ [10, p. 762]. They then derive from (IV-66) and (IV-71) equations for computing suboptimal estimates $r\hat{Q}_s(k|k)\Gamma^T$ and $\hat{R}_s(k|k)$. These equations require only the estimates $\hat{x}(j|j-1)$ and $\hat{x}(j|j)$ produced by the Kalman filter. We now present a development of their suboptimal method.

In the suboptimal design to follow we first assume that the estimates for $rQ\Gamma^T$ and R will be good enough that the Kalman filter using them will be nearly optimal. We therefore assume that the error covariances $P(k|k-1)$ and $P(k|k)$ are computed correctly by the Kalman filter.

We first replace $\hat{R}(k|k-1)$ in (IV-71) with a suboptimal estimate $\hat{A}(k|k-1)$ which does not require smoothing:

$$\hat{A}(k|k-1) = \frac{1}{k-1} \sum_{j=1}^{k-1} [y(j) - H\hat{x}(j|j-1)][y(j) - H\hat{x}(j|j-1)]^T \quad (\text{IV-72.A})$$

$$= \frac{1}{k-1} \sum_{j=1}^{k-1} v(j)v^T(j) \quad (\text{IV-72})$$

where $v(j)$ is the innovations residual given by (IV-8). To be unbiased, $\hat{A}(k|k-1)$ must have R as its expected value:

$$E\{\hat{A}(k|k-1)\} = \frac{1}{k-1} \sum_{j=1}^{k-1} E\{v(j)v^T(j)\} \quad (\text{IV-73})$$

$$E\{v(j)v^T(j)\} = W = HP(j|j-1)H^T + R \quad (\text{IV-74})$$

where W is the steady-state innovations covariance, given by (IV-13).

$E\{\hat{A}(k|k-1)\}$ thus equals W , so that $\hat{A}(k|k-1)$ is biased. We note however that $HP(j|j-1)H^T$ is computed in the Kalman filter's gain equation (III-12), and can therefore be subtracted out of the summation term to produce an unbiased estimate:

$$\hat{R}_s(k|k-1) = \frac{1}{k-1} \sum_{j=1}^{k-1} v(j)v^T(j) - HP(j|j-1)H^T \quad (\text{IV-75})$$

We now replace $r\hat{Q}(k|k)r^T$ in (IV-66) with a new suboptimal estimate:

$$\hat{A}(k|k) = \frac{1}{k} \sum_{j=1}^k [\hat{x}(j|j) - \phi\hat{x}(j|j-1)][\hat{x}(j|j) - \phi\hat{x}(j|j-1)]^T \quad (\text{IV-76.A})$$

$$= \frac{1}{k} \sum_{j=1}^k [K(j)v(j)][K(j)v(j)]^T \quad (\text{IV-76})$$

where (IV-76) follows from noting that $K(j)v(j)$ is the difference between estimates $\hat{x}(j|j)$ and $\hat{x}(j|j-1)$ in (III-13). To find whether $\hat{A}(k|k)$ is unbiased we compute:

$$E\{\hat{A}(k|k-1)\} = \frac{1}{k} \sum_{j=1}^k K(j)E\{v(j)v^T(j)\}K^T(j) \quad (\text{IV-77})$$

$$K(j)E\{v(j)v^T(j)\}K^T(j) = K(j)W(j)K^T(j) \quad (\text{IV-78.A})$$

$$= K(j)W(j)[P(j|j-1)H^TW^{-1}(j)]^T \quad (\text{IV-78.B})$$

$$= K(j)HP(j|j-1) \quad (\text{IV-78.C})$$

$$= P(j|j-1) - P(j|j) \quad (\text{IV-78.D})$$

$$= \phi P(j-1|j-1)\phi^T + rQr^T - P(j|j) \quad (\text{IV-78})$$

(IV-78.B) results from substituting (III-12) for $K(k)$, while (IV-78.C) results from noting that $P(j|j-1)$ and $W(j)$ are symmetric by definition. We then obtain (IV-78.D) from (III-14) and (IV-78) from (III-11). $\hat{A}(k|k)$ is biased, but we note that $\phi P(j-1|j-1)\phi^T$ and $P(j|j)$ are computed by the Kalman filter and can be removed from the summation. We therefore obtain the suboptimal estimate for rQr^T :

$$r\hat{Q}_s(k|k)r^T = \frac{1}{k} \sum_{j=1}^k K(j)v(j)v^T(j)K^T(j) + P(j|j) - \phi P(j-1|j-1)\phi^T \quad (\text{IV-79})$$

We now write (IV-75) and (IV-79) in recursive form:

$$\hat{R}_s(k|k-1) = \frac{1}{k-1} [(k-2)\hat{R}(k-1|k-2) + v(k-1)v^T(k-1) - HP(k-1|k-2)H^T] \quad (\text{IV-80})$$

$$\begin{aligned} \Gamma\hat{Q}_s(k|k)\Gamma^T &= \frac{1}{k} [(k-1)\Gamma\hat{Q}(k-1|k-1)\Gamma^T + K(k)v(k)v^T(k)K^T(k) \\ &\quad + P(k|k) - \phi P(k-1|k-1)\phi^T] \end{aligned} \quad (\text{IV-81})$$

Sage and Husa devise a suboptimal state estimation algorithm by merely using the Kalman filter equations (III-10)-(III-14) and substituting the estimates of (IV-80) and (IV-81) for the true values R and rQr^T . We modify this algorithm in Chapter IV to work for time-varying Q and R . The algorithm is given below:

$$\hat{x}(k|k-1) = \phi\hat{x}(k-1|k-1) \quad (\text{IV-82})$$

$$P(k|k-1) = \phi P(k-1|k-1)\phi^T + \Gamma\hat{Q}(k-1|k-1)\Gamma^T \quad (\text{IV-83})$$

$$v(k) = y(k) - H\hat{x}(k|k-1) \quad (\text{IV-84})$$

$$K(k) = P(k|k-1)H^T [HP(k|k-1)H^T + \hat{R}(k|k-1)]^{-1} \quad (\text{IV-85})$$

$$\hat{x}(k|k) = \hat{x}(k|k-1) + K(k)v(k) \quad (\text{IV-86})$$

$$P(k|k) = P(k|k-1) - K(k)HP(k|k-1) \quad (\text{IV-87})$$

$$\hat{R}(k+1|k) = \frac{1}{k-1} [(k-2)\hat{R}(k|k-1) + v(k)v^T(k) - HP(k|k-1)H^T] \quad (\text{IV-88})$$

$$\begin{aligned} \Gamma \hat{Q}(k|k) \Gamma^T &= \frac{1}{k} [(k-1) \Gamma \hat{Q}(k-1|k-1) \Gamma^T + K(k) v(k) v^T(k) K^T(k) \\ &+ P(k|k) - \Phi \hat{P}(k-1|k-1) \Phi^T] \end{aligned} \quad (\text{IV-89})$$

The Method of Magill

The method of Magill assumes that the unknown covariances can take on a finite number of possible combinations. A bank of parallel stationary Kalman filters is run, where each filter assumes a different allowable combination of Q and R . The adaptive Kalman filter estimate $\hat{x}(k|k)$ then becomes a weighted sum of the estimates produced by the parallel filters [13].

We first assume the system model of (IV-1)-(IV-4), where the noise covariances are constant and thus denoted as Q and R . The unknown elements of Q and R are contained in the vector α ; we sometimes use the notation $Q(\alpha)$ and $R(\alpha)$ to indicate that a knowledge of α specifies Q and R . Magill assumes that α can take on one of L possible values:

$$\alpha \in \{\alpha_1, \alpha_2, \dots, \alpha_L\} \quad (\text{IV-90})$$

where the i th value has an a priori probability density $p[\alpha_i]$.

We recall from (III-9) that the optimal minimum variance estimate $\hat{x}(k|k)$ is the conditional mean of $x(k)$ given the measurements Y_k :

$$\hat{x}(k|k) = E\{x(k) | Y_k\} \quad (\text{IV-91.A})$$

$$= \int_X x p[x | Y_k] dx \quad (\text{IV-91})$$

where X is the space of all $x(k)$. Defining A as the space of all α , we

have:

$$p[x|Y_k] = \int_A p[x, \alpha|Y_k] d\alpha \quad (\text{IV-92})$$

By the definition of conditional probability:

$$p[x, \alpha|Y_k] = p[x|\alpha, Y_k] p[\alpha|Y_k] \quad (\text{IV-93})$$

Substituting (IV-92) and (IV-93) into (IV-91):

$$\hat{x}(k|k) = \int_X \int_A x p[x|\alpha, Y_k] p[\alpha|Y_k] d\alpha dx \quad (\text{IV-94.A})$$

$$= \int_A \{ \int_X x p[x|\alpha, Y_k] dx \} p[\alpha|Y_k] d\alpha \quad (\text{IV-94})$$

where the last step is accomplished by reversing the order of integration. From (IV-91) we recognize the term in brackets in (IV-94) as the optimal estimate of $x(k)$ given α (Magill calls this the optimal conditional estimate). (IV-94) thus becomes:

$$\hat{x}(k|k) = \int_A \hat{x}(k|k, \alpha) p[\alpha|Y_k] d\alpha \quad (\text{IV-95})$$

$$= \sum_{i=1}^L \hat{x}(k|k, \alpha_i) p[\alpha_i|Y_k] \quad (\text{IV-96})$$

where (IV-96) follows from the quantization of α .

Magill notes here that the optimal estimation of $x(k)$ has been factored into the linear calculation of a set of conditional estimates and the nonlinear calculation of a set of weighting coefficients [13, p. 434]. The first half of this factorization is easily obtained, since the

optimal conditional estimate $\hat{x}(k|k, \alpha_i)$ is the linear Kalman filter estimate produced by assuming α to be α_i :

$$\hat{x}(k|k-1, \alpha_i) = \Phi \hat{x}(k-1|k-1, \alpha_i) \quad (\text{IV-97})$$

$$P(k|k-1, \alpha_i) = \Phi P(k-1|k-1, \alpha_i) + \Gamma Q(\alpha_i) \Gamma^T \quad (\text{IV-98})$$

$$v(k|\alpha_i) = y(k) - H \hat{x}(k|k-1, \alpha_i) \quad (\text{IV-99})$$

$$W(k|\alpha_i) = H P(k|k-1, \alpha_i) H^T + R(\alpha_i) \quad (\text{IV-100})$$

$$K(k|\alpha_i) = P(k|k-1, \alpha_i) H^T W^{-1}(k|\alpha_i) \quad (\text{IV-101})$$

$$\hat{x}(k|k, \alpha_i) = \hat{x}(k|k-1, \alpha_i) + K(k|\alpha_i) v(k|\alpha_i) \quad (\text{IV-102})$$

$$P(k|k, \alpha_i) = P(k|k-1, \alpha_i) - K(k|\alpha_i) H P(k|k-1, \alpha_i) \quad (\text{IV-103})$$

The remaining problem is to find the weighting coefficient $p[\alpha_i | Y_k]$.

We recognize the conditional density $p[\alpha_i | Y_k]$ as the a posteriori density of the unknown noise covariance elements given the measurements.

From Bayes Law we have:

$$p[\alpha_i | Y_k] = \frac{p[Y_k | \alpha_i] p[\alpha_i]}{p[Y_k]} \quad (\text{IV-104.A})$$

$$= C p[Y_k | \alpha_i] p[\alpha_i] \quad (\text{IV-104})$$

where $p[Y_k]$ is independent of i and thereby represented by a constant C whose value is chosen so that the sum of $p[\alpha_i | Y_k]$ over all i is unity. We now write:

$$p[Y_k | \alpha_i] = p[Y(k), Y_{k-1} | \alpha_i] \quad (\text{IV-105.A})$$

$$= p[Y(k) | Y_{k-1}, \alpha_i] p[Y_{k-1} | \alpha_i] \quad (\text{IV-105})$$

We know from (IV-19) that:

$$p[Y(k) | Y_{k-1}] = N[H\hat{x}(k|k-1), W(k)] \quad (\text{IV-106})$$

where $\hat{x}(k|k-1)$ and $W(k)$ are given by the optimal filter. Given that $\alpha = \alpha_i$, we have the optimal filter and write:

$$p[Y(k) | Y_{k-1}, \alpha_i] = N[H\hat{x}(k|k-1; \alpha_i), W(k|\alpha_i)] \quad (\text{IV-107})$$

Reapplying (IV-105) to obtain $p[Y_k | \alpha_i]$ for use in (IV-104), we have:

$$p[\alpha_i | Y_k] = Cp[\alpha_i] \prod_{j=1}^k p[Y(j) | Y_{j-1}, \alpha_i] \quad (\text{IV-108.A})$$

$$= Cp[\alpha_i] \prod_{j=1}^k N[H\hat{x}(j|j-1, \alpha_i), W(j|\alpha_i)] \quad (\text{IV-108.B})$$

$$= Cp[\alpha_i] \prod_{j=1}^k |W(j|\alpha_i)|^{-\frac{1}{2}} \exp\{-\frac{1}{2}v^T(j|\alpha_i)W^{-1}(j|\alpha_i)v(j|\alpha_i)\} \quad (\text{IV-108})$$

The adaptive Kalman filter algorithm of Magill is now defined. For

the i th stationary parallel filter we compute $\hat{x}(k|k, \alpha_i)$ from (IV-97)-(IV-103) and $p[\alpha_i|Y_k]$ from (IV-108). The adaptive filter estimate $\hat{x}(k|k)$ follows from (IV-96).

Two modifications will improve the practical implementation of Magill's algorithm. First, Sims and Lainiotis note that (IV-108) can be realized by a faster recursive form requiring less storage [14]. We reproduce their result here by rewriting (IV-108):

$$p[\alpha_i|Y_k] = Cp[\alpha_i]|W(k|\alpha_i)|^{-\frac{1}{2}} \exp\{-\frac{1}{2}v^T(k|\alpha_i)W^{-1}(k|\alpha_i)v(k|\alpha_i)\} \quad (IV-109.A)$$

$$\times \prod_{j=1}^{k-1} |W(j|\alpha_i)|^{-\frac{1}{2}} \exp\{-\frac{1}{2}v^T(j|\alpha_i)W^{-1}(j|\alpha_i)v(j|\alpha_i)\}$$

$$= C|W(k|\alpha_i)|^{-\frac{1}{2}} \exp\{-\frac{1}{2}v^T(k|\alpha_i)W^{-1}(k|\alpha_i)v(k|\alpha_i)\} p[\alpha_i|Y_{k-1}] \quad (IV-109)$$

The second modification results from noting that since the parallel Kalman filters are stationary, their gains and covariances reach constant, steady-state values. Before actual implementation the gain and covariance equations for each parallel filter can be run until $K(k|\alpha_i)$ and $W(k|\alpha_i)$ reach steady-state values $K(\alpha_i)$ and $W(\alpha_i)$. Then (IV-97)-(IV-103) for the adaptive filter can be replaced by:

$$\hat{x}(k|k-1, \alpha_i) = \hat{\phi}\hat{x}(k-1|k-1, \alpha_i) \quad (IV-110)$$

$$v(k|\alpha_i) = y(k) - H\hat{x}(k|k-1, \alpha_i) \quad (IV-111)$$

$$\hat{x}(k|k, \alpha_i) = \hat{x}(k|k-1, \alpha_i) + K(\alpha_i)v(k|\alpha_i) \quad (IV-112)$$

$W(\alpha_i)$ replaces $W(k|\alpha_i)$ in (IV-109).

The Method of Alspach

The method of Alspach assumes that the unknown optimal gain $K(k)$ of the Kalman filter is a random variable with a posteriori density $p[K|Y_k]$. Alspach runs a bank of parallel stationary Kalman filters with enough gains K_i to cover the space of allowable K . The innovations sequence of the i th filter is used to obtain the density $p[K_i|Y_k]$. The resulting discretized a posteriori density is then used to compute an estimate $\hat{K}(k)$ of the optimal gain for use in an adaptive Kalman filter.

We assume the system model of (IV-1)-(IV-4), where the noise covariances Q and R are unknown constants. For known Q and R the optimal state estimate is given by the stationary Kalman filter:

$$\hat{x}(k|k-1) = \Phi\hat{x}(k-1|k-1) \quad (IV-113)$$

$$\hat{x}(k|k) = \hat{x}(k|k-1) + K_{OPT}[y(k) - H\hat{x}(k|k-1)] \quad (IV-114)$$

where K_{OPT} is the gain $K(k)$ when the Kalman filter equations (III-10)-(III-14) are run to steady-state. For the problem here K_{OPT} is unknown and is assumed at time k to be a random variable with an a posteriori density $p_{K_{OPT}}[K|Y_k]$. We next implement a bank of L stationary Kalman filters running in parallel, where the i th filter has a fixed suboptimal gain K_i :

$$\hat{x}(k|k-1, K_i) = \Phi \hat{x}(k-1|k-1, K_i) \quad (\text{IV-115})$$

$$v(k|K_i) = y(k) - H\hat{x}(k|k-1, K_i) \quad (\text{IV-116})$$

$$\hat{x}(k|k, K_i) = \hat{x}(k|k-1, K_i) + K_i v(k|K_i) \quad (\text{IV-117})$$

The gains $\{K_1, K_2, \dots, K_L\}$ are chosen to cover the space of allowable K_{OPT} . We desire to use the observed statistical properties of the i th filter to compute the conditional density $p_{K_{\text{OPT}}} [K_i | Y_k]$. By computing $p_{K_{\text{OPT}}} [K_i | Y_k]$ as a function of K_i for a sufficient number of gains we can identify the a posteriori density of K_{OPT} well enough to estimate its value.

We define W_{OPT} as the steady-state innovations covariance of the optimal filter. Alspach first solves for the joint a posteriori density of K_{OPT} and W_{OPT} , which by Bayes Law becomes:

$$p_{K_{\text{OPT}}, W_{\text{OPT}}} [K, W | Y_k] = \frac{p[Y_k | K, W] p_{K_{\text{OPT}}, W_{\text{OPT}}} [K, W]}{p[Y_k]} \quad (\text{IV-118.A})$$

$$= C p[Y_k | K, W] p[K, W] \quad (\text{IV-118})$$

where $p[Y_k]$ is constant for all K, W and therefore replaced by C .

$p_{K_{\text{OPT}}, W_{\text{OPT}}} [K, W]$ is the a priori density of K and W , representing any knowledge of K_{OPT} and W_{OPT} without measurement information. The subscripts on $p[\cdot]$ are dropped where no confusion results. From the definition of conditional probability we can rewrite (IV-118):

$$p[K, W|Y_k] = Cp[Y_k|K, W]p[W|K]p[K] \quad (\text{IV-119})$$

We then write:

$$p[Y_k|K, W] = p[y(k), Y_{k-1}|K, W] \quad (\text{IV-120.A})$$

$$= p[y(k)|Y_{k-1}, K, W]p[Y_{k-1}|KW] \quad (\text{IV-120})$$

From (IV-19) we know that:

$$p[y(k)|Y_{k-1}] = N[\hat{Hx}(k|k-1, K_{OPT}), W_{OPT}] \quad (\text{IV-121})$$

Given that $K_{OPT} = K$, $W_{OPT} = W$, we can therefore impute:

$$p[y(k)|Y_{k-1}, K, W] = N[\hat{Hx}(k|k-1, K), W] \quad (\text{IV-122})$$

Applying this result to (IV-120) we have:

$$p[Y_k|K, W] = \prod_{j=1}^k p[y(j)|Y_{j-1}, K, W] \quad (\text{IV-123.A})$$

$$= \prod_{j=1}^k N[\hat{Hx}(j|j-1, K), W] \quad (\text{IV-123})$$

We now rewrite (IV-119):

$$p[K, W, |Y_k] = Cp[W|K]p[K] \prod_{j=1}^k |W|^{-\frac{1}{2}} \exp\{-\frac{1}{2}[y(j) - \hat{Hx}(j|j-1, K)]^T \\ \times W^{-1}[y(j) - \hat{Hx}(j|j-1, K)]\} \quad (\text{IV-124.A})$$

$$= C_p[W|K]p[K]|W|^{-\frac{k}{2}} \exp\left\{-\frac{1}{2} \sum_{j=1}^k v^T(j|K)W^{-1}v(j|K)\right\} \quad (\text{IV-124})$$

Alspach now specializes the adaptive Kalman filtering development to the case of scalar noise and measurements. This is general enough to cover our specific aircraft model of (III-1)-(III-4). Q , R , and W_{OPT} are now scalars, and (IV-124) becomes:

$$p[K, W|Y_k] = p[W|K]p[K]W^{-\frac{k}{2}} \exp\left\{-\frac{1}{2} \sum_{j=1}^k \frac{v^2(j|K)}{W}\right\} \quad (\text{IV-125})$$

We define the sample covariance of $v(k|K)$ by:

$$\hat{W}(k|K) = \frac{1}{k} \sum_{j=1}^k v^2(j|K) \quad (\text{IV-126})$$

For stationary Gaussian noise $\hat{W}(k|K)$ is an unbiased estimate of W . (IV-125) thus becomes:

$$p[K, W|Y_k] = p[W|K]p[K]W^{-\frac{k}{2}} \exp\left\{-\frac{k}{2} \frac{\hat{W}(k|K)}{W}\right\} \quad (\text{IV-127})$$

We now express W_{OPT} in terms of K_{OPT} by using (III-32):

$$W_{opt} = R/[1 - HK_{OPT}] \quad (\text{IV-128})$$

Assume that the only a priori information we have about Q and R is that they are bounded by the values Q_{MAX} and R_{MAX} . Then given K_{OPT} , the only information we have about W_{OPT} is that it lies somewhere between zero and

an upper bound $W_{MAX}(K_{OPT})$:

$$W_{MAX}(K_{OPT}) = R_{MAX}/[1 - HK_{OPT}] \quad (IV-129)$$

Alspach therefore assumes that the conditional density of W_{OPT} given K_{OPT} is uniform:

$$p(W|K) = \begin{cases} \frac{1}{W_{MAX}} & : 0 \leq W \leq W_{MAX}(K) \\ 0 & : \text{otherwise} \end{cases} \quad (IV-130)$$

Substituting (IV-130) for $p[K|W]$, we can obtain $p[K|Y_k]$ by integrating the joint conditional density of (IV-127) over the range of W :

$$p[K|Y_k] = \int_{-\infty}^{\infty} p[K, W|Y_k] dW \quad (IV-131.A)$$

$$= \frac{Cp[K]}{W_{MAX}(K)} \int_0^{W_{MAX}(K)} W^{-\frac{k}{2}} \exp\left\{-\frac{\hat{W}(k|K)}{W}\right\} dW \quad (IV-131)$$

Using the variable of integration $z = \frac{k\hat{W}(k|K)}{2W}$, (IV-131) becomes:

$$p[K|Y_k] = \frac{Cp[K]}{W_{MAX}(K)} [\hat{W}(k|K)]^{-(k-2)/2} \int_a^{\infty} z^{-(k-4)/2} e^{-z} dz \quad (IV-132.A)$$

$$= \frac{Cp[K]}{W_{MAX}(K)} [\hat{W}(k|K)]^{-(k-2)/2} WT(k, K) \quad (IV-132)$$

where

$$a \triangleq \frac{k}{2} \hat{W}(k|K) / W_{MAX}(K) \quad (IV-133)$$

$WT(k, K)$ is the integral of (IV-132.A) and is a function of the ratio $\hat{W}(k|K) / W_{MAX}(K)$. We define M as the value $(k - 4)/2$. When M is an integer (meaning k is even and greater than 2) we can evaluate WT :

$$WT(k, K) = \int_a^\infty z^M e^{-z} dz \quad (IV-134.A)$$

$$= M! e^{-a} \sum_{j=0}^M \frac{a^{M-j}}{(M-j)!} \quad (IV-134.B)$$

$$= \left(\frac{k-4}{2}\right)! \exp\left\{-\frac{k}{2} \frac{\hat{W}(k|K)}{W_{MAX}(K)}\right\} \sum_{j=0}^{(k-4)/2} \frac{\left[\frac{k}{2} \frac{\hat{W}(k|K)}{W_{MAX}(K)}\right]^{(k-4)/2-j}}{\left[\frac{k-4}{2} - j\right]!} \quad (IV-134)$$

Alsopach plots $WT(k|K)$ as a function of $\hat{W}(k|K) / W_{MAX}(K)$ for different values of k . His results are reproduced in Figure IV-2. He notes that for k above 1000, $WT(k, K)$ can be approximated as a unit step which falls to zero at $\hat{W}(k|K) = W_{MAX}(K)$ (This is not a bad assumption even for $k = 50$ or 100). Thus $WT(k, K)$ acts to discriminate against gains for which the sample innovations covariance exceeds the maximum value:

$$p[K|Y_k] = \begin{cases} \frac{Cp[K]}{W_{MAX}(K)} [\hat{W}(k|K)]^{-(k-2)/2} : \hat{W}(k|K) \leq W_{MAX}(K) \\ 0 : \hat{W}(k|K) > W_{MAX}(K) \end{cases} \quad (IV-135)$$

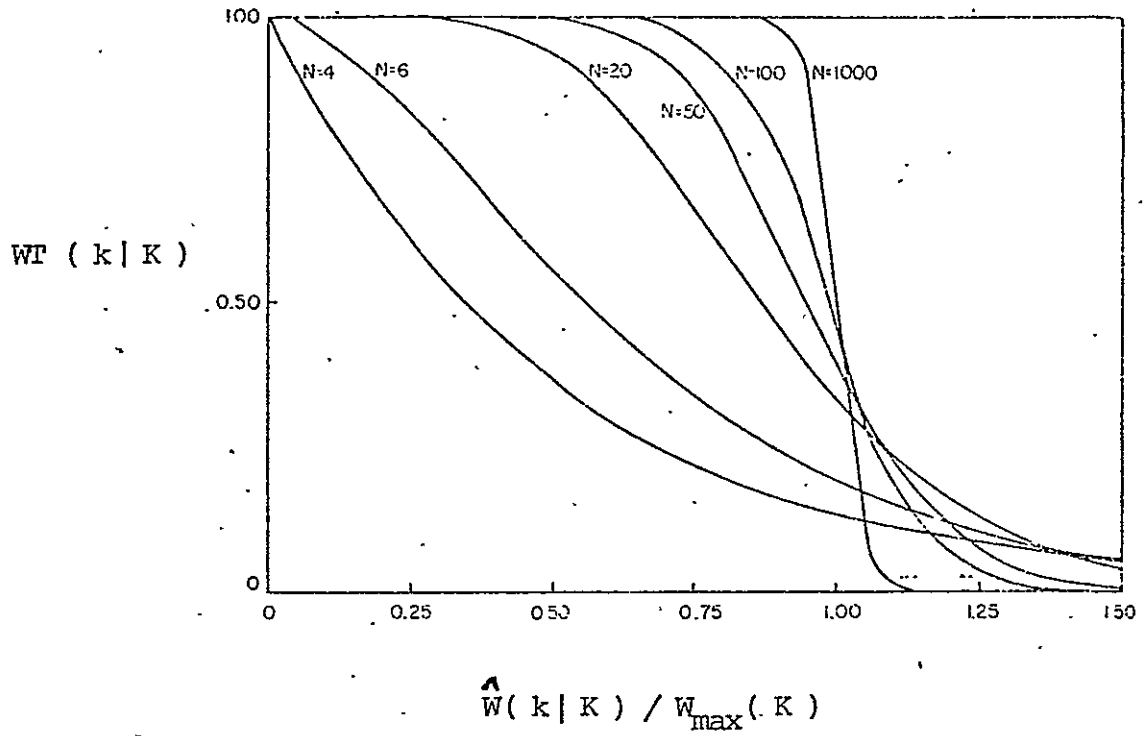


Figure IV - 2. $Wf(k|K)$ vs. $\hat{W}(k|K) / W_{\max}(K)$

[8, p. 272]

We now assume no a priori information about Q and R , so that Q_{MAX} and R_{MAX} become infinite. Since nothing is known about K_{OPT} , $p[K]$ can be made uniform over the limits of allowable gain. $w_{MAX}(k)$ now approaches infinity, so that $WT(k|K)$ becomes unity for all $\hat{W}(k|K)$. We now have:

$$p[K|Y_k] = \begin{cases} c[\hat{W}(k|K)]^{-(k-2)/2}, & \text{allowable gain} \\ 0, & \text{otherwise} \end{cases} \quad (IV-136)$$

The adaptive Kalman filter of Alspach is now ready for implementation. For each of the parallel suboptimal filters the estimate $\hat{x}(k|k, K_i)$ and innovations residual $v(k|K_i)$ are obtained from (IV-115)-(IV-117). The a posteriori gain density $p[K_i|Y_k]$ is then computed by (IV-136), using the sample innovations covariance of (IV-126), which Alspach writes in recursive form:

$$\hat{W}(k|K) = \frac{1}{k} [(k-1)\hat{W}(k-1|K) + v^2(k|K)] \quad (IV-137)$$

The adaptive filter implementation is greatly simplified when we recall from Chapter III that for scalar noise and measurements the optimal gain K_{OPT} is known when only one element is specified. ($K_2(k)$ is given as a function of $K_1(k)$ in (III-42) for our aircraft model). Also, the gain K_{OPT} is always bounded. We can therefore implement the parallel filters by uniformly incrementing the first gain element between limits K_{1MIN} and K_{1MAX} , allowing K_{ji} ($2 \leq j \leq n$) to be determined by the appropriate functional relation. We can therefore use (IV-136) to find $p[K_{1i}|Y_k]$ and thus estimate K_{1OPT} . Alspach does not specify what

estimation scheme to use in computing $\hat{K}_1(k)$. However, since we know the conditional mean $E\{K_1|Y_k\}$ to be the optimal minimum variance estimate from (II-9), we use it here:

$$\hat{K}_1(k) = \sum_{i=1}^L K_i p[K_i|Y_k] \quad (\text{IV-138})$$

$\hat{K}_1(k)$ automatically defines $\hat{K}(k)$, which is then used in the adaptive filter of (IV-5) and (IV-6).

Alspach admits that his algorithm may be impractical for use in a general-purpose digital computer where the L suboptimal stationary filters must be implemented serially. However, in a special-purpose parallel implementation the stationary filters can run simultaneously, producing a fast adaptive algorithm. He also notes that, though similar to the parallel filters method of Magill, his algorithm is simpler, requiring fewer parallel paths. Consider the scalar noise case where Q and R are both unknown. For n possible values of Q and m values of R , we would need $n \times m$ parallel filters in Magill's algorithm. The number of allowable Q and R values may increase further if we do not know their upper bounds Q_{MAX} and R_{MAX} , which can approach infinity. In Alspach's algorithm the only unknown is K_1 , which is always bounded. We need only to use enough parallel filters to adequately cover the range of allowable K_1 values.

The Minimum Innovations Covariance Method

The last adaptive Kalman filtering method presented here is an intuitive scheme which has some theoretical backing. As in the methods

of Magill and Alspach, a bank of parallel fixed-gain Kalman filters is run. The gain of that filter with the minimum innovations sample covariance is chosen as the gain $\hat{K}(k)$ for use in the adaptive Kalman filter.

We again assume the system model of (IV-1) to (IV-4), but with scalar noise and measurements, so that Q and R are unknown scalar constants. From (III-13) we recall that the steady-state innovations covariance W is minimum when the suboptimal filter gain becomes the optimal Kalman gain. Let us revisit Figure III-1 and IV-1, where $P_{11}(k|k)$; the mean-square error in $\hat{\theta}(k|k)$, and W are plotted as functions of suboptimal gain \hat{K}_1 for the aircraft system of (III-1)-(III-4) with stationary noise (\hat{K}_2 is given by (III-42)). Not only are $P_{11}(k|k)$ and W minimum for $\hat{K}_1 = K_{1\text{OPT}}$, but both increase monotonically when \hat{K}_1 either increases or decreases from the optimal gain. We can assert that the innovations covariance W is a direct indicator of a suboptimal filter's error performance.

We now implement a bank of parallel fixed-gain Kalman filters, where, as in the algorithm of Alspach, the gain K_1 is incremented between the limits $K_{1\text{MIN}}$ and $K_{1\text{MAX}}$. The i th filter is realized, just as in Alspach, by (IV-115)-(IV-117). The sample covariance $\hat{W}(k|\alpha_i)$ of the innovations sequence is computed from (IV-137). We note that $\hat{W}(k|K)$ is the standard covariance estimate for a stationary scalar process with zero mean, and is therefore our best estimate of $W(k|K)$. It would thus seem reasonable to choose that parallel filter with the lowest value of $\hat{W}(k|K_i)$ as the one whose gain is closest to $K_{1\text{OPT}}$. We therefore choose the gain of this filter as the gain $\hat{K}(k)$ of our adaptive Kalman filter:

$$\hat{K}(k) = K_i: \hat{W}(k|K_i) \leq \hat{W}(k|K_j), 1 \leq j \leq L \quad (\text{IV-139})$$

The adaptive filter is given by (IV-5) and (IV-6).

This intuitive scheme has a theoretical appeal when we recall (IV-136), which gives $p[K_i|Y_k]$ for the i th parallel fixed-gain filter. The gain K_i which minimizes $\hat{W}(k|K_i)$ is the same gain which maximizes the a posteriori density $p[K_i|Y_k]$, as derived by Alspach. Instead of the conditional mean estimate of K_{OPT} , we are choosing the maximum a posteriori estimate of K_{OPT} . The intuitive, minimum sample covariance estimate $\hat{K}(k)$ may therefore be considered the MAP gain estimate of Alspach. Of course, this MAP estimate does not require the calculation of $p[K_i|Y_k]$, and is therefore easier to implement than the method of Alspach.

CHAPTER V

ADAPTIVE KALMAN FILTERING WITH TIME-VARYING NOISE STATISTICS

In Chapter IV we presented four methods of adaptive Kalman filtering for use in problems where the noise is stationary. We recall our general system model of (IV-1)-(IV-4). The noise covariances $Q(k-1)$ and $R(k)$ were unknown constants. In this chapter we remove the stationary noise assumption and allow $Q(k-1)$ and $R(k)$ to vary with time. We modify the adaptive filtering methods to work for the non-stationary noise case and then specialize them to our aircraft system model.

The Method of Alspach

We recall that Alspach assumes that the measurements and noise terms of the system model (IV-1)-(IV-4) are scalars. The a posteriori density of the optimal gain $K(k)$ is found by computing the sample innovations covariance $\hat{W}(k|K_i)$ for each of the parallel stationary filters:

$$\hat{W}(k|K_i) = \frac{1}{k} [(k-1)\hat{W}(k-1|K_i) + v^2(k|K_i)] \quad (V-1)$$

Alspach points out that as k becomes large, the present innovations residual $v(k|K_i)$ has little effect upon the value $\hat{W}(k|K_i)$. In order to prevent $\hat{W}(k|K_i)$ from becoming insensitive to new information he suggests the following change [15, p. 553]:

$$\hat{W}(k|K_i) = \begin{cases} \frac{1}{k}[(k-1)\hat{W}(k-1|K_i) + v^2(k|K_i)]; & k \leq N \\ \frac{1}{N}[(N-1)\hat{W}(k-1|K_i) + v^2(k|K_i)]; & k > N \end{cases} \quad (V-2)$$

where N is chosen for the stationary noise case such that $\hat{W}(k|K_i)$ is within some acceptable r.m.s. deviation of the true covariance $W(k|K_i)$ for $k > N$. We can view (V-2) as a fading-memory estimate of $W(k|K_i)$, where old innovations residuals are deweighted: values $v(j|K_i)$ will have little effect on $\hat{W}(k|K_i)$ for $j < (k - N)$. $\hat{W}(k|K_i)$ becomes the output of a first-order lowpass filter with input $v^2(k)$ and time constant $N\Delta t$.

If the noise covariances $Q(k-1)$ and $R(k)$ are slowly changing with time, we can approximate them as being constant for N iterations. We can then estimate the state with stationary noise methods where only the last N innovations residuals are used. Alspach has done this by using (V-2) to estimate $W(k|K_i)$ as it changes with $Q(k-1)$ and $R(k)$. Of course, the more slowly changing the noise covariances are, the larger N becomes, making $\hat{W}(k|K_i)$ more accurate. Alspach also modifies (IV-136) for computing the a posteriori density of the gain:

$$p[K_i|Y_k] = \begin{cases} C[\hat{W}(k|K_i)]^{-(k-2)/2}, & k \leq N \\ C[\hat{W}(k|K_i)]^{-(N-2)/2}, & k > N \end{cases} \quad (V-3)$$

The adaptive algorithm of Alspach remains the same as for the stationary case, with (V-2) replacing (IV-137) and (V-3) replacing (IV-136). Alspach adds another modification by restricting the range of $\hat{W}(k|K_i)$ among parallel filters. This is done to enhance the adaptive filter's

ability to follow time changes in the noise covariances, and is illustrated by example:

Consider two filters in the parallel filter bank, one with very low gain K_j and the second with high gain K_1 . Consider also the case where the ratio $Q(k-1)/R(k)$ is large, so that the optimal gain is near K_1 . Recalling Figures III-1 and IV-1, we expect $\hat{W}(k|K_1)$ to be low while $\hat{W}(k|K_j)$ becomes very high, indicating a diverging filter. $p[K_j|Y_k]$ will be nearly zero, so that only the higher gains contribute to $\hat{K}(k)$. Now assume that $Q(k-1)/R(k)$ suddenly becomes small, so that the optimal gain is near K_j . The true innovations covariance $W(k|K_j)$ becomes small, but the sample covariance $\hat{W}(k|K_j)$ will not show this effect for a considerable time; the old residuals $v(k|K_j)$ taken while the filter was divergent must be deweighted and replaced by new residuals of lower covariance. Such a process could require more than a time constant of the fading memory filter of (V-2).

Alspach has therefore placed a ceiling on $\hat{W}(k|K_j)$. If $\hat{W}(k|K_1)$ is the minimum sample covariance among all parallel filters, then $\hat{W}(k|K_j)$ is not allowed to exceed an upper bound $f_{MAX} \times \hat{W}(k|K_1)$. Whenever this limit is exceeded, we replace the estimate $\hat{x}(k|k, K_j)$ with $\hat{x}(k|k, K_1)$. This modification allows $p[K_j|Y_k]$ to quickly become significant when the optimal gain suddenly shifts toward K_j .

Alspach also modifies his algorithm to allow the value N to adapt to changes in the time variations of $Q(k-1)$ and $R(k)$. A fading memory estimate $\hat{W}(k|\hat{K})$ of the adaptive filter's innovations covariance is computed using (V-2). A second estimate $\hat{W}_2(k|\hat{K})$ is computed by replacing N in (V-2) with a smaller time constant N_2 (we could make N_2 some fraction,

say 20 percent, of the nominal value of N). If N is large and $Q(k-1)/R(k)$ suddenly changes, the small time constant filter will soon detect this change by changing $\hat{W}_2(k|\hat{K})$. When $\hat{W}(k|\hat{K})$ and $\hat{W}_2(k|\hat{K})$ differ by more than an allowable amount, N will be decreased.

Alspach uses the following procedure for changing N : for stationary noise we know that the variance in the unbiased estimate $\hat{W}_2(k|\hat{K})$ is:

$$\text{Var}\{\hat{W}_2(k|\hat{K})\} = 2W^2(k|\hat{K})/N_2 \quad (\text{V-4})$$

Assuming $\hat{W}(k|\hat{K})$ to be our best estimate of $W(k|\hat{K})$, we can measure standard deviation in $\hat{W}_2(k|\hat{K})$:

$$\sigma_2 = \hat{W}(k|\hat{K})/\sqrt{N_2/2} \quad (\text{V-5})$$

Alspach then modifies N according to the rule:

$$\Delta = |\hat{W}(k|\hat{K}) - \hat{W}_2(k|\hat{K})| \quad (\text{V-6.A})$$

$$\text{IF } \Delta < \sigma_2: N \rightarrow N + N_2 \quad (\text{V-6.B})$$

$$\text{IF } \Delta > 2\sigma_2: N \rightarrow N - \text{Integer}\left[\frac{\Delta}{\sigma_2} N_2\right] \quad (\text{V-6.C})$$

The above procedure works for situations where changes in $Q(k-1)$ and $R(k)$ produce a wide dynamic range in the values of $W(k|\hat{K})$. In the simulation testing described in Chapter VI this was not the case, with $W(k|\hat{K})$ never changing by more than 25 percent. N was chosen experimentally from various simulation runs and left constant.

Figure V-1 is a block diagram of the adaptive algorithm of Alspach for the specific MLS aircraft model of (III-1)-(III-4). The algorithm is implemented as a computer subroutine, where during the k th iteration the measurement y is received and estimates $\hat{\theta}_{AD}$ and $\hat{\sigma}_{AD}$ are computed and returned to the main program (the subroutine is not given the noise covariances $Q(k-1)$ and $R(k)$). The adaptive filter has L parallel stationary filters, implemented according to (IV-115)-(IV-117). The conditional density $p[K_i | Y_k]$ is computed for each filter according to (V-3), using the sample innovations covariance $\hat{W}(k | K_i)$ of (V-2). The adaptive Kalman filter is then updated using the gain \hat{K} computed from (IV-138).

The block diagram shown here is for an algorithm using constant N . FIRST is a logical variable which is TRUE until k is greater than N . We should point out that since this algorithm will be implemented as a subroutine in a digital computer simulation, the parallel filters must be run serially. In an actual parallel implementation, the i -loops in the block diagram would not exist: the parallel filters would run simultaneously.

We now proceed to modify the other three adaptive filtering algorithms for use in problems where the noise statistics are time varying. We make use of Alspach's fading memory approach to deweighting old innovations information. Each algorithm is then specialized to our aircraft problem model of (III-1)-(III-4).

The Minimum Innovations Covariance Method

As stated in Chapter IV, this method is actually that of Alspach, where the maximum a posteriori (MAP) estimate of the gain $K(k)$ is used by

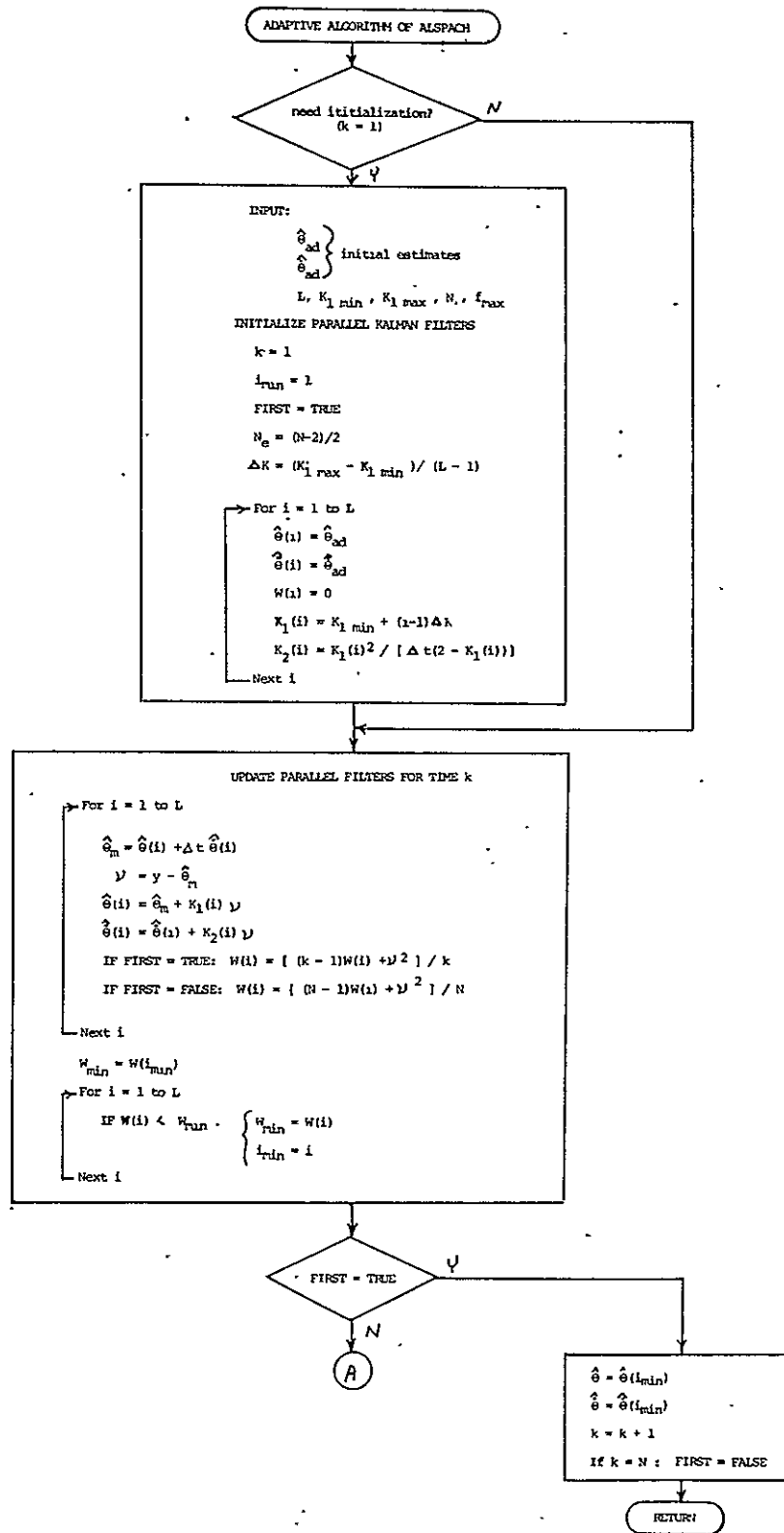


Figure V - 1. Adaptive Algorithm of Alspach

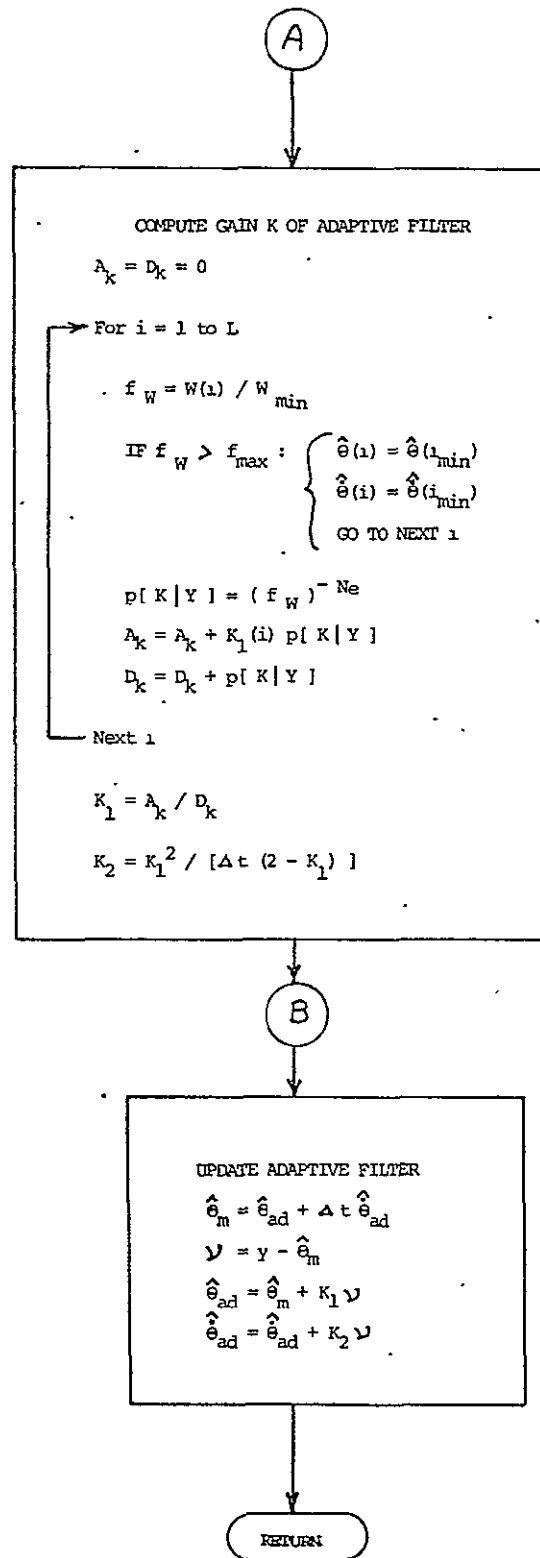


Figure V - 1.A Algorithm of Alspach (continued)

the adaptive filter. The adaptive filter algorithm looks like that of Alspach, except that the conditional density $p[K_i|Y_k]$ is not computed. Instead, the adaptive gain \hat{K} is just set equal to the gain of the parallel filter with lowest sample covariance $\hat{W}(k|K_i)$. We can therefore use the block diagram of Alspach in Figure V-1, where the only modifications necessary are between points A and B. These modifications are shown in Figure V-2.

The Method of Sage and Husa

The suboptimal algorithm of Sage and Husa is that of a discrete Kalman filter where the unknown noise covariances $Q(k-1)$ and $R(k)$ are replaced by the estimates of (IV-75) and (IV-79). We can make these estimates responsive to changes in the noise covariances by using only the last N innovations residuals:

$$\Gamma \hat{Q}_S(k|k) \Gamma^T = \frac{1}{N} \sum_{j=k-N}^k K(j) v(j) v^T(j) K^T(j) + P(j|j) - \Phi P(j-1|j-1) \Phi^T \quad (V-7)$$

$$\hat{R}_S(k|k-1) = \frac{1}{N} \sum_{j=k-N-1}^{k-1} v(j) v^T(j) - H P(j|j-1) H^T \quad (V-8)$$

We now use recursive approximations:

$$\Gamma \hat{Q}_S(k|k) \Gamma^T = \begin{cases} \frac{1}{k} [(k-1) \Gamma \hat{Q}_S(k-1|k-1) \Gamma^T + K(k) v(k) v^T(k) K^T(k) \\ \quad + P(k|k) - \Phi P(k-1|k-1) \Phi^T], & k \leq N \\ \frac{1}{N} [(N-1) \Gamma \hat{Q}_S(k|k) \Gamma^T + K(k) v(k) v^T(k) K^T(k) \\ \quad + P(k|k) - \Phi P(k-1|k-1) \Phi^T], & k > N \end{cases} \quad (V-9)$$

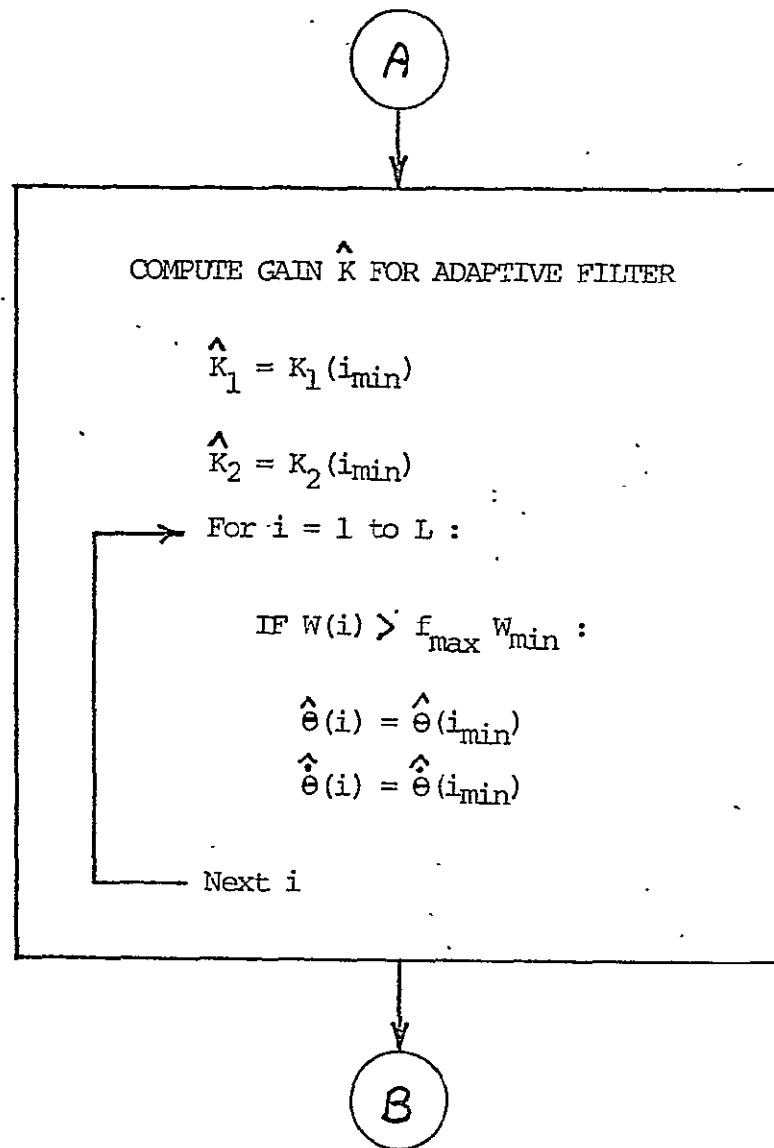


Figure V - 2. Modifications to Block Diagram of Alspach for Implementation of Minimum Innovations Covariance Filter

2-1
 1-1

$$\hat{R}_s(k|k-1) = \begin{cases} \frac{1}{k-1}[(k-2)\hat{R}_s(k-1|k-2) + v(k)v^T(k) - HP(k|k-1)H^T], & k \leq N \\ \frac{1}{N}[(N-1)\hat{R}_s(k-1|k-2) + v(k)v^T(k) - HP(k|k-1)H^T], & k > N \end{cases} \quad (V-10)$$

We note that the equations in (V-9) and (V-10) for $k \leq N$ are the recursive equations (IV-88) and (IV-89) in the original algorithm of Sage and Husa. We can obtain a more practical form of (V-9), in terms of quantities already computed by the Kalman filter, by recalling from (IV-83) that $\phi P(k-1|k-1)\phi^T$ equals $P(k|k-1) - \Gamma\hat{Q}_s(k-1|k-1)\Gamma^T$:

$$\Gamma\hat{Q}_s(k|k)\Gamma^T = \begin{cases} \Gamma\hat{Q}_s(k-1|k-1)\Gamma^T + \frac{1}{k}[K(k)v(k)v^T(k)K^T(k) \\ \quad + P(k|k) - P(k|k-1)], & k \leq N \\ \Gamma\hat{Q}_s(k-1|k-1)\Gamma^T + \frac{1}{N}[K(k)v(k)v^T(k)K^T(k) \\ \quad + P(k|k) - P(k|k-1)], & k > N \end{cases} \quad (V-11)$$

The adaptive algorithm of Sage and Husa is now given by the original algorithm of (IV-82)-(IV-89) with (V-10) replacing (IV-88) and (V-11) replacing (IV-89). Figure V-3 is a block diagram of this algorithm for the specific aircraft model of (III-1)-(III-4). The Kalman filter equations (IV-83)-(IV-87) are given by the specific equations (III-18)-(III-28), with $\Gamma\hat{Q}_s(k|k)\Gamma^T$ replacing $\Gamma Q(k)\Gamma^T$. $R(k)$ is known in this problem, and so $\hat{R}_s(k|k)$ is not needed.

The Method of Magill

Here we modify the algorithm of Magill for the case of scalar measurements and noise. We make the conditional density $p[\alpha_i|Y_k]$ in

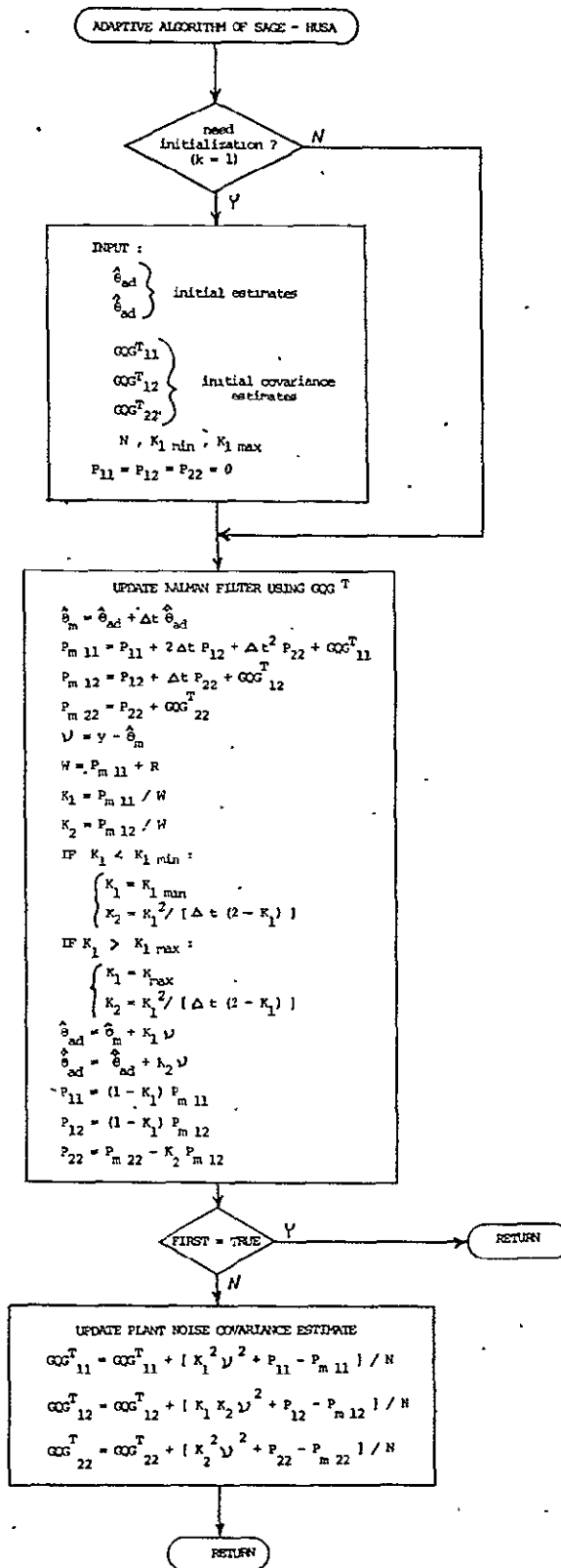


Figure V - 3. Adaptive Algorithm of Sage - Husa

(IV-108) a function of only the N most recent innovations residuals:

$$p[\alpha_i | Y_k] = Cp[\alpha_i] \prod_{j=k-N}^k W^{-\frac{1}{2}}(j|\alpha_i) \exp\left\{-\frac{1}{2} \frac{v^2(j|\alpha_i)}{W(j|\alpha_i)}\right\} \quad (V-12)$$

We then use the recursive approximation:

$$p[\alpha_i | Y_k] = \begin{cases} CW^{-\frac{1}{2}}(k|\alpha_i) \exp\left\{-\frac{1}{2} \frac{v^2(k|\alpha_i)}{W(k|\alpha_i)}\right\} p[\alpha_i | Y_{k-1}] & , k \leq N \\ CW^{-\frac{1}{2}}(k|\alpha_i) \exp\left\{-\frac{1}{2} \frac{v^2(k|\alpha_i)}{W(k|\alpha_i)}\right\} (p[\alpha_i | Y_{k-1}])^{\frac{N-1}{N}} & , k > N \end{cases} \quad (V-13)$$

where $p[\alpha_i | Y_0] = p[\alpha_i]$.

We recall that for our specific problem model (III-1)-(III-4) only the plant noise covariance $Q(k-1)$ is unknown. We can therefore set the unknown parameter vector α equal to the scalar $Q(k-1)$. We implement L parallel Kalman filters: the i th filter uses the true value $R(k)$ and an estimate Q_i for $Q(k-1)$.

The i th parallel filter is not stationary, since $R(k)$ is time varying. The gain $K_i(k)$ is not a steady-state value as in Chapter IV, and this requires running all the Kalman gain and covariance equations. This problem can be avoided in our case by noting that Q_i is never explicitly used in computing $p[Q_i | Y_k]$; only $K(k|Q_i)$ and $W(k|Q_i)$ are needed (here we have replaced α_i with Q_i). Since for every Q_i and $R(k)$ there exists a unique $K(k|Q_i)$, we might ask why the gain could not be a conditioning variable instead of Q_i . We embrace this approach here. For our problem $K_1(k)$ is bounded between 0 and 1. We therefore implement a bank of

parallel stationary filters with first gain elements K_{1i} uniformly spaced between these limits. K_{2i} is given by (III-42). We can use (III-32) to obtain $W(k|K_i)$:

$$W(k|K_i) = R(k)/[1 - K_{1i}] \quad (V-14)$$

The conditional estimates for the i th filter are given by:

$$\hat{x}(k|k-1, K_i) = \phi \hat{x}(k-1|k-1, K_i) \quad (V-15)$$

$$v(k|K_i) = y(k) - H\hat{x}(k|k-1, K_i) \quad (V-16)$$

$$\hat{x}(k|k, K_i) = \hat{x}(k|k-1, K_i) + K_i v(k|K_i) \quad (V-17)$$

We obtain $p[K_i|Y_k]$ from (V-13), realizing that it is equal to $p[\alpha_i|Y_k]$ where α_i is that value Q_i which results in a Kalman gain of K_i :

$$p[K_i|Y_k] = \begin{cases} CW^{-\frac{1}{2}}(k|K_i) \exp\left\{-\frac{v^2(k|K_i)}{W(k|K_i)}\right\} p[K_i|Y_{k-1}] & , k \leq N \\ CW^{-\frac{1}{2}}(k|K_i) \exp\left\{-\frac{v^2(k|K_i)}{W(k|K_i)}\right\} (p[K_i|Y_{k-1}])^{\frac{N-1}{N}} & , k > N \end{cases} \quad (V-18)$$

We then obtain the adaptive state estimate from (IV-96):

$$\hat{x}(k|k) = \sum_{i=1}^L \hat{x}(k|k, K_i) p[K_i|Y_k] \quad (V-19)$$

The advantage of this approach is that only the Kalman estimate

equations must be run for the i th parallel filter, since the gain K_i is fixed. Also, as noted by Alspach, the optimal gain is bounded, while $Q(k-1)$ may take on any positive value. For the general problem where $Q(k-1)$ and $R(k)$ are both unknown, this modification of Magill cannot be used. Given only K_i , we do not know $W(k|K_i)$ and thus $p[K_i|Y_k]$ remains unknown. We must then resort to using parallel filters where various combinations of Q and R are assumed.

Figure V-4 provides a flowchart of the modified Magill algorithm for the aircraft system model (III-1)-(III-4). As for the other algorithms, the adaptive filter is implemented as a subroutine, receiving $y(k)$ and $R(k)$ and returning estimates $\hat{\theta}_{AP}(k|k)$ and $\hat{\theta}(k|k)$. The a priori density of the gain $K_1(k)$ is assumed uniform.

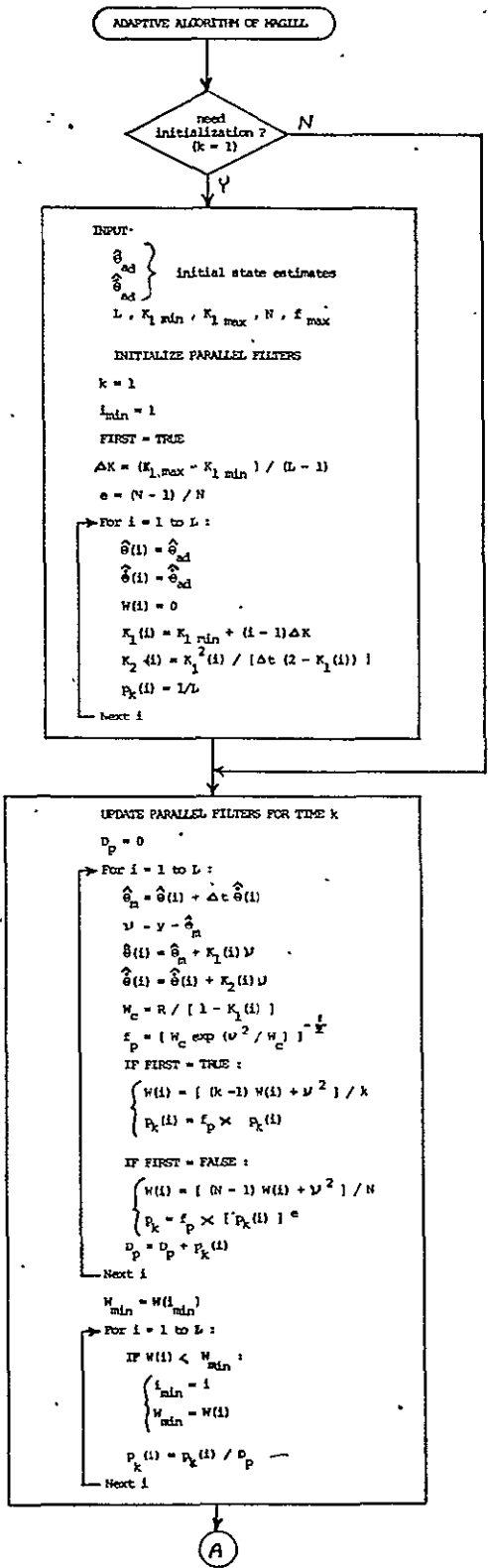


Figure V - 4. Adaptive Algorithm of Magill.

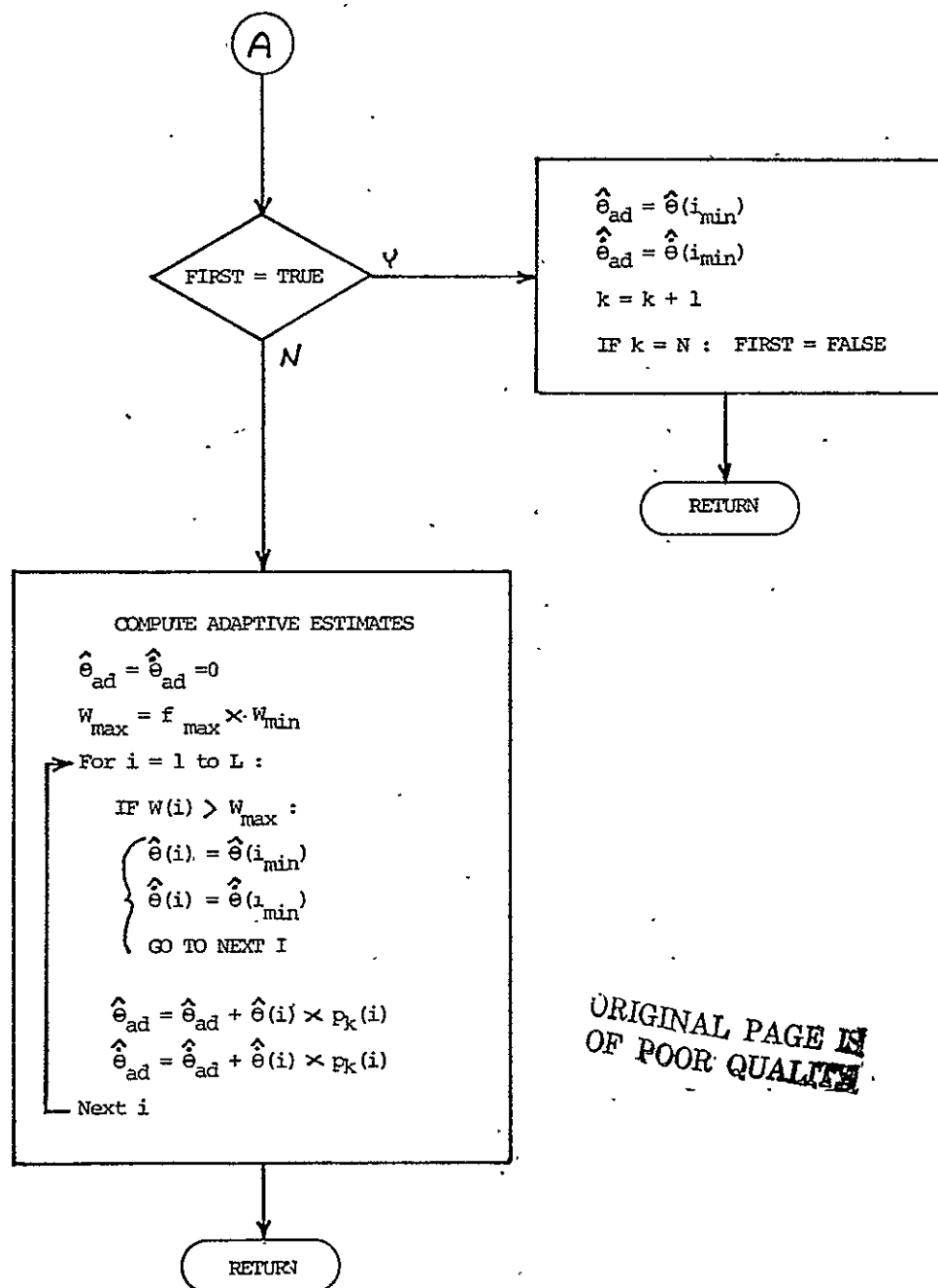


Figure V - 4.A Algorithm of Magill (continued)

CHAPTER VI

COMPUTER SIMULATION TESTING

We now develop and employ a digital computer simulation for testing the candidate adaptive filters for our aircraft landing problem. We realize at the onset that poor performance can occur for one of two reasons: first, an adaptive Kalman filter may be a poor estimator, given the stochastic state model for which it was developed; secondly, the assumed state model may inadequately describe the physical system for which the adaptive filter is used. Our testing is therefore conducted in two phases. We first simulate the state model (III-1)-(III-4), repeated below:

$$\begin{bmatrix} \theta(k) \\ \dot{\theta}(k) \end{bmatrix} = \begin{bmatrix} 1 & \Delta t \\ 0 & 1 \end{bmatrix} \begin{bmatrix} \theta(k-1) \\ \dot{\theta}(k-1) \end{bmatrix} + \begin{bmatrix} 0 \\ 1 \end{bmatrix} \omega(k-1) \quad (\text{VI-1})$$

$$y(k) = [1 \quad 0] \begin{bmatrix} \theta(k) \\ \dot{\theta}(k) \end{bmatrix} + v(k) \quad (\text{VI-2})$$

$$p[\omega(k-1)] = WN[0, Q(k-1)] \quad (\text{VI-3})$$

$$p[v(k)] = WN[0, R(k)] \quad (\text{VI-4})$$

At each new time increment the measurement $y(k)$ and the error covariance $R(k)$ are sent to the candidate adaptive filter, which computes state estimates $\hat{\theta}(k|k)$ and $\hat{\dot{\theta}}(k|k)$. In the second test phase we remove the state model (VI-1) and update $\theta(k)$ deterministically, as in (II-1):

$$\theta = f(k) \quad (\text{VI-5})$$

where $f(\cdot)$ describes the evolution of $\theta(k)$ for aircraft motion along a given flightpath. The measurement model (VI-2), (VI-4) is retained, and the adaptive filter is retested. In this two-prong approach we establish the performance of each candidate filter for both the assumed state model and the actual landing approach.

In simulating the stochastic system model (VI-1)-(VI-4) we must select realistic functions for $Q(k)$ and $R(k)$. $R(k)$ is the covariance of the error in the estimate $y(k)$ computed by the locally optimum estimation algorithm in the envelope processor. This covariance has been computed as a function of receiver signal-to-noise ratio in earlier simulations [5, pp. 25-27]. $Q(k)$ is the covariance of the Gaussian white noise driving the system. We recall from Chapter II that our state model (VI-1) was derived from a continuous-time model where acceleration $\ddot{\theta}(t)$ was represented by white noise. The mean square of the noise was set equal to the square of the acceleration. From (II-11) and (II-22) the discrete model noise covariance is given by:

$$Q(k-1) = \Delta t \ddot{\theta}^2(t_k) \quad (\text{VI-6})$$

Of course, the aircraft does not know $\ddot{\theta}(t_k)$, so $Q(k-1)$ is unknown as well.

In light of (VI-6) we use the following scheme for propagating the state model of (VI-1). The true acceleration $\ddot{\theta}(t_k)$ is computed in a subroutine for a typical deterministic flightpath and passed to the main

program. Here $Q(k - 1)$ is computed using (VI-6). The system state is then updated using a sample from a white Gaussian population with covariance $Q(k - 1)$. We are careful here not to confuse $\theta(k)$ and $\dot{\theta}(k)$ with $\bar{\theta}(t_k)$. The former are states of a stochastic process driven by white noise. $\bar{\theta}(t_k)$, a deterministic quantity, is a tool for setting $Q(k - 1)$ in the simulation and has nothing to do with the state.

The same subroutine which computes $\bar{\theta}(t_k)$ for aircraft motion along a given flightpath also computes $\theta(t_k)$ and $\dot{\theta}(t_k)$. In the second phase of simulation, where $\theta(k)$ is updated deterministically, these values are merely passed to the main program, which sets $\theta(k)$ equal to $\theta(t_k)$ and $\dot{\theta}(k)$ equal to $\dot{\theta}(t_k)$. We now address the task of realizing a suitable flightpath for updating both $Q(k)$ in the stochastic case and $\theta(k)$ in the deterministic case.

The Landing Approach

Before assuming a test landing pattern, we first place some restrictions on the set of allowable flightpaths. Let $f(k)$ describe the evolution of $\theta(k)$ as the aircraft travels a given flightpath. We recall from Chapter II that, while unknown, $f(k)$ is a member of a known class of functions. We restrict this class to include those functions attributable to aircraft motion along a restricted family of flightpaths. This family includes what we assume to be reasonable flightpaths, thus ruling out unrealistic approaches for which adaptive filtering could not work. For example, a missed approach where the aircraft crosses the runway at high speed within a mile of the azimuth antenna, produces very high and rapidly changing values of $\ddot{\theta}(t)$. The resulting covariance $Q(k)$ in the

system model would be too rapidly varying to be followed by an adaptive filter. We therefore place the following restrictions on the landing approach:

1. Maximum airspeed = 200 knots
2. Minimum turn radius = 1 N. mile
3. Flightpath must be coincident with runway centerline before runway is reached (no missed approaches)

We assume these conditions to be those of a worst-case approach.

Given these restrictions, $\ddot{\theta}(t)$ has been observed in simulation to remain below $0.1^\circ/\text{sec.}^2$ [6, p. 40]. From (VI-6) we can therefore place an upper limit on $Q(k)$:

$$Q_{\text{MAX}} = (.075)(.1)^2 = 7.5 \times 10^{-4} \quad (\text{VI-7})$$

where $\Delta t = .075$ seconds, the time between the start of successive azimuth scans (at a 13 1/3 Hz update rate).

We now return to the task of finding a suitable test flightpath within the above restrictions. Figure VI-1 shows a representative landing approach selected for this simulation. The aircraft travels at 120 knots along an S-curve flightpath, staying on runway centerline for the last 3 N. miles of the approach. The runway is 2 N. miles long, with the azimuth antenna at the stop end.

We have developed a FORTRAN computer subroutine for computing $\theta(t)$ and its derivatives as the aircraft follows an S-curve approach of variable dimension. This general flightpath, shown in Figure VI-2, has the

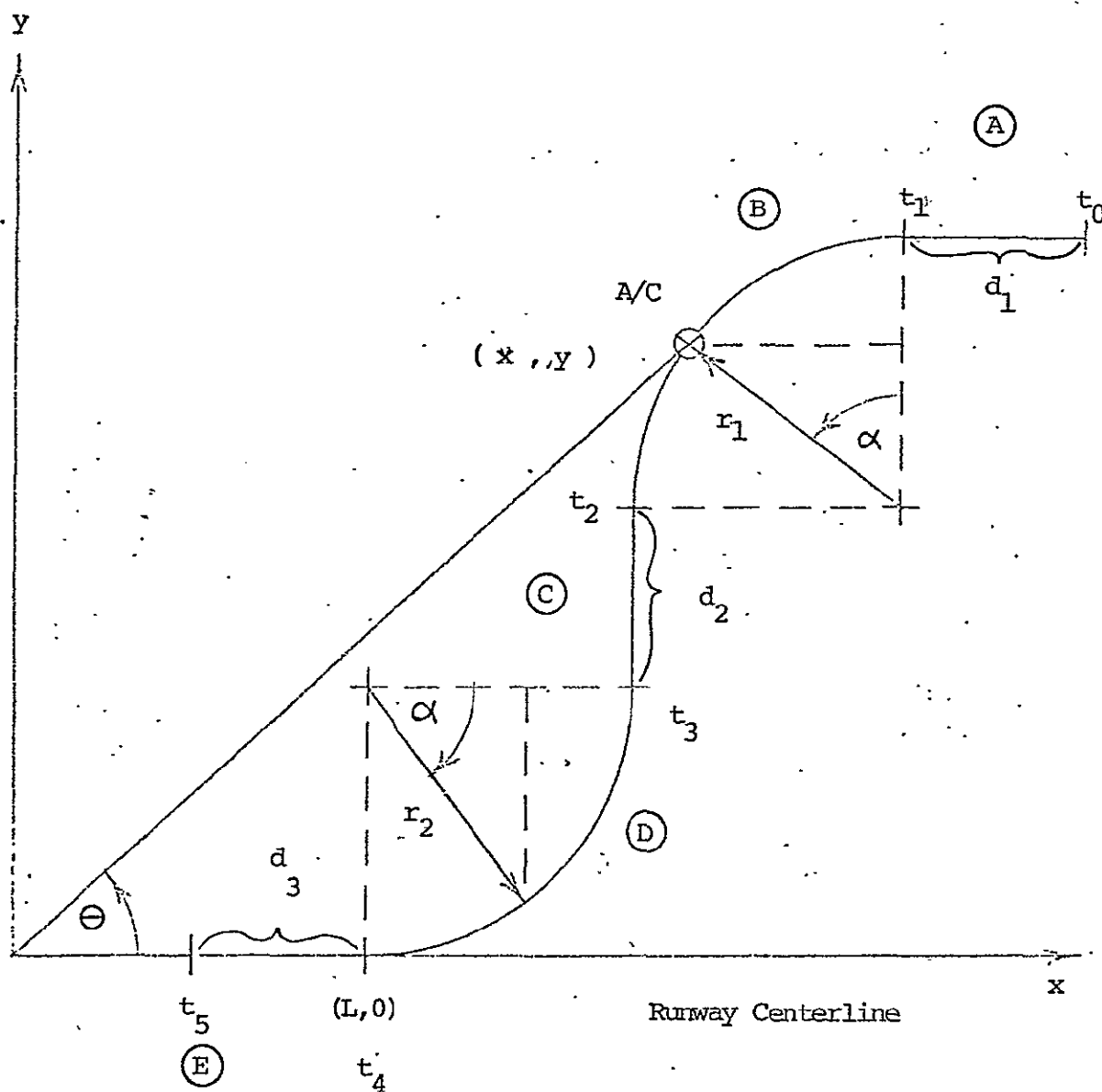


Figure VI - 2. General S - Curve Flightpath.

MISSING
 PRECEDING PAGE ~~XXXXXXXXXX~~ NOT FILMED

following programmable parameters:

- v = airspeed (knots)
- d_1, d_2, d_3 = lengths of the straight segments of the flightpath, as shown in Figure VI-2 (N. miles)
- r_1, r_2 = turn radii (N. miles)
- l = distance (N. miles) from azimuth antenna to that point where the approach first coincides with the runway centerline (5 N. miles for Figure VI-1).

A flowchart of the flightpath subroutine is given in Figure VI-3. The various straight and curved sections of the approach are labeled from A to E on both the flowchart and Figure VI-2. The simulated flight runs from time t_0 to t_5 , with t_1 through t_4 marking transition times from one flightpath section to the next. The subroutine receives the present azimuth scan number and computes the time t . Based upon which flightpath section the aircraft is currently following, its cartesian coordinates x and y and their derivatives are computed. The subroutine then computes $\theta(t)$, $\dot{\theta}(t)$, and $\ddot{\theta}(t)$:

$$\theta = \arctan(y/x) \quad (\text{VI-8})$$

$$\dot{\theta} = (x\dot{y} - \dot{x}y)/(x^2 + y^2) \quad (\text{VI-9})$$

$$\ddot{\theta} = [x\ddot{y} - \ddot{x}y - 2\dot{\theta}(x\dot{x} + y\dot{y})]/(x^2 + y^2) \quad (\text{VI-10})$$

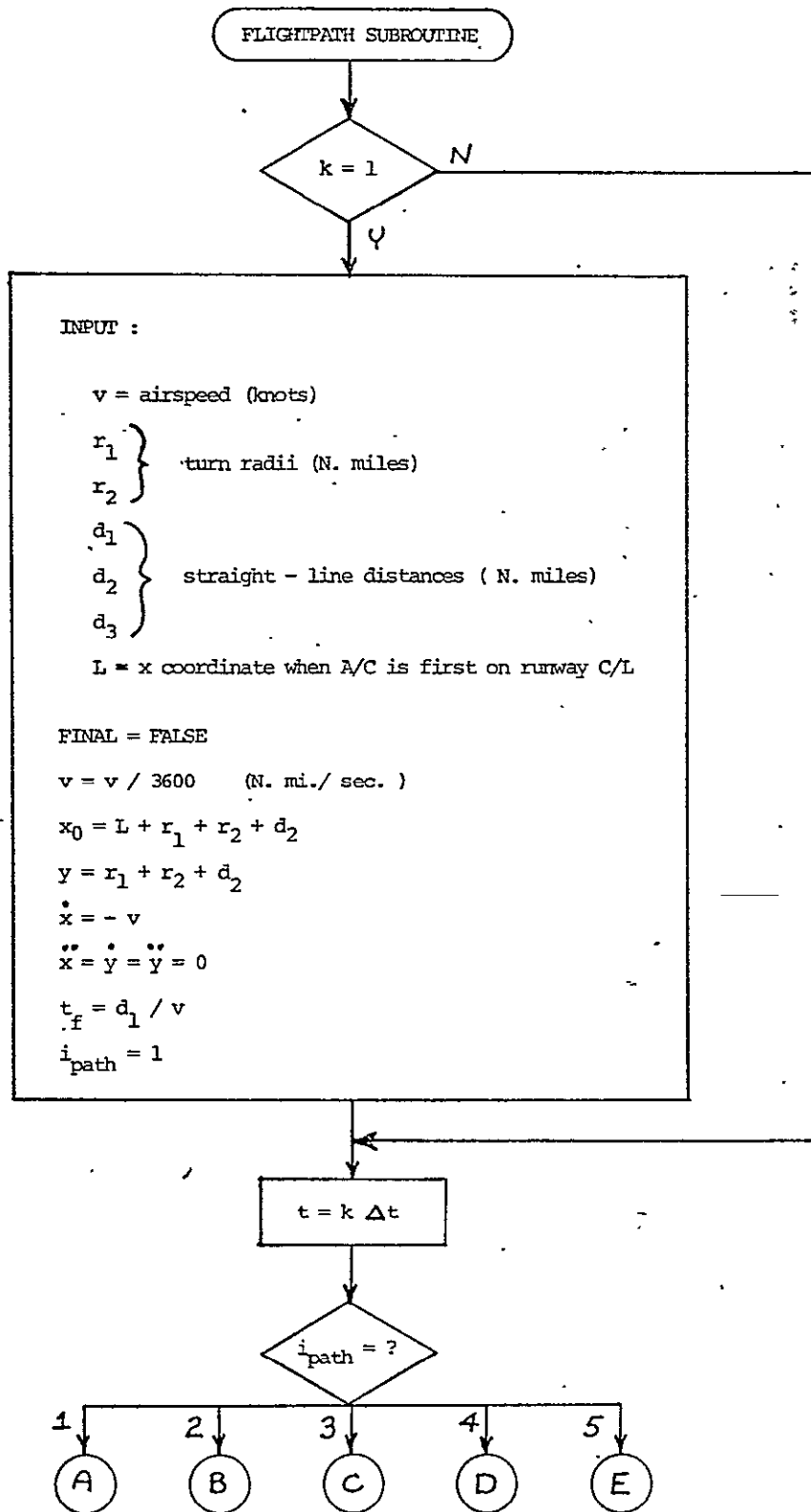


Figure VI - 3. Flightpath Subroutine

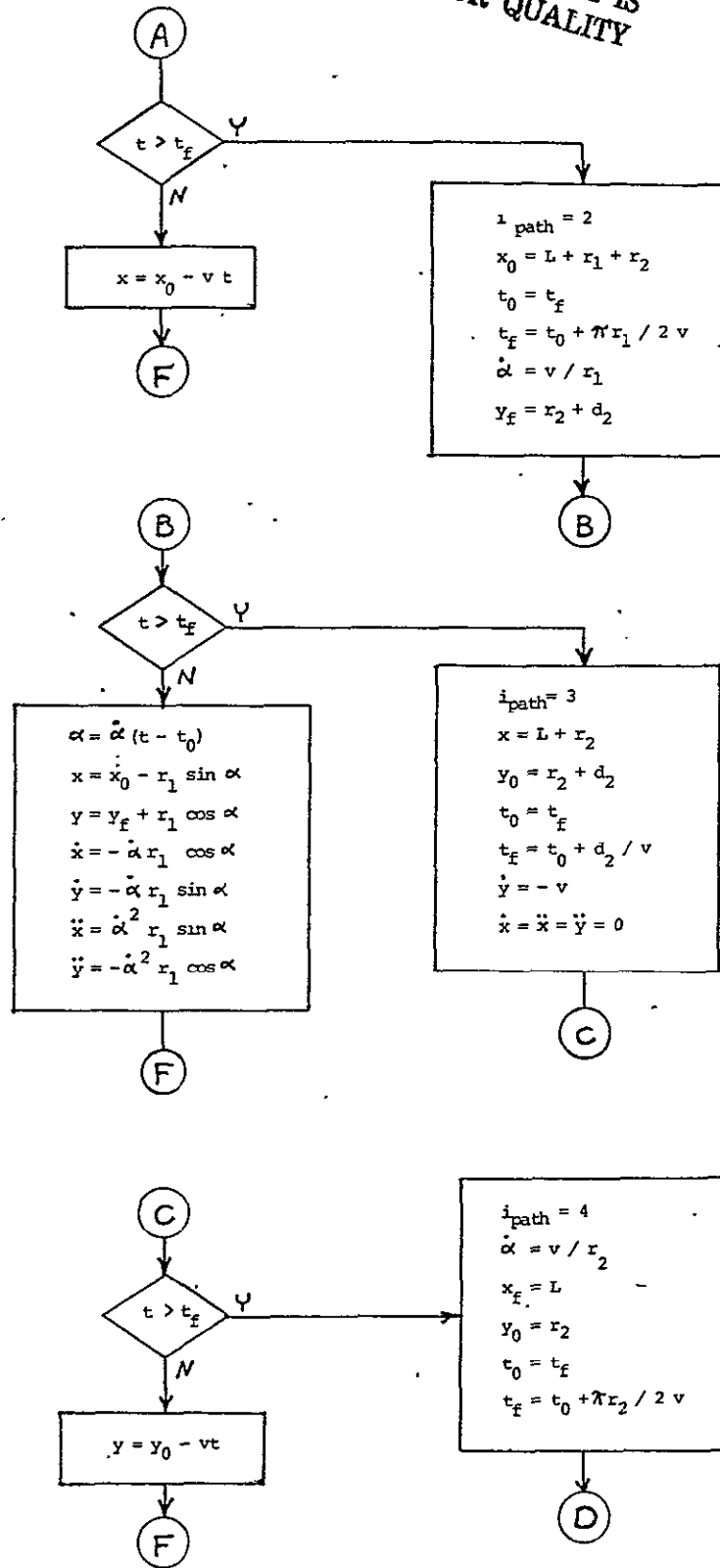


Figure VI - 3.A Flightpath Subroutine (continued)

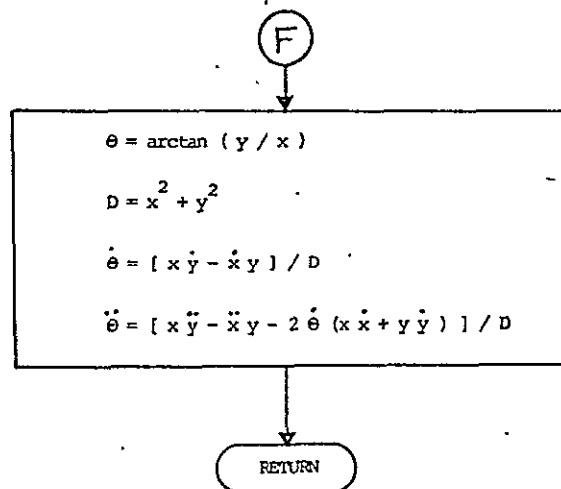
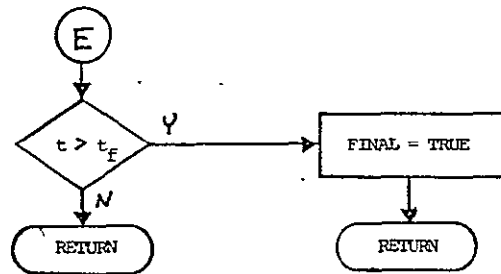
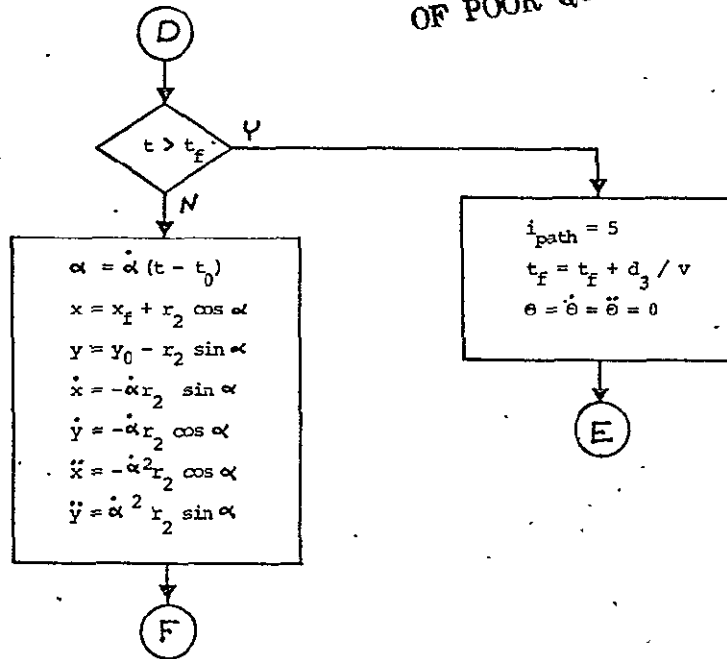


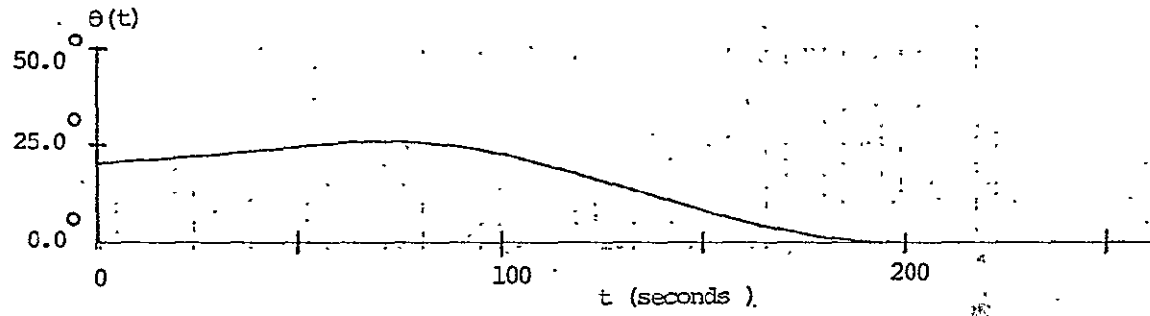
Figure VI - 3.B Flightpath Subroutine (continued)

The values $\theta(t)$, $\dot{\theta}(t)$, and $\ddot{\theta}(t)$ are returned to the main simulation program, along with the logical variable FINAL, which is set to TRUE when the simulated approach has been completed.

Figure VI-4 shows the time functions $\theta(t)$, $\dot{\theta}(t)$, and $\ddot{\theta}(t)$ for the S-curve flightpath of Figure VI-1. The simulated approach begins with the aircraft 2 N. miles ahead of the first 90° turn and ends 2 N. miles beyond the second turn, or 1 N. mile before the runway is reached ($d_1 = d_3 = 2$ N. miles). At 120 knots the aircraft covers 8.88 N. miles in 266 seconds, or 3550 azimuth scan periods (scan update rate = 13 1/3 Hz). Figure VI-4 also shows the plant noise covariance $Q(k)$ for the stochastic modeling of this flightpath, computed from (VI-5).

Computer Simulation Structure

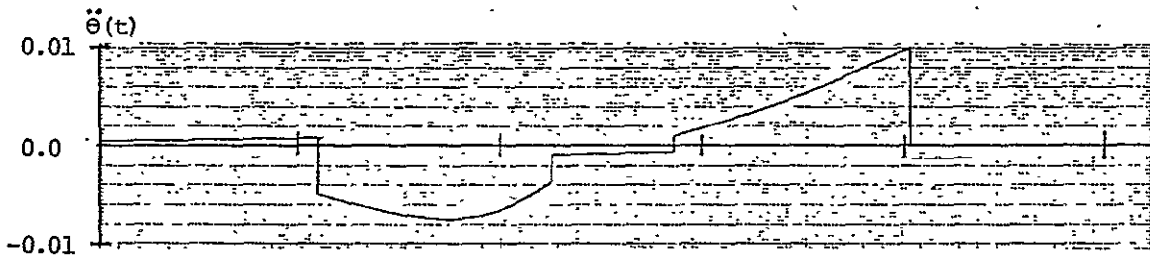
We now describe the actual test simulation, implemented as a FORTRAN computer program. A flowchart of the overall simulation is given in Figure VI-5. At the k th scan period the main program calls the flightpath subroutine, which updates $\theta(t)$, $\dot{\theta}(t)$, and $\ddot{\theta}(t)$ according to deterministic aircraft motion along the S-curve flightpath. The main program then updates the state values $\theta(k)$ and $\dot{\theta}(k)$, either stochastically with white noise or deterministically, depending on the value of the logical variable MODEL. When MODEL is TRUE, the state is updated with noise according to (VI-1). $Q(k-1)$ is computed from $\ddot{\theta}(t)$ using (VI-6). The white noise term $\omega(k-1)$ is then obtained from $Q(k-1)$ and the output of GAUSS, a subroutine which uses the machine random number generator to produce independent samples of a standard Gaussian population (zero mean, unity covariance). When MODEL is FALSE, the state is updated



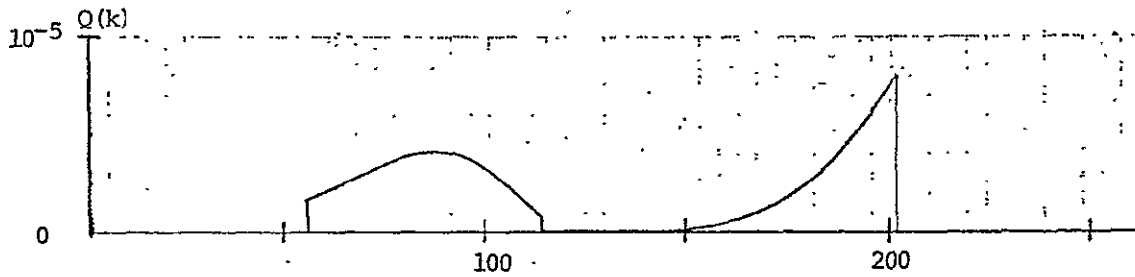
A. $\theta(t)$ vs. t



B. Velocity $\dot{\theta}(t)$ (deg./sec.)



C. Acceleration $\ddot{\theta}(t)$ (deg./sec.²)



D. State Noise Covariance $Q(k)$

Figure VI - 4. Azimuth Angle $\theta(t)$ and Derrivatives for S - Curve Flightpath

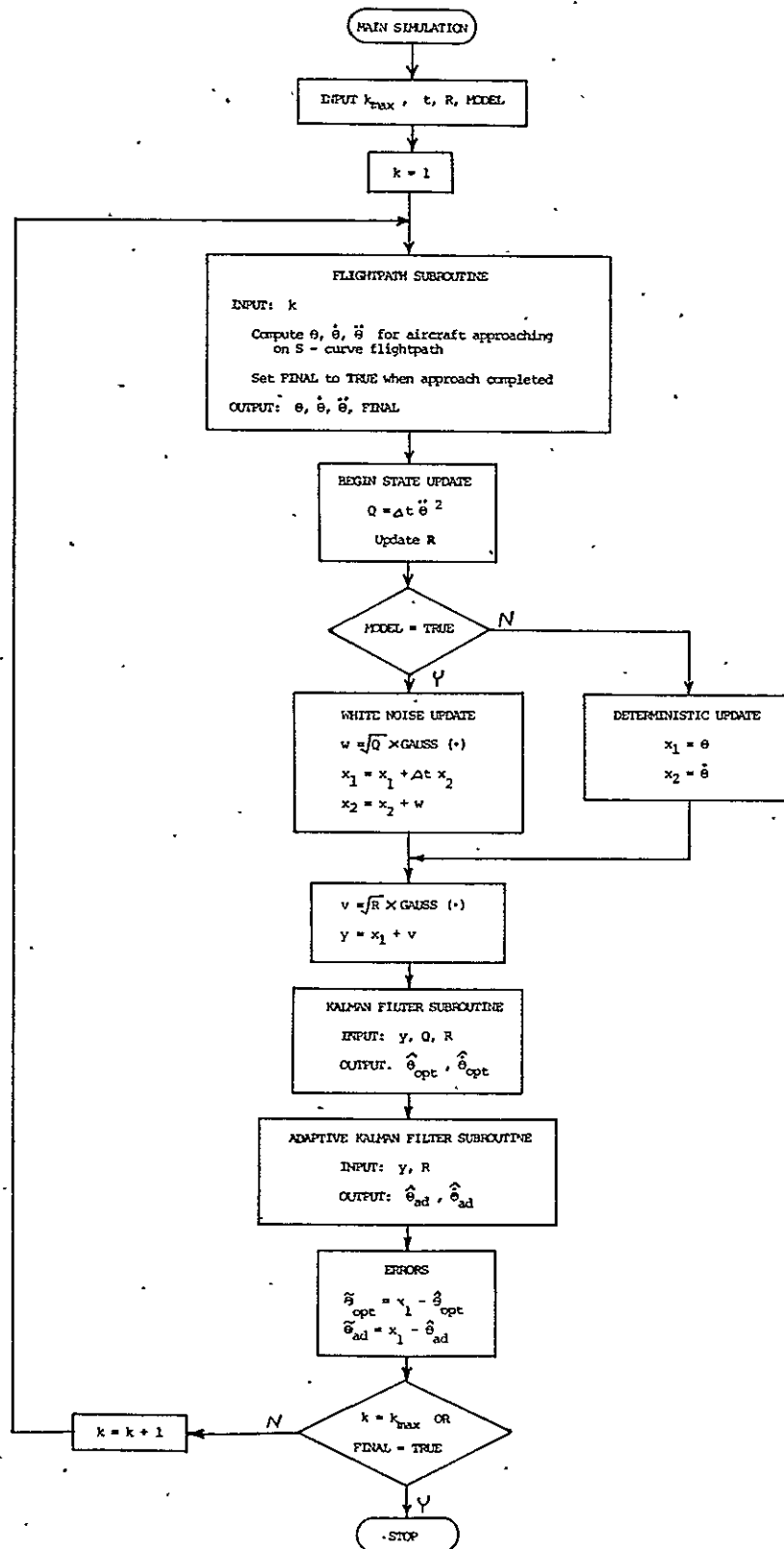


Figure VI - 5. Main Simulation Program

deterministically by merely setting $\theta(k)$ to $\theta(t)$ and $\dot{\theta}(k)$ to $\dot{\theta}(t)$ (x_1 and x_2 are used for $\theta(k)$ and $\dot{\theta}(k)$ in the actual program to avoid confusion with $\theta(t)$ and $\dot{\theta}(t)$ when the stochastic model is used -- see flowchart in Figure VI-4).

The main program now uses GAUSS and $R(k)$ to produce an additively corrupted measurement $y(k)$ of the state, as in (VI-2). $Q(k-1)$, $R(k)$, and $y(k)$ are then sent to the Kalman filter subroutine, which computes the optimal state estimates $\hat{\theta}_{OPT}(k|k)$ and $\hat{\dot{\theta}}_{OPT}(k|k)$ (these estimates are optimal when the assumed state variable model (VI-1)-(VI-4) is correct). $R(k)$ and $y(k)$ are then sent to the candidate adaptive Kalman filter subroutine, which, without knowledge of $Q(k-1)$, computes the suboptimal state estimates $\hat{\theta}_{AD}(k|k)$ and $\hat{\dot{\theta}}_{AD}(k|k)$. The main program computes errors in estimates of $\theta(k)$ and increments k to the next scan period.

Simulation Testing: The Stochastic Model Case

The S-curve flightpath of Figure VI-1 is used in both the stochastic and deterministic phases of simulation testing. Here we use $Q(k)$ from Figure VI-4 to update the state variable model (VI-1).

As a result of the restrictions placed on the family of allowable flightpaths, we can limit the adaptive gain K_1 . We recall from (IV-7) that $Q(k)$ is bounded at $Q_{MAX} = 7.5 \times 10^{-4}$. We also recall from Chapter III that the Kalman gain $K_1(k)$ is a monotone increasing function of $Q(k-1)/R(k)$. Given Q_{MAX} , we can thus limit K_1 by placing a lower bound on R . In earlier simulations we have found the r.m.s. error in the envelope processor estimate $y(k)$ to remain above $.01^\circ$ for the expected range of signal-to-noise ratios (20 db or less) [5, p. 27]. We assume a lower

limit on r.m.s. error in $y(k)$ of $.005^\circ$, yielding the bound

$R_{\text{MIN}} = 2.5 \times 10^{-5}$. When Q_{MAX} and R_{MIN} are used in our system model the Kalman filter has a steady-state gain $K_1 = .602$. We assume the upper bound $K_{1\text{MAX}} = .625$.

Three of the adaptive filters tested here use a bank of parallel stationary Kalman filters. In each case we use 24 parallel filters, incrementing K_1 uniformly from $.05$ to $.625$. For each of the three adaptive filters we use a fading memory time constant N of 80 scan periods in computing the sample innovations covariances. This value has been chosen experimentally by studying the effect of different values of N on filter performance for various flightpaths (from typical to worst-case approaches). The adaptive filter of Sage and Husa uses a constant N of 30 scan periods.

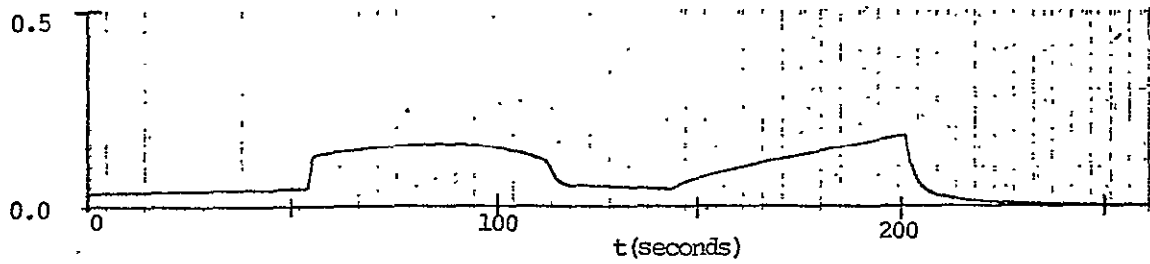
In addition to the adaptive filters of Chapters VI and V we also test a suboptimal filter which does not adapt to changes in $Q(k)$. This estimator is merely a Kalman filter which uses the true value $R(k)$, but which replaces the unknown $Q(k)$ with the limit Q_{MAX} of 7.5×10^{-4} , from (VI-7). Such an estimator, which is much simpler than an adaptive filter, has some intuitive appeal. Since $R(k)$ is known, the filter gain $\hat{K}_1(k)$ is always greater than or equal to the optimal gain $K_1(k)$ (as $Q_{\text{MAX}} \geq Q(k)$). Recalling Figure III-1, such a filter, while not always optimal, always has a mean square error in $\hat{\theta}(k|k)$ less than $R(k)$. We test a second constant- Q filter which has knowledge of maximum acceleration $\ddot{\theta}(t)$ for the actual flightpath to be used. For this simulation the S-curve approach produces a peak $\ddot{\theta}(t)$ just above $.01^\circ/\text{sec}^2$, while $Q(k)$ peaks at

8×10^{-6} (see Figure VI-4.C, D). We have assumed in the problem definition of Chapter II that nothing is known about the actual flightpath except that it belongs to a given family of approaches. We nevertheless include this filter for test comparison with the other candidate filters.

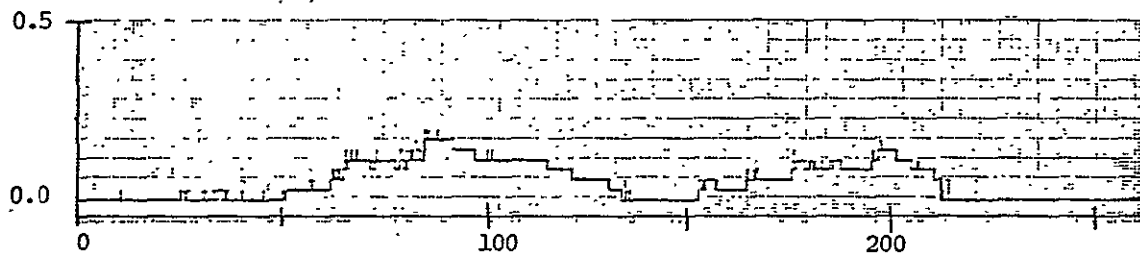
We assume a constant $R(k)$ of 10^{-4} for the simulation (r.m.s. error in $y(k) = .01^\circ$). This is not too realistic, because the signal-to-noise ratio slowly rises as the aircraft approaches the runway. A slowly decreasing function for $R(k)$ would seem more reasonable. But judging from Figure VI-4.D, we would expect the more rapid variations in $Q(k)$ to cause the most difficulty in adaptive estimation. A constant- R simulation should give a fair indication as to whether or not adaptive filtering will work.

The candidate adaptive filters have been tested in a FORTRAN simulation on a PDP-1103 computer. The stochastic state model (VI-1)-(VI-4) is implemented, with $Q(k)$ updated as shown in Figure VI-4.D. $R(k)$ is constant at 10^{-4} . The nonadaptive filter using Q_{MAX} has a steady-state gain $\hat{K}_1 = .476$. The second constant- Q filter, which has knowledge of maximum acceleration for the actual flightpath, has a steady-state gain $\hat{K}_1 = .190$.

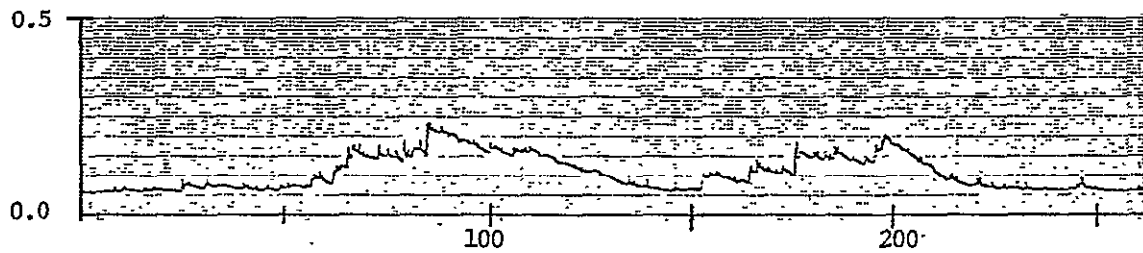
Figure VI-6 shows the optimal gain $K_1(k)$ and the adaptive filter gains $\hat{K}_1(k)$ for the simulation. No plot is shown for Magill's algorithm, which computes the adaptive state estimate from (V-19) as a weighted sum of parallel filter estimates and consequently does not use $\hat{K}_1(k)$. The optimal gain goes through three near-step changes; at $t = 55$ sec., 115 sec., and 200 sec. For all adaptive gain plots shown, $\hat{K}_1(k)$ lags $K_1(k)$ at each of these three times in changing to the new gain level. This



A. Optimal (Kalman)



B. Minimum Innovations Covariance



C. Alspach



D. Sage - Husa

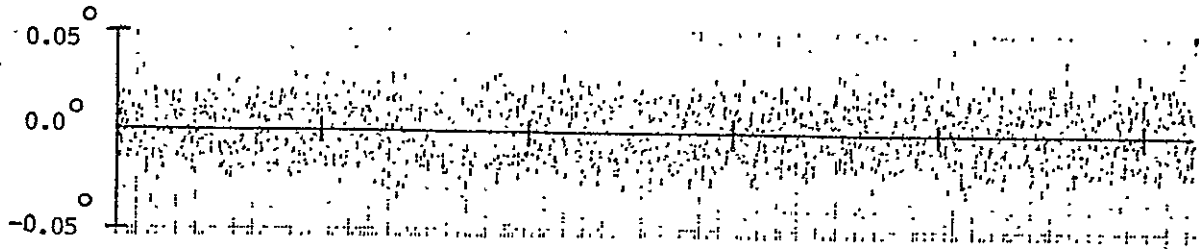
Figure VI - 6. Gain \hat{K}_1 vs. Time for Adaptive Filters

(State updated by white noise)

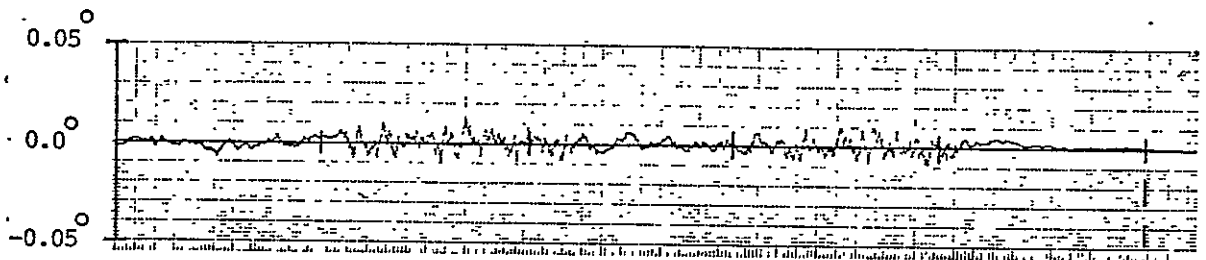
time lag is most noticeable in the filter of Sage and Husa, which has the most difficulty in estimating the optimal gain. We recall that the adaptive filters all use sample innovations covariances, either of an assumed optimal filter in the method of Sage and Husa, or of each of a group of parallel filters for the other methods. The true innovations covariances change immediately whenever $K_1(k)$ changes, but the sample covariances are time averages and consequently change more slowly. The time lag in $\hat{K}_1(k)$ is most critical at $t = 55$ sec. Here the adaptive gain remains low when the optimal gain is high, a condition which can produce high mean square errors in $\hat{\theta}(k|k)$ (see Figure III-1).

Figure VI-7 shows the error $\theta(k) - y(k)$ in the envelope processor, as well as the error $\theta(k) - \hat{\theta}(k|k)$ for the optimal and constant-Q filters. The reduction in error produced by the optimal filter is obvious. The nonadaptive filter with gain $\hat{K}_1 = .476$ (Q set to Q_{MAX}) reduces the error in $y(k)$, but not as well as the optimal filter. The filter with gain \hat{K}_1 of .190 works about as well as the optimal, except for $t > 200$ seconds, where Q and $K_1(k)$ go to zero. Figure VI-8 compares the optimal filter's error in $\hat{\theta}(k|k)$ with that of the adaptive filters. All of these filters seem to work about as well as the optimal, except near the end of the approach, when $Q(k)$ goes to zero.

We realize that results of a single simulation run cannot provide us with a firm basis for any meaningful conclusions. The results shown here are to some degree dependent upon the noise sequences $\omega(k)$ and $v(k)$ peculiar to this particular run. We therefore repeat the above simulation 100 times: the simulation is repeated without reinitializing the machine random number generator, so that noise samples used in one

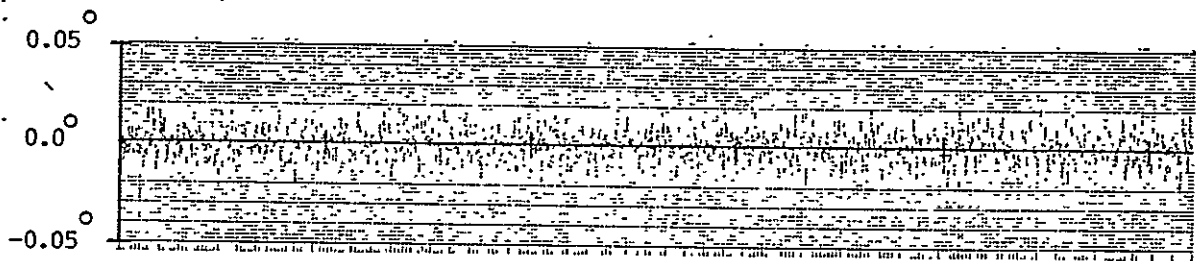
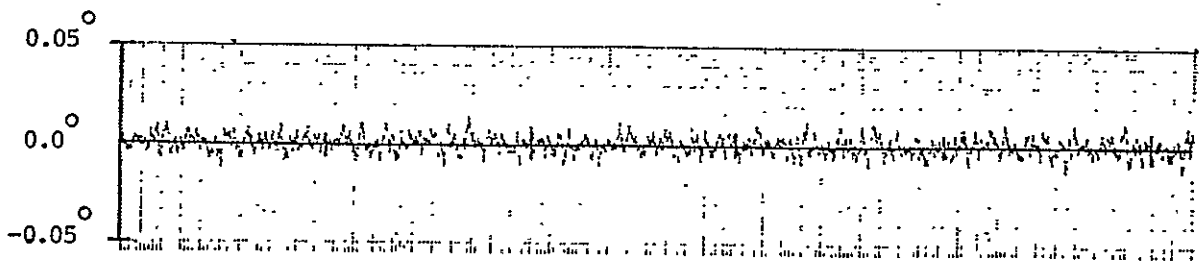


A. Envelope processor (filter input)

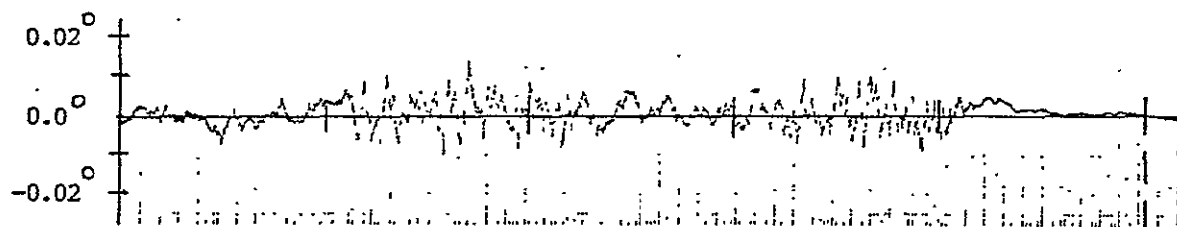


B. Optimal Filter

t = 250 sec.

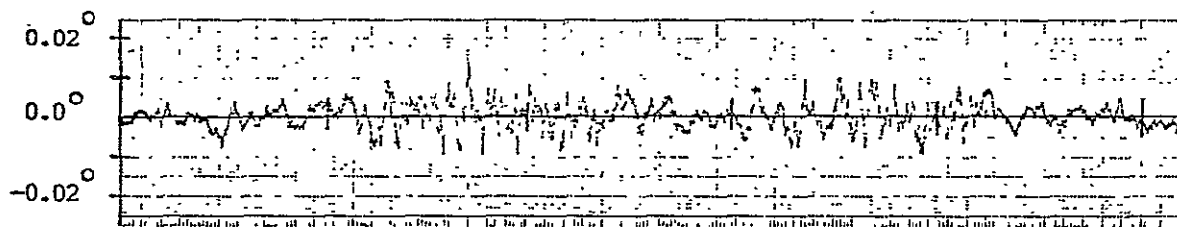
C. Nonadaptive Filter : $K_1 = .476$ D. Nonadaptive Filter : $K_1 = .190$ Figure VI - 7. Error in $\hat{\Theta}(k|k)$ for Different Estimators

(State updated by white noise)

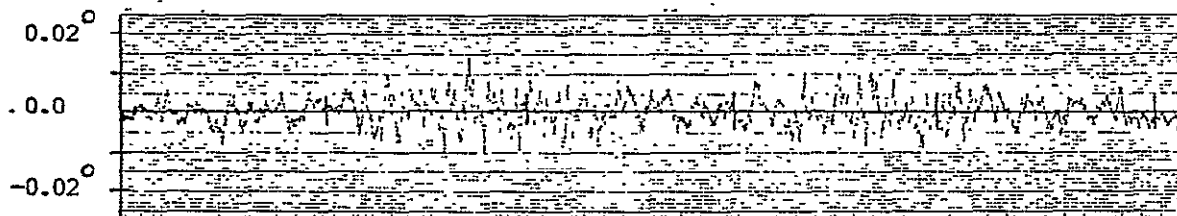


A. Optimal

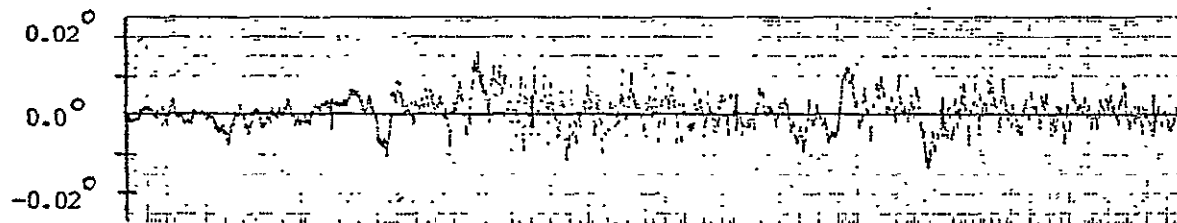
t = 250 sec.



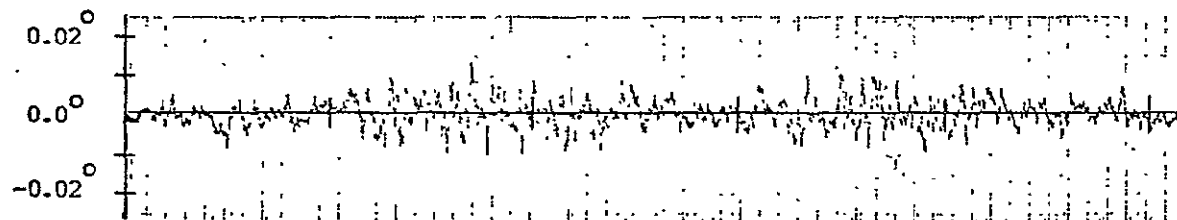
B. Minimum Innovations Covariance



C. Alspach



D. Sage - Husa



E. Magill

Figure VI 8. Error in $\hat{\theta}(k|k)$ for Adaptive Kalman Filters

experimental run are independent of those used in the other runs. We then obtain an ensemble average of the mean square error in $\hat{\theta}(k|k)$ for a given candidate filter. Let $\tilde{\theta}_i(k|k)$ be the error in $\hat{\theta}(k|k)$ for the i th simulation run:

$$\tilde{\theta}_i(k|k) = \theta(k) - \hat{\theta}(k|k); \text{ ith run} \quad (\text{VI-11})$$

We obtain a sample mean square error by averaging the square error at time k for all simulation runs:

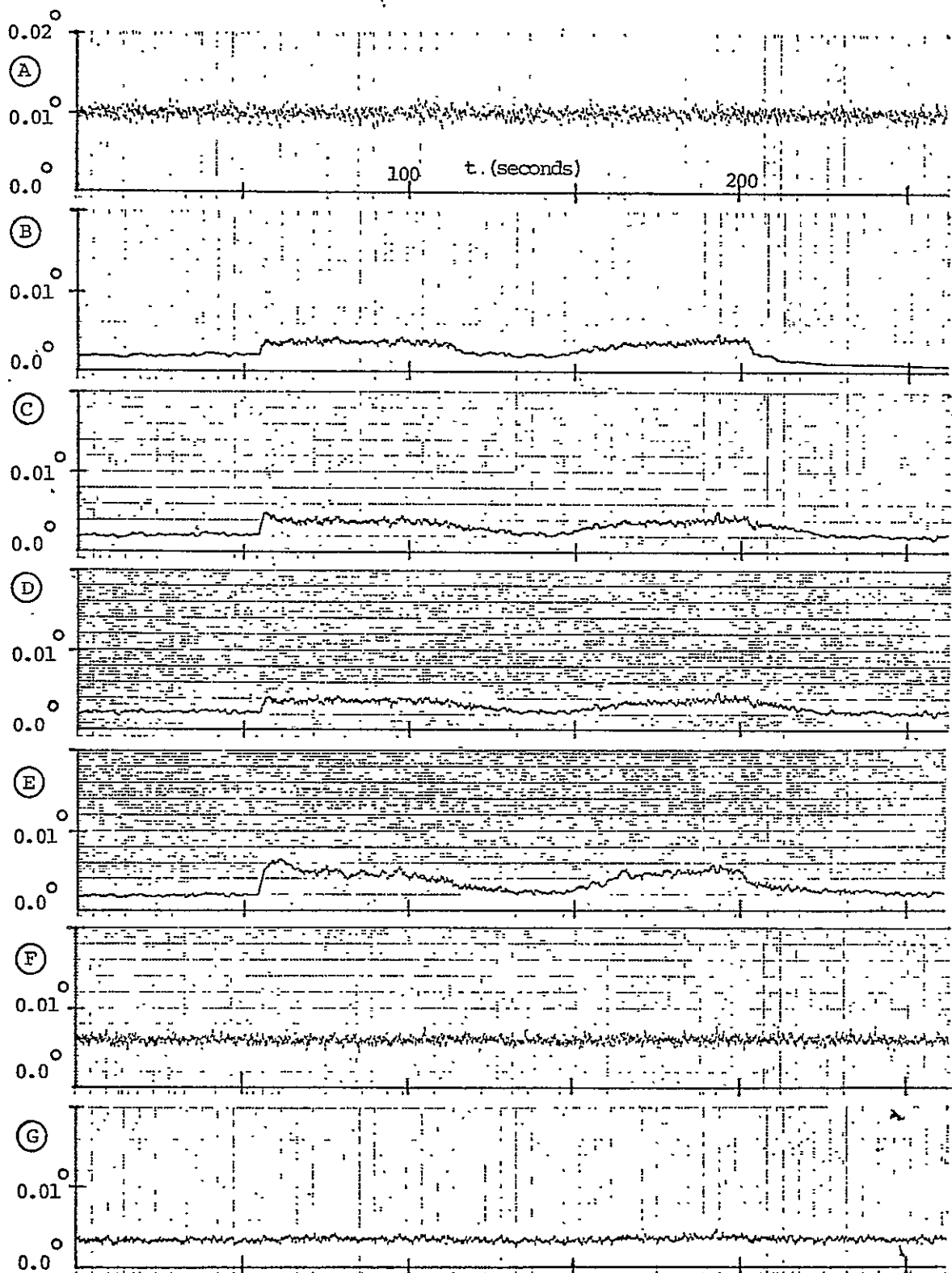
$$\hat{P}(k|k) = \frac{1}{100} \sum_{i=1}^{100} \tilde{\theta}_i^2(k|k) \quad (\text{VI-12})$$

Assuming $\hat{\theta}(k|k)$ to be unbiased, $\hat{P}(k|k)$ is a variance estimate. From (V-4) we know that the standard deviation in this estimate is given by

$$\sigma_p = P(k|k)/\sqrt{100/2} = .141P(k|k) \quad (\text{VI-13})$$

where $P(k|k)$ is the true error covariance for $\hat{\theta}(k|k)$ (which we know only for the optimal filter). We thus expect our sample error covariance $\hat{P}(k|k)$ to be within 14 percent of the true covariance most of the time. Here we use the square root of $\hat{P}(k|k)$ as a sample r.m.s. error in $\hat{\theta}(k|k)$.

Figure VI-9 shows the sample r.m.s. error in $\hat{\theta}(k|k)$ computed from 100 simulation runs for each of the estimators tested. The error in the envelope processor estimate $y(k)$ stays near $.01^\circ$; this is consistent with a constant covariance $R(k)$ of 10^{-4} . The optimal filter significantly lowers the error, usually holding it below $.004^\circ$. The minimum innovations covariance and Alspach adaptive filters work nearly as well as the



A. Envelope Processor; B. Optimal; C. Min. Innov. Cov.; D. Alspach;

E. Sage - Husa; F. $K_1 = .476$; G. $K_1 = .190$

Figure VI - 9. Sample RMS error in $\hat{\theta}(k|k)$; State Driven by White Noise

optimal; only for $t > 200$ seconds, where $Q(k)$ goes to zero, does the optimal filter have a noticeably smaller r.m.s. error. The adaptive filter of Sage-Husa does almost as well, with a peak r.m.s. error of about $.006^\circ$. The Magill filter was not tested here. It was much slower than the other adaptive filters, and the time required to run a 100-record simulation was too great to be practical (recall that the bank of parallel stationary filters must be implemented serially in simulation). We note, however, that the single-run results for this filter look very much like those of Alspach. This is not surprising, as both methods compute the a posteriori gain density $p[K_i|Y_k]$ from parallel filters.

We note in Figure VI-9 that the constant-Q filter with gain \hat{K}_1 of $.476$ has an r.m.s. error of about $.006^\circ$. This is somewhat higher than the error associated with the adaptive filters. The nonadaptive filter with \hat{K}_1 at $.190$ does very well, however, with the r.m.s. error staying near $.004^\circ$. This compares favorably with the optimal and adaptive filters. Only when $Q(k)$ becomes very small, as for $t < 50$ seconds and $t > 200$ seconds, do the adaptive filters work significantly better than this filter.

Simulation Testing: The Deterministic Case

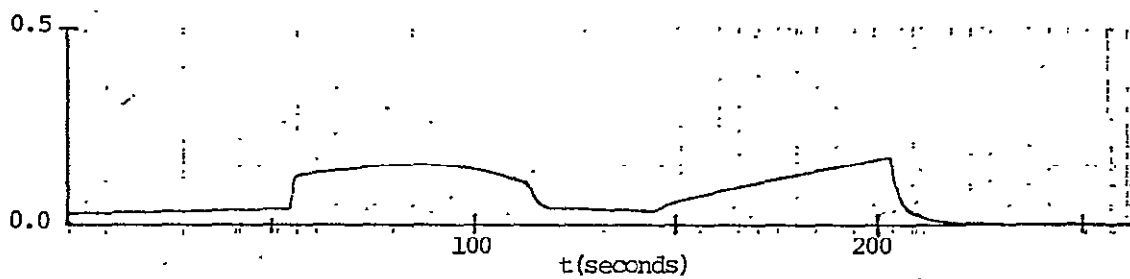
We have established that the candidate adaptive and constant-Q filters work reasonably well when the assumed state model is implemented. We must now find out how well they can work in a true physical environment, where the aircraft is actually moving along a given flightpath. This of course is our original objective: to find an adaptive Kalman filtering scheme for computing a minimum mean square error estimate

$\hat{\theta}(k|k)$, using the estimates Y_k output by the airborne receiver's envelope processor.

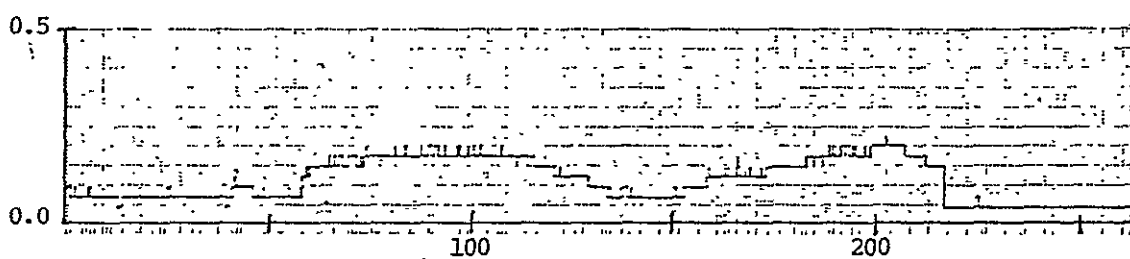
The entire simulation of the preceding section has been repeated, with the logical variable MODEL now changed to FALSE. $\theta(k)$ is now updated deterministically as the aircraft travels at 120 knots along the S-curve approach of Figure VI-1 (Recall that $\theta(t)$, $\dot{\theta}(t)$, and $\ddot{\theta}(t)$ are shown for this flightpath in Figure VI-4). $R(k)$ is still held constant at 10^{-4} , giving an r.m.s. error of $.01^\circ$ in the envelope processor estimate $y(k)$. In addition to the candidate adaptive and constant-Q filters we also run the same optimal filter as before, setting $Q(k-1)$ to $\Delta t \ddot{\theta}(t_k)$. Of course, this filter is unrealizable, since $\ddot{\theta}(t_k)$ is unknown to the aircraft.

Results for the single simulation run are given in Figures VI-10, 11, 12. Figure VI-10 depicts the gain $K_1(k)$ for the optimal and adaptive Kalman filters. The adaptive gains look about the same as for the stochastic model simulation, with the Sage-Husa filter again having the most difficulty in estimating the optimal gain.

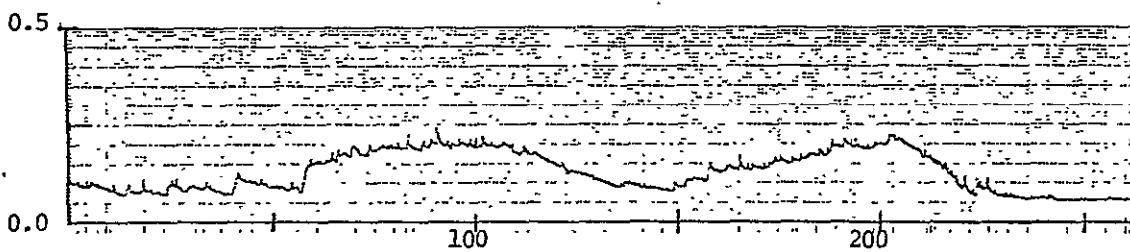
Figure VI-11 gives the error in $\hat{\theta}(k|k)$ for the envelope processor as well as the optimal and constant-Q filters. Again, these plots look about the same as for the stochastic case. The optimal filter significantly lowers the envelope processor error, while the filter with constant gain \hat{K}_1 at $.476$ also lowers the original error, but not as much. The filter with \hat{K}_1 at $.190$ performs about as well as the optimal filter, except for $t > 200$ seconds. Here, where the aircraft is on runway centerline, the optimal filter has less error. Figure VI-12 compares the optimal filter's error with that of the adaptive filters. The minimum



A. Optimal



B. Minimum Innovations Covariance

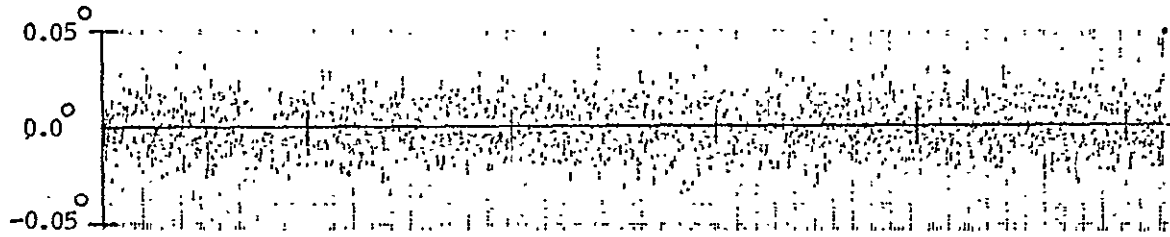


C. Alspach

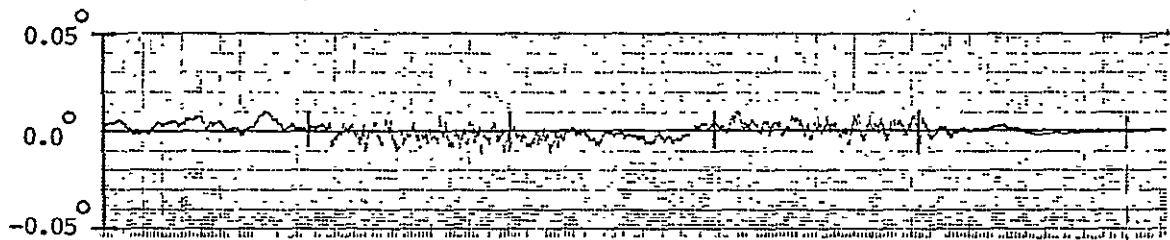


D. Sage - Husa

Figure VI - 10. Gain \hat{K}_1 for Adaptive Filters; $\Theta(k)$ updated deterministically

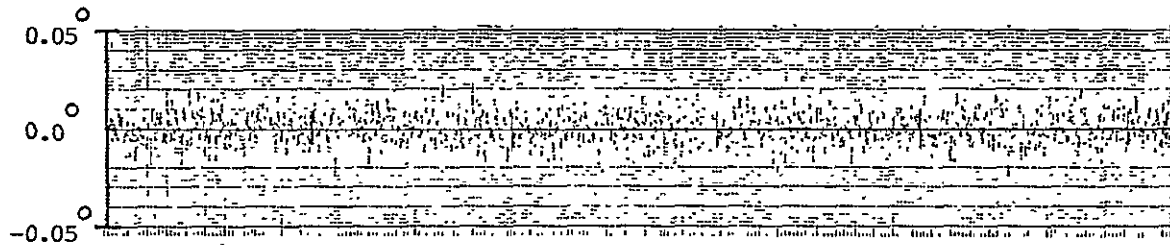


A. Envelope Processor (filter input)

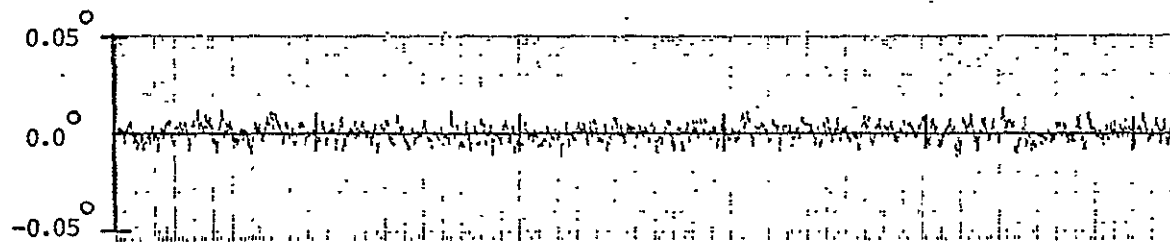


B. Optimal Filter

t = 250 sec.

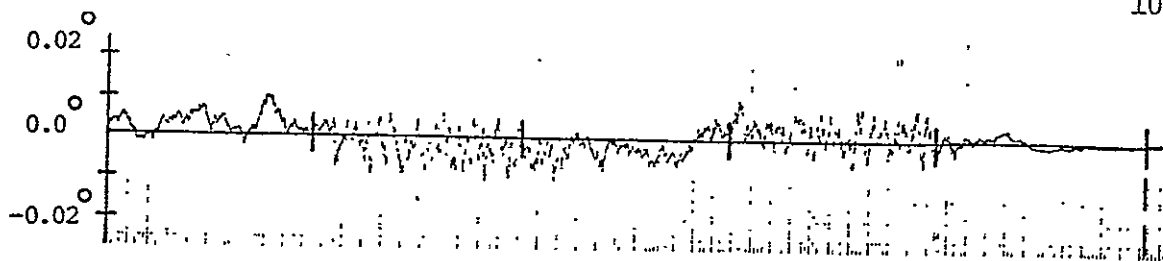


C. Nonadaptive Filter : $K_1 = .476$



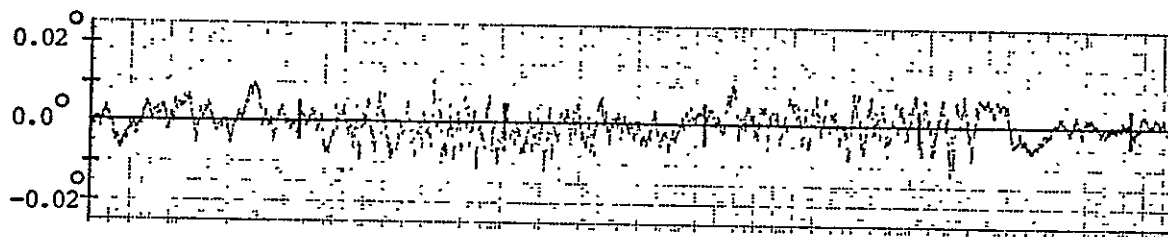
D. Nonadaptive Filter : $K_1 = .190$

Figure VI -11. Error in $\hat{\theta}(k)$; $\theta(k)$ updated according to S - curve flightpath

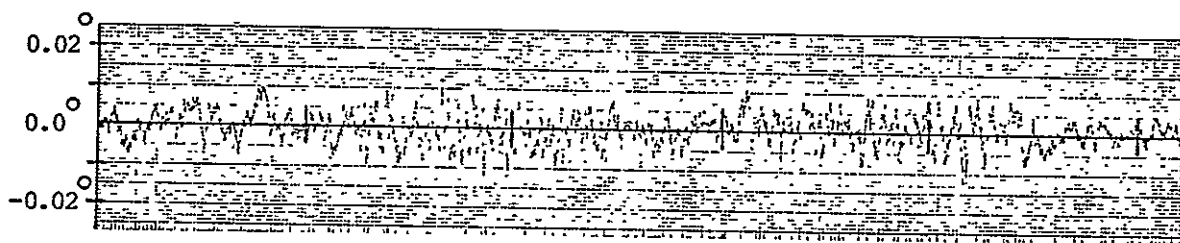


A. Optimal

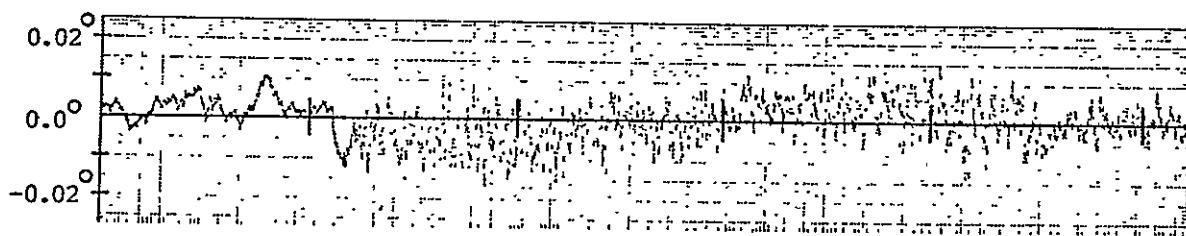
t = 250 sec.



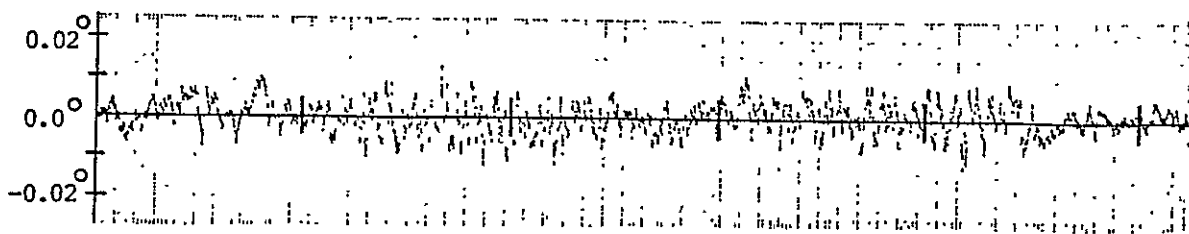
B. Minimum Innovations Covariance



C. Alspach



D. Sage - Husa



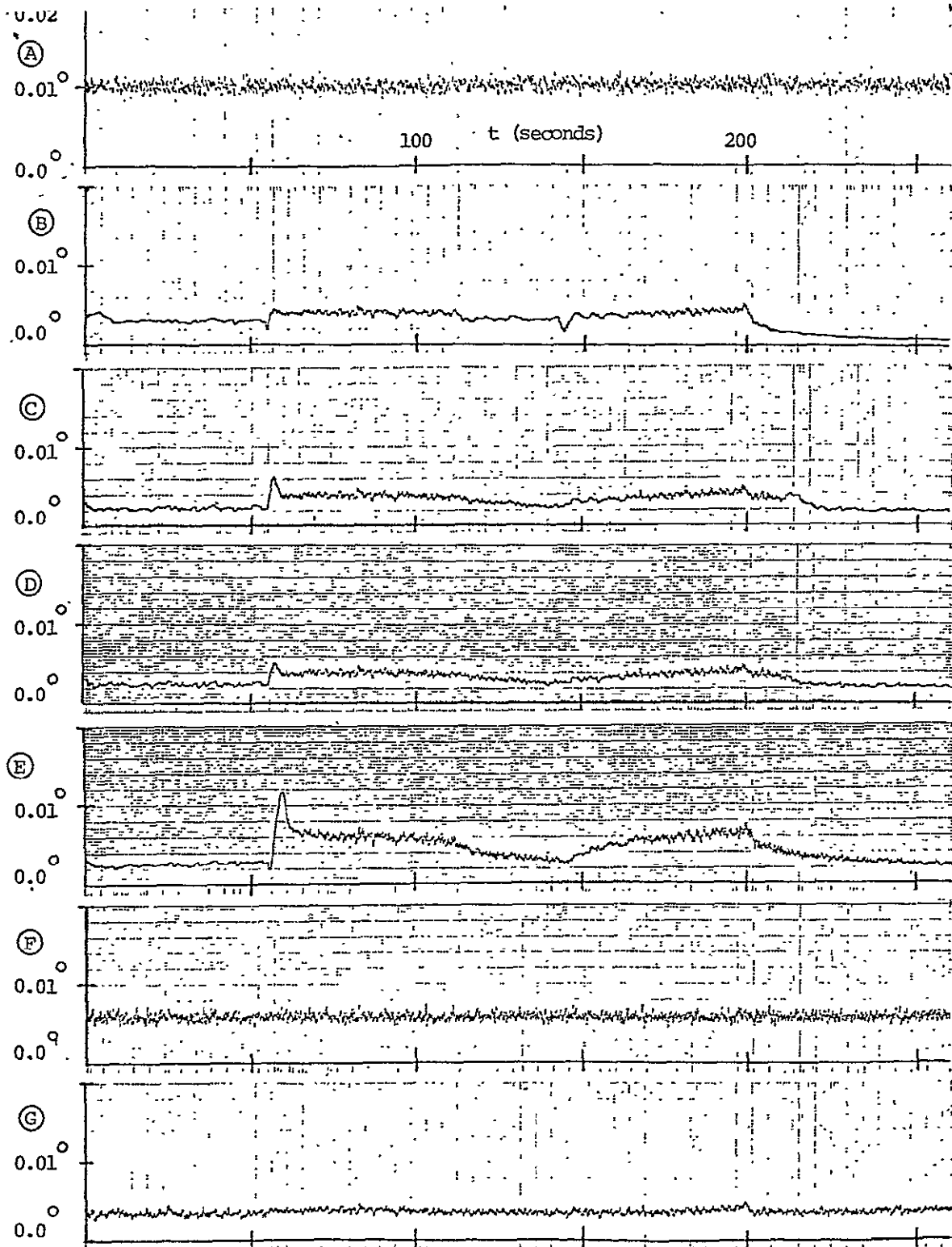
E. Magill

Figure VI - 12. Error in $\hat{\theta}(k|k)$ for Adaptive Filters; $\theta(k)$ deterministic

innovations covariance, Alspach, and Magill filters compare favorably with the optimal. The Sage-Husa filter experiences some difficulty, however, having a noticeable error bias, especially in the time region between 50 and 100 seconds.

Figure VI-13 shows the sample r.m.s. error in $\hat{\theta}(k|k)$ for 100 simulation runs for each of the filters tested. The r.m.s. error in the envelope processor estimate $y(k)$ stays near $.01^\circ$, as expected. The minimum innovations covariance and Alspach filters significantly reduce this error, generally holding it to $.004^\circ$ or less. Both filters show a brief rise in error at $t = 55$ seconds, where the acceleration $\ddot{\theta}(t)$ suddenly changes (see Figure VI-4.C). Here the adaptive gain $\hat{K}_1(k)$ lags the optimal gain, using a low suboptimal gain until the sample innovations covariances in the parallel filter bank can respond to the change in $\ddot{\theta}(t)$. Except for this temporary error increase, these two filters work about as well as the assumed optimal filter. The adaptive algorithm of Sage-Husa lowers the r.m.s. error in the envelope processor, but not to the same degree as the other adaptive filters. The error increase at $t = 55$ seconds is much more pronounced, rising almost to $.012^\circ$.

The nonadaptive Q_{MAX} filter with \hat{K}_1 at $.476$ has an r.m.s. error of about $.006^\circ$. This is higher than the $.004^\circ$ error often present with the best adaptive filters. A reduction of error from $.006^\circ$ to $.004^\circ$ seems rather marginal, though, when we consider the added sophistication required by the adaptive filters. If we assume that maximum $\ddot{\theta}(t)$ is known for the actual flightpath, then the constant-Q filter with \hat{K}_1 at $.190$ can be used. This filter has an r.m.s. error of about $.004^\circ$; this error performance is only slightly different from that of the adaptive



A. Envelope Processor; B. Optimal; C. Minimum Innov. Cov.; D. Alspach
 E. Sage - Husa; F. $K_1 = .476$; G. $K_1 = .190$

Figure VI - 13. Sample RMS Error in $\hat{\theta}(k|k)$; $\theta(k)$ set by S- curve flightpath.

filters. We note that the adaptive filters lower the r.m.s. error to about $.002^\circ$ when t is less than 50 seconds or greater than 200 seconds. Citing Figure VI-4.C, $\ddot{\theta}(t)$ is nearly zero for $t < 50$ seconds, and it equals zero for $t > 200$ seconds (here the aircraft is flying on runway centerline). Thus the adaptive filters work best only when the acceleration is near zero.

From these results it would seem wise to use the constant-Q filter with knowledge of maximum $\ddot{\theta}(t)$ for estimating $\theta(k)$. This filter works nearly as well as the best adaptive filters, and is much simpler to implement. The constant-Q filter uses the same equations as the Kalman filter of (III-18)-(III-28). On the other hand, the minimum innovations covariance and Alspach adaptive filters, which have the best error performance, must implement parallel Kalman filters. While such parallel processing would be fast, especially for the minimum innovations covariance filter, the hardware cost involved in realizing a bank of parallel filters seems unjustified by the marginal improvement in estimation error.

The constant-Q filter use here with gain \hat{K}_1 of .190 requires a knowledge of the maximum acceleration $\ddot{\theta}_{MAX}$ for the actual landing approach. In the general problem statement of this paper we have assumed the landing approach to be unknown; we can compute $\ddot{\theta}_{MAX}$ only for the family of allowable flightpaths. We therefore cannot realize this filter for our estimation problem as formally described. Yet we assume that the approach pattern used at a given airport and runway is standard. In such a case $\ddot{\theta}_{MAX}$ could be computed and stored until needed by an aircraft landing at that runway. At the beginning of the standard approach, this

value $\ddot{\theta}_{MAX}$ could be transmitted to the aircraft, which could then use the above constant-Q filter.

If the landing approach is not standard, or if there is no provision for communicating $\ddot{\theta}_{MAX}$ to the aircraft, we can still use the constant-Q filter which uses $\ddot{\theta}_{MAX}$ for the family of allowable flightpaths (the filter with gain $\hat{K}_1 = .476$ in our simulation). This filter has a higher r.m.s. error in $\hat{\theta}(k|k)$ than the best adaptive filters: $.006^\circ$ compared to $.004^\circ$ when the aircraft is maneuvering. Yet the improvement in performance for the adaptive filters is still not very significant when weighed against their added complexity.

In general the adaptive filters work well. The filter of Alspach and the minimum innovations covariance filter lower the envelope processor error in estimating $\theta(k)$ from $.01^\circ$ to $.004^\circ$ or less: a 60% reduction. But for our specific problem adaptive filtering does not appear to be necessary. The constant-Q filters work nearly as well and greatly simplify the estimation procedure. We should point out that use of the constant-Q filters is made possible by the fact that the measurement noise covariance $R(k)$ is known in our problem. In the general adaptive estimation problem, where $Q(k)$ and $R(k)$ are both unknown, we would expect the constant-Q filter to be highly suboptimal, with the superiority of the adaptive Kalman filters becoming clearly evident. We note that the minimum innovations covariance and Alspach filters do not use $R(k)$ anyway. These filters would work just as well for our problem if $R(k)$ had been unknown.

We digress here to make a general observation regarding adaptive filtering which may be useful in future work. Both in the simulation

runs presented here and in other runs the filter of Sage and Husa was slower than the other adaptive filters in responding to changes in $Q(k)$. The adaptive gain $\hat{K}(k)$ did not follow the optimal gain $K(k)$ as well, and the time lags between $K(k)$ and $\hat{K}(k)$ were much more pronounced when $Q(k)$ varied rapidly. We can speculate as to why this happened. The Sage-Husa filter uses the sample innovations covariance of the adaptive filter in computing $\hat{K}(k)$. If $Q(k)$ experiences a step change, the sample covariance eventually detects this change, causing $\hat{K}(k)$ to move toward the new steady-state gain. Yet the sample innovations covariance cannot immediately show the effect of using the new adaptive gain $\hat{K}(k)$, since most of the innovations residuals used in this statistic are those computed when $\hat{K}(k)$ was at the old value. The other adaptive algorithms use banks of fixed-gain parallel Kalman filters. When the adaptive gain moves to a new value $\hat{K}(k)$ as the result of a change in $Q(k)$, we already have a parallel filter operating with a gain close to $\hat{K}(k)$. This parallel filter has always been running at the same gain, so that the effects of $\hat{K}(k)$ upon the sample innovations covariance for the new value of $Q(k)$ are felt much sooner.

We should bear in mind that the filter of Sage-Husa was designed for problems where the noise was stationary. Also, we elected to use the suboptimal algorithm of Sage-Husa, rather than their more complicated optimal design based on MAP estimation. We speculate that this filter, by using smoothed state estimates, would be much faster in adapting to changes in $Q(k)$ and $R(k)$.

CHAPTER VII

CONCLUSION

We have examined adaptive Kalman filtering for use in estimating an aircraft's azimuth angle $\theta(k)$ in the Microwave Landing System. Adaptive filters from the literature were modified for application to the MLS problem and then tested in a simulated landing approach. The airborne receiver's envelope processor azimuth estimate $y(k)$ was used as an input to each candidate filter. The filter's task was to produce a new estimate $\hat{\theta}(k|k)$ having less mean-square error than $y(k)$. In the simulation testing conducted here, where an S-curve flightpath was used, two adaptive filters performed well: the r.m.s. error in $y(k)$ was lowered during various phases of the approach by 60 percent or more. A suboptimal, non-adaptive estimation scheme was found to work almost as well.

In Figure VI-13 we presented the results of our S-curve landing simulation, where the square error in $\hat{\theta}(k|k)$ was averaged for time k over 100 simulated approaches. The minimum innovations covariance filter and the filter of AIspace proved to be the best adaptive filters, generally holding the r.m.s. error in $\hat{\theta}(k|k)$ to $.004^\circ$ or less. This compares to a constant r.m.s. error in the envelope processor estimate $y(k)$ of $.01^\circ$. An r.m.s. error of about $.004^\circ$ was obtained by a suboptimal filter using a fixed estimate of the state noise covariance $Q(k)$ in the assumed stochastic model for $\theta(k)$. The estimate of Q was based upon knowledge of the maximum acceleration $\ddot{\theta}_{MAX}$ for the actual S-curve flightpath. When $\ddot{\theta}_{MAX}$ for the flightpath was unknown a second value of $\ddot{\theta}_{MAX}$ was used,

based on maximum acceleration for an allowable family of flightpaths. A filter using a constant Q estimate based on this value of $\ddot{\theta}_{MAX}$ estimated $\theta(k)$ with an r.m.s. error of about $.006^\circ$.

In Figure VI-13 we note that the adaptive filters lower the r.m.s. error to about $.002^\circ$ for t above 230 seconds; here the aircraft has been on runway centerline for about a mile. This is the only phase of the landing approach where the adaptive filters significantly outperform the best fixed- Q filter (the filter with steady-state gain \hat{K}_1 of .190 for our simulation).

While this constant- Q filter has an error performance comparable to that of the adaptive filters, it is not realizable under the formal constraints of our problem as defined in Chapter II. We assumed that the flightpath of the aircraft was unknown to the candidate filter; only the restrictions on the family of allowable flightpaths were given. Thus we would not know $\ddot{\theta}_{MAX}$ for the actual landing approach. As explained in Chapter VI, however, this filter could be used at an airport runway where the landing approach is standard. $\ddot{\theta}_{MAX}$ could be computed and stored for a given standard approach, and its value subsequently transmitted to an approaching aircraft.

If there is no provision for making the value $\ddot{\theta}_{MAX}$ for the given flightpath available to the aircraft's MLS receiver, we can resort to the less optimal constant- Q filter where $\ddot{\theta}_{MAX}$ for the set of allowable flightpaths is used. In our simulation this filter compared reasonably well with the best adaptive filters in error performance ($.006^\circ$ r.m.s. error vs. $.004^\circ$ r.m.s. error for large segments of the approach).

The fixed- Q filters use the Kalman filter equations of (III-18)-

(III-28), replacing $Q(k)$ with Q_{MAX} . Revisiting the algorithm flowcharts in Figures V-1 to V-4, we note that the adaptive Kalman filters are much more complex. The minimum innovations covariance and Alspach filters can run nearly as fast as the Kalman filter, but only when the parallel stationary filters run simultaneously. This requires the use of a special-purpose digital machine with parallel processing capability.

We conclude that, for a curved landing pattern similar to the S-curve approach used here, adaptive Kalman filtering is not needed. A nonadaptive, fixed-Q filter can estimate $\theta(k)$ with a mean-square error performance comparable to optimal. While adaptive filters can lower this mean-square error further, the marginal improvement is judged to be insignificant in comparison with the added complexity and cost of realizing a bank of parallel filters.

The success of the constant-Q filter results from the fact that the measurement noise covariance $R(k)$ is known in our problem. Given a knowledge of $R(k)$, we can be assured that our nonadaptive filter will not diverge by merely setting our estimate of $Q(k)$ to some maximum limit never exceeded by the true value. The more accurately we can bound $Q(k)$, the closer to optimal this filter becomes. In the more general problem where $Q(k)$ and $R(k)$ are both unknown, we speculate that an adaptive filter would be clearly superior. We note that the minimum innovations covariance and Alspach adaptive filters make no use of $R(k)$ in our problem, but assume it to be unknown. Thus their error performance would remain unchanged if knowledge of $R(k)$ were lost.

REFERENCES

1. H. W. Sorenson, "Kalman Filtering Techniques," Advances in Control Systems, Vol. 3, New York: Academic Press, 1974.
2. A. H. Jazwinski, Stochastic Processes and Filtering Theory, New York: Academic Press, 1970.
3. "Microwave Landing System," Final Report of the Scanning Beam Working Group, prepared for the Department of Transportation, Federal Aviation Administration, December, 1974.
4. G. A. McAlpine, J. H. Highfill, III, S. H. Irwin, Jr., J. E. Padgett, "Optimization of MLS Receivers for Multipath Environments," Report No. EE-4033-101-75, Research Laboratories for the Engineering Sciences, School of Engineering and Applied Science, University of Virginia, Charlottesville, Virginia, December, 1975.
5. G. A. McAlpine, J. H. Highfill, III, "Optimization of MLS Receivers for Multipath Environments," Report No. EE-4033-102-76, Research Laboratories for the Engineering Sciences, School of Engineering and Applied Science, University of Virginia, Charlottesville, Virginia, March, 1976.
6. G. A. McAlpine, J. H. Highfill, III, S. H. Irwin, Jr., "Optimization of MLS Receivers for Multipath Environments," Report No. UVA/528062/EE 76/103, Research Laboratories for the Engineering Sciences, School of Engineering and Applied Science, University of Virginia, Charlottesville, Virginia, December 1976.
7. A. Gelb, editor, Applied Optimal Estimation, Cambridge, Massachusetts: The M.I.T. Press, 1974.
8. D. L. Alspach, L. L. Scharf, A. Abiri, "A Bayesian Solution to the Problem of State Estimation in an Unknown Noise Environment," International Journal of Control, Vol. 19, No. 2, February, 1974, pp. 265-287.
9. R. K. Mehra, "On the Identification of Variances and Adaptive Kalman Filtering," IEEE Transactions on Automatic Control, Vol. AC-15:2, April, 1970, pp. 175-184.
10. A. P. Sage and G. W. Husa, "Adaptive Filtering with Unknown Prior Statistics," Proceedings, Joint Automatic Control Conference, pp. 760-769, 1969.

11. A. P. Sage and G. W. Husa, "Algorithms for Sequential Adaptive Estimation of Prior Statistics," Proceedings, IEEE Symposium on Adaptive Processes, Pennsylvania State University, University Park, Pennsylvania, November, 1969.
12. M. Aoki, Optimization of Stochastic Systems, New York: Academic Press, 1967.
13. D. T. Magill, "Optimal Adaptive Estimation of Sampled Stochastic Processes," IEEE Transactions on Automatic Control, Vol. AC-10:4, October, 1965, pp. 434-439.
14. F. L. Sims and D. G. Lainiotis, "Recursive Algorithm for the Calculation of Adaptive Kalman Filter Weighting Coefficients," IEEE Transactions on Automatic Control, Vol. AC-14:2, April, 1969, pp. 215-218.
15. D. L. Alspach, "A Parallel Filtering Algorithm for Linear Systems with Unknown Time Varying Noise Statistics," IEEE Transactions on Automatic Control, Vol. AC-19:5, October, 1974, pp. 552-556.

DISTRIBUTION LIST

Copy No.

1 - 2 NASA Scientific and Technical
Information Facility
P. O. Box 8757
Baltimore/Washington International Airport
Maryland 21240

3 - 13 Flight Electronics Division
National Aeronautics and Space Administration
Langley Research Center
Hampton, Virginia 23665
Attn: Mr. L. R. Shultz
Technical Officer

14 - 15 G. A. McAlpine

16 - 19 J. H. Highfill, III

20 S. H. Irwin, Jr.

21 R. E. Nelson

22 Ghassem Koleyni

23 J. N. Warfield

24 I. A. Fischer

25 - 26 E. H. Pancake
Science/Technology Information Center
Clark Hall

27 RLES Files

UNIVERSITY OF VIRGINIA

School of Engineering and Applied Science

The University of Virginia's School of Engineering and Applied Science has an undergraduate enrollment of approximately 1,000 students with a graduate enrollment of 350. There are approximately 120 faculty members, a majority of whom conduct research in addition to teaching.

Research is an integral part of the educational program and interests parallel academic specialties. These range from the classical engineering departments of Chemical, Civil, Electrical, and Mechanical to departments of Biomedical Engineering, Engineering Science and Systems, Materials Science, Nuclear Engineering, and Applied Mathematics and Computer Science. In addition to these departments, there are interdepartmental groups in the areas of Automatic Controls and Applied Mechanics. All departments offer the doctorate; the Biomedical and Materials Science Departments grant only graduate degrees.

The School of Engineering and Applied Science is an integral part of the University (approximately 1,400 full-time faculty with a total enrollment of about 14,000 full-time students), which also has professional schools of Architecture, Law, Medicine, Commerce, and Business Administration. In addition, the College of Arts and Sciences houses departments of Mathematics, Physics, Chemistry and others relevant to the engineering research program. This University community provides opportunities for interdisciplinary work in pursuit of the basic goals of education, research, and public service.